

THE SYNTHESIS OF FUNCTIONALIZED CYCLOPARAPHENYLENES AS NOVEL  
BIOCOMPATIBLE FLUORESCENT PROBES  
AND ORGANIC MATERIALS

by

BRITTANY MARIE WHITE

A DISSERTATION

Presented to the Department of Chemistry and Biochemistry  
and the Graduate School of the University of Oregon  
in partial fulfillment of the requirements  
for the degree of  
Doctor of Philosophy

December 2018

DISSERTATION APPROVAL PAGE

Student: Brittany Marie White

Title: The Synthesis of Functionalized Cycloparaphenylenes as Novel Biocompatible Fluorescent Probes and Organic Materials

This dissertation has been accepted and approved in partial fulfillment of the requirements for the Doctor of Philosophy degree in the Department of Chemistry and Biochemistry by:

Michael Haley	Chairperson
Ramesh Jasti	Advisor
Darren Johnson	Core Member
Tristan Ursell	Institutional Representative

and

Janet Woodruff-Borden	Vice Provost and Dean of the Graduate School
-----------------------	--

Original approval signatures are on file with the University of Oregon Graduate School.

Degree awarded December 2018

© 2018 Brittany Marie White

## DISSERTATION ABSTRACT

Brittany Marie White

Doctor of Philosophy

Department of Chemistry and Biochemistry

December 2018

Title: The Synthesis of Functionalized Cycloparaphenylenes as Novel Biocompatible Fluorescent Probes and Organic Materials

Conjugated macrocycles have emerged as novel structural motifs that modulate the electronic properties of organic molecules because of their strained and contorted structures. Cycloparaphenylenes, known as nanohoops, are a particularly attractive scaffold for the design of new types of carbon nanomaterials because of their size-selective synthesis, radially oriented  $\pi$ -systems and tunable electronic properties. The development of modular syntheses of nanohoops over the past decade should enable the preparation of substituted derivatives that can be tuned for applications in biology and materials science.

Chapter **I** provides a brief overview of conjugated macrocycles recently reported in the literature with a discussion of the structural effects that are responsible for the remarkable properties of this class of molecules. Chapter **II** highlights a scalable and mild synthetic approach developed in our lab to prepare nanohoop conjugated macrocycles and expands the generality of this methodology with the formal synthesis of natural product Acerogenin E. Chapter **III** describes the synthesis of cycloparaphenylenes with versatile functional handles and uncovers the reactivity of the strain nanohoop backbone under reaction conditions that promote the formation of radical cations. Chapter **IV** takes

advantage of the functional groups described in chapter **III** to develop the first example of nanohoops as a new class of biocompatible fluorophores. Chapter **V** details a novel synthetic approach that enables the incorporation of the linear acene pentacene into the nanohoop backbone and reports our findings on the impact that the macrocyclic structure has on the properties of this organic semiconductor. In summary, the findings discussed in this dissertation provide synthetic strategies for the selective functionalization of nanohoops and highlight this class of molecules as a novel scaffold for the design of new types of carbon nanomaterials.

This dissertation includes previously published and unpublished co-authored material.

## CURRICULUM VITAE

NAME OF AUTHOR: Brittany Marie White

### GRADUATE AND UNDERGRADUATE SCHOOLS ATTENDED:

University of Oregon, Eugene  
Boston University, Boston  
University of New Hampshire, Durham

### DEGREES AWARDED:

Doctor of Philosophy, Chemistry, 2018, University of Oregon  
Bachelor of Science, Chemistry, 2013, University of New Hampshire

### AREAS OF SPECIAL INTEREST:

Synthetic Organic Chemistry  
Physical Organic Chemistry  
Chemical Biology

### PROFESSIONAL EXPERIENCE:

Teaching Fellow, University of Oregon, 2014-2018  
Teaching Fellow, Boston University, 2013-2014

### GRANTS, AWARDS, AND HONORS:

Travel Award, Division of Organic Chemistry, National Organic Chemistry Symposium, 2017  
Raymond B. Seymour Award, University of New Hampshire, Department of Chemistry, 2013  
Craig West Award for Undergraduate Professional Development, University of New Hampshire, Department of Chemistry, 2012  
George and Dorothy Costarakis Galanes Endowment, University of New Hampshire, Department of Chemistry, 2012 and 2011

Mike and Bea Dolton Scholarship, University of New Hampshire, College of  
Chemistry, Engineering and Physical Sciences, 2011

PUBLICATIONS:

White, B. M.; Zhao, Y.; Kawashima, T. K.; Branchaud, B. P.; Pluth M. D.;  
Jasti, R. Expanding the chemical space of biocompatible fluorophores:  
Nanohoops in cells. *ACS Cent. Sci.* **2018**, *4*, 1173-1178.

White, B. M.; Zhao, Y.; Kawashima, T. K.; Branchaud, B. P.; Pluth M. D.;  
Jasti, R. Expanding the chemical space of biocompatible fluorophores:  
Nanohoops in cells. *ChemRxiv* **2018**, DOI: 10.26434/chemrxiv.6261884.v1.

Darzi, E. R.; White, B. M.; Loventhal, L. K.; Zakhovov, L. N.; Jasti, R. An  
operationally simple and mild oxidative homocoupling of aryl boronic  
esters to access conformationally constrained macrocycles. *J. Am. Chem.  
Soc.* **2017**, *139*, 3109-3115.

Sisto, T. J.; Zakhovov L. N.; White, B. M.; Jasti, R. Towards Pi-Extended  
Cycloparaphenylenes as Seeds for CNT Growth: Investigating Strain  
Relieving Ring-Openings and Rearrangements. *Chem. Sci.* **2016**, *7*, 3681-  
3688.

## ACKNOWLEDGMENTS

I would like to first acknowledge the mentors I had the pleasure of learning from at the beginning of my scientific career that have had a profound impact on my development as a scientist. Professor Richard Johnson for welcoming me into his lab as an undergraduate researcher, Dr. Sarah Skraba for being an excellent role model of a female scientist in chemistry, Dr. Rajesh Thamatan for taking me under his wing as a young scientist and teaching me skills that have been invaluable to my career inside and outside of the lab and all of the Professors, Graduate students and Staff in the Department of Chemistry at the University of New Hampshire that prepared me so well for my journey into graduate school.

I would like to express sincere appreciation to my graduate advisor Professor Ramesh Jasti for his continued support and guidance throughout my graduate career and for leading by example as a mentor. To the graduate students in the Jasti lab that moved across the country to start the lab at the University of Oregon, Thomas Sisto, Paul Evans, Matthew Golder, Evan Darzi and Penghao Li, words cannot express how grateful I am for the memories we share in Eugene and the continued support I've received from every one of you. A special thanks to Gabby Macias and Evan Darzi for becoming my Eugene family, Matt Golder for all of his guidance during my graduate career, Dan Seidenkranz, Gabe Rudebusch, the rest of the Haley lab and the all of the Professors and Staff in the Chemistry Department at the University of Oregon for welcoming the Jasti lab to Eugene and Elizabeth Hirst for believing in me as a young graduate student.

I am extremely grateful for undergraduate students Taryn Kawashima and Cyrus Waters that I have had the privilege of working with in the lab, I hope I've been able to



teach you as much as you've taught me. Thank you to all of the current members of the Jasti Lab Tobias Schaub, Jeff Van Raden, Curtis Colwell, Erik Leonhardt, Terri Lovell, Ruth Maust and Claire Ottenson for contributing scientifically and personally to create a productive space for discovery. Especially Erik, Ruth and Jeff for their support and friendship particularly during challenging times of my graduate career.

A heartfelt thanks to my parents Joseph White and Dana Lussier and my step parents Nadine White and Robert Lussier for their patience while I've been in graduate school and for teaching me to believe in myself, work hard and never give up on my goals in life. Thank you to my sisters and brothers Caitlin Chaput, Lindsey Lussier, Joshua Lussier and Joshua Skerry for their unending love and supporting and my godson Jacob Chaput for the inspiration and motivation to finish the last years of graduate school strong. I would like to acknowledge the rest of my family and friends especially Lisa Trahan and Jean Mathieu, thank you for all of your inspiration, love and support.

Finally I would like to express my deepest appreciation and gratitude to my fiancé Spencer Mathieu. You are the light of my life and your constant love and support has lifted me up to make me the person I am today. None of this work would have been possible without you. Thank you for always believing in me, believing in us and joining me on this journey that led us all the way across the country.

Dedicated to my loving fiancé Spencer Mathieu and sisters and brothers Caitlin Chaput,  
Lindsey Lussier, Joshua Lussier and Joshua Skerry

## TABLE OF CONTENTS

Chapter	Page
I. THE UNIQUE PROPERTIES OF CONJUGATED MACROCYCLIC STRUCTURES .....	1
1.1. Introduction .....	1
1.2. Synthesis of Conjugated Macrocycles.....	3
1.3. The Electronic Properties of Cyclic Oligothiophenes .....	8
1.4. Organic Materials from PDI Containing Macrocycles.....	10
1.5. Porphyrin Nanorings as Synthetic Light Harvesting Systems .....	13
1.6. The Unique Optical Properties of Cycloparaphenylenes .....	15
1.7. Conclusion.....	17
1.8. Bridge to Chapter II.....	18
II. THE FORMAL SYNTHESIS OF ACEROGENIN E VIA OXIDATIVE HOMOCOUPLING .....	19
2.1. Introduction .....	20
2.2. Results and Discussion.....	21
2.2.1. Natural Product Acerogenin E.....	21
2.2.2. Oxidative Homocoupling for the Formal Synthesis of Acerogenin E .....	23
2.2.3. Variable Temperature <sup>1</sup> H NMR.....	25
2.3. Conclusion.....	20
2.4. Experimental Sections .....	20
2.4.1. General Experimental Details.....	27
2.4.2. Synthetic Details.....	28
2.4.3. Crystallographic Data.....	34

Chapter	Page
2.4.4. Homodesmotic Reactions .....	35
2.4.5. Computational Coordinates of Minimized Geometries.....	35
2.5. Bridge to Chapter III .....	40
III. THE SYNTHESIS OF SUBSTITUTED CYCLOPARAPHENYLENES AND THEIR REACTIVITY .....	41
3.1. Introduction .....	41
3.2. Results and Discussion .....	44
3.2.1. The Synthesis of Methyl Substituted Nanohoops .....	44
3.2.2. The Synthesis of a Nanohoop with Benzyl Alcohol Functionality .....	47
3.3. Conclusion .....	49
3.4. Experimental Sections .....	50
3.4.1. General Experimental Details.....	50
3.4.2. Synthetic Details.....	51
3.5. Bridge to Chapter IV .....	64
IV. EXPANDING THE CHEMICAL SPACE OF BIOCOMPATIBLE FLUOROPHORES: NANOHOOPS IN CELLS.....	65
4.1. Introduction .....	65
4.2. Results and Discussion .....	68
4.3. Conclusion .....	73
4.4. Experimental Sections .....	74
4.4.1. General Experimental Details.....	74
4.4.2. Synthetic Details.....	75
4.5. Bridge to Chapter V.....	104

Chapter	Page
V. THE SYNTHESIS OF A PENTACENE INCORPORATED NANOHOOP .....	105
5.1. Introduction .....	105
5.2. Results .....	107
5.3. Discussion.....	110
5.4. Conclusion and Future Work.....	111
5.5. Experimental Sections .....	111
5.5.1. General Experimental Details.....	111
5.5.2. Synthetic Details.....	112
5.5.3. Computational Coordinates of Minimized Geometries and HOMO, LUMO levels .....	119
CONCLUDING REMARKS .....	124
REFERENCES CITED .....	125

## LIST OF FIGURES

Figure	Page
1.1. Conjugated macrocycles presented in this chapter: cyclic oligothiophene <b>I.1</b> , PDI containing macrocycle <b>I.2</b> , porphyrin nanoring <b>I.3</b> and cycloparaphenylene <b>I.4</b> . .....	3
1.2. Synthetic methods for the preparation of $C_n$ Ts developed by Bäuerle and coworkers. ....	4
1.3. Synthesis of PDI containing macrocycle <b>I.2</b> using the platinum templation strategy. ....	5
1.4. Templation strategy developed by Anderson to produce porphyrin nanoring <b>I.3</b> . ....	6
1.5. Synthetic methods for the preparation of $[n]$ CPPs pioneered by Jasti, Itami and Yamago. ....	8
1.6. Linear analog <b>I.35</b> for comparison to macrocyclic $C_n$ Ts. ....	9
1.7. Linear analogs <b>I.36</b> , <b>I.37</b> , <b>I.38</b> and <b>I.39</b> for comparison to conjugated macrocycle <b>I.2</b> . ....	12
1.8. Structures of porphyrin nanoring <b>I.40</b> , templated nanoring <b>I.41</b> , template <b>I.42</b> and linear analogs <b>I.43</b> and <b>I.44</b> for comparison to the macrocyclic compounds. ....	14
1.9. HOMO-LUMO gaps of $[n]$ CPPs <b>I.32</b> , <b>I.45</b> , <b>I.46</b> , <b>I.4</b> , <b>I.27</b> , <b>I.47</b> , <b>I.48</b> and <b>I.28</b> compared to their linear p-oligophenylene counterparts ( <b>I.49</b> ). ....	16
2.1. a) The original oxidative homocoupling reaction conditions. b) Our optimized conditions. c) The substrate scope of the oxidative homocoupling. ....	21
2.2. The reported total synthesis of Acerogenin E ( <b>II.7</b> ). ....	22
2.3. The minimized structure of <b>II.5</b> and a view of its planar $\pi$ -system down the aryl-aryl bond. ....	23
2.4. Ortho-metalation as a strategy to install aryl boronic acid pinacol ester functionality. ....	24
2.5. Our optimized reaction sequence for the preparation of <b>II.8</b> and its oxidative homocoupling to give <b>II.5</b> . ....	25

Figure	Page
2.6. VT- <sup>1</sup> H NMR of <b>II.5</b> . Peaks are assigned to hydrogens in <b>II.5</b> as indicated by the colored squares at 0 °C and 78 °C. ....	26
2.7. Proton-carbon HSQC of the alkyl region of macrocycle <b>II.5</b> . The proton spectrum is displayed on the x-axis (peaks and position, top and bottom respectively) and the carbon spectrum is displayed in the y-axis (peaks and position, left and right respectively). ....	34
2.8. ORTEP representation of x-ray crystallographic structure of macrocycle <b>II.5</b> . ....	34
2.9. Homodesmotic reaction used to approximate the strain of compound <b>II.5</b> . ....	35
2.10. Structure of macrocycle <b>II.5</b> represented by the computation coordinates listed below. ....	35
2.11. Structure of homodesmotic product <b>II.13</b> represented with the computational coordinates listed below. ....	37
3.1. a) Nanohoops as the smallest cross-sectional segment of an armchair carbon nanotube (CNT). b) The size-dependent optical properties of [5]-[12]CPP (solid lines are absorbance and dashed lines are fluorescence) and the x-ray crystal structure of the C <sub>60</sub> @[10]CPP host-guest complex. c) The scalable and modular synthesis of nanohoops. d) Structures of the nanohoops investigated in this chapter. ....	44
3.2. The synthesis of methyl substituted [6]CPP <b>III.1</b> . ....	45
3.3. The synthesis of methyl substituted [8]CPP <b>III.2</b> . ....	46
3.4. a) The decomposition of <b>III.1</b> and <b>III.2</b> under benzylic bromination reaction conditions. B) A mechanism of rearrangement for [6]CPP after single electron oxidation. ....	47
3.5. The synthesis of benzyl alcohol [8]CPP <b>III.3</b> and benzyl bromide [8]CPP <b>III.4</b> . ....	49
4.1. Traditional organic dye scaffolds and the new nanohoop fluorophore scaffold. ....	66

- 4.2. Characterization of disulfonate[8]CPP (**IV.1**). (a) Summary of nanohoop photophysical properties. (footnote a) Contains 0.1% SDS. (footnote b) Standard deviation is <5% of the measurement ( $n=3$ ). (footnote c) 0.01 M KOH in ethanol. (b)  $\lambda_{\text{ex}}$  and  $\lambda_{\text{em}}$  of 2  $\mu\text{M}$  solutions of [8]CPP (black), **IV.1** in DMSO (green), and **IV.1** in PBS buffer with 0.1% SDS (yellow). (c) pH vs fluorescence (FL) intensity of **IV.1** and fluorescein in a 1:1 MeOH:100 mM KCl, 100 mM KOH solution. Error bars represent standard deviation ( $n = 3$ ). ..... 70
- 4.3. DIC and fluorescent images of live HeLa cells in the absence (A-D) or presence (E-H) of disulfonate[8]CPP (**IV.1**). (A,E) DIC; (B,F) NucRed live 647 imaged in CY5 channel; (C, G) **IV.1** imaged in DAPI-long-pass channel; and (D,H) merge of the CY5/DAPI-long-pass channel showing no significant colocalization. Scale bar = 100  $\mu\text{m}$ . ..... 71
- 4.4. (a) Synthesis of folate-[8]CPP conjugate using copper catalyzed azide-alkyne click chemistry. (b) DIC and fluorescent images of live HeLa cells in the presence of **IV.11** (A, B, E, F) and absence of **IV.11** (C, D, G, H). As controls cells were treated with folic acid (E-F) and **IV.9** (G-H). (A, C, E, G) DIC channel; (B, D, F, H) DAPI-long-pass channel. Scale bar = 50  $\mu\text{m}$ . ..... 72
- 4.5. Fluorescent images of [8]CPP and [12]CPP in live cells. HeLa cells were incubated with nuclear stain NucRed® live 647 (A-F) in the presence of a [8]CPP in a 5 wt% solution of pluronic F108 (A-C) or in the presence of a [12]CPP in a 5 wt% solution of pluronic F108 (D-F) for 1 hour and washed before imaging. The channels shown are the differential interference contrast (A and D), CY5 (colored red, B and E), DAPI-LP (colored green, C) and DAPI (colored blue, F). Channels C and F were treated with 3x3 binning and 3s exposure times to visualize the fluorescent emission. .... 93
- 4.6. Fluorescent images of [8]CPP and [12]CPP in live cells. HeLa cells were incubated with nuclear stain NucRed® live 647 (A-F) in the presence of a [8]CPP in a 5 wt% solution of pluronic F108 and cetrimonium bromide (CTBA) (A-C) or in the presence of a [12]CPP in a 5 wt% solution of pluronic F108 and CTAB (D-F) for 1 hour and washed before imaging. The channels shown are the differential interference contrast (A and D), CY5 (colored red, B and E), DAPI-LP (colored green to represent the emission of [8]CPP, C) and DAPI (colored blue to represent the emission of [12]CPP, F). Channels C and F were treated with 3x3 binning to visualize the fluorescent emission. Large aggregated structures are clearly visible in the nanohoop channels (C and F). ..... 94



Figure	Page
4.7. Cell viability of disulfonate[8]CPP <b>IV.1</b> in HeLa cells. The results are expressed as the mean with error bars representing the standard error in measurement (n=6). .....	95
4.8. Long-term cell viability of disulfonate[8]CPP <b>IV.1</b> in HeLa cells. The results are expressed as the mean with error bars representing the standard error in measurement (n=6). .....	95
4.9. DIC and fluorescent images of live HeLa cells for colocalization experiments of disulfonate[8]CPP <b>IV.1</b> with CellTracker Red CMTPX (A-D), ER-Tracker Red (E-H) and MitoTracker Red RM (I-L). DIC (A, E, I); CY5 (B, F, J); DAPI-long-pass (C, G, K); CY5 and DAPI-long-pass overlay (C, H, L). .....	96
4.10. Quantum yield measurement of <b>IV.1</b> in DMSO. . .....	98
4.11. Quantum yield measurement of <b>IV.1</b> in PBS Buffer with 0.1% SDS. ....	98
4.12. Quantum yield measurement of <b>IV.9</b> in dichloromethane. ....	99
4.13. Molar absorptivity measurement of <b>IV.1</b> in DMSO. ....	99
4.14. Molar absorptivity measurement of <b>IV.1</b> in PBS Buffer with 0.1% SDS. ....	100
4.15. Molar absorptivity measurement of <b>IV.9</b> in dichloromethane. ....	100
4.16. The absorbance of <b>IV.1</b> at 330 nm remains constant as pH changes while the absorbance of fluorescein at 494 nm is pH dependent. Error bars represent standard deviation (n=3). .....	101
4.17. Photobleaching of nano hoop <b>IV.1</b> and fluorescein under constant irradiation over time in a cuvette. The nano hoop was excited at 328 nm and the emission was monitored at 510 nm while fluorescein was excited 494 nm and the emission was monitored 512 nm. ....	102
4.18. The fluorescence of <b>IV.1</b> (excitation at 330 nm) in PBS buffer solution with 10% fetal bovine serum (FBS). The initial increase in fluorescence is likely due to increased solubility of <b>IV.1</b> in the 10% FBS solution. ....	102
4.19. Absorption spectra of [8] and [12]CPP stock solutions (nano hoop in deionized water with 1wt% pluronic F108). Absorption normalized by scaling the maxima to 1. ....	103

Figure	Page
4.20. Emission spectra of [8] and [12]CPP stock solutions (nanohoop in deionized water with 1 wt% pluronic F108). Emission normalized by scaling the maxima to 1. ....	103
4.21. Cell viability of [8]CPP in HeLa cells with 1 wt% pluronic F108. Error bars show standard error in measurement (n=6). ....	103
4.22. Cell viability of [12]CPP in HeLa cells with 1 wt% pluronic F108. Error bars show standard error in measurement (n=6). ....	103
5.1. Pentacene and [10]cycloparaphenylene combine to create novel organic nanomaterial <b>V.1</b> . ....	107
5.2. Synthesis of pentacene containing macrocycles utilizing endoperoxide formation to access <i>cis</i> -stereochemistry. ....	108
5.3. Reduction and oxidation attempts to prepare target compound <b>V.1</b> . ....	109
5.4. VT- <sup>1</sup> H NMR of macrocycle <b>V.7</b> . ....	116
5.5. Structure of macrocycle <b>V.1</b> represented with the computational coordinates listed below ....	119
5.6. HOMO and LUMO surfaces of <b>V.1</b> . ....	124

## LIST OF TABLES

Table	Page
1.1. Optical properties of $C_nT$ s <b>I.10-I.15</b> and linear analog <b>I.35</b> . .....	9
1.2. A summary of the electronic properties of $[n]$ CPPs. ....	17
4.1. Details for the cubes used in the experiments outlined in this document and in the manuscript. ....	92
4.2. Pearson's colocalization coefficients for the images shown in <b>Figure 4.8</b> and <b>Figure 4.3</b> . ....	97
5.2. HOMO and LUMO levels of <b>V.1</b> from its minimized structure (in hartrees and eV). ....	124

## LIST OF SCHEMES

Scheme	Page
4.1 The synthesis of disulfonate[8]CPP. ....	69

## CHAPTER I

### THE UNIQUE PROPERTIES OF CONJUGATED MACROCYCLIC STRUCTURES

This chapter was written by myself and edited by Professor Ramesh Jasti.

Chapter **II** includes co-authored material with excerpts from work published in *The Journal of the American Chemical Society*. The excerpt included was written by myself with assistance from Dr. Evan R. Darzi. The experimental work included from the published material was performed by myself with assistance from Dr. Evan R. Darzi. Dr. Lev N. Zakharov provided crystal structure analysis of the final product discussed in the experimental section. Professor Ramesh Jasti provided editorially assistance.

Chapter **III** includes unpublished co-authored material. This chapter was written by and includes experimental work performed by myself. Professor Ramesh Jasti provided editorial assistance.

Chapter **IV** is based on published material in *ACS Central Science*. This manuscript was written by myself with editorial assistance from Professor Ramesh Jasti, Professor Michael D. Pluth and Professor Bruce P. Branchaud. Experimental work included in this chapter was performed by myself or with Dr. Yu Zhao and Taryn E. Kawashima under my direction. Experimental guidance was provided by Professor Ramesh Jasti and Professor Michael D. Pluth.

Chapter **V** includes unpublished co-authored material. Experimental work was performed by either myself or Cyrus Waters under my direction. This chapter was written by myself with editorial assistance from Professor Ramesh Jasti.

#### **1.1. Introduction**

Macrocyclic molecules are cyclic molecular frameworks consisting of at least twelve atoms.<sup>1,2</sup> This unique class of compounds possesses unconventional molecular shapes, unusual bond geometries and unique spatial orientations that offer remarkable properties.<sup>3</sup> For example, macrocycles found in nature achieve structural preorganization of binding sites that minimize entropic loss when interacting with protein pockets in

biological systems.<sup>1</sup> This can result in increased compound potency and selectivity as evident by the development of several macrocyclic natural product oncology drugs that have been approved for clinical use.<sup>4-7</sup> Natural light-harvesting systems take advantage of this architecture with proteins that hold macrocyclic chlorophyll molecules together in a cyclic arrangement to enable electronic delocalization and enhance the light harvesting ability of these chromophores.<sup>8</sup> Additionally, recent studies show that structural deformation of individual chlorophyll molecules play a major role in the harvesting abilities of these systems by increasing conjugation through orbital overlap.<sup>9</sup>

Inspired by the macrocyclic molecules that nature has invented, organic chemists have sought to harness the beneficial properties of these systems with the synthesis of natural products for decades. More recently, advances in synthetic techniques have prompted the design of completely new scaffolds where macrocyclic architecture provides access to unconventional electronic structures. In particular, the preparation of fully conjugated macrocycles has provided access to molecules distorted  $\pi$ -systems and small highest molecular orbital-lowest unoccupied molecular orbital (HOMO $\rightarrow$ LUMO) gaps to afford materials with advantageous properties.<sup>10-13</sup>

This chapter focuses on four related compound classes that are recent examples of conjugated macrocyclic structures with unique electronic properties: 1) cyclic oligothiophenes, 2) perylene diimide (PDI) containing macrocycles, 3) fully conjugated porphyrin nanorings and 4) cycloparaphenylenes (**Figure 1.1**). The chapter begins with a brief overview of the key synthetic steps to access these molecules and the proceeding discussions highlight studies where the electronic structure of these conjugated macrocycles are compared to their linear counterparts.

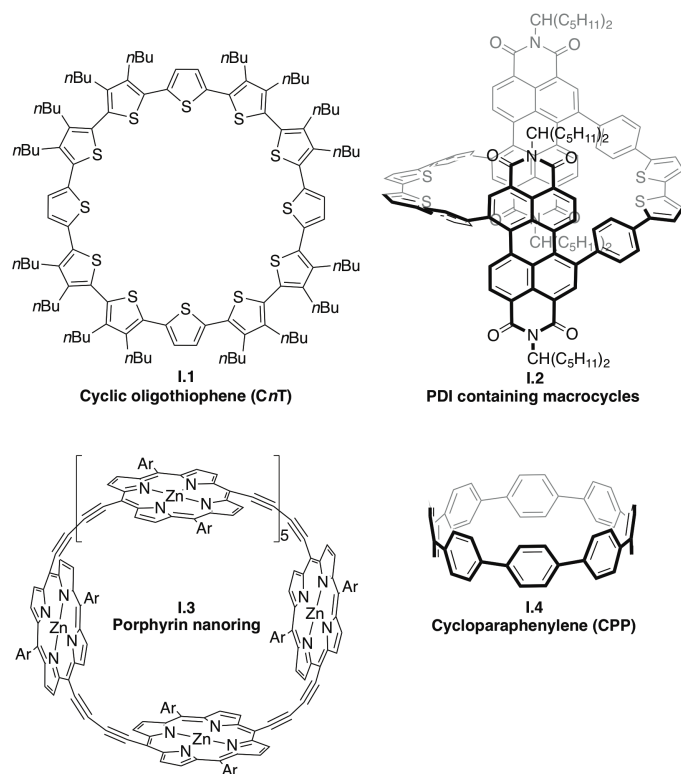


**Figure 1.1.** Conjugated macrocycles presented in this chapter: cyclic oligothiophene **I.1**, PDI containing macrocycle **I.2**, porphyrin nanoring **I.3**, cycloparaphenylene **I.4**.

## 1.2. Synthesis of Conjugated Macrocycles

The ability to study new types of conjugated macrocycles is directly related to the synthetic methods available to prepare them. These structures can be especially challenging to synthesize with standard methods because of their highly strained nature or contorted structure based on the bond linkages of the macrocyclic architecture.<sup>10, 14, 15</sup> The careful design of advanced intermediates, templates and selection of reaction conditions that promote macrocycle formation have been key to the successful preparation of **I.1**, **I.2**, **I.3** and **I.4**. The synthetic strategies outlined in this section have enabled studies of these conjugated macrocycles, discussed in the remaining sections of this chapter.

Cyclic oligothiophenes (C<sub>n</sub>Ts), where *n* represents the number of thiophenes in a ring, were first synthesized in 2000 by Bäuerle using copper mediated alkyne homocoupling of thienylbutadiynes (**I.5**) followed by reaction with sodium sulfide

(Figure 1.2).<sup>10, 11, 16</sup> The amount of material that is produced with this sequence is limited by the homocoupling macrocyclization step where a statistical mixture of products is prepared with low yields (2-12%) under pseudo-dilute reaction conditions. This was exacerbated even further during the sulfur nucleophilic step to give the final products C12T **I.1**, C14T **I.6** and C16T **I.7** in 23%, 7% and 27% yield respectively. To mitigate these issues Bäuerle and coworkers reported an improved synthetic route in 2009 that utilizes Pt<sup>II</sup> as a templating building block to assemble oligothiophene linear precursor **I.8** (Figure 1.2).<sup>17,18</sup> This method again produced a statistical mixture macrocycles but gave multinuclear platinum compounds (**I.9**) in 80% combined yield with mild reaction conditions. The final C<sub>n</sub>Ts were prepared by refluxing intermediate mixture **I.9** in toluene to give C10T **I.10**, C15T **I.11**, C20T **I.12**, C25T **I.13**, C30T **I.14** and C35T **I.15** as a mixture in a 57% combined yield. The high yields and mild reaction conditions used for the Pt<sup>II</sup> templating strategy has made this approach one of the most popular methods for the preparation of conjugated macrocyclic precursors.

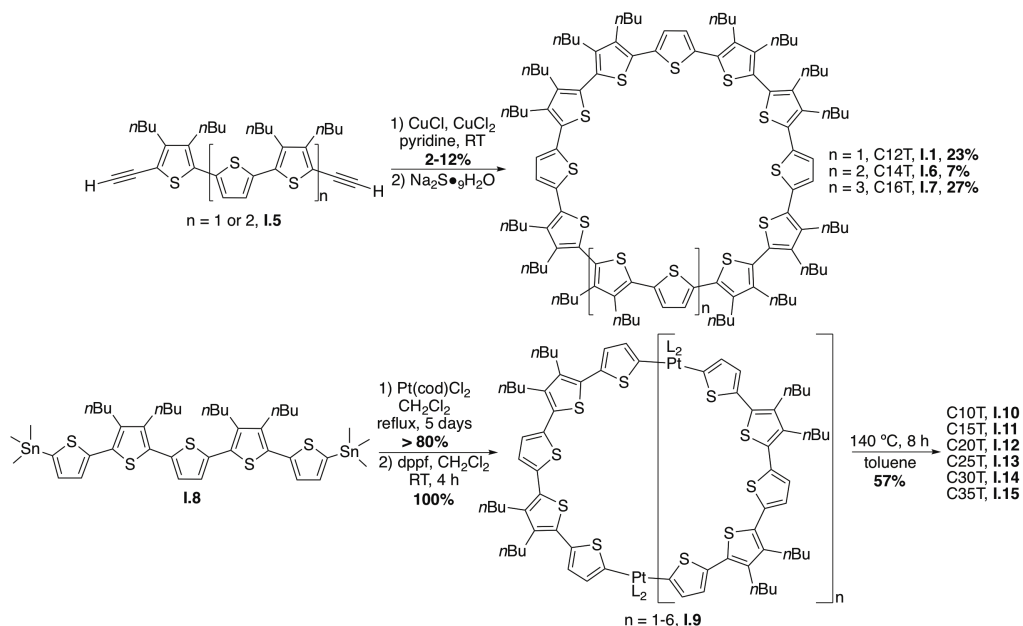


**Figure 1.2.** Synthetic methods for the preparation of C<sub>n</sub>Ts developed by Bäuerle and coworkers.

Very recently, the Nuckolls lab reported the synthesis of “conjugated corrals” that consist of two diphenyl perylene diimide (PDI) and two bithiophene units arranged



in an alternating fashion (**Figure 1.3**).<sup>19</sup> With guidance from the platinum templation methods described by Bäuerle<sup>17,18</sup> and Yamago<sup>20</sup> (*vide infra*), bisplatinated diphenyl-PDI **I.16** and bithiophene **I.17** were reacted to give multinuclear platinum macrocyclic intermediate **I.18**. Reductive elimination of the platinum centers with triphenylphosphine gave the desired compound **I.2** in 8% yield over two steps. The low yield observed in this reaction sequence is likely due to the large amount of strain built into **I.2** during the last step. This is a major drawback of the Pt<sup>II</sup> templation strategy from linear precursors where yields decrease precipitously as macrocyclic strain increases.

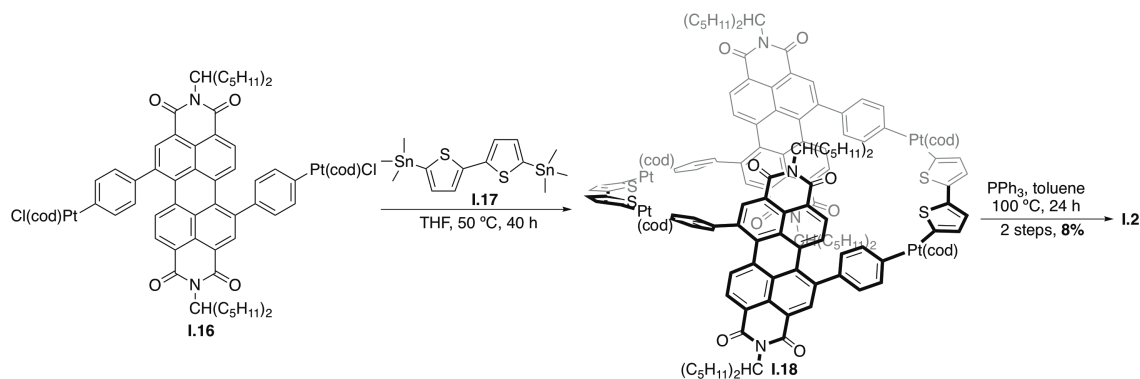


**Figure 1.3.** Synthesis of PDI containing macrocycle **I.2** using the platinum templation strategy.

The first fully conjugated porphyrin nanoring was prepared by Anderson and colleagues using an impressive wheel and spoke templation strategy in 2007.<sup>21</sup> Stirring linear octamer **I.19** with octadentate ligand **I.20** results in the formation a strong 1:1 complex between the reaction partners (**Figure 1.4**). This complex effectively wraps **I.19** around **I.20** while bringing the terminal alkynes of **I.19** together in close proximity. Treatment of this supramolecular complex with copper/palladium mediate oxidative alkyne homomcoupling conditions gave butadiyne linked porphyrin macrocycle **I.21** in 14% yield. Remarkably, this strategy produces macrocyclic products from completely linear starting materials. The template can be removed from this structure by ligand exchange with pyridine to give the free porphyrin nanoring **I.3**. Since the original synthesis, this templation strategy has been leveraged to prepare smaller and larger porphyrin nanorings with low to moderate yields (15-32%).<sup>22-26</sup>

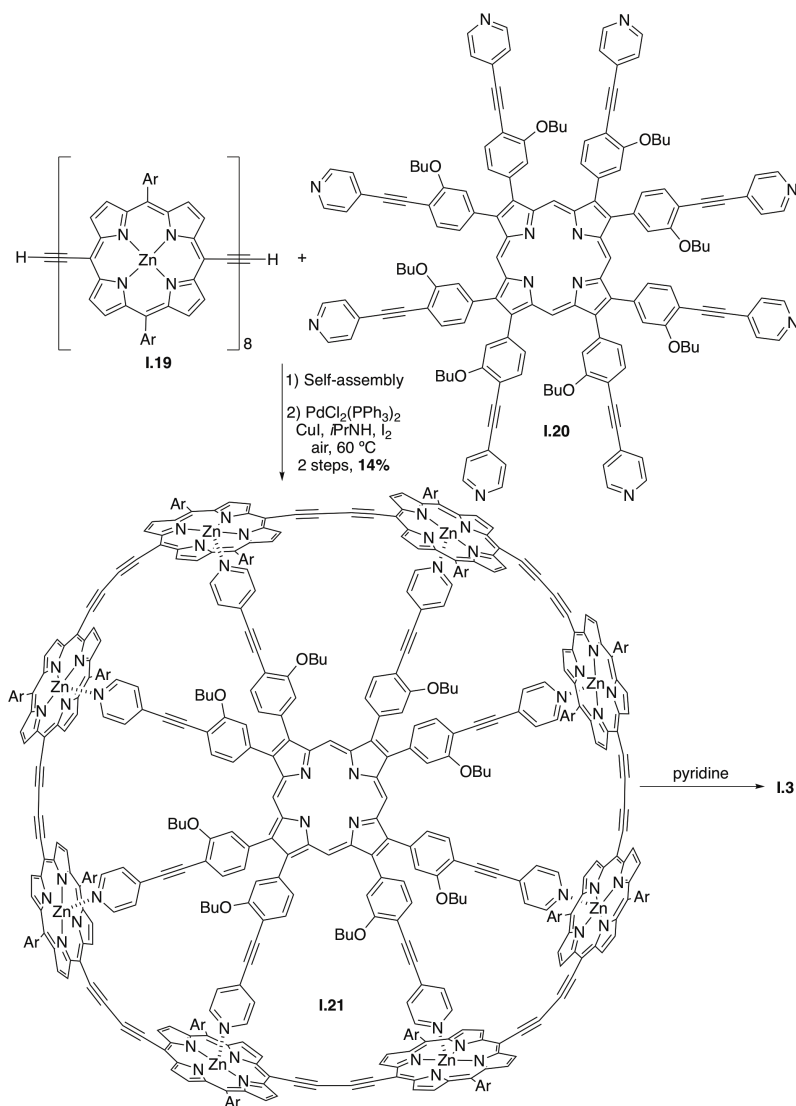


**Figure 1.4.** Templatation strategy developed by Anderson to produce porphyrin nanoring **I.3**.

Macrocyclic precursors towards the synthesis of cycloparaphenylenes ( $n$ CPPs, where  $n$  represents the number of benzene rings in the macrocycle) or nano hoops were first prepared in 2008 by Jasti and Bertozzi using a palladium catalyzed “shot-gun” synthesis of monomers **I.22** and **I.23** with dilute reaction conditions (**Figure 1.5**).<sup>27</sup> Similar to the original synthesis of  $C_n$ Ts by Bäuerle, a statistical mixture of macrocycles **I.24**, **I.25**, and **I.26** were prepared in 2%, 10% and 10% respectively with this method. The key feature of this synthetic approach is the incorporation of cyclohexadiene rings

that act as masked aromatic rings in the penultimate macrocyclic intermediate and provide curvature to linear precursors. Reductive aromatization using a single-electron reducing agent then delivered [9]CPP **I.27**, [12]CPP **I.28** and [18]CPP **I.29**. Our laboratory has since expanded upon this methodology with the preparation of macrocyclic intermediates in moderate yields (20-50%) that allow for gram scale and size selective syntheses of [5]-[12]CPP.<sup>28-33</sup> For example, the oxidative homocoupling of bisboronate **I.30** gave macrocyclic intermediate **I.31** in 50% yield and ultimately led to the synthesis of [5]CPP (**I.32**), the smallest nanohoop prepared to date.<sup>33</sup> The Itami lab has used a similar strategy to prepare nanohoops where cyclohexadienes are replaced with cyclohexane units to give macrocyclic precursors such as **I.33** in high yields (51%, **Figure 1.5**).<sup>34</sup> In contrast to the synthetic route developed in our lab, oxidative aromatization of **I.33** under acid catalysis gave **I.28** in 62% yield. Finally, the Yamago lab has developed methodology based on platinum templation strategy to give macrocyclic precursors such as **I.34** in 57% yield from linear precursors (**Figure 1.5**).<sup>20</sup> Similar to the strategies previously discussed in this section by Bäuerle and Nuckolls, reduction the platinum centers gave [8]CPP **I.4** in 49% yield.

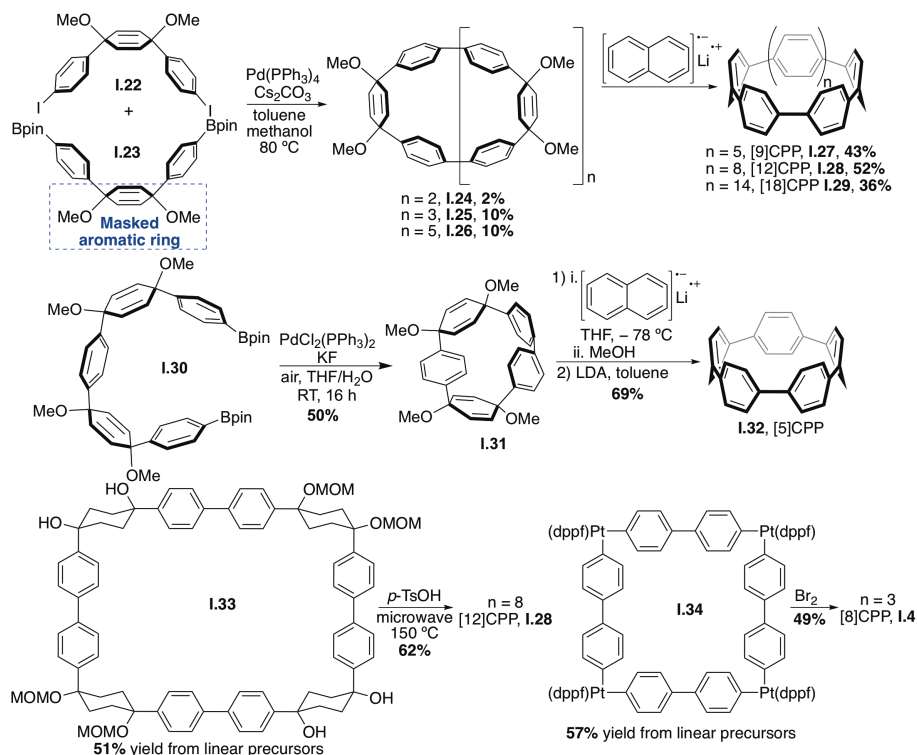


**Figure 1.5.** Synthetic methods for the preparation of  $[n]$ CPPs pioneered by Jasti, Itami and Yamago.

### 1.3. The Electronic Properties of Cyclic Oligothiophenes

Linear polyoligothiophenes are superior materials for the development of organic electronics because of their charge-transport abilities and unique optoelectronic properties that stem from their highly conjugated structure.<sup>10, 11, 18, 35</sup> However, the end groups of these polymeric systems create defects that act as trap sites for charges moving through devices fabricated from these types of materials.<sup>36</sup> Therefore,  $C_nT$  macrocycles have the potential to act as superior organic materials with infinitely conjugated  $\pi$ -systems.

After the synthetic methods developed by Bäuerle group gave access to various sizes of  $C_nT$ s, the characterization of their electronic properties provided insight on the unique effects imparted by the macrocyclic structure. **Table 1.1** summarizes the optical data and oxidation potentials for  $C_nT$ s **1.10**, **1.11**, **1.12**, **1.13**, **1.14**, **1.15** (**Figure 1.2**) and linear oligothiophene **1.35** (**Figure 1.6**).<sup>18</sup> The highly symmetric and delocalized nature of

the molecular orbitals in these molecules render the  $S_0 \rightarrow S_1$  optical transition dipole forbidden making  $S_0 \rightarrow S_2$  transitions the predominate feature in the absorption spectra for all  $C_nT$ s.<sup>37</sup> As the size of the macrocycle increases, the maximum absorption ( $\lambda_{abs}$ ) red-shifts slightly and the molar absorptivity ( $\epsilon$ ) increases. This suggests that conjugation increases as the size of the  $C_nT$  increases. In contrast, the fluorescence ( $\lambda_{em}$ ) blue shifts as the size of the ring increases with **1.10** and **1.11** having decreased fluorescence intensity as a result of increased ring strain in these smaller macrocycles. When the  $\lambda_{abs}$  and  $\epsilon$  of linear **I.35** (Figure 1.6) are compared to  $C_nT$  of the same size (**1.10**), a blue shifting and increase in  $\epsilon$  is observed respectively upon macrocycle formation. The blue shifting observed in this case is due to the fact that the absorption transitions in the two systems are different (**I.35**  $\lambda_{abs}$  is the result of a  $S_0 \rightarrow S_1$  transition) while the increase in  $\epsilon$  indicates an increase in conjugation from linear **I.35** to macrocyclic **I.10**. Interestingly, due to structural deformation in the small macrocycle **I.10**, the  $S_0 \rightarrow S_1$  becomes partially allowed resulting in a second absorption band of this  $C_nT$  at 490 nm that is significantly red-shifted when compared to linear **I.35**.<sup>37</sup>

**Table 1.1.** Optical properties of  $C_nT$ s **I.10** – **I.15** and linear analog **I.35**.

$C_nT$	$\lambda_{abs}$ (nm)	$\epsilon$ (L mol <sup>-1</sup> cm <sup>-1</sup> )	$\lambda_{em}$ (nm)	$E_{oxidation}$ (V)
<b>I.35</b>	435	51000	519	0.25
<b>I.10</b>	417	86000	685	0.03
<b>I.11</b>	423	119000	582	0.08
<b>I.12</b>	434	130000	572	0.08
<b>I.13</b>	440	163000	570	0.09
<b>I.14</b>	444	183000	568	0.16
<b>I.15</b>	445	196000	567	0.16

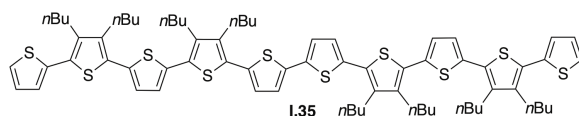


**Figure 1.6.** Linear analog **I.35** for comparison to macrocyclic  $C_nT$ s.

An increase in conjugation for these *CnTs* when compared to linear **I.35** is also evident by the ease of which these macrocycles are oxidized, measured with cyclic voltammetry (CV). *CnT I.10*, has an extremely low reversible oxidation potential that increases as the size of the macrocycle increases with the oxidation potential of **I.15** being only slightly lower than linear **I.35**. The ease at which **I.10** can be oxidized when compared to larger *CnTs* is attributed to destabilization of the HOMO as a result of the large amount of ring strain in this small macrocycle.<sup>18</sup> Preferential dimerization of radical cations is observed upon the oxidation of *CnTs* indicated by CV and mass spectrometry. In this case, dimerization is a result of the formation of favorable intermolecular  $\pi$ - $\pi$  interactions, a hallmark of conjugated materials with planar, perpendicular  $\pi$ -systems. The conjugated, planar structure also results in the formation of polaron-pair when **I.10** is oxidized to **I.10**<sup>2(+)</sup>.<sup>38</sup>

Despite the promising electronic properties exhibited by this class of conjugated macrocycles, the use of these compounds as components in organic electronics is currently limited. The non-selective, shot-gun approach used to prepare *CnTs* requires separation of six different compounds in the final step and makes derivatization of these structures challenging. Therefore, recent efforts towards the application of these molecules have been focused on  $\pi$ -expanded oligothiophenes to give functional macrocycles with properties that emulate the parent *CnTs*.<sup>10, 11, 39, 40</sup> In these derivatives, acetylenes or alkenes are inserted between thiophene units that act as flexible linkers to facilitate size selective syntheses and improve the materials properties of these molecules. This has led to the development of cyclic oligothiophenes that exhibit photoisomerism, polymorphism, large two-photon cross sections, hole transport ability and light harvesting characteristics.<sup>10, 11, 36, 41</sup>

#### 1.4. Organic Materials from PDI Containing Macrocycles

A common strategy to engineer the electronic properties of linear organic materials is through the incorporation of donor and acceptor molecules into polymeric and oligomeric structures.<sup>19, 41, 42</sup> Such materials have decreased HOMO→LUMO gaps

and increased absorption in the visible region due to intermolecular charge transfer between the donor and the acceptor units. Ultimately, these types of changes in the electronic structure of organic materials increase their hole/electron transport abilities and improve their performance in photovoltaic devices. The synthesis of macrocyclic molecules such PDI containing macrocycles provide an excellent opportunity to study the effect that the macrocyclic architecture has on the properties of organic donor-acceptor materials.

In these types of conjugated macrocycles two PDI units and two bithiophene units act as acceptor and donor motifs respectively (**Figure 1.1**). By virtue of their connectivity, some of these structures (i.e. **I.2**) are chiral and are converted between their R and S states through an achiral intermediate at room temperature.<sup>19</sup> Thus, **I.2** provides a unique opportunity to design supramolecular, chiral recognition materials, although the application of **I.2** in this way has yet to be realized.

As expected, optical characterization of **I.2** shows advantageous properties as a result of its donor-acceptor components and macrocyclic architecture. First, the absorption spectrum shows multiple peaks corresponding to thiophene→thiophene, PDI→PDI and thiophene→PDI intramolecular charge transfer transitions resulting in an overall broad absorption that covers almost the entire visible spectrum.<sup>19</sup> The major absorption that occurs at approximately 397 nm is a result of a  $S_0 \rightarrow S_2$  transition, similar to the major transitions observed for the cyclic oligothiophenes.<sup>43</sup> When compared to the linear **I.36** and **I.17**, the absorption of **I.2** is more red-shifted because of increased conjugation in the macrocyclic system (**Figure 1.7**). A similar trend is observed when comparing the absorption characteristics of **I.2** to linear donor-acceptor fragments (**I.37** and **I.38**) and polymers (**I.39**).<sup>44</sup>

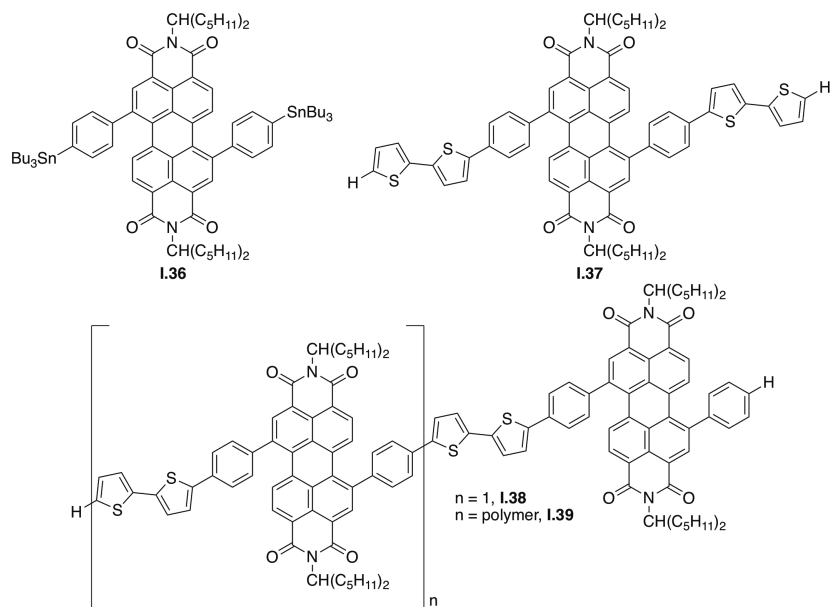


**Figure 1.7.** Linear analogs **I.36**, **I.37**, **I.38** and **I.39** for comparison to conjugated macrocycle **I.2**.

In order to determine the effect that macrocyclic structure has on the performance of donor acceptor materials as organic photovoltaic (OPV) materials, **I.2**, **I.37**, **I.38** and **I.39** were fabricated into devices. Overall, the photocurrent generation in **I.2** outperformed all of the acyclic structures because of the smaller HOMO→LUMO gap, higher hole mobility and better film morphology of the macrocyclic system.<sup>44</sup> For example, linear **I.37** and **I.38** self-aggregate in thin films to give large domains of phase segregation where carrier recombination can occur resulting poor device performance. Conversely, the contorted macrocyclic structure of **I.2** prevents aggregation to give more uniform films and smaller domains.

The seminal studies on the performance of PDI containing macrocycles as new types of organic materials have highlighted the enormous potential that conjugated macrocyclic have in this field. The tunable nature of these compounds have enabled the synthesis derivatives of **I.2** that act as superior organic photodetectors<sup>45</sup> or giant PDI contain macrocycles that are molecularly flexible transport materials.<sup>46</sup> Recently, halogenated derivatives showed self-assembly on surfaces where the macrocyclic pore



enables this derivatives to act as an organic semiconductor gas sensors and nanoreactors.<sup>47</sup>

### 1.5. Porphyrin Nanorings as Synthetic Light Harvesting Systems

In nature, systems with infinitely delocalized excited states and ultra-fast energy migration act as light harvesting systems during photosynthesis.<sup>8,9</sup> Synthetic compounds that mimic the harvesting abilities of natural systems are of great interest because of their potential to act as superior light absorbing components in solar cells. As such, organic semiconductors designed for photovoltaic devices that absorb large amounts of visible light and exhibit charge separation after absorption of light are promising in this context.<sup>48,49</sup> Unfortunately, the majority of these compounds have localized excitation states or exhibit decoupling of delocalized chromophores as a result of vibrations and distortions of the molecular system.<sup>49</sup> Porphyrin nanorings present themselves as alternatives to traditional organic light harvesting systems as a result of their rigid, conjugated and macrocyclic structure.

Since the seminal synthesis of **I.3** by the Anderson group, the preparation of smaller and larger nanorings have enabled the study of the size-dependent properties of this class of conjugated macrocycles.<sup>22-26</sup> In particular, studies of the electrochemical and photophysical properties of **I.40** and its templated analog **I.41** highlight the advantages that porphyrin nanorings have over their linear analogs (**Figure 1.8**).<sup>50</sup> Electrochemical measurements show that **I.41** has a smaller HOMO→LUMO gap when compared to infinite polymer **I.43** indicating that **I.41** is more conjugated than the polymer. Interestingly, when template **I.42** is removed to give free nanoring **I.40** the HOMO→LUMO gap increases implying that the increased electronic coupling in **I.41** is a result of the distorted macrocyclic structure of the porphyrin nanoring and the rigid geometry enforced by template **I.42**. This is supported further by the photophysical properties of the porphyrin nanorings where the major absorbance red-shifts from linear **I.44** to **I.40** and is even further red-shifted for rigid **I.41**. In accordance with the conjugated macrocycles **I.1** and **I.2** discussed in this chapter, the major absorbance of

macrocycles **I.40** and **I.41** are a result of  $S_0 \rightarrow S_2$  transitions because of the symmetrical nature of their molecular orbitals.<sup>50</sup>

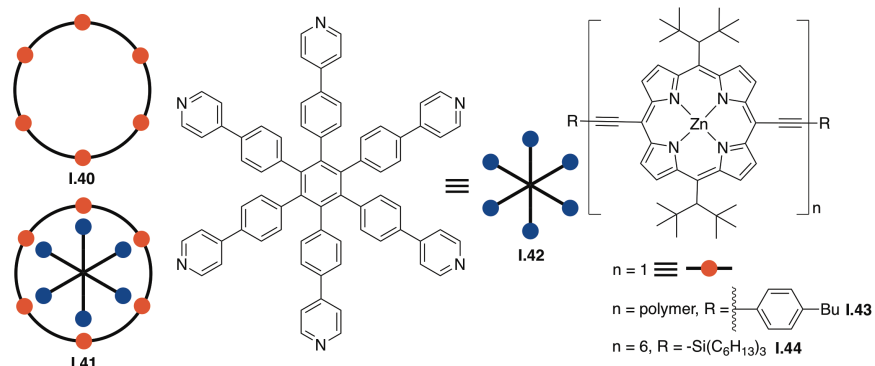


**Figure 1.8.** Structures of porphyrin nanoring **I.40**, templated nanoring **I.41**, template **I.42** and linear analogs **I.43** and **I.44** for comparison to the macrocyclic compounds.

After excitation of **I.40** and **I.41** Herberg – Teller coupling enables intensity sharing between the  $S_2$  and  $S_1$  excited states to give a fluorescence emission of these macrocycles from  $S_1 \rightarrow S_0$  radiation.<sup>50</sup> The emission of **I.40** and **I.41** extends into NIR region (800 – 1300 nm) while linear **I.44** has a broad emission from 750 – 1100 nm. Again, because of its rigid structure, **I.41** has a more red-shifted emission accompanied by a decrease in fluorescence quantum yield (QY). The effect that rigidity has on the QY is also manifested in the macrocyclic structure of **I.40** where the QY decreases from 8% to 0.79% for **I.44** and **I.40** respectively. Finally, fluorescence decay times indicate that the emissive  $S_1$  excited state is delocalized across the entire nanoring of **I.40** and **I.41** in contrast to many linear and macrocyclic conjugated compounds that have localized emissive excited states.

The electronic properties described here have been expanded to derivatives of porphyrin nanorings with thermally enhanced emission, “Russian doll” complexes that exhibit delocalization across multiple nanorings<sup>51</sup> and smaller ethylene linked nanorings with red-shifted absorbance, fluorescence and stronger electronic coupling.<sup>26</sup> Interestingly, the acetylene linkage between the porphyrin nanorings in these systems is essential as directly linked porphyrin macrocycles have optical properties that are almost identical to linear, monomeric porphyrin units.<sup>52</sup> The advantageous photophysical

properties of porphyrin nanorings make this class of molecules ideal synthetic analogs of natural light harvesting systems.<sup>49</sup>

## 1.6. The Unique Optical Properties of Cycloparaphenylenes

Oligomeric carbon based nanomaterials such as carbon nanotubes (CNTs) and graphene have emerged as powerful organic materials with a variety of different applications from components in organic electronics to imaging agents in live animals.<sup>53, 54</sup> However, the lack of synthetic methods to prepare and functionalize these materials in a precise fashion limits their potential because of molecular inhomogeneity introduced during their preparation. Cycloparaphenylenes ( $[n]$ CPPs), termed nanohoops because of their structural relationship to CNTs, present themselves as alternatives to these materials because they are prepared in a molecularly precise fashion. Additionally, the cyclic structure of the hoop provides yet another opportunity to prepare conjugated macrocycles with desirable electronic properties.

The size-dependent electronic properties of nanohoops have recently been reviewed in detail revealing subtle structural effects that result in electrochemical and photophysical properties that are unique to this class of molecules.<sup>12, 55, 56</sup> Briefly, computationally predicted (B3LYP/6-31G(d)) HOMO→LUMO gaps for  $[5]$ – $[12]$ CPP (**I.32**, **I.45**, **I.46**, **I.4**, **I.27**, **I.47**, **I.48**, **I.28**) show that as the size of the nanohoop decreases the HOMO→LUMO gap decreases (**Figure 1.9**).<sup>55</sup> This is in stark contrast to linear p-phenylene oligomers (**I.49**) where HOMO→LUMO gaps decrease as the number of phenyl ring increase because of increased conjugation. As summarized in **Table I.2**, this results in smaller nanohoops that are easier to oxidize electrochemically, similar to the trend observed with  $C_n$ Ts.

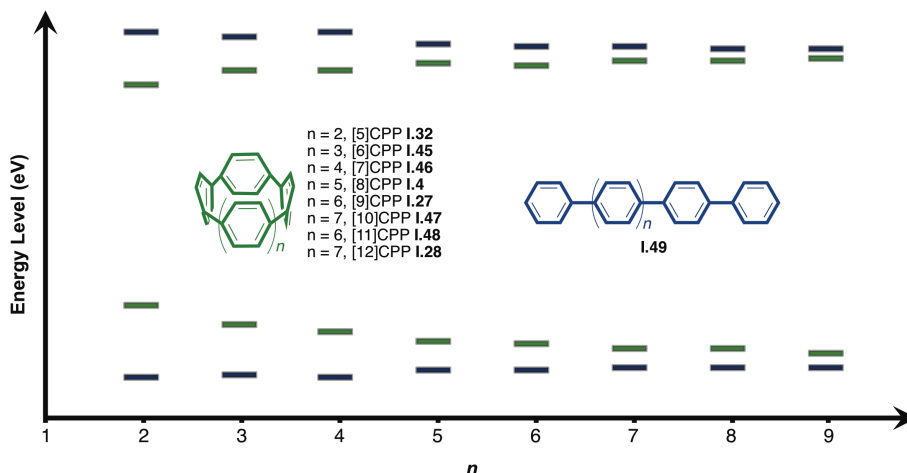


**Figure 1.9.** HOMO→LUMO gaps of [n]CPPs **I.32**, **I.44**, **I.45**, **I.4**, **I.27**, **I.47**, **I.48** and **I.28** compared to their linear p-oligophenylene counterparts (**I.49**).

In line with all of the conjugated macrocycles discussed here, the symmetric nature of these molecules results in forbidden  $S_0 \rightarrow S_1$  transitions in all nanohoops. Instead, all of these molecules share a common major absorption that is a result of HOMO→LUMO+1, HOMO→LUMO+2, HOMO→1-LUMO or HOMO→2-LUMO transitions between 335–340 nm with large  $\epsilon$  values, highlighting the increased conjugation in these macrocyclic systems (**Table I.2**).<sup>57</sup> Structural deformation of the smaller nanohoops results in  $S_0 \rightarrow S_1$  transitions that become slightly allowed, as observed in smaller  $C_n$ Ts. Finally, as the size of the hoop decreases, the fluorescence emission red-shifts coupled with a decrease in QY where **I.32** and **I.45** are no longer fluorescent. Unlike porphyrin nanorings, relaxation of the excited state to an  $S_1'$  state results in a localized emissive state for **I.46**, **I.4**, **I.27**, **I.47**, **I.48** and **I.28**. As the size of the nanohoop decreases, the rigidity of the smaller nanohoops results in a  $S_1'$  excited state that is delocalized across the entire molecule. This results in a  $S_1' \rightarrow S_0$  transition that is forbidden, decreasing emission from the excited state, accounting for the decrease of QY and lack of fluorescence in **I.32** and **I.45**.<sup>57</sup> Together, the absorption and emission of the nanohoop results in large effective Stokes shifts for all sizes (**Table I.2**).

**Table 1.2.** A summary of the electronic properties of [*n*]CPPs.

[ <i>n</i> ]CPP	$\lambda_{\text{abs}}$ (nm)	$\lambda_{\text{em}}$ (nm)	Stokes shift ( $\lambda_{\text{abs}} - \lambda_{\text{em}}$ , nm)	$\epsilon$ (L mol <sup>-1</sup> cm <sup>-1</sup> )	E <sub>oxidation</sub> (V)
<b>I.32</b>	335	--	--	57000	0.25
<b>I.45</b>	340	--	--	--	0.44
<b>I.46</b>	340	587	247	69000	0.55
<b>I.4</b>	340	533	193	110000	0.59
<b>I.27</b>	340	494	154	120000	0.70
<b>I.47</b>	338	466	128	130000	0.74
<b>I.48</b>	340	458	118	130000	0.83
<b>I.28</b>	339	450	111	140000	0.85

The unique properties afforded by the radially oriented  $\pi$ -systems of nanohoops make this class of molecules attractive for a variety of applications. Specifically, the size dependent optical properties and small HOMO→LUMO gaps make nanohoops appealing targets for the development of novel organic materials.<sup>58</sup> Modification of the nanohoop backbone further tunes this gap highlighting the advantage of their selective, building block synthesis.<sup>59-61</sup> Additionally, large  $\epsilon$  and Stokes shifts make these compounds promising materials for imaging applications.

## 1.7. Conclusion

Just as nature has evolved to develop synthetic tools that provide access to macrocyclic structures with vital function, chemists can invent methodologies to prepare compounds with desirable electronic properties. Conjugated macrocycles offer an unique opportunity to develop new organic materials because their cyclic structure provides compounds with small HOMO→LUMO gaps as a result of increased conjugation and strain. This results in molecules with optical and transport properties that are superior to their oligomeric and polymeric linear counterparts. Importantly, in each case the macrocycles discussed here provide valuable insight into the different structural components that result in their desirable electronic properties. New types of macrocyclic

compounds that combine all of these strategies offer a bright future for the development of novel types of organic materials.

### **I.8. Bridge to Chapter II**

This chapter highlights the unique electronic properties observed in conjugated macrocycles because of the cyclic structure of these molecules. Our ability to develop these types of materials and study their structural property relationship is limited by the synthetic methods available to prepare them. Therefore, reactions that provide efficient routes towards macrocyclic compounds will expand our understanding of this class of molecules. The next chapter discusses the development of an efficient and scalable macrocyclization strategy to provide access to conjugated macrocycles and macrocyclic natural products.

## CHAPTER II

### THE FORMAL SYNTHESIS OF ACEROGENIN E VIA OXIDATIVE HOMOCOUPLING

Adapted with permission from Darzi, E. R.; White, B. W.; Loventhal, L. K.; Zakharov, L. N.; Jasti, R. An operationally simple and mild oxidative homocoupling of aryl boronic esters to access conformationally constrained macrocycles. *J. Am. Chem. Soc.* **2017**, *139*, 3106-3114. Copyright 2017 American Chemical Society. The excerpt included was written by myself with assistance from Dr. Evan R. Darzi. The experimental work included from the published material was performed by myself with assistance from Dr. Evan R. Darzi. Dr. Lev N. Zakharov provided crystal structure analysis of the final product discussed in the experimental section. Professor Ramesh Jasti provided editorially assistance.

Constrained macrocyclic scaffolds are recognized as challenging synthetic motifs with few general macrocyclization methods capable of accessing these types of systems. Although palladium catalyzed oxidative homocoupling of aryl boronic acids and esters to biphenyls has been recognized as a common byproduct in Suzuki–Miyaura cross-couplings for decades, this reactivity has not been leveraged for the synthesis of challenging molecules. We recently reported an oxidative boronic ester homocoupling reaction as a mild method for the synthesis of strained and conformationally restricted macrocycles including strained polyphenylene macrocycles and strained cycloalkynes. Here we expand the substrate scope of this reaction with the formal synthesis of Acerogenin E. Higher yields and better efficiencies are observed for the intramolecular macrocyclization step when directly compared to the analogous intramolecular Suzuki–Miyaura cross-coupling. Notably, this oxidative homocoupling reaction is performed at room temperature, open to atmosphere, and without the need to rigorously exclude water, thus representing an operationally simple alternative to traditional cross-coupling macrocyclizations. The conformationally restricted nature of the advanced intermediate en route to Acerogenin E is also investigated with variable temperature (VT) <sup>1</sup>H NMR.

## 2.1. Introduction

Macrocyclic molecules are widely recognized as useful structural motifs across disciplines including materials science,<sup>1-4</sup> medicinal chemistry,<sup>5-6</sup> and supramolecular chemistry.<sup>7-14</sup> Synthetic methods towards efficient macrocycle formation, however, remain a challenge and often represent the limiting step in a synthetic sequence. This limitation becomes increasingly apparent when the desired macrocycle is sterically congested, conformationally restricted, or distorted from ideal geometry. Examples of challenging biaryl containing macrocycles range from natural products such as haouamine A<sup>15, 16</sup> or vancomycin<sup>17-20</sup> to the “bent and battered” benzene rings found in cyclophanes.<sup>21</sup> Moreover, the strain and conformational restriction imparted by the macrocyclic motif is often directly responsible for the desirable properties of these molecules.

Constrained macrocycles have served as motivation for developing methodology utilizing mild transition metal catalyzed conditions, such as Suzuki-Miyaura cross-coupling, to construct these challenging systems. In 2014, our lab prepared macrocycle **II.2** as a key intermediate towards the synthesis and characterization of [5]CPP, a highly strained molecular fragment of C<sub>60</sub> (118 kcal/mol of strain energy), using a palladium catalyzed homocoupling of diboronic ester **II.1** (**Figure 2.1a**).<sup>22</sup> This palladium catalyzed reaction was found to operate efficiently at room temperature and open to air. Although the oxidative homocoupling process has long been appreciated as a side product in Suzuki-Miyaura cross-coupling reactions, only few studies have been devoted to exploring this reaction in the context of complex molecule synthesis.<sup>23-25</sup> Recently, we provided a detailed study of this oxidative aryl-aryl bond forming reaction and used this information to optimize the reaction conditions (**Figure 2.1b**).<sup>26</sup> We expanded the substrate scope of this reaction through the preparation of a variety of highly strained macrocycles such as a *p*-quaterphenyl containing macrocycle **II.3** and strained alkyne **II.4** (**Figure 2.1c**). Interestingly, our mechanistic studies also suggested that the reaction is efficiently catalyzed with palladium nanoparticles. To established this reaction as an operationally simple alternative to traditional cross-coupling reactions, we aimed to



further demonstrate its generality with the preparation of **II.5** for the formal synthesis of Acerogenin E. Herein, the detailed synthetic steps towards the synthesis of biaryl containing macrocycle **II.5** are described. The conformationally restricted nature of **II.5** is explored with variable temperature nuclear magnetic resonance (VT-NMR) spectroscopy. This study demonstrates the oxidative homocoupling of boronic esters as a general strategy for the preparation of conformationally restricted and strained natural products.

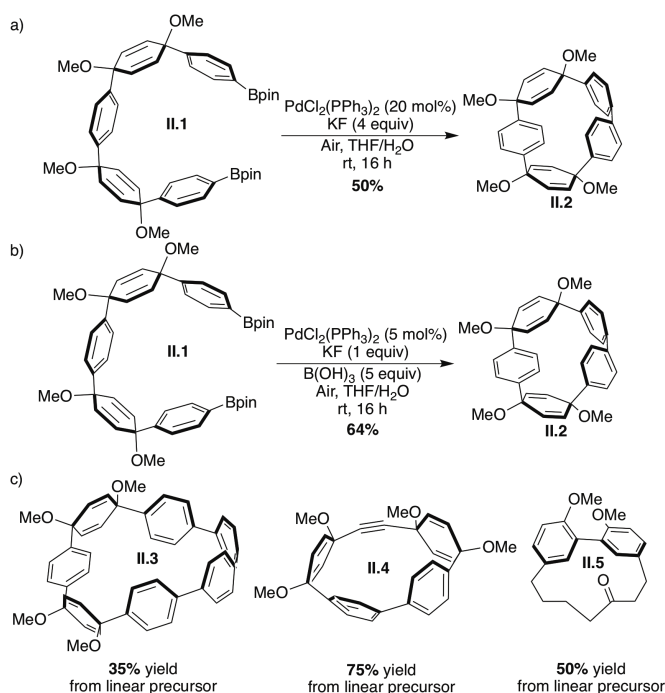


**Figure 2.1.** a) The original oxidative homocoupling reaction conditions. b) Our optimized conditions. c) The substrate scope of the oxidative homocoupling.

## 2.2. Results and Discussion

### 2.2.1. Natural Product Acerogenin E

Acerogenin E (**II.7**, **Figure 2.2**) is a naturally occurring compound that has been isolated from *Acer nikoense* MAXIM stem bark.<sup>27, 28</sup> Pharmacological studies of **II.7** and related structures have revealed the anti-inflammatory, anti-tumor, anti-obesity and anti-oxidative properties of these molecules prompting investigations into the total synthesis of this compound.<sup>29</sup> The macrocyclic architecture of **II.7** is expected to limit its

conformational freedom, an effect that undoubtedly impacts its biological activity. Unfortunately, the synthesis of molecules such as **II.7** is difficult because of the inherent challenges associated with macrocycle formation from a linear precursors. This makes the impact that conformation restriction has on the bioactivity of molecules such as **II.7** poorly understood.<sup>5, 29-31</sup>

When we began this study, the only reported synthesis of **II.7** utilized in situ monoborylation followed by intramolecular Suzuki coupling of diiodide **II.6** to give Acerogenin E precursor **II.5** in 34% yield (**Figure 2.2**). Deprotection of the methyl ethers in **II.5** with boron tribromide ultimately gave **II.7** nearly quantitatively.<sup>29</sup> The intramolecular palladium catalyzed step of the reaction sequence suggested that the macrocyclization could be amenable to the oxidative homocoupling conditions developed in our lab.

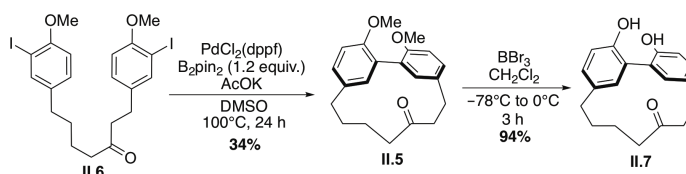


**Figure 2.2.** The reported total synthesis of Acerogenin E (**II.7**).

Homodesmotic reaction calculations (B3LYP/6-31d\*) of **II.5** revealed that this macrocycle has a small amount of strain energy (4 kcal/mol) when compared to highly strained molecules previously prepared with our method (for example **II.3** has 41 kcal/mol of strain energy). The strain of **II.5** is spread out over 19 carbons to give a total of 0.21 kcal/mol of strain energy per carbon. However, the connectivity of **II.5** results in a biaryl system that is nearly planar, in stark contrast to nanohoop precursors **II.3** and **II.4** (**Figure 2.3**). The planarity of the  $\pi$ -systems suggests that the majority of this strain resides on the  $\text{sp}^3$  positions of the macrocycle and may result in conformational restriction along the alkyl chain.

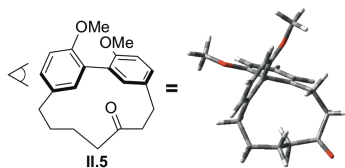


**Figure 2.3.** The minimized structure of **II.5** and a view of its planar  $\pi$ -system down the aryl-aryl bond.

Synthesis of **II.5** with our optimized conditions would act as a proof-of-principle that the oxidative homocoupling of aryl boronic esters is a general route towards the formation of biaryl macrocycles. Access to large quantities of **II.5** could enable studies into the conformational restriction of the macrocycle and its natural product analog **II.7**. This study will also allow us to compare our oxidative homocoupling conditions with traditional intramolecular Suzuki cross-coupling methods reported in the literature. Finally, preparation of **II.5** with our optimized conditions will expand the scope of this reaction to include constrained macrocycles beyond the highly strained precursors utilized for nanohoop synthesis.

### 2.2.2 Oxidative Homocoupling for the Formal Synthesis of Acerogenin E

The preparation of **II.5** with our optimized homocoupling conditions required first the synthesis of advanced intermediate diboronate **II.8** (**Figure 2.4**). With guidance from the seminal synthesis of **II.5**,<sup>29</sup> we sought to access **II.8** through Miyaura borylation of diiodide **II.6**. However, under these conditions we only ever isolated a mixture of borylated products and starting material **II.6**. In addition, **II.6** was not bench stable and appeared to decompose over time resulting in the loss of material. To circumvent these issues, we next aimed to install the boronate functionality directly from starting material **II.9** using ortho-metalation (**Figure 2.4**). After protection of the ketone in **II.9** with ethylene glycol, reaction of **II.10** with tert-butyllithium followed by addition of a boronic acid pinacol ester electrophile gave the desired borylated product **II.11** in 34% yield.<sup>32</sup>

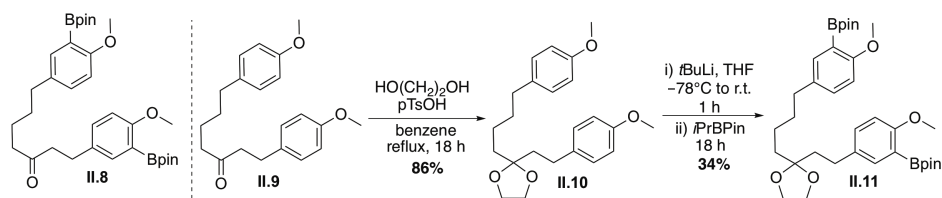


**Figure 2.4.** Ortho-metalation as a strategy to install aryl boronic acid pinacol ester functionality.

While this synthetic route provided access to an advanced intermediate towards desired product, it was difficult to reproduce the moderate yield of this reaction on large scale. Analysis of the crude reaction mixture revealed a considerable amount of recovered starting material (**II.10**) and apparent decomposition of **II.10** and **II.11**, evident by the appearance of new peaks in the alkyl region of the  $^1\text{H}$  NMR. These results led us to consider a decomposition pathway where the acetal protecting group of **II.10** and **II.11** also act as a directing group to promote deprotonation of the alkyl protons in these molecules.<sup>33</sup> This decomposition mechanism would also result in the recovery of **II.10** as tert-butyllithium is consumed through deprotonation, consistent with our crude reaction mixture.

To avoid this deleterious pathway we increased the reactivity of the protons in the ortho-position of **II.11** through complexation with  $\text{Cr}(\text{CO})_6$  (**Figure 2.5**).<sup>34, 35</sup> The strong electron withdrawing nature of the  $\text{Cr}(\text{CO})_3$  functional group pulls electron density away from the aromatic ring to increase the acidity of the aryl protons and favor deprotonation at the ortho-position. Thus, deprotonation of the resulting chromium complex (**II.12**) with a more mild reagent at  $-78^\circ\text{C}$ , followed by treatment with an electrophilic boron source and decomplexation of chromium with manganese oxide, gave dibornate **II.11** in 47% yield in gram-scale quantities. Deprotection of the ketone followed by reprotection of the boronate with pinacol finally gave the desired product **II.8** in 93% yield. With gram quantities of dibornate **II.8** in hand, we prepared macrocycle **II.5** in 50% yield after stirring **II.8** at room temperature and open to air for 2 hours with our optimized conditions. The structure of **II.5** was determined by x-ray crystallography confirming its distorted macrocyclic structure.

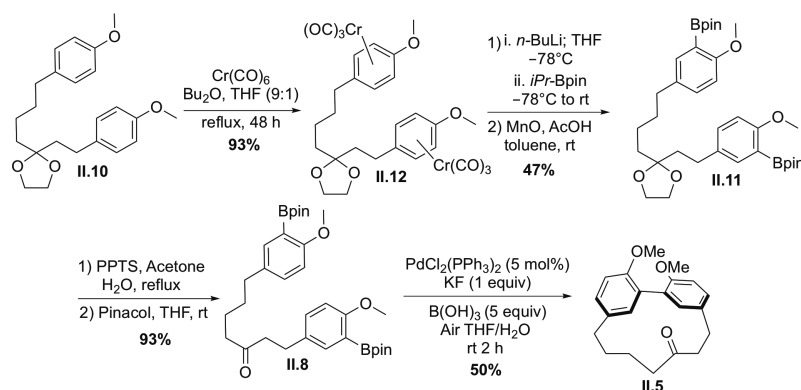


**Figure 2.5.** Our optimized reaction sequence for the preparation of **II.8** and its oxidative homocoupling to give **II.5**.

### 2.2.3. Variable Temperature $^1\text{H}$ NMR

While **II.5** is significantly less strained than the nanohoop precursors previously prepared with this method, its behavior in solution alluded to the conformationally restricted nature of this molecule. At room temperature (25 °C), the peaks associated with hydrogens attached to  $\text{sp}^3$  carbons in the alkyl bridge of **II.5** are broad (**Figure 2.6**). This indicates that these protons are populating multiple conformations that are slowly interconverting on the NMR timescale as a result of limited rotation about  $\text{sp}^3$  carbons throughout the alkyl chain. In addition, some peaks integrate to only one proton suggesting that hydrogens attached to the same carbon are in different electronic environments as a result of restricted nature of the macrocycle. Proton-carbon HSQC of **II.5** confirmed this as most of the alkyl carbons are correlated with two different proton signals (**Figure 2.7**). The aromatic region of the  $^1\text{H}$  NMR of **II.5** at room temperature shows different peaks for each unique proton with no indication of restricted rotation about the aryl-aryl bond.

To further elucidate the conformational restriction of **II.5**, we analyzed the structure using VT- $^1\text{H}$  NMR. **Figure 2.6** shows the  $^1\text{H}$  NMR spectra for **II.5** at 0 °C, 10 °C, 25 °C, 40 °C, 50 °C, 60 °C, 70 °C and 78 °C. The alkyl proton peaks are assigned to hydrogens on the aliphatic bridge of **II.5** as indicated by colored squares at 0 °C and 78 °C. As rotation is restricted even further by cooling to 0 °C, the alkyl proton peaks become more resolved indicating that the macrocycle has begun to populate one

conformation. Conversely, as the temperature is increased to 78 °C these peaks coalesce consistent with increased rotation about  $sp^3$  carbons throughout the alkyl chain that is fast on the NMR time scale. The increased rotation results in protons becoming equivalent to give one peak for hydrogens attached to the same  $sp^3$  carbon. The aromatic region remains mostly unchanged with only the protons ortho of the methoxy group separating further and coalescing to one peak at low and high temperatures respectively. These findings are consistent with our analysis of the minimized structure where the majority of the strain in **II.5** resides on the alkyl chain.

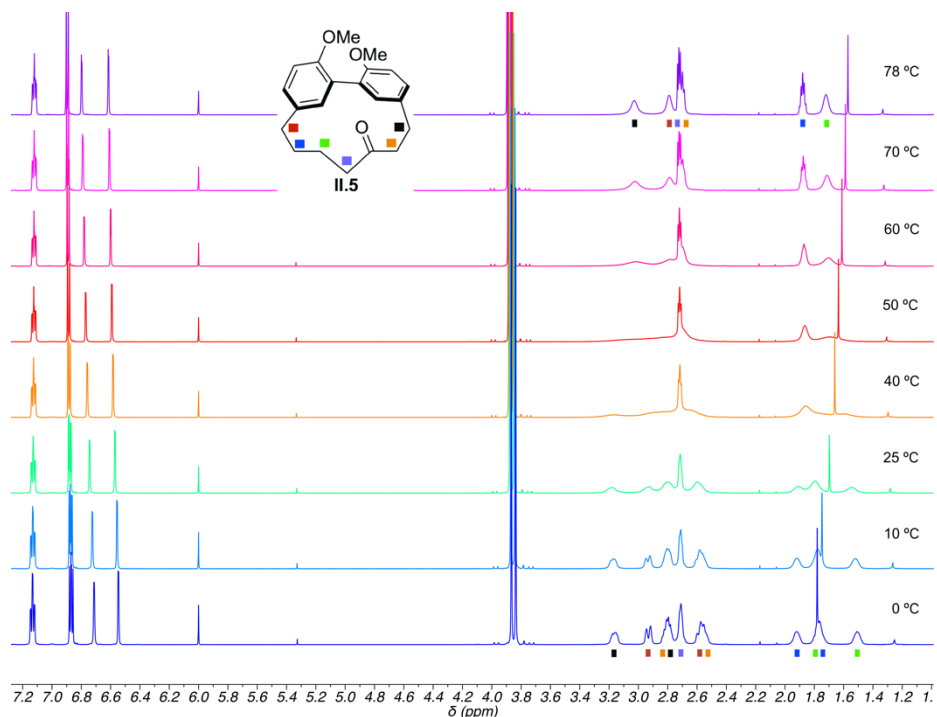


**Figure 2.6.** VT- $^1\text{H}$  NMR of **II.5**. Peaks are assigned to hydrogens in **II.5** as indicated by the colored squares at 0 °C and 78 °C

### 2.3. Conclusion

The oxidative homocoupling of aryl boronic esters is an efficient method to prepare conformationally restricted macrocycle **II.5**. When compared to traditional intramolecular Suzuki-Miyaura cross-coupling conditions previously reported to prepare **II.5**, our conditions are more mild and scalable. This enabled us to prepare **II.5** efficiently and analyze its conformationally restricted macrocyclic structure with x-ray

crystallography and VT-<sup>1</sup>H NMR. This study acts as proof-of-principle to show that our optimized homocoupling reaction provides a general route towards the synthesis of macrocyclic biaryl containing natural products. Access to such structures on scale should facilitate the study of this class of molecules and expand our understanding on the unique structural-property relationship of macrocyclic natural products.

## 2.4. Experimental Sections

### 2.4.1. General Experimental Details

Moisture sensitive reactions were carried out under an inert atmosphere of nitrogen using standard Schlenk technique. <sup>1</sup>H NMR spectra were recorded at 400 MHz, 500 MHz, or 600 MHz on a (400 MHz or 500 MHz) Varian VNMR spectrometer or at 600 MHz on a Bruker Avance-III-HD NMR spectrometer. <sup>13</sup>C NMR spectra were recorded at 100 MHz or 125 MHz on a Varian VNMR Spectrometer or at 150 MHz on a Bruker Avance-III-HD NMR spectrometer. All <sup>1</sup>H NMR spectra were taken in CDCl<sub>3</sub> (referenced to TMS, δ 0.00 ppm) or 1,1,2,2-Tetrachloroethane *d*<sub>2</sub> (referenced to residual C<sub>2</sub>H<sub>2</sub>Cl<sub>4</sub>, δ 6.00 ppm). All <sup>13</sup>C NMR spectra were taken in CDCl<sub>3</sub> (referenced to chloroform, δ 77.16 ppm) or acetone-*d*<sub>6</sub> (referenced to acetone, δ 29.84 ppm).

THF, dichloromethane, and DMF were dried by filtration through alumina according to the methods described by Grubbs.<sup>36</sup> All homocoupling reactions were done with THF filtered through alumina. Silica column chromatography was conducted with Zeochem Zeoprep 60 Eco 40-63 μm silica gel. Thin Layer Chromatography (TLC) was performed using Sorbent Technologies Silica Gel XHT TLC plates. Developed plates were visualized using UV light at wavelengths of 254 and 265 nm. All glassware was oven or flame dried and cooled under an inert atmosphere of nitrogen unless otherwise noted. IR spectra were recorded on a Thermo Nicolet 6700 FT-IR. Recycling gel permeation chromatography (GPC) was performed using a Japan Analytical Industry LC-9101 preparative HPLC with JAIGEL-1H/JAIGEL-2H columns in series using CHCl<sub>3</sub>. Automated flash chromatography was performed using a Biotage Isolera One.

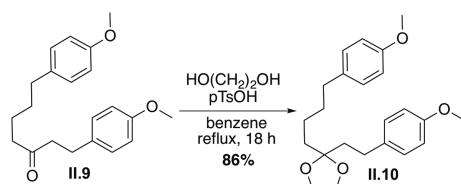
Diffraction intensities for **II.5** were collected at 173 K on a Bruker Apex2 CCD diffractometer using CuKα radiations, 1.54178 Å. The space group was determined

based on systematic absences. Absorption corrections were applied by SADABS.<sup>37</sup> Structures were solved by direct methods and Fourier techniques and refined on  $F^2$  using full matrix least-squares procedures. All non-H atoms were refined with anisotropic thermal parameters. All H atoms were refined in calculated positions in a rigid group model. Diffraction data for **II.5** were collected up to  $2\theta_{\max} = 135^\circ$ , but only reflection with  $2\theta_{\max} = 115^\circ$  have been used in the final refinement due to very weak reflections at the high angles. The bridge  $-(\text{CH}_2)_4\text{-C(=O)-}(\text{CH}_2)_2\text{-}$  chain in **II.5** is disordered over two positions. Our evaluation shown that contribution of the second position is less than 10% and it was taken into consideration in the final refinement. All calculations were performed by the Bruker SHELXL-2013 package.<sup>38</sup>

Compounds **II.6** and **II.9** were prepared in accordance with previously reported procedures and all spectra matched previously reported.<sup>29</sup> All reagents were obtained commercially unless otherwise noted.

All calculations were carried out with Gaussian 09 package at B3LYP/6-31g\* level of theory.<sup>39</sup> Geometries were optimized in the gas phase. The fully optimized structures were confirmed to be true minima by vibrational analysis. Structures were minimized with no symmetry restrictions.

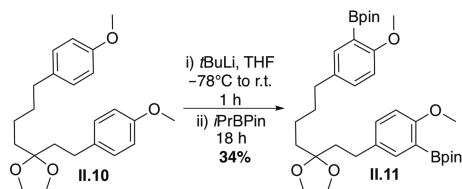
#### 2.4.2. Synthetic Details



1,7-Bis-(4-methoxyphenyl)-heptane-3-one **II.9** (6.00 g, 18.4 mmol, 1.00 equiv) was stirred with p-toluene sulfonic acid monohydrate (670 mg 3.68 mmol, 0.200 equiv) and distilled ethylene glycol (1.50 mL, 27.6 mmol, 1.50 equiv) in benzene (80.0 mL) in a flask attached to a Dean-Stark apparatus. The reaction mixture was stirred under reflux for 18 hours then cooled to room temperature and quenched with saturated sodium bicarbonate. The resulting organic layer was separated and dried over sodium sulfate to give a light brown oil. The crude reaction mixture was purified via column

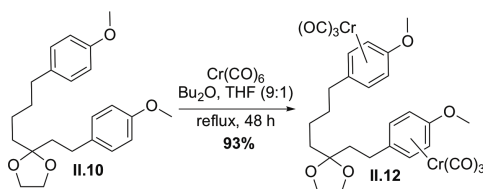


chromatography (5-30% ethyl acetate/hexanes) to give the product **II.10** as a white solid after crystallization from hexanes (5.70 g, 86%). mp 44-45 °C. <sup>1</sup>H NMR (600 MHz, CDCl<sub>3</sub>): δ 7.09 (d, *J* = 8.7 Hz, 2H), 7.09 (d, *J* = 8.6 Hz, 2H), 6.82 (d, *J* = 8.7 Hz, 2H), 6.82 (d, *J* = 8.6 Hz, 2H), 3.96 (s, 4H), 3.78 (s, 3H), 3.78 (s, 3H), 2.60 (m, 2H), 2.55 (t, *J* = 7.7 Hz, 2H), 1.88 (m, 2H), 1.42 (m, 2H), 1.59 (m, 2H), 1.67 (m, 2H); <sup>13</sup>C NMR (150 MHz, CDCl<sub>3</sub>): δ 157.85, 157.78, 134.83, 134.45, 129.38, 129.31, 113.98, 113.84, 111.51, 65.18, 55.42, 55.40, 39.40, 37.35, 35.12, 32.16, 29.27, 23.72; HRMS (TOF, ES+) (*m/z*): [M+Na]<sup>+</sup> calculated for C<sub>23</sub>H<sub>30</sub>O<sub>4</sub>, 393.2042; found: 393.2034. IR (neat): 2940, 2909, 2864, 1611, 1607, 1511, 1464, 1376, 1301, 1255, 1241, 1179, 1172, 1134, 1127, 1062, 1029, 950, 905, 901, 829, 815, 778, 750, 674, 647, 647, 614, 557 cm<sup>-1</sup>.



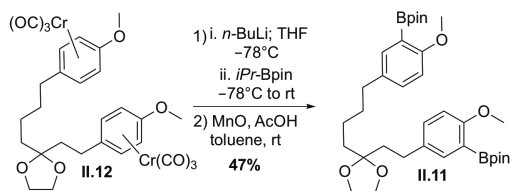
1,7-Bis-(4-methoxyphenyl)-heptane-3-[1,3]dioxolane **II.10** (250 mg, 0.695 mmol, 1.00 equiv) was dissolved in THF (35 mL) and cooled to -78 °C for 30 min. Tert-butyl lithium (1.7 M in hexanes, 2.90 mL, 4.85 mmol, 7.00 equiv) was then added dropwise to the cooled reaction mixture and stirred at this temperature for 30 min. The resulting yellow reaction solution was warmed to room temperature and stirred for 18 hours. 2-Isopropoxy-4,4,5,5-tetramethyl-1,3,2-dioxaborolane (0.710 mL, 3.47 mmol, 5.00 equiv) was then added to the mixture dropwise and the reaction was stirred at room temperature for 6 hours. The reaction was then quenched with a saturated solution of ammonium chloride (50 mL) and the product was extracted with dichloromethane (3 x 50 mL). The organic layers were combined and washed with deionized water (2 x 50 mL) then brine (1 x 50 mL), dried over sodium sulfate and concentrated to give a yellow oil crude reaction mixture. The product was purified with gel permeation chromatography HPLC in chloroform to give the **II.11** as clear viscous oil (145 mg, 34%). <sup>1</sup>H NMR (500 MHz, CDCl<sub>3</sub>): δ 7.49 (d, *J* = 2.4 Hz, 1H), 7.47 (d, *J* = 2.4 Hz, 1H), 7.19 (dd, *J* = 8.5 Hz, 2.3 Hz, 1H), 7.19 (dd, *J* = 8.4 Hz, 2.3 Hz, 1H), 6.78 (d, *J* = 8.4 Hz, 1H), 6.77 (d, *J* = 8.5 Hz, 1H), 3.96 (m, 4H), 3.80 (s, 6H), 3.80 (s, 6H), 2.61 (m, 2H), 2.54 (m, 2H), 1.89 (m, 2H), 1.68

(m, 2H), 1.59 (m, 2H), 1.43 (m, 2H), 1.35 (s, 12H), 1.35 (s, 12H);  $^{13}\text{C}$  NMR (125 MHz,  $\text{CDCl}_3$ ):  $\delta$  162.64, 162.59, 136.67, 136.57, 134.27, 133.80, 132.35, 132.33, 111.56, 110.83, 110.73, 83.54, 83.50, 65.21, 56.18, 39.49, 37.41, 35.09, 32.29, 29.15, 24.97, 23.84; HRMS (TOF, ES+) ( $m/z$ ):  $[\text{M}+\text{Na}]^+$  calculated for  $\text{C}_{35}\text{H}_{52}\text{B}_2\text{O}_8$ , 645.3759; found: 645.3741. IR (neat): 2974, 2930, 2858, 2830, 1606, 1609, 1492, 1461, 1413, 1369, 1342, 1310, 1276, 1268, 1244, 1204, 1179, 1167, 1140, 1107, 1068, 1026, 965, 947, 912, 856, 824, 813, 763, 745, 731, 691, 673, 578, 553  $\text{cm}^{-1}$ .



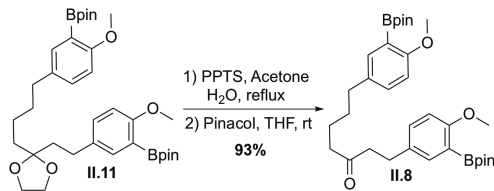
1,7-Bis-(4-methoxyphenyl)-heptane-3-[1,3]dioxolane **II.10** (3.00 g, 8.32 mmol, 1.00 equiv) and chromium carbonyl (4.76 g, 21.6 mmol, 2.60 equiv) were charged to a Schlenk flask equipped with a reflux condenser. The mixture was diluted with dibutyl ether (111 mL) and THF (12.0 mL) and subjected to freeze-pump-thaw cycles (3 x 15 min) and then refluxed at 150 °C. At 4 and 24 hours of reaction time, THF (2.00 mL) was added to the top of the reflux condenser to dissolve any chromium carbonyl that sublimed in the condenser. After 48 hours, the reaction mixture was cooled to room temperature and filtered through a pad of silica. The silica pad was rinsed with diethyl ether (3 x 250 mL) and dichloromethane (3 x 250 mL) the resulting filtrate was concentrated to give a yellow solid. The crude reaction mixture was purified via column chromatography (20-70% ethyl acetate/hexane then 70% ethyl acetate/dichloromethane) to give the product **II.12** as a yellow solid (5.97 g, 93%). mp 126-127 °C.  $^1\text{H}$  NMR (600 MHz,  $\text{CDCl}_3$ ):  $\delta$  5.45 (d,  $J$  = 6.9 Hz, 2H), 5.43 (d,  $J$  = 6.8 Hz, 2H), 5.11 (d,  $J$  = 6.6 Hz, 2H), 5.10 (d,  $J$  = 6.3 Hz, 2H), 1.42 (m, 2H), 3.95 (s, 4H), 3.68 (s, 6H), 2.33 (m, 2H), 2.26 (t,  $J$  = 7.7 Hz, 2H), 1.84 (m, 2H), 1.62 (m, 2H), 1.55 (m, 2H);  $^{13}\text{C}$  NMR (150 MHz,  $\text{CDCl}_3$ ):  $\delta$  142.28, 142.17, 110.70, 106.36, 106.28, 95.43, 95.37, 78.49, 78.28, 65.23, 55.86, 38.92, 37.14, 34.03, 31.74, 27.98, 23.53; HRMS (TOF, ES+) ( $m/z$ ):  $[\text{M}+\text{Na}]^+$  calculated for  $\text{C}_{29}\text{H}_{30}\text{Cr}_2\text{O}_{10}$ , 665.0548; found: 665.0532. IR (neat): 3091, 3072, 3051, 2977, 2975, 2938, 2908, 2881, 2863, 2834, 1941, 1846, 1841, 1610, 1607, 1542, 1511, 1485, 1462,

1435, 1356, 1278, 1271, 1248, 1245, 1221, 1178, 1134, 1132, 1107, 1075, 1062, 1060, 1028, 1015, 954, 950, 939, 905, 872, 835, 823, 817, 744, 662, 670, 626 cm<sup>-1</sup>.



1,7-Bis-[(4-methoxyphenyl)chromium-tricarbonyl]-heptane-3-[1,3]dioxolane **II.12** (4.55 g, 7.09 mmol, 1.00 equiv) was dissolved in THF (120 mL) and cooled to -78 °C. *n*-BuLi (2.32 M in hexanes, 7.55 mL, 17.5 mmol, 2.50 equiv) was added to the cooled reaction mixture dropwise and the reaction was stirred at this temperature for 1 hour. 2-Isopropoxy-4,4,5,5-tetramethyl-1,3,2-dioxaborolane (5.00 mL, 24.5 mmol, 3.50 equiv) was then added to the mixture dropwise and the reaction was stirred at -78 °C for 1 hour. The reaction was then quenched with water and warmed to room temperature. The product was extracted with dichloromethane (3 x 100 mL) and the combined organic layers were washed with deionized water (3 x 100 mL), once with brine and dried over sodium sulfate to give the a yellow-orange foam after filtration and concentration. The foam was carried on crude.

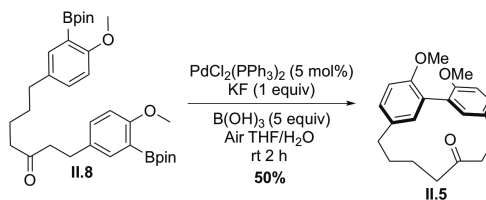
To foam from above was added AcOH (10.0 mL) after dilution with toluene (50.0 mL). Activated manganese oxide (4.00 g, 46.0 mmol, 6.50 equiv) was added in portions to the reaction mixture and this slurry was stirred open to the atmosphere for 16 hours. The reaction was then diluted with EtOAc (20.0 mL) and filtered over a short pad of silica. The pad was rinsed with EtOAc (3 x 125 mL) and filtrate was concentrated to give a yellow oil. The crude reaction mixture was purified via column chromatography (15-50% ethyl acetate/hexane) to give the product **II.11** as a clear, viscous oil (2.05 g, 47%). Characterization of this compound was consistent with the previous synthesis reported in this document.



1,7-Bis-[3-(4,4,5,5-tetramethyl-[1,3,2]dioxaborolane-2-yl)4-methoxyphenyl]-heptane-3-[1,3]dioxolane **II.11** (1.77 g, 2.84 mmol, 1.00 equiv) was refluxed in acetone (29.0 mL) and water (12.0 mL) with pyridinium paratoluenesulfonate (243 mg, 0.967 mmol, 0.340 equiv) for 16 hours. The reaction mixture was then cooled to room temperature and quenched with saturated sodium bicarbonate (15.0 mL). The product was extracted with ethyl acetate (3 x 75.0 mL) and the combined organic layers were washed with deionized water (3 x 100 mL) and brine (1 x 100 mL) then dried over sodium sulfate and concentrated to give a colorless viscous oil. The crude reaction mixture was carried on crude.

The oil from above was stirred with 2,3-dimethyl-2,3-butanediol (1.01 g, 8.53 mmol, 3.00 equiv) in THF (28.0 mL) and molecular sieves for 48 hours. The reaction mixture was then filtered over a pad of celite that was rinsed with dichloromethane (3 x 25.0 mL) and the filtrate was concentrated to give a colorless viscous oil. The crude mixture was purified via column chromatography (15-50% ethyl acetate/hexane) to give the product and 2,3-dimethyl-2,3-butanediol as a mixture. The mixture was then diluted with dichloromethane (50.0 mL) and rinsed with deionized (4 x 10.0 mL) then dried with sodium sulfate and concentrated to give the desired product **II.8** as a colorless viscous oil (1.54 g, 93%). <sup>1</sup>H NMR (500 MHz, CDCl<sub>3</sub>): δ 7.46 (d, *J* = 2.3 Hz, 1H), 7.45 (d, *J* = 2.3 Hz, 1H), 7.19 (dd, *J* = 8.8 Hz, 2.2 Hz, 1H), 7.17 (dd, *J* = 8.9 Hz, 2.2 Hz, 1H), 6.77 (d, *J* = 8.5 Hz, 1H), 6.77 (d, *J* = 8.5 Hz, 1H), 3.80 (s, 3H), 3.80 (s, 3H), 2.81 (t, *J* = 7.7, 2H), 2.67 (t, *J* = 7.7, 2H), 2.53 (t, *J* = 7.2, 2H), 2.39 (t, *J* = 6.9 2H), 1.58 (m, 4H), 1.43 (m, 2H), 1.35 (s, 24H); <sup>13</sup>C NMR (125 MHz, CDCl<sub>3</sub>): δ 210.38, 162.72, 162.54, 136.53, 136.37, 133.71, 132.55, 132.36, 132.26, 110.71, 110.62, 83.47, 83.41, 56.05, 56.01, 44.69, 42.89, 34.77, 31.33, 28.94, 24.88, 23.51; HRMS (TOF, ES<sup>+</sup>) (*m/z*): [M+Na]<sup>+</sup> calculated for C<sub>33</sub>H<sub>48</sub>B<sub>2</sub>O<sub>7</sub>, 601.4395; found: 601.3493. IR (neat): 3535, 2973, 2931, 2856, 2836, 1708, 1606, 1609, 1493, 1460, 1415, 1370, 1343, 1315, 1284, 1267, 1245,

1205, 1176, 1164, 1140, 1107, 1069, 1030, 964, 949, 912, 854, 834, 816, 762, 744, 732, 712, 671, 653, 578, 556 cm<sup>-1</sup>.



1,7-Bis-[3-(4,4,5,5-tetramethyl-[1,3,2]dioxaborolane-2-yl)4-methoxyphenyl]-heptane-3-one **II.8** (1.50 g, 2.59 mmol, 1.00 equiv) was added to a 4 L jar with bis(triphenylphosphine)palladium(II) dichloride (91.0 mg, 0.130 mmol, 5.00 mol%) and boric acid (802 mg, 13.0 mmol, 5.00 equiv). The solid were dissolved in THF (2,590 mL) and the mixture was stirred vigorously for 10 min. Potassium fluoride (151 mg, 2.59 mmol, 1.00 equiv) was dissolved in water (260 mL) and added immediately to the reaction. The reaction was stirred at room temperature open to the atmosphere for 2 hours. The THF was removed under vacuum and the resulting solution was extracted with dichloromethane (3 x 100 mL). The combined organic layers were washed with deionized water (3 x 100 mL) and brine (1 x 100 mL) then dried over sodium sulfate and concentrated to give a brown oil. The crude reaction mixture was purified via column chromatography (100% dichloromethane) to give the desired product **II.5** as a white crystalline solid (416 mg, 50%). mp 145-146 °C. <sup>1</sup>H NMR (600 MHz, CDCl<sub>3</sub>): δ 7.08 (dd, *J* = 8.3 Hz, 2.3 Hz, 1H), 7.07 (dd, *J* = 8.4 Hz, 2.3 Hz, 1H), 6.84 (d, *J* = 8.4, 1H), 6.84 (d, *J* = 8.3 Hz, 1H), 6.74 (d, *J* = 2.4 Hz, 1H), 6.60 (d, *J* = 2.5 Hz, 1H), 3.85 (s, 3H), 1.57 (app brs, 1H), 3.82 (s, 3H), 3.22 (app brs, 1H), 2.91 (app brs, 1H), 2.76 (app brs, 2H), 2.67 (t, *J* = 5.8 2H), 2.60 (app brs, 2H), 1.90 (app brs, 1H), 1.78 (app brs, 2H); <sup>13</sup>C NMR (150 MHz, CDCl<sub>3</sub>): δ 213.94, 155.50, 155.05, 134.97, 134.57, 132.72, 131.68, 129.55, 129.41, 128.54, 128.30, 111.88, 111.55, 56.26, 56.21, 47.27, 42.87, 31.96, 29.93, 25.67, 21.00; HRMS (TOF, ES<sup>+</sup>) (*m/z*): [M+Na]<sup>+</sup> calculated for C<sub>21</sub>H<sub>24</sub>O<sub>3</sub>, 347.1623; found: 347.1616. IR (neat): 3366, 3052, 2998, 2923, 2891, 2837, 2828, 1695, 1606, 1605, 1502, 1463, 1460, 1436, 1404 1366, 1350, 1291, 1287, 1249, 1238, 1177, 1166, 1150, 1134, 1083, 1045, 1025, 993, 903, 905, 890, 818, 809, 803, 757, 732, 728, 702, 680, 644, 648, 502, 585, 584 cm<sup>-1</sup>.

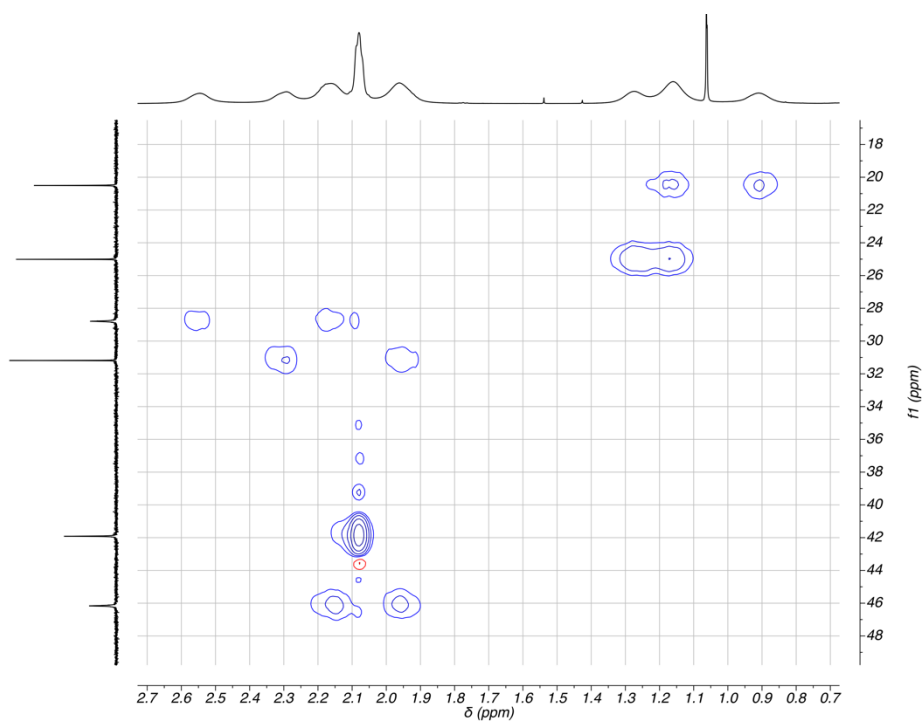


**Figure 2.7.** Proton-carbon HSQC of the of alkyl region macrocycle **II.5**. The proton spectrum is displayed on the x-axis (peaks and position, top and bottom respectively) and the carbon spectrum is displayed on the y-axis (peaks and position, left and right respectively).

### 2.4.3. Crystallographic Data

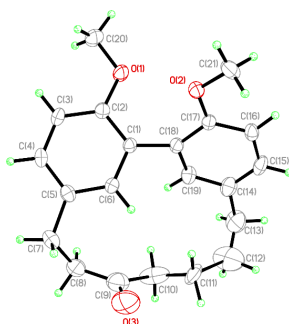


**Figure 2.8.** ORTEP representation of x-ray crystallographic structure of macrocycle **II.5**.

Crystallographic Data for **II.5**: C<sub>21</sub>H<sub>24</sub>O<sub>3</sub>, M = 324.40, 0.10 x 0.06 x 0.04 mm, T = 173(2) K, Monoclinic, space group *P*2<sub>1</sub>/*c*, *a* = 10.4271(4) Å, *b* = 14.8854(5) Å, *c* = 12.0952(4) Å, β = 113.424(2)°, V = 1722.60(11) Å<sup>3</sup>, Z = 4, D<sub>c</sub> = 1.251 Mg/m<sup>3</sup>, μ(Cu) = 0.654 mm<sup>-1</sup>, F(000) = 696, 2θ<sub>max</sub> = 115.0°, 9981 reflections, 2291 independent reflections [R<sub>int</sub> = 0.0357], R1 = 0.1075, wR2 = 0.2954 and GOF = 1.015 for 2291 reflections (218 parameters) with I > 2σ(I), R1 = 0.1240, wR2 = 0.3146 and GOF = 1.015 for all reflections, max/min residual electron density +0.898/-0.521 eÅ<sup>3</sup>.

#### 2.4.4. Homodesmotic Reactions

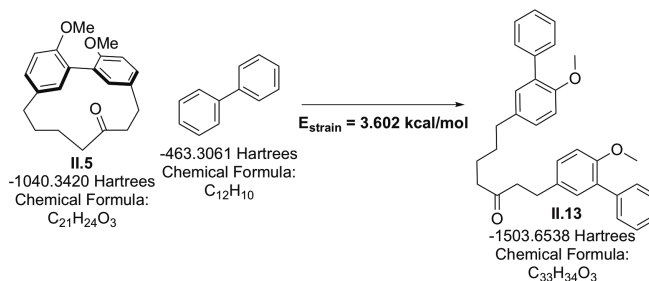


**Figure 2.9.** Homodesmotic reaction used to approximate the strain of compound **II.5**.

#### 2.4.5. Computational Coordinates of Minimized Geometries

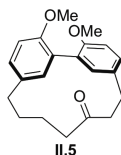


**Figure 2.10.** Structure of macrocycle **II.5** represented with the computational coordinates listed below.

C	-2.43541	-0.87566	0.34829
C	-1.05881	-0.6374	0.3189
C	-0.49686	0.35772	1.15865
C	-1.33141	1.32828	1.72085
C	-2.72398	1.15435	1.66329

C	-3.27101	0.02165	1.0314
H	-2.8497	-1.72179	-0.159
H	-3.3709	1.88131	2.10811
H	-4.32668	-0.15017	1.06322
C	1.02783	0.38426	1.40377
C	1.73344	1.49885	0.94242
C	1.76232	-0.65826	2.05791
C	3.12211	1.40491	0.76799
C	3.10737	-0.83301	1.7209
C	3.78915	0.20315	1.06619
H	3.67208	2.24357	0.39503
H	3.61929	-1.73477	1.9848
H	4.82065	0.08507	0.8074
O	1.04401	2.70842	0.61602
O	-0.77282	2.47437	2.36846
C	-1.67312	3.57831	2.24375
H	-2.60764	3.32986	2.7018
H	-1.25523	4.43588	2.72833
H	-1.83013	3.79522	1.20781
C	1.9116	3.82455	0.8313
H	1.39571	4.72961	0.58709
H	2.21109	3.85066	1.85821
H	2.77721	3.72856	0.20967
C	-0.13384	-1.39515	-0.69933
H	-0.10263	-0.8322	-1.60872
H	0.85023	-1.4735	-0.28661
C	1.19512	-1.56278	3.23364
H	0.12576	-1.59962	3.22938
H	1.54021	-1.10486	4.13702
C	-0.65305	-2.80799	-1.01406
H	-1.65166	-2.77824	-1.39723



H	-0.02407	-3.28986	-1.73316
C	1.73298	-3.01306	3.1642
H	2.75697	-2.98111	2.85546
H	1.66623	-3.51157	4.10864
C	0.8351	-3.76297	2.20191
C	-0.59302	-3.51918	0.29077
H	-1.2289	-3.0051	0.9809
H	-0.90894	-4.53902	0.21979
C	0.8598	-3.42583	0.75575
H	1.4976	-4.07087	0.1883
H	1.20487	-2.41831	0.65217
O	0.02333	-4.62205	2.63388

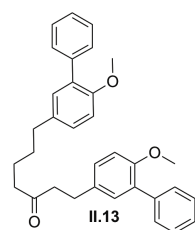


**Figure 2.11.** Structure of homodesmotic product **II.13** represented with the computational coordinates listed below.

C	-1.70304	1.14848	-1.32814
C	-0.8525	0.12486	-1.76691
C	-0.67541	-0.09946	-3.13879
C	-1.34664	0.70189	-4.07192
C	-2.19705	1.72586	-3.6332
C	-2.37559	1.94882	-2.26132
H	-1.83887	1.31925	-0.28063
H	-2.71007	2.33737	-4.3457
H	-3.0254	2.7302	-1.9263
C	3.21179	-0.74554	2.48311
C	2.77854	0.51593	2.05386

C	3.43739	-1.76474	1.5483
C	2.56883	0.75775	0.68945
C	3.22725	-1.52347	0.18392
C	2.79279	-0.26202	-0.24545
H	2.23765	1.72086	0.3615
H	3.39864	-2.30187	-0.52992
H	2.63203	-0.07756	-1.28719
O	2.55052	1.55604	3.00819
O	-1.16435	0.47495	-5.47187
C	-2.35264	0.84928	-6.17365
H	-2.55575	1.88591	-6.00321
H	-2.21638	0.68001	-7.22127
H	-3.17492	0.26216	-5.8214
C	2.80908	2.82485	2.40154
H	2.63891	3.60304	3.11593
H	3.82587	2.86109	2.07019
H	2.15623	2.95984	1.56473
C	-0.11204	-0.75362	-0.74172
H	0.81959	-1.07711	-1.1566
H	0.07097	-0.18712	0.14738
C	3.91653	-3.14909	2.02295
H	3.54447	-3.3357	3.00861
H	4.98629	-3.17089	2.03508
C	-0.97476	-1.98225	-0.39989
H	-1.90658	-1.66021	0.01542
H	-1.15741	-2.54805	-1.28975
C	3.39215	-4.23391	1.06351
H	3.76368	-4.04863	0.07728
H	3.72621	-5.19446	1.39596
C	1.85239	-4.2039	1.04603
C	-0.23241	-2.86114	0.6237

H	-0.05146	-2.29663	1.51445
H	-0.83024	-3.71675	0.85903
C	1.11029	-3.32086	0.02574
H	0.92946	-3.88293	-0.86651
H	1.70853	-2.46472	-0.20693
O	1.20034	-4.90165	1.86546
C	0.25609	-1.22698	-3.62073
C	1.19231	-0.97763	-4.63324
C	0.1671	-2.50247	-3.04703
C	2.03971	-2.00399	-5.07221
H	1.26016	-0.00372	-5.07128
C	1.01393	-3.52902	-3.48649
H	-0.54749	-2.69271	-2.27361
C	1.95035	-3.27983	-4.49909
H	2.75486	-1.81348	-5.84504
H	0.94544	-4.50322	-3.04904
H	2.59701	-4.06355	-4.83448
C	3.44015	-1.01332	3.98242
C	4.73446	-1.25963	4.45967
C	2.35488	-1.0112	4.86925
C	4.94389	-1.50435	5.82348
H	5.56308	-1.26089	3.78268
C	2.56429	-1.25584	6.23339
H	1.36654	-0.82283	4.50517
C	3.85885	-1.50251	6.71053
H	5.93246	-1.69256	6.18765
H	1.73571	-1.25425	6.91069
H	4.01878	-1.68948	7.75198

## 2.5. Bridge to Chapter III

This chapter describes the development of synthetic methods to prepare biaryl-containing macrocycles using an efficient and scalable oxidative homocoupling of aryl boronic esters. The reaction enabled the synthesis of large quantities of the desired product, **11.5**, to facilitate our study into the structural properties of this constricted macrocycle. In the next chapter, this oxidative homocoupling is used to prepare cycloparaphenylenes with versatile function handles towards nanomaterials that exploit the inherent properties of the nanohoop scaffold.

## CHAPTER III

### THE SYNTHESIS OF SUBSTITUTED CYCLOPARAPHENYLENES AND THEIR REACTIVITY

This chapter includes unpublished co-authored material, was written by and includes experimental work performed by myself. Professor Ramesh Jasti provided editorial assistance.

Oligomeric carbon nanostructures, such as carbon nanotubes, offer unique properties based on their molecular arrangement. The application of these molecules is limited because of structural inhomogeneity that arises during their synthesis and functionalization. Similarly cycloparaphenylenes, that can be thought of as the smallest cross-sectional segment of armchair carbon nanotubes, exhibit size-dependent electronic properties due to their highly conjugated structure. The modular synthetic approach that is used to prepare cycloparaphenylenes present them as appealing types of carbon based structures in biology and materials science. However, that lack of synthetic methods available to prepare functionalized versions of these nanohoops in a controlled manner has limited their study in this context. Here we report the synthesis of cycloparaphenylenes with versatile functional handles as an important step towards their application in biology and materials science. Our initial approach revealed the reactive nature of the strained nanohoop backbone under conditions that promote the formation of a radical cation. Ultimately, incorporation of benzyl alcohol functionality into our synthetic sequence provided access to nanohoops with nucleophilic and electrophilic centers for further manipulation.

#### 3.1. Introduction

Carbon nanotubes (CNTs) are oligomeric, cylindrical molecules that exhibit extraordinary properties depending on the arrangement of their  $sp^2$  carbon atoms to give armchair, zig-zag or chiral nanotubes.<sup>1</sup> CNTs can be more conductive than copper,

stronger than steel, and exhibit semiconducting behavior with tunable band gaps.<sup>2-6</sup> These phenomenal properties make nanotubes promising carbon based structures for applications in materials science and biology, but their utilization is currently limited due to the inability to produce homogeneous types of CNTs.<sup>7-9</sup> State of the art synthesis of CNTs involves treatment of a carbon source, such as ethylene, with a high energy source in the presence of a metal catalyst to give mixtures of armchair, zig-zag and chiral tubes of various diameters and length.<sup>7, 10-11</sup> Separation of a single nanotube type from this mixture is demanding on large scale and the polymeric nature of the nanotubes make selective functionalization for a specific application difficult.<sup>7, 12</sup> This limits their application especially in biological settings where molecular inhomogeneity makes toxicology studies nearly impossible.<sup>9</sup>

Small molecules that are isostructural to CNTs are appealing as seeds towards the controlled growth of a single type of nanotube.<sup>7, 13, 14</sup> Such molecules may also offer advantageous properties through the preparation of carbon materials with molecular precision. [*n*]Cycloparaphenylenes, that are the smallest cross-sectional segment of armchair CNTs, have emerged as new types of nanomaterials in this context (**Figure 3.1a**). These molecules, termed nanohoops because of their structural relationship to nanotubes, can be envisioned as *n* number of benzene rings linked in the para-position to form a macrocycle. The connection between nanohoops and CNTs motivated the first successful synthesis of [9]-, [12]- and [18]-CPP in 2008 by Jasti and Bertozzi and their application as seeds towards the controlled growth of nanotubes is an active area of research.<sup>13, 15-21</sup>

Since the seminal synthesis of nanohoops, the development of modular synthetic strategies towards size-selective or gram-scale synthesis of [5]-[12]CPP has uncovered the unique physical properties of this novel class of molecules.<sup>22-36</sup> This includes tunable, size-dependent HOMO→LUMO energy gaps that dramatically impact the electronic structure of the nanohoop.<sup>37-39</sup> For example, all CPPs share a common absorption with a red-shifted fluorescence as the size of the hoop decreases (**Figure 3.1b**). Upon host-guest complexation, this fluorescence is quenched as observed in the concave-convex interaction of [10]CPP and Buckminsterfullerene (C<sub>60</sub>) (**Figure 3.1b**).<sup>24, 40</sup> Crystal

structures of nanohoops also reveal that these molecules are tightly packed with long-range channels that can be tuned with structural modification CPP backbone.<sup>37, 38, 41, 42</sup>

The physical properties of nanohoops highlight their potential as novel types of carbon nanomaterials that can be prepared in a molecularly precise and scalable fashion (**Figure 3.1c**).<sup>43-45</sup> For example, exploitation of the unique optical properties of nanohoops in a biological setting should enable the development of a new class of fluorescent probes based on this unique scaffold. Water-soluble derivatives should promote the formation of host-guest complexes with fluoresce turn off behavior for size-selective sensing of guests. Furthermore, incorporation of nanohoops into polymeric networks may improve the macroscopic properties of these traditional organic materials through extended  $\pi$ -conjugation. Currently, reports of synthetic strategies that appended reactive groups to the nanohoop backbone and enable selective functionalization of these materials are sparse, limiting their application in biology and materials science.<sup>46-49</sup> In this study we describe our approach to incorporate versatile functional handles on to the nanohoop backbone. Leveraging the modular synthetic strategy developed in our lab, we prepare functionalized nanohoops **III.1**, **III.2**, **III.3** and **III.4** (**Figure 3.1d**), and provide insight on the reactivity of these functional groups and the nanohoop backbone. The ensuing discussion highlights challenges involved in selecting a robust functional group that survives the reaction conditions required for nanohoop synthesis and avoids conditions that promote nanohoop decomposition during functional group manipulation. This work takes an important first step towards the application of this novel class of carbon nanomaterials in biology and materials science.

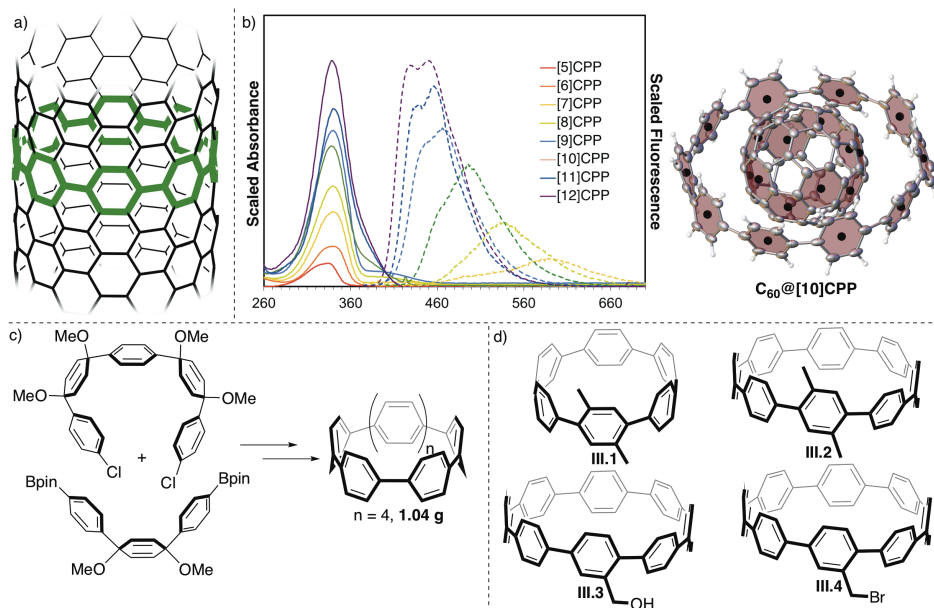


**Figure 3.1.** a) Nano hoops as the smallest cross-sectional segment of an armchair carbon nanotube (CNT). b) The size-dependent optical properties of [5]-[12]CPP (solid lines are absorbance and dashed lines are fluorescence) and the x-ray crystal structure of the  $C_{60}@[10]CPP$  host-guest complex. c) The scalable and modular synthesis of nano hoops. d) Structures of the nano hoops investigated in this chapter.

## 3.2. Results and Discussion

### 3.2.1. The Synthesis of Methyl Substituted Nano hoops

With the goal of producing nano hoops with versatile functional handles, we evaluated which group would provide orthogonal reactivity to the transformations required in our current synthetic route. The original CPP synthetic sequence calls for lithium halogen exchange under basic conditions, deprotection under mildly acidic conditions, transition metal catalyzed coupling and in the last step harsh reducing conditions for aromatization with sodium naphthalenide. Namely, the reducing conditions the concluding step of the sequence are not suitable for most functional handles and led us to first investigate the synthesis of methyl substituted [6]CPP (**III.1**) and methyl substituted [8]CPP (**III.2**). We envisioned that the robust methyl substituents would provide access to a variety of different functional groups through bromination at the



benzylic position, paving the way for the application of these molecules in biology and materials science.

The synthesis of **III.1** began with the lithiation of 1,4-dibromo-2,5-dimethylbenzene and addition of the resulting nucleophile into deprotonated chloro ketone **III.5**, prepared from a previously reported procedure (**Figure 3.2**).<sup>50</sup> Under these reaction conditions the desired *cis*-isomer was prepared in a ratio of 20:1 over the *trans*-isomer to give **III.6** after protection with methyl iodide in 83% yield. Suzuki-Miyaura cross-coupling of **III.6** with 4-chlorophenylboronic acid gave six ringed intermediate **III.7** in 73% yield. Miyaura borylation of **III.7** in high yield (91 %) gave **III.8** that was subjected to our optimized palladium catalyzed oxidative homocoupling conditions to give **III.9** 40% yield.<sup>51</sup> Aromatization of **III.9** with sodium naphthalenide gave the desired nanohoop **III.1** in 60% yield.

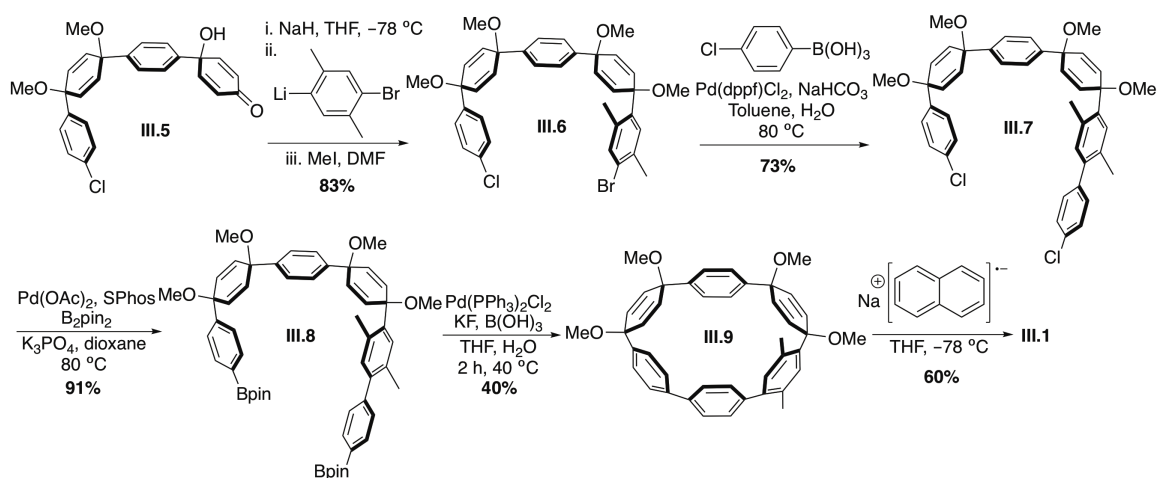


**Figure 3.2.** The synthesis of methyl substituted [6]CPP **III.1**.

Nanohoop **III.2** was prepared in a similar fashion to nanohoop **III.1** (**Figure 3.3**). First, lithiated 1,4-dibromo-2,5-dimethylbenzene was added to deprotonated bromo-ketone **III.10**, prepared from a previously reported procedure, to give **III.11** after protection with methyl iodide in 50% yield.<sup>23</sup> Lithium halogen exchange of **III.11** with *n*-butyllithium followed by treatment with electrophilic boron source 2-isopropoxy-4,4,5,5,tertramethyl-1,3,2-dioaborolane gave borylated intermediate **III.12** in 75% yield. Suzuki-Miyuara cross-coupling of **III.12** and previously reported dichloride **III.13** gave

macrocycle **III.14** in 12% yield that was aromatized with sodium naphthalenide to give nanohoop **III.2** in 66% yield.<sup>50</sup>

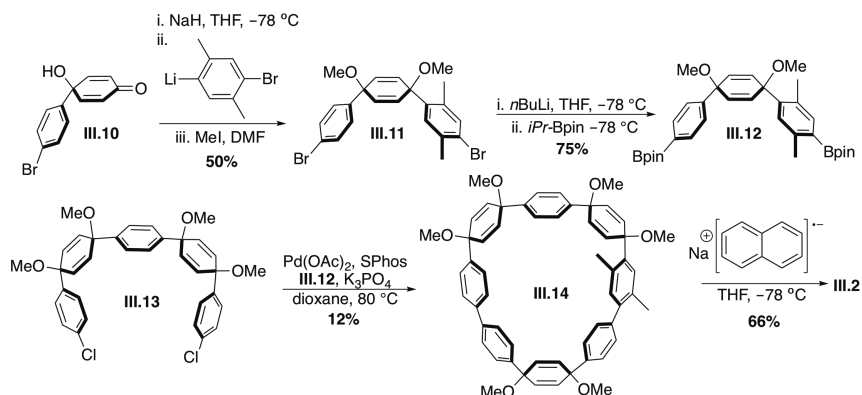


**Figure 3.3.** The synthesis of methyl substituted [8]CPP **III.2**.

With nanohoops **III.1** and **III.2** in hand we began investigating the benzylic bromination of these functionalized nanohoops with optimized reaction conditions using *N*-bromosuccinamide (NBS) and benzoyl peroxide as a radical initiator. Surprisingly, treatment of **III.2** with these conditions resulted in complete consumption of starting material with no evidence of the expected brominated product by <sup>1</sup>H NMR (**Figure 3.4a**). Instead, we observed new peaks in the alkyl region and many additional aromatic protons consistent with the formation of nanohoop derivatives with broken symmetry. We speculated that these unsymmetrical products may be a result of the nanohoop backbone reacting with the radical initiator. However, exposure of **III.1** to only benzoyl peroxide resulted in recovery of starting material while subjecting **III.1** to NBS gave unsymmetrical product (**Figure 3.4a**). To determine if the observed reaction pathway was related to the highly strained nature of nanohoop **III.1** we subjected **III.2** to the same bromination conditions. Again, we observed full consumption of starting material **III.2** and unsymmetrical nanohoop derivatives by <sup>1</sup>H NMR. Indeed, under these conditions the reaction pathway of **III.2** is similar to that of **III.1** as subjecting **III.2** to only NBS also gave unsymmetrical products.

The nanohoop derivatives observed under these reaction conditions are consistent with a recent study from our lab where the CPP backbone rearranges or ring opens in the presence of a strong acid or reagents that promote radical cation formation.<sup>52</sup> In this

study, we investigated reaction pathways that led to nanohoop rearrangement or ring opening theoretically and found that such derivatives are thermodynamically favored when compared to the para-connected parent compound. Specifically, [8]CPP with a single meta-shift was almost 20 kcal/mol lower in energy than the all para-precursor and each additional meta-shift throughout the backbone provides about 20 kcal/mol of further thermodynamic stabilization. Ring opened products were also found to be nearly 40 kcal/mol more stable than their circular parent compounds, providing sufficient driving force for this process under conditions where cations are formed at the nanohoop backbone. The reactive, highly strained nature of nanohoops **III.1** and **III.2** should facilitate this type of reaction after a single electron oxidation with NBS to give a radical cation in the nanohoop backbone. **Figure 3.4b** shows an example of this rearrangement mechanism with [6]CPP to give a ring opened product for simplicity.

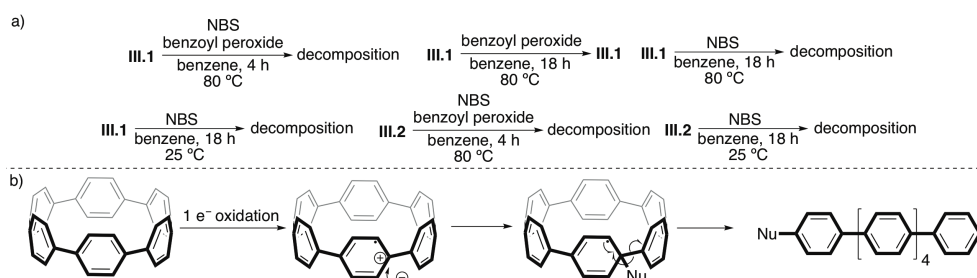


**Figure 3.4.** a) The decomposition of **III.1** and **III.2** under benzylic bromination reaction conditions. b) A mechanism of rearrangement for [6]CPP after single electron oxidation.

### 3.2.2. The Synthesis of a Nanohoop with Benzyl Alcohol Functionality

During the course of our studies, Yamago and co-workers reported a synthetic route where triethyl silane (TES) protected alcohols were used in place of the methyl ether protecting groups developed in our strategy. Macrocyclic formation then deprotection of the alcohols permitted the synthesis of [5]-[12]CPP after aromatization with H<sub>2</sub>SnCl<sub>4</sub> mediated mild reduction conditions.<sup>32, 34, 35</sup> Building off this key advancement, we aimed to introduce benzylic alcohol functionality into the nanohoop backbone in the form of [8]CPP analog **III.3**. This handle can be manipulated with mild reaction conditions after nanohoop formation and should survive the mild aromatization conditions detailed by Yamago.

The synthesis of nanohoop **III.3** required the preparation of a coupling partner with benzylic alcohol functionality. This intermediate was prepared first by the deprotonation of previously reported chloro-ketone **III.15** with sodium hydride followed by addition of mono-lithiated bromobenzene prepared from lithium halogen exchange of 1,4-dibromobenzene.<sup>50</sup> Protection of the resulting alkoxides with chlorotriethylsilane gave TES protected bromo-chloro three ring **III.16** in 92% yield. Lithiation of **III.16** followed by addition to previously reported quinone monoketal **III.17** gave chloroketone **III.18** in 55% yield after acetal deprotection.<sup>50</sup> Lithium halogen exchange of previously reported *tert*-butyldimethylsilyl protected benzyl alcohol and addition of the resulting nucleophile into deprotonated **III.18** gave dichloride **III.19** in 43% yield after TES protection to install the benzyl alcohol functionality.<sup>20</sup> Suzuki-Miyuara cross-coupling of **III.19** and previously reported **III.20** gave macrocycle **III.21** in 10% yield.<sup>53</sup> Deprotection of **III.21** followed by aromatization with H<sub>2</sub>SnCl<sub>4</sub> gave nanohoop **III.3** with the benzylic alcohol functionality intact in 22% after two steps.

Deprotonation of the benzylic alcohol in **III.3** will provide a nucleophilic center for functional group incorporation. We were interested in expanding the transformation scope of this reactive handle through the formation of an electrophilic center. Treatment of **III.3** with bromotrimethylsilane (TMSBr) gave benzyl bromide **III.4** in 83% yield as a functional group that can be manipulated with nucleophilic reaction partners.<sup>54</sup>

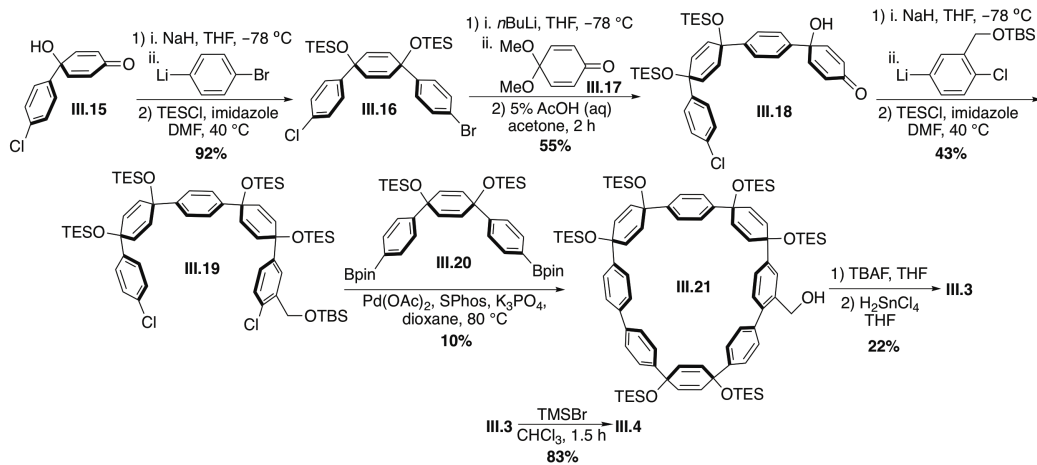


**Figure 3.5.** The synthesis of benzyl alcohol [8]CPP **III.3** and benzyl bromide [8]CPP **III.4**.

With functionalized nano hoops **III.3** and **III.4** in hand, we are now prepared to transform these reactive handles into functional groups that facilitate the use of CPPs in biology and material science. The modular synthetic sequence reported herein should enable the synthesis of nano hoop derivatives with multiple functional groups to tune the physical properties of this unique scaffold. We will first investigate groups that impart water solubility onto the backbone using derivatives of either **III.3** or **III.4** towards the development of nano hoops as a new class of fluorophores. These solubilizing groups will also facilitate investigations into the supramolecular properties of nano hoops as sensors in aqueous media. Furthermore, the functional groups provide a strategy for the incorporation of nano hoops into larger polymeric materials as a tool to tune macroscopic properties on a molecular level.

### 3.3. Conclusion

During our investigation of strategies that facilitate the incorporation of a versatile functional handle onto the nano hoop backbone, we uncovered a decomposition pathway with reaction conditions that promote radical cation formation at the nano hoop backbone. The development of new synthetic strategies for nano hoop synthesis that utilize mild

reducing conditions as the final step in the reaction sequence enabled the synthesis of derivatives of [8]CPP with benzyl alcohol and benzyl bromide functionality. Studies are currently underway to transform these functional handles and expand the utility of the nanohoop scaffold in biology and materials science.

### 3.4. Experimental Sections

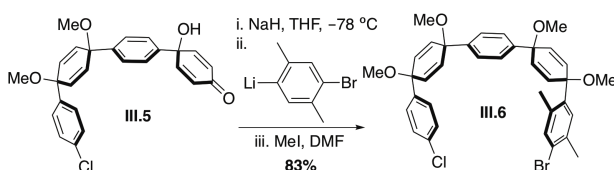
#### 3.4.1. General Experimental Details

Moisture sensitive reactions were carried out under an inert atmosphere of nitrogen using standard Schlenk technique.  $^1\text{H}$  NMR spectra were recorded at 400 MHz, 500 MHz, or 600 MHz on a (400 MHz or 500 MHz) Varian VNMR spectrometer or at 600 MHz on a Bruker Avance-III-HD NMR spectrometer.  $^{13}\text{C}$  NMR spectra were recorded at 100 MHz or 125 MHz on a Varian VNMR Spectrometer or at 150 MHz on a Bruker Avance-III-HD NMR spectrometer. All  $^1\text{H}$  NMR spectra were taken in  $\text{CDCl}_3$  (referenced to TMS,  $\delta$  0.00 ppm). All  $^{13}\text{C}$  NMR spectra were taken in  $\text{CDCl}_3$  (referenced to chloroform,  $\delta$  77.16 ppm).

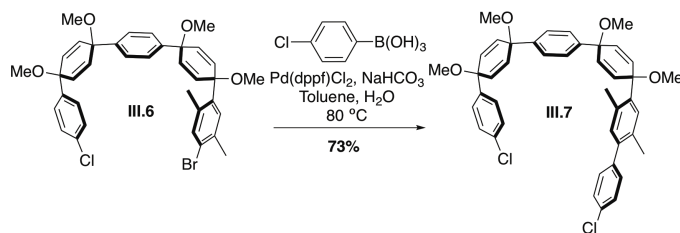
THF, dichloromethane, toluene and DMF were dried by filtration through alumina according to the methods described by Grubbs.<sup>55</sup> All homocoupling reactions were done with THF filtered through alumina. Silica column chromatography was conducted with Zeochem Zeoprep 60 Eco 40-63  $\mu\text{m}$  silica gel. Thin Layer Chromatography (TLC) was performed using Sorbent Technologies Silica Gel XHT TLC plates. Developed plates were visualized using UV light at wavelengths of 254 and 265 nm. All glassware was oven or flame dried and cooled under an inert atmosphere of nitrogen unless otherwise noted.

Compounds **III.5**,<sup>50</sup> **III.10**,<sup>23</sup> **III.13**,<sup>50</sup> **III.15**,<sup>50</sup> **III.17**,<sup>50</sup> **III.19**<sup>54</sup> and **III.22**<sup>20</sup> were prepared in accordance with previously reported procedures and all spectra matched previously reported. All reagents were obtained commercially unless otherwise noted.

### 3.4.2. Synthetic Details

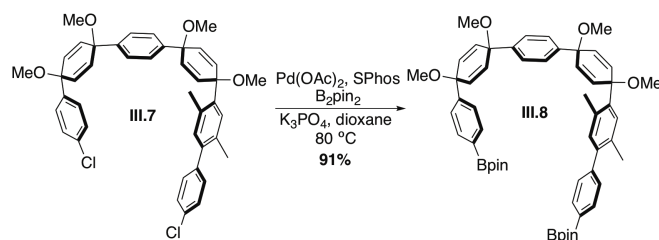


1,4-dibromo-1,6-dimethylbenzene (5.31 g, 20.2 mmole, 2.30 equiv) was dissolved in THF (40 mL) and cooled to  $-78\text{ }^{\circ}\text{C}$  for 30 min. *n*BuLi (2.5 M in hexanes, 8.10 mL, 20.2 mmole, 2.30 equiv) was added dropwise to the solution to form a white precipitate that was stirred for 1 hour at this temperature. In a separate flask, sodium hydride (501 mg, 12.5 mmole, 1.40 equiv) was suspended in THF (24 mL) and cooled to  $-78\text{ }^{\circ}\text{C}$  for 30 minutes. A solution of **III.5** (3.84 g, 8.83 mmole, 1.00 equiv) dissolved in THF (18 mL) was added via cannula dropwise to the solution of sodium hydride and stirred and  $-78\text{ }^{\circ}\text{C}$  for 30 min. The solution of lithiated 1,4-dibromo-1,6-dimethylbenzene was then cannulated into the solution of deprotonated **III.5** and stirred for 1 hour. After 1 hour, DMF (50 mL) and methyl iodide (5.73 mL, 92.0 mmole, 10.4 equiv) were added to the reaction mixture, the solution was warmed to room temperature and stirred for an additional 48 hours. The reaction was quenched by the slow addition of deionized water (50 mL) and extracted with diethyl ether (3 x 100 mL). The combined organic layers were washed with a 5% solution of LiCl in deionized water (7 x 100 mL), deionized water (1 x 100 mL), brine (1 x 100 mL) and dried over sodium sulfate. The resulting solution was concentrated under reduced pressure to give an off white solid. The resulting solid was recrystallized in hexanes to give a pure **III.6** white solid (4.76 g, 83%)  $^1\text{H}$  NMR (400 MHz,  $\text{CDCl}_3$ ):  $\delta$  7.35 (s, 1H), 7.30 (d,  $J = 8.6\text{ Hz}$ , 2H), 7.27-7.24 (overlap, 8H), 6.99 (s, 1H), 6.29 (d,  $J = 10\text{ Hz}$ , 2H), 6.09 (d,  $J = 5.1\text{ Hz}$ , 2H), 6.06 (d,  $J = 5.1\text{ Hz}$ , 2H), 6.03 (d,  $J = 10\text{ Hz}$ , 2H), 3.41 (s, 3H), 3.40 (s, 3H), 3.39 (s, 3H), 3.36 (s, 3H), 2.54 (s, 3H), 2.21 (s, 3H).  $^{13}\text{C}$  NMR (100 MHz,  $\text{CDCl}_3$ ):  $\delta$  142.67, 142.48, 142.19, 139.37, 136.66, 136.34, 136.32, 134.84, 133.82, 133.54, 133.13, 131.85, 129.89, 128.67, 127.58, 126.16, 126.04, 124.00, 76.18, 74.73, 74.63, 74.57, 52.17, 52.15, 51.53, 51.51, 22.33, 21.03.

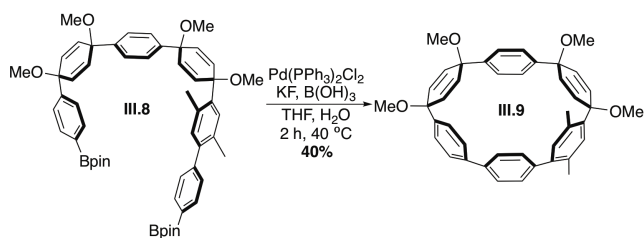


Toluene (155 mL) and deionized water (155 mL) were sparged with N<sub>2</sub> for 1 hour. **III.6** (2.00 g, 3.09 mmole, 1.00 equiv), 4-chlorophenylboronic acid (724 mg, 4.63 mmole, 1.50 equiv), [1,1'-bis(diphenylphosphine)ferrocene]dichloro-palladium(II) (126 mg, 0.154 mmole, 0.0500 equiv) and sodium bicarbonate (1.30 mg, 15.4 mmole, 5.00 equiv) were added to a round bottom flask. The flask was evacuated and backfilled with N<sub>2</sub> (5 x), capped with a septum and purged with N<sub>2</sub> for 30 minutes. The sparged toluene was added to the flask via cannula and the mixture was placed in an 80°C oil bath. The sparged deionized water was cannulated into the mixture and the solution was stirred at this temperature for 18 hours. The reaction was cooled to room temperature and filtered over celite. The filtrate was extracted with DCM (3 x 100 mL) and the combined organic layers were washed with deionized water (3 x 100 mL), brine (1 x 100 mL), dried over sodium sulfate and concentrated under reduced pressure to give a brown solid. The product was recrystallized from hexanes to give **III.7** as a white solid. (1.54 g, 73%). <sup>1</sup>H NMR (400 MHz, CDCl<sub>3</sub>): δ 7.36 (d, *J* = 8.4 Hz, 2H), 7.34 (d, *J* = 8.4 Hz, 2H), 7.30 (d, *J* = 8.0 Hz, 2H), 7.28 (d, *J* = 8.0 Hz, 2H), 7.23 (d, *J* = 8.2, 4H), 7.07 (s, 1H), 7.03 (s, 1H), 6.37 (d, *J* = 10 Hz, 2H), 6.09 (d, *J* = 4.3 Hz, 2H), 6.07 (d, *J* = 4.3 Hz, 2H), 6.02 (d, *J* = 10.3 Hz, 2H), 3.44 (s, 3H), 3.40 (s, 6H), 3.38 (s, 3H), 2.60 (s, 3H), 2.10 (s, 3H). <sup>13</sup>C NMR (100 MHz, CDCl<sub>3</sub>): δ 142.78, 142.58, 142.22, 140.03, 139.95, 139.41, 134.61, 134.45, 133.82, 133.62, 133.49, 133.09, 132.96, 132.36, 132.25, 130.68, 129.69, 128.64, 128.41, 127.58, 126.23, 126.02, 76.33, 74.77, 74.63, 74.57, 52.16, 52.14, 51.58, 51.56, 21.30, 20.02.

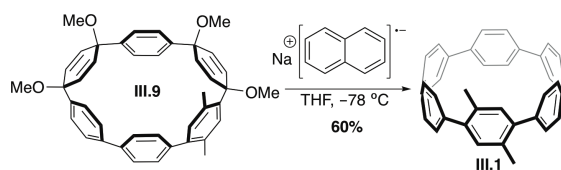




Dioxane (22 mL) was sparged with N<sub>2</sub> for 1 hour. Dichloride **III.7** (3.00 g, 4.41 mmole, 1.00 equiv), dry potassium phosphate (7.49 g, 35.3 mmole, 8.00 equiv), bis(pinacolato)diboron (8.97 g, 35.3 mmole, 8.00 equiv), palladium (II) acetate (297 mg, 0.441 mmole, 0.100 equiv) and 2-dicyclohexylphosphino-2',6'-dimethoxybiphenyl (452 mg, 1.10 mmole, 0.250 equiv) were added to a round bottom flask. The flask was evacuated and backfilled with N<sub>2</sub> (5 x). The flask was capped with a septum and purged with N<sub>2</sub> for 30 minutes. The sparged dioxane was added to the flask via cannula and the reaction mixture was stirred in an 80°C oil bath for 18 hours. The mixture was cooled to room temperature and filtered over celite. The filtrate was extracted with dichloromethane (3 x 100 mL) and the combined organic layers were rinsed with denionized water (3 x 100 mL), brine (1 x 100 mL), dried over sodium sulfate and concentrated under reduced pressure to give a black solid. The product was purified via silica gel column chromatography (5% to 20% ethyl acetate in hexanes) to give **III.8** as a white solid that crystallizes upon standing in hexanes (3.63 g, 91%). <sup>1</sup>H NMR (400 MHz, CDCl<sub>3</sub>): δ 7.84 (d, *J* = 7.8 Hz, 2H), 7.73 (d, *J* = 8.1 Hz, 2H), 7.38 (d, *J* = 8.1 Hz, 2H), 7.34-7.29 (overlap, 6H), 7.07 (s, 1H), 7.06 (s, 1H), 6.38 (d, *J* = 10 Hz, 2H), 6.08 (d, *J* = 10 Hz, 2H), 6.05 (s, 4H), 3.44 (s, 3H), 3.41 (s, 3H), 3.40 (s, 3H), 3.39 (s, 3H), 2.60 (s, 3H), 2.11 (s, 3H), 1.36 (s, 12H), 1.31 (s, 12H). <sup>13</sup>C NMR (100 MHz, CDCl<sub>3</sub>): δ 146.63, 144.69, 142.74, 142.68, 141.05, 139.16, 135.09, 134.69, 134.45, 134.40, 133.57, 133.48, 133.36, 132.45, 132.20, 129.67, 128.78, 126.23, 126.08, 125.44, 83.95, 76.35, 75.09, 74.80, 74.74, 52.14, 52.13, 51.54, 51.53, 25.09, 25.05, 21.30, 20.09.

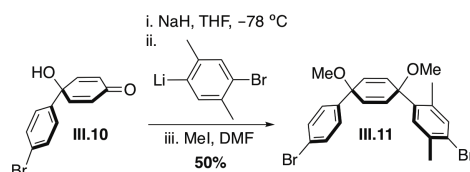


Bisboronate **III.8** (100 mg, 0.115 mmole, 1.00 equiv), boronic acid (35.8 mg, 0.580 mmole, 5.00 equiv), bis(thiophenylphosphine)palladium(II) dichloride (16.3 mg, 0.0232 mmole, 0.200 equiv) and potassium fluoride (6.73 mg, 0.116 mmole, 1.00 equiv) were dissolved in THF (150 mL) in a round bottom flask and the flask was placed into a 40°C oil bath. Deionized water (30 mL) was added to the mixture and the reaction was stirred open to air for 2 hours. The mixture was cooled to room temperature and filtered over celite. The filtrate was extracted with dichloromethane (3 x 50 mL) and the combined organic layers were washed with deionized water (3 x 50 mL) and brine (1 x 50 mL), dried over sodium sulfate and concentrated under reduced pressure to give a brown oil. The product was purified via silica gel column chromatography (25% ethyl acetate in hexanes) to give **III.9** as a white solid (28.5 mg, 40%). <sup>1</sup>H NMR (600 MHz, CDCl<sub>3</sub>): δ 7.47 (d, *J* = 8.7 Hz, 2H), 7.34 (d, *J* = 8.6 Hz, 2H), 7.32 (d, *J* = 8.7 Hz, 2H), 7.22 (d, *J* = 8.6 Hz, 2H), 7.12 (s, 1H), 7.04 (s, 1H), 6.80 (d, *J* = 8.5 Hz, 2H), 6.75 (d, *J* = 8.5 Hz, 2H), 6.34 (d, *J* = 10 Hz, 2H), 6.29 (d, *J* = 10 Hz, 2H), 5.73 (d, *J* = 10 Hz, 2H), 5.68 (d, *J* = 10 Hz, 2H), 3.44 (s, 3H), 3.44 (s, 3H), 3.29 (s, 3H), 3.29 (s, 3H), 2.46 (s, 3H), 1.98 (s, 3H). <sup>13</sup>C NMR (150 MHz, CDCl<sub>3</sub>): δ 142.94, 142.81, 142.14, 141.05, 140.18, 139.85, 139.22, 138.91, 134.65, 133.76, 133.67, 133.29, 132.84, 132.19, 132.05, 131.96, 130.93, 128.50, 128.28, 127.01, 125.84, 125.83, 76.39, 74.25, 74.08, 52.84, 52.17, 51.35, 51.33, 22.01, 21.32.



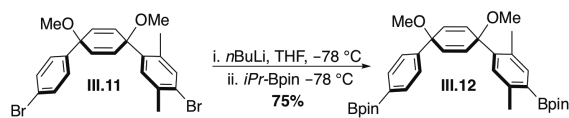
Macrocycle **III.9** (120 mg, 0.197 mmole, 1.00 equiv) was dissolved in THF (10 mL) and cooled to -78°C for 30 minutes. Sodium naphthalenide in THF (1 M, 7.90 mL, 1.97 mmole, 10.0 eq) was added dropwise to the solution of **III.9** and the reaction was stirred

for 30 minutes. The reaction was quenched with a 1M solution of iodine in THF (4 mL) and the reaction was warmed to room temperature. After the addition of saturated sodium thiosulfate (10 mL) the reaction was diluted with dichloromethane (50 mL). The reaction mixture was washed with deionized (3 x 25 mL) and brine (1 x 25 mL), dried over sodium sulfate and concentrated under reduced pressure to give a red-orange solid. The product was purified via silica gel column chromatography (0% to 20% dichloromethane/hexanes) to give **III.1** as a red-orange solid (54.2 mg, 60%). <sup>1</sup>H NMR (600 MHz, CDCl<sub>3</sub>): δ 7.57 (d, *J* = 8.0 Hz, 2H), 7.56-7.55 (overlap, 6H), 7.45 (d, *J* = 8.6 Hz, 4H), 7.41 (d, *J* = 8.5 Hz, 4H), 7.39 (d, *J* = 8.6 Hz, 4H), 7.14 (s, 2H), 2.52 (s, 3H). <sup>13</sup>C NMR (150 MHz, CDCl<sub>3</sub>): δ 137.83, 137.11, 136.79, 136.57, 135.55, 135.53, 132.68, 132.14, 127.92, 127.25, 127.16, 22.03.

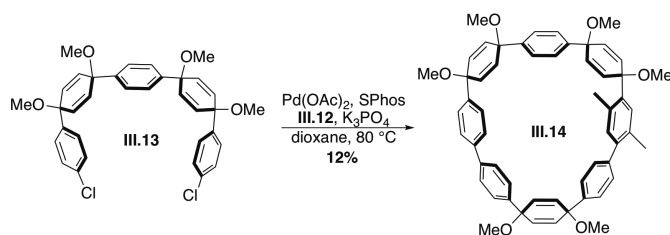


Sodium hydride (3.94 g, 98.5 mmole, 1.30 equiv) was suspended in THF (197 mL) and cooled to  $-78^{\circ}\text{C}$  for 1 hour. In a separated flask 2,5-dibromo-1,4-dimethylbenzene (43.6 g, 167 mmole, 2.20 equiv) was dissolved in THF (334 mL) and cooled to  $-78^{\circ}\text{C}$  for 1 hour. *n*BuLi (2.4 M in hexanes, 67.0 mL, 167 mmole, 2.20 equiv) was added to a separate flask and cooled to  $-78^{\circ}\text{C}$  for 30 minutes. In a separate flask bromoketone **III.10** (20.0 g, 75.8 mmole, 1.00 equiv) was dissolved in THF (151 mL) and cannulated into the sodium hydride slurry dropwise. The resulting mixture was stirred at  $-78^{\circ}\text{C}$  1 hour. The *n*BuLi was cannulated into the solution of 2,5-dibromo-1,4-dimethylbenzene dropwise to form a white precipitate. The reaction was stirred for 30 minutes at  $-78^{\circ}\text{C}$ . The lithiated 2,5-dibromo-1,4-dimethylbenzene was cannulated into the solution of deprotonated **III.10** and the mixture was stirred at  $-78^{\circ}\text{C}$  for 1.5 hours. DMF (87 mL) and methyl iodide (19.0 mL, 303 mmole, 4.00 equiv) was added to the mixture and the reaction was warmed to room temperature. The warmed solution was stirred at room temperature for 48 hours. The product was extracted with ethyl acetate (3 x 150 mL) and the combined organic layers were washed with a 5% solution of lithium chloride in deionized water (5 x 75 mL), deionized water (3 x 100 mL) and brine (1 x 100 mL), dried

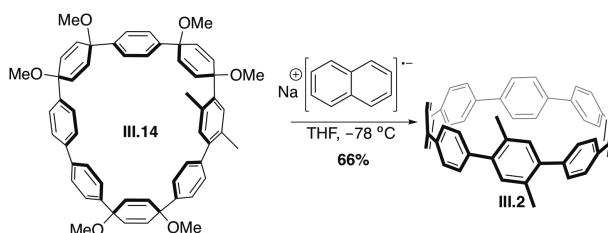
over sodium sulfate and concentrated under reduced pressure to give a light yellow solid. The solid was recrystallized in hexanes to give **III.11** as an off white solid (22.0 g, 50%). <sup>1</sup>H NMR (600 MHz, CDCl<sub>3</sub>): δ 7.37 (d, *J* = 8.6 Hz, 2H), 7.37 (s, 1H), 7.17 (d, *J* = 8.6 Hz, 2H), 6.96 (s, 1H), 6.31 (d, *J* = 10 Hz, 2H), 6.02 (d, *J* = 10, Hz, 2H), 3.41 (s, 3H), 3.35 (s, 3H), 2.55 (s 3H), 2.23 (s, 3H). <sup>13</sup>C NMR (150 MHz, CDCl<sub>3</sub>): δ 142.18, 139.20, 136.73, 136.45, 134.95, 133.54, 132.19, 131.47, 129.78, 127.88, 124.15, 121.69, 76.18, 74.64, 52.17, 51.55, 22.34, 21.01.



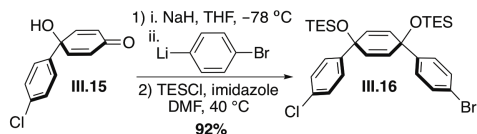
Dibromide **III.11** (20.0 g, 41.8 mmole, 1.00 equiv) was dissolved in THF (210 mL) and cooled to  $-78^{\circ}\text{C}$  for 1 hour. *n*BuLi (2.5 M in hexanes, 36.8 mL, 92.0 mmole, 2.20 eq) was added to a separate round bottom flask and cooled to  $-78^{\circ}\text{C}$  for 30 minutes. The *n*BuLi was then cannulated into the solution of **III.11**. 2-isopropoxy-4,4,5,5-tetramethyl-1,3,2-dioxaborolane (34.0 mL, 167.0 mmole, 4.00 eq) was added to the flask immediately afterward and the mixture was stirred  $-78^{\circ}\text{C}$  for 30 minutes. The reaction was quenched with the addition of deionized water (100 mL) and the mixture was warmed to room temperature. The product was extracted with ethyl acetate (3 x 150 mL) and the combined organic layers were washed with deionized water (3 x 100 mL) and brine (1 x 100 mL), dried over sodium sulfate and concentrated under reduced pressure to give an off-white solid. The solid was rinsed with hexanes to give **III.12** as a white solid (18.0 g, 75%). <sup>1</sup>H NMR (600 MHz, CDCl<sub>3</sub>): δ 7.73 (d, *J* = 8.2 Hz, 2H), 7.61 (s, 1H), 7.37 (d, *J* = 8.2 Hz, 2H), 7.05 (s, 1H), 6.37 (d, *J* = 10 Hz, 2H), 6.04 (d, *J* = 10 Hz, 2H), 3.45 (s, 3H), 3.38 (s, 3H), 2.60 (s, 3H), 2.44 (s, 3H), 1.37 (s, 12H), 1.35 (s, 12H). <sup>13</sup>C NMR (151 MHz, CDCl<sub>3</sub>): δ 146.45, 142.45, 142.41, 140.58, 134.96, 133.27, 133.20, 132.07, 129.19, 125.43, 83.91, 83.59, 76.47, 75.08, 52.08, 51.44, 25.11, 25.05, 21.89, 21.10.



Dioxane (580 mL) and deionized water (83 mL) were sparged with N<sub>2</sub> for 1 hour. Dibpin **III.12** (1.19 g, 2.09 mmole, 1.20 equiv), Dichloride **III.13** (1.00 g, 1.74 mmole, 1.00 equiv), palladium(II) acetate (81.9 mg, 0.122 mmole, 0.0700 equiv), 2-dicyclohexylphosphino-2',6'-dimethoxybiphenyl (285 mg, 0.695 mmole, 0.400 equiv) and potassium phosphate (736 mg, 3.48 mmole, 2.00 equiv) were added to a round bottom flask. The flask was evacuated and backfilled with N<sub>2</sub> (5 x). The flask was capped with a septum and purged with N<sub>2</sub> for 30 minutes. The sparged dioxane was added to the flask via cannula and the flask was placed in an 80 °C oil bath. The sparged deionized water was added to the flask via cannula and the mixture was stirred at this temperature for 18 hours. The mixture was cooled to room temperature and filtered over celite. The product was extracted with dichloromethane (3 x 100 mL) and the combined organic layers were washed with deionized water (3 x 100 mL) and brine (1 x 100 mL), dried over sodium sulfate and concentrated under reduced pressure to give a black solid. The product was purified via silica gel chromatography (25% ethyl acetate in hexanes) to give **III.14** as a white solid (200 mg, 12%). <sup>1</sup>H NMR (600 MHz, CDCl<sub>3</sub>): δ 7.54 (s, 4H), 7.47 (d, *J* = 3.4 Hz), 7.46 (d, *J* = 2.2, Hz), 7.32 (d, *J* = 8.4 Hz, 2H), 7.21 (d, *J* = 8.3 Hz, 2H), 7.10 (d, *J* = 8.4 Hz, 2H), 7.01 (s, 1H), 6.57 (s, 1H), 6.51 (d, *J* = 10.2 Hz, 2H), 6.23 (d, *J* = 10.2 Hz, 2H), 6.15 (d, *J* = 7.5 Hz, 2H), 6.13 (d, *J* = 7.5 Hz, 2H), 6.07 (d, *J* = 10 Hz, 2H), 6.03 (d, *J* = 10.2 Hz, 2H), 3.48 (s, 3H), 3.47 (s, 3H), 3.44 (s, 3H), 3.42 (s, 3H), 3.41 (s, 3H), 3.41 (s, 3H), 2.64 (s, 3H), 1.79 (s, 3H). <sup>13</sup>C NMR (150 MHz, CDCl<sub>3</sub>): δ 143.42, 143.37, 142.78, 142.17, 140.64, 140.60, 140.10, 139.79, 139.50, 136.54, 134.24, 133.90, 133.62, 133.44, 133.32, 132.85, 132.83, 132.42, 131.56, 130.56, 128.95, 127.01, 126.68, 126.39, 126.36, 126.28, 126.27, 125.52, 77.66, 76.03, 74.66, 74.61, 74.18, 74.16, 52.13, 52.13, 52.08, 51.89, 51.88, 51.66, 51.66, 20.78, 19.80.



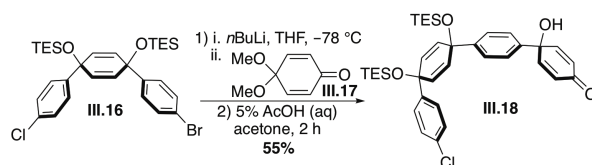
Macrocycle **III.14** (160 mg, 0.194 mmole, 1.00 equiv) was dissolved in THF (9.73 mL) and cooled to  $-78^{\circ}\text{C}$  for 30 minutes. Sodium naphthalenide in THF (0.5 M, 7.00 mL, 4.86 mmole, 25.0 equiv) was added dropwise to the solution of **III.14** and the reaction was stirred for 1 hour. The reaction was quenched with a 1M solution of iodine in THF (10 mL) and the reaction was warmed to room temperature. After the addition of saturated sodium thiosulfate (15 mL) the reaction was diluted with dichloromethane (50 mL). The reaction mixture was washed with deionized (3 x 25 mL) and brine (1 x 25 mL), dried over sodium sulfate and concentrated under reduced pressure to give a yellow solid. The product was purified via silica gel column chromatography (0% to 100% dichloromethane in hexanes) to give **III.2** as a yellow solid (82.1 mg, 67%).  $^1\text{H}$  NMR (600 MHz,  $\text{CDCl}_3$ ):  $\delta$  7.57 (d,  $J = 8.8$  Hz, 4H), 7.55 (d,  $J = 8.8$  Hz, 4H), 7.49 (d,  $J = 8.6$  Hz, 4H), 7.49 (s, 4H), 7.47 (d,  $J = 8.8$  Hz, 4H), 7.41 (dd,  $J = 8.6, 1.7$  Hz, 4H), 7.28 (d,  $J = 8.8$  Hz), 6.96 (s, 2H), 2.31 (s, 6H).  $^{13}\text{C}$  NMR (151 MHz,  $\text{CDCl}_3$ ):  $\delta$  139.84, 139.44, 138.89, 138.65, 138.10, 137.98, 137.74, 137.64, 133.11, 133.03, 130.62, 128.11, 127.76, 127.74, 127.54, 127.53, 127.34, 21.01.



Chloroketone **III.15** (8.50 g, 38.7 mmole, 1.00 equiv) was dissolved in THF (155 mL) and cooled to  $-78^{\circ}\text{C}$  for 1 hour. Sodium hydride (1.86 mg, 46.4 mmole, 1.20 equiv) was added to the solution of **III.15** and the reaction was stirred for 2 hours. In a separated flask 1,4-dibromobenzene (20.1 g, 85.1 mmole, 2.20 equiv) was dissolved in THF (284 mL) and cooled to  $-78^{\circ}\text{C}$  for 1 hour.  $n\text{BuLi}$  (2.3 M in hexanes, 37 mL, 85.1 mmole, 2.20 equiv) was added to a separate flask and cooled to  $-78^{\circ}\text{C}$  for 30 minutes. The  $n\text{BuLi}$  was cannulated into the solution of 1,4-dibromobenzene dropwise to form a white precipitate. The reaction was stirred for 30 minutes at  $-78^{\circ}\text{C}$ . The lithiated 1,4-dibromobenzene was

cannulated into the solution of deprotonated **III.15** and the mixture was stirred at  $-78^{\circ}\text{C}$  for 1.5 hours. The reaction was quenched with deionized water (50 mL) and warmed to room temperature. The product was extracted with ethyl acetate (3 x 100 mL) and the combined organic layers were washed deionized water (3 x 100 mL) and brine (1 x 100 mL), dried over sodium sulfate and concentrated under reduced pressure to give a brown oil.

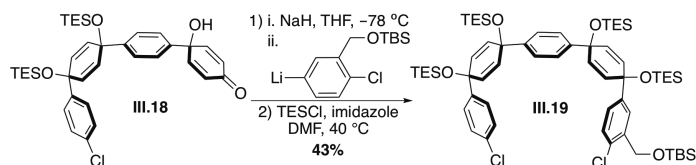
Imidazole (10.6 g, 155 mmole, 4.00 equiv) was added to a round bottom flask and the flask was purged under nitrogen. The crude brown oil was diluted with DMF (105 mL) and added to the reaction flask with imidazole. The flask contained the crude brown oil was rinsed further (3 x 30 mL) with each rinse being added to the reaction flask adding a total of 195 mL of DMF to the reaction mixture. Chlorotriethylsilane (19.5 mL, 116 mmole, 3.00 equiv) was added to the reaction mixture dropwise and the flask was placed in a  $40^{\circ}\text{C}$  oil bath and was stirred at this temperature for 18 hours. The reaction was cooled to room temperature and quenched with a saturated solution of sodium bicarbonate in deionized water (150 mL). The product was extracted with ethyl acetate (3 x 200 mL) and the combined organic layers were washed with deionized water (2 x 200 mL) and brine (1 x 200 mL), dried over sodium sulfate and concentrated under reduced pressure to give a yellow oil. The product was purified via silica gel column chromatography (5% ethyl acetate in hexanes) to give **III.16** as a clear oil that crystallized to a white solid upon standing (22 g, 92%).  $^1\text{H}$  NMR (500 MHz,  $\text{CDCl}_3$ ):  $\delta$  7.38 (d,  $J = 8.6$  Hz, 2H), 7.23 (s, 4H), 7.17 (d,  $J = 8.6$  Hz, 2H), 5.95 (s, 4H), 0.93 (t,  $J = 7.9$  Hz, 9H), 0.92 (t,  $J = 7.9$  Hz, 9H), 0.62-0.57 (overlap, 16H).  $^{13}\text{C}$  NMR (125 MHz,  $\text{CDCl}_3$ ) 145.12, 144.56, 133.26, 131.61, 131.52, 131.40, 128.45, 127.75, 127.39, 121.44, 71.25, 71.18, 7.15, 6.55.



Compound **III.16** (20.0 g, 34.0 mmole, 1.00 equiv) was dissolved in THF (110 mL) and cooled to  $-78^{\circ}\text{C}$  for 30 minutes. *n*BuLi (2.3 M in hexanes, 17.2 mL, 39.6 mmole, 1.20 equiv) was added dropwise to the solution and the mixture was stirred for 30 minutes. Ketal **III.17** (6.93 mL, 49.5 mmole, 1.50 equiv) was added to the mixture dropwise to the mixture and the reaction was stirred for 1.5 hours at this temperature. The reaction was quenched with the addition of deionized water (100 mL) and warmed to room temperature. The product was extracted with ethyl acetate (3 x 100 mL) and the combined organic layers were washed with deionized water (2 x 150 mL) and brine (1 x 150 mL), dried over sodium sulfate and concentrated under reduced pressure to give a brown-red oil.

The oil was diluted with a minimum amount of acetone (100 mL). An equal amount of 5% acetic acid in deionized water (100 mL) was added to the mixture and the reaction was stirred for 1 hour at room temperature. The mixture was quenched with the addition of a saturated solution of sodium bicarbonate in water (50 mL) and the product was extracted with ethyl acetate (3 x 100 mL). The combined organic layers were washed with a saturated solution of sodium bicarbonate (1 x 100 mL), deionized water (2 x 100 mL) and brine (1 x 100 mL), dried over sodium sulfate and concentrated to give a brown oil. The product was purified via silica gel column chromatography (20% ethyl acetate in hexanes) to give an orange oil. When diluted with hexanes pure **III.18** precipitates as an off white solid (11.6 g, 55%).  $^1\text{H}$  NMR (600 MHz,  $\text{CDCl}_3$ ):  $\delta$  7.37 (d,  $J = 8.5$  Hz, 2H), 7.32 (d,  $J = 8.5$  Hz, 2H), 7.27 (d,  $J = 8.7$  Hz, 2H), 7.24 (d,  $J = 8.6$  Hz, 2H), 6.88 (d,  $J = 10$  Hz, 2H), 6.23 (d,  $J = 10$  Hz, 2H), 5.97 (d,  $J = 10$  Hz, 2H), 5.95 (d,  $J = 10$  Hz, 2H), 0.94-0.90 (overlap, 18H), 0.61 (q,  $J = 7.9$  Hz, 6H), 0.58 (q,  $J = 7.9$  Hz, 6H).  $^{13}\text{C}$  NMR (150 MHz,  $\text{CDCl}_3$ ):  $\delta$  185.75, 150.71, 146.54, 144.80, 137.86, 133.31, 131.81, 131.49, 128.52, 127.49, 127.19, 126.57, 125.35, 71.41, 71.18, 71.15, 7.23, 6.62.

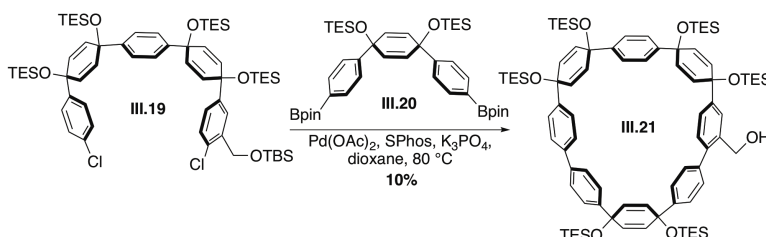




Chloroketone **III.18** (10.0 g, 15.7 mmole, 1.00 equiv) was dissolved in THF (63 mL) and cooled to  $-78^{\circ}\text{C}$  for 1 hour. Sodium hydride (756 mg, 18.9 mmole, 1.20 equiv) was added to the solution of **III.18** and the reaction was stirred for 2 hours. In a separated flask, *tert*-butyldimethylsilyl protected benzylic alcohol **III.22** (11.6 mg, 34.6 mmole, 2.20 equiv) was dissolved in THF (115 mL) and cooled to  $-78^{\circ}\text{C}$  for 1 hour. *n*BuLi (2.5 M in hexanes, 14.0 mL, 34.6 mmole, 2.20 equiv) was added the solution of **III.22** dropwise to form and the reaction was stirred for 30 minuets at  $-78^{\circ}\text{C}$ . The lithiated **III.22** was cannulated into the solution of deprotonated **III.18** and the mixture was stirred at  $-78^{\circ}\text{C}$  for 1.5 hours. The reaction was quenched with deionized water (100 mL) and warmed to room temperature. The product was extracted with ethyl acetate (3 x 100 mL) and the combined organic layers were washed deionized water (3 x 100 mL) and brine (1 x 100 mL), dried over sodium sulfate and concentrated under reduced pressure to give a yellow-brown oil.

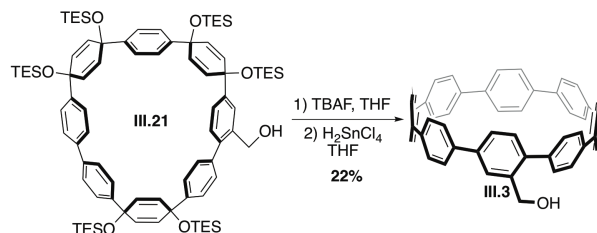
Imidazole (4.29 mg, 63.0 mmole, 4.00 equiv) was added to a round bottom flask and the flask was purged under nitrogen. The crude brown oil was diluted with DMF (50 mL) and added to the reaction flask with imidazole. The flask contained the crude brown oil was rinsed further (3 x 10 mL) with each rinse being added to the reaction flask adding a total of 80 mL of DMF to the reaction mixture. Triethylsilane chloride (7.93 mL, 47.2 mmole, 3.00 equiv) was added to the reaction mixture dropwise and the flask was placed in a  $40^{\circ}\text{C}$  oil bath and was stirred at this temperature for 18 hours. The reaction was cooled to room temperature and quenched with a saturated solution of sodium bicarbonate in deionized water (100 mL). The product was extracted with ethyl acetate (3 x 150 mL) and the combined organic layers were washed with deionized water (2 x 150 mL), a 5% LiCl solution in deionized water (4 x 75 mL) and brine (1 x 150 mL), dried over sodium sulfate and concentrated under reduced pressure to give a yellow oil. The product was purified via silica gel column chromatography (0% to 20% ethyl acetate in hexanes) to give **III.19** as a yellow oil that crystallizes to a yellow solid upon standing

(7.65 g, 43%).  $^1\text{H}$  NMR (600 MHz,  $\text{CDCl}_3$ ):  $\delta$  7.81 (s, 1H), 7.23-7.21 (overlap, 5H), 7.19 (d,  $J = 8.5$  Hz, 2H), 7.10 (d,  $J = 8.3$  Hz, 1H), 6.89 (d,  $J = 8.3$  Hz, 1H), 5.98 (d,  $J = 10$  Hz, 4H), 5.95 (d,  $J = 10$  Hz, 2H), 5.89 (d,  $J = 9.8$ , 2H), 4.76 (s, 2H), 0.94-0.89 (overlap, 45H) 0.63-0.54 (overlap, 24H), 0.10 (s).  $^{13}\text{C}$  NMR (150 MHz,  $\text{CDCl}_3$ ):  $\delta$  145.21, 145.03, 144.99, 144.87, 138.85, 133.12, 131.98, 131.85, 131.45, 131.27, 130.37, 128.38, 128.37, 127.46, 125.88, 125.85, 125.53, 125.48, 71.42, 71.37, 71.36, 62.68, 53.64, 26.18, 18.63, 7.28, 7.26, 7.25, 6.67, 6.66, 6.62, 6.60, 0.22, -5.12.



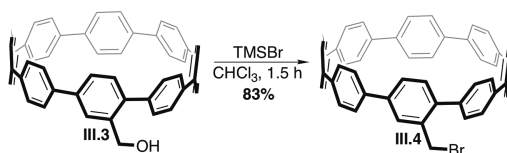
Dioxane (450 mL) and deionized water (67 mL) were sparged with  $\text{N}_2$  for 1 hour. Bisboronate **III.20** (1.20 g, 1.61 mmole, 1.20 equiv), dichloride **III.19** (1.51 g, 1.34 mmole, 1.00 equiv), palladium(II) acetate (63.3 mg, 0.0940 mmole, 0.07 equiv), 2-dicyclohexylphosphino-2',6'-dimethoxybiphenyl (220 mg, 0.537 mmole, 0.4 equiv) and potassium phosphate (596 mg, 2.69 mmole, 2.00 equiv) were added to a round bottom flask. The flask was evacuated and backfilled with  $\text{N}_2$  (5 x). The flask was capped with a septum and purged with  $\text{N}_2$  for 30 minutes. The sparged dioxane was added to the flask via cannula and the flask was placed in an  $80^\circ\text{C}$  oil bath. The spared deionized water was added to the flask via cannula and the mixture was stirred at this temperature for 18 hours. The mixture was cooled to room temperature and filtered over celite. The product was extracted with dichloromethane (3 x 100 mL) and the combined organic layers were washed with deionized water (3 x 100 mL) and brine (1 x 100 mL), dried over sodium sulfate and concentrated under reduced pressure to give a black solid. The product was purified via silica gel chromatography (2% to 5% ethyl acetate in hexanes) to give a white solid. The solid was rinsed with acetone to give **III.21** as a white solid (192 mg, 10%).  $^1\text{H}$  NMR (600 MHz,  $\text{CDCl}_3$ ):  $\delta$ (ppm) 7.50-7.46 (overlap, 6H), 7.45 (s, 1H), 7.44 (d,  $J = 7.9$  Hz, 1H), 7.39 (d,  $J = 8.4$ , 2H), 7.34 (d,  $J = 8.4$  Hz, 2H), 7.19 (d,  $J = 7.8$  Hz, 1H), 7.19 (d,  $J = 8.3$  Hz, 2H), 7.14 (d,  $J = 8.4$  Hz, 2H), 7.05 (d,  $J = 8.3$ , 2H), 6.19 (d,  $J = 10.0$  Hz, 2H), 6.08 (d,  $J = 10.0$  Hz, 2H), 6.07 (d,  $J = 10.2$  Hz, 2H), 6.05 (d,  $J = 10.0$  Hz,

2H), 5.93 (d,  $J = 10.2$  Hz, 2H), 5.91 (d,  $J = 10.0$  Hz, 2H), 4.60 (d,  $J = 6.1$  Hz, 2H), 1.36, (t,  $J = 6.1$  Hz, 1H), 1.01-0.91 (overlap, 54H), 0.74-0.62 (overlap, 24H), 0.54 (d,  $J = 7.7$  Hz, 12H).



Macrocycle **III.21** (300 mg, 0.1404 mmole, 1.00 equiv) was dissolved in THF (1.40 mL). Tetra-*n*-butylammonium fluoride (1 M in THF, 1.00 mL, 1.00 mmole, 7.00 equiv) was added dropwise to the solution of **III.21** at room temperature and the reaction was stirred for 2 hours. The reaction was quenched with deionized water and the THF was evaporated under reduced pressure. The resulting solid product was filtered and rinsed with dichloromethane (2 x 10 mL) and deionized water (2 x 10 mL) to give the deprotected macrocycle as an off white solid that was carried on crude to the aromatization reaction

A 0.04M solution of  $\text{H}_2\text{SnCl}_4$  was prepared by stirring tin(II) dichloride dihydrate (180 mg, 0.798 mmole, 1.00 equiv) was dissolved in THF (20.0 mL) with HCl (12 M, 0.130 mL, 1.56 mmole, 1.95 equiv) for 30 minutes. In a separate flask, the deprotected macrocycle (104 mg, 0.1404 mmole, 1.00 equiv) was added to the round bottom flask and suspended in THF (11.7 mL). The solution of  $\text{H}_2\text{SnCl}_4$  (0.04 M, 11.6 mL, 0.463 mmol, 3.30 equiv.) was added to the flask and the reaction was stirred for 30 minutes. The mixture was quenched with a solution of saturated sodium bicarbonate in deionized water (10 mL) and the product was extracted with dichloromethane (3 x 20 mL) and the combined organic layers were rinsed with deionized water (2 x 20 mL), brine (1 x 20 mL) dried over sodium sulfate and concentrated to give a green-yellow solid. The product was purified via column chromatography (100% dichloromethane) to give **III.3** as a yellow-green solid (19.6 mg, 22%).  $^1\text{H}$  NMR (500 MHz,  $\text{CDCl}_3$ ):  $\delta$  7.87 (d,  $J = 2.0$  Hz, 1H), 7.56-7.44 (overlap, 24H), 7.40 (d,  $J = 8.4$  Hz, 2H), 7.32 (d,  $J = 8.6$  Hz, 2H), 7.05 (dd,  $J = 8.4, 2.0$  Hz, 1H), 6.89 (d,  $J = 8.4$  Hz, 1H), 5.05 (s, 2H), 3.67 (brs, 1H).



Nanohoop **III.3** (65.1 mg, 0.102 mmole, 1.00 equiv) was dissolved in chloroform (20.2 mL). To this solution was added bromotrimethylsilane (20.2  $\mu$ L, 0.153 mmole, 1.50 equiv) and the reaction was stirred for 1.5 hours. The reaction was quenched with the addition of a solution of saturated sodium bicarbonate in deionized water (10 mL) and the product was extracted with dichloromethane (3 x 20 mL) and the combined organic layers were rinsed with deionized water (2 x 20 mL), brine (1 x 20 mL) dried over sodium sulfate and concentrated to give a pure **III.4** as a yellow-green solid (59.4 mg, 83%).  $^1\text{H}$  NMR (500 MHz,  $\text{CDCl}_3$ ):  $\delta$  7.89 (d,  $J$  = 2.0 Hz, 1H), 7.55 (d,  $J$  = 8.9 Hz, 2H), 7.53-7.50 (overlap, 6H), 7.48 (d,  $J$  = 6.4 Hz, 4H), 7.47-7.46 (overlap, 8H), 7.43 (d,  $J$  = 8.9 Hz, 2H), 7.41 (d,  $J$  = 8.3 Hz, 4H), 7.38 (d,  $J$  = 8.9 Hz, 2H), 6.97 (dd,  $J$  = 8.5, 2.0 Hz, 1H), 6.79 (d,  $J$  = 8.4 Hz, 1H), 4.89 (s, 2H).  $^{13}\text{C}$  NMR (125 MHz,  $\text{CDCl}_3$ ):  $\delta$  139.60, 139.30, 139.01, 138.48, 138.12, 137.99, 137.97, 137.95, 137.93, 137.88, 137.61, 137.47, 134.60, 133.51, 130.84, 129.48, 128.31, 128.05, 127.86, 127.69, 127.66, 127.64, 127.55, 127.51, 127.49, 127.48, 33.00.

### 3.5. Bridge to Chapter IV

This chapter describes the development of nano hoops with functional groups that should facilitate the use of these molecules in materials science and biology. In the next chapter, we describe the synthesis of a nano hoop that is soluble in aqueous media through the manipulation of the benzyl alcohol functional group. The solubilized nano hoop enabled the first study of these compounds as a new class of fluorescent dyes as detailed in the next chapter.

## CHAPTER IV

### EXPANDING THE CHEMICAL SPACE OF BIOCOMPATIBLE FLUOROPHORES: NANOHOOPS IN CELLS

From White, B. M.; Zhao, Y.; Kawashima, T. E.; Branchaud, B. P.; Pluth, M. D.; Jasti, R. Expanding the chemical space of biocompatible fluorophores: Nanohoops in cells. *ACS Cent. Sci.* **2018**, *4*, 1173-1178.

<https://pubs.acs.org/doi/10.1021/acscentsci.8b00346>. Further permissions related to the use of the material excerpted in this chapter should be directed to the ACS. This manuscript was written by myself with editorial assistance from Professor Ramesh Jasti, Professor Michael D. Pluth and Professor Bruce P. Branchaud. Experimental work included in this chapter was performed by myself or with Dr. Yu Zhao and Taryn E. Kawashima under my direction. Experimental guidance was provided by Professor Ramesh Jasti and Professor Michael D. Pluth.

The design and optimization of fluorescent molecules has driven the ability to interrogate complex biological events in real time. Notably, most advances in bioimaging fluorophores are based on optimization of core structures that have been known for over a century. Recently, new synthetic methods have resulted in an explosion of nonplanar conjugated macrocyclic molecules with unique optical properties yet to be harnessed in a biological context. Herein we report the synthesis of the first aqueous-soluble carbon nanohoop (i.e., a macrocyclic slice of a carbon nanotube prepared via organic synthesis) and demonstrate its bioimaging capabilities in live cells. Moreover, we illustrate that these scaffolds can be easily modified by well-established “click” chemistry to enable targeted live cell imaging. This work establishes the nanohoops as an exciting new class of macrocyclic fluorophores poised for further development as novel bioimaging tools.

#### 4.1. Introduction

Fluorescent molecules have fueled the now widespread use of optical imaging to observe biological processes in living systems.<sup>1-3</sup> The power of such imaging methods

has led to increased interest in identifying new types of dyes, optically active materials, and nanoparticles that have enhanced photophysical properties suitable for multimodal, multiplexed, and super-resolution imaging.<sup>4-14</sup> Because fluorophores play such a critical role in understanding biological processes, it is somewhat surprising that most advances in small molecule dye technology today rely on structural modifications of scaffolds discovered over a century ago.<sup>15</sup> For example, the robust Janelia Fluor and some AlexaFluor dyes are structurally modified versions of rhodamine scaffolds discovered 130 years ago. Similarly, commercially available CyDyes, which have found widespread use as probes for targeted live cell imaging, are based off the cyanine core structure synthesized first in 1924 (**Figure 4.1**).<sup>7</sup> Clearly the modification of these core dye scaffolds is still yielding fruitful discoveries (e.g., Janelia Fluor 549),<sup>16, 17</sup> however, fundamentally new types of fluorophore scaffolds could offer advantageous photophysical properties for exploitation in biological contexts.<sup>18-21</sup> Inspired by this prospect, we report here the first biological studies demonstrating carbon nano hoops, short macrocyclic slices of carbon nanotubes prepared by organic synthesis, as exciting new biocompatible fluorophore scaffolds (**Figure 4.1**).

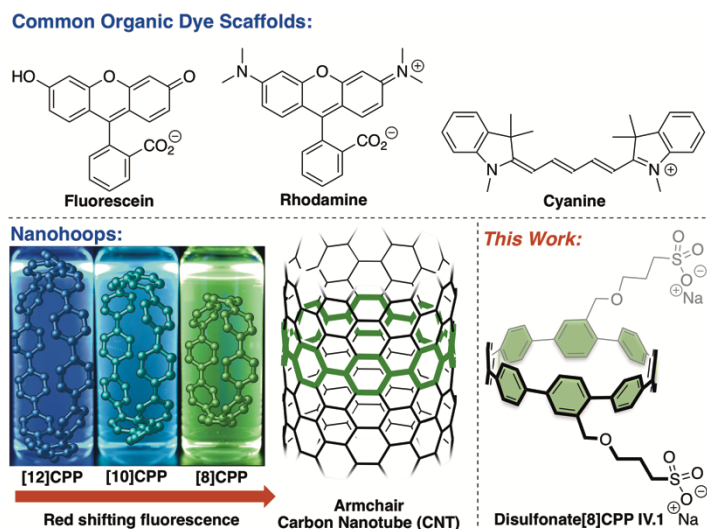


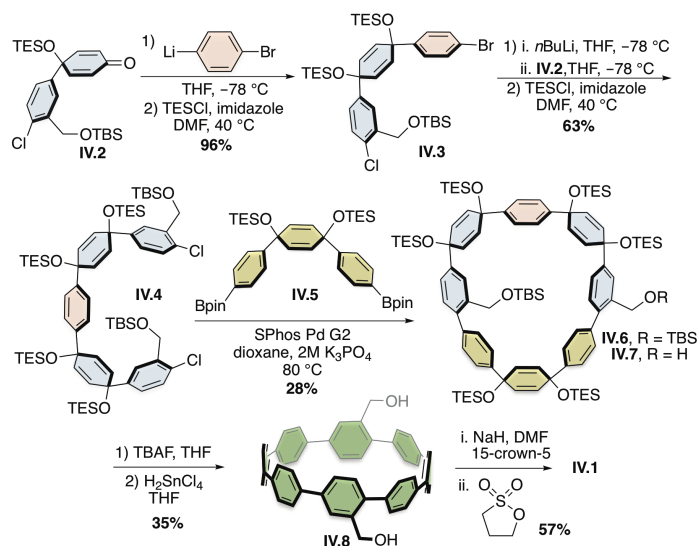
**Figure 4.1.** Traditional organic dye scaffolds and the new nanohoop fluorophore scaffold.

The [n]cycloparaphenylenes ([n]CPPs, n = number of benzene rings) are the smallest macrocyclic slices of carbon nanotubes (CNTs). These structures, coined “carbon nanohoops” due to their structural relationship to carbon nanotubes, were intensely pursued synthetic targets for over 70 years before finally succumbing to synthesis in 2008 (**Figure 4.1**).<sup>22-23</sup> Since then, the development of synthetic methods to prepare nanohoops has unveiled several unique, size-dependent photophysical properties that are a direct result of the radially oriented  $\pi$ -system of this unusual architecture.<sup>24-27</sup> First, the bending of the  $\pi$ -system increases delocalization around the hoop due to induction of a small amount of quinoidal character in these strained systems.<sup>28</sup> Second, the hoop architecture forces neighboring aromatic units to have smaller dihedral angles than in an acyclic oligomeric system due to conformational constraints of the macrocyclic geometry, again leading to increased conjugation.<sup>29</sup> These two factors together result in a size-dependent fluorescence emission ( $\lambda_{em}$ ) where the HOMO $\rightarrow$ LUMO gap narrows as nanohoop diameter decreases.<sup>30</sup> Additionally, due to Laporte forbidden HOMO $\rightarrow$ LUMO transitions, all nanohoops share a common absorption maxima ( $\lambda_{abs} = 340$  nm) with high absorption coefficients ( $\epsilon$ ) and large effective Stokes shifts ranging from 100 to 200 nm depending on size.<sup>31-34</sup> Taken together, the nanohoop scaffold offers the possibility of multiplexed imaging using a single excitation source. Moreover, the nonplanarity of the benzene rings in the nanohoop also leads to better solubility when compared to planar aromatic systems. Lastly, despite molecular strain, nanohoops are only reactive under forcing reaction conditions.<sup>35</sup> The inherent attributes provided by the nanohoop structure highlight their potential as new fluorophores for biological imaging. Despite this exciting proposition, to date, there are no reported biological investigations of these small molecular slices of carbon nanotubes. Herein for the first time we report a strategy to prepare an aqueous-soluble nanohoop (**IV.1**), demonstrate that the desirable optical properties of this scaffold are maintained in aqueous buffer and in live cells, and provide insights into the toxicity and permeability of the nanohoop. We also demonstrate that targeting groups can be easily appended to the nanohoop using copper catalyzed “click” chemistry. This study provides the foundation for the study of nanohoops and their derivatives as an exciting new class of biological imaging tools.

## 4.2. Results and Discussion

Numerous studies have documented the promise of carbon nanotubes as biological imaging agents.<sup>36</sup> Inspired by some of these works, we initially investigated the use of surfactant Pluronic F108 to solubilize the unfunctionalized nanohoops in aqueous media for biological studies—a strategy that has been successful for CNTs.<sup>37</sup> Although the solubility of the nanohoop increased in the presence of surfactant, cell imaging experiments were plagued by low signal response and aggregation (Experimental section, **Figure 4.5** and **Figure 4.6**). This complication prompted the synthesis of **IV.1** (**Figure 4.1**), a nanohoop functionalized with sulfonate groups to promote solubility in aqueous media. The synthesis of **IV.1** relies on the incorporation of alcohol functional groups into the nanohoop backbone for late stage manipulation (**Scheme 4.1**). The synthesis begins with the monolithiation of 1,4-dibromobenzene and subsequent nucleophilic addition into ketone **IV.2**, followed by protection of the resulting alcohol with triethylsilyl (TES) chloride to give **IV.3** (96% yield, dr: >20:1). Lithiation of **IV.3** followed by nucleophilic addition to a second equivalent of ketone **IV.2** and TES protection provided dichloride **IV.4** with two tert-butyl dimethylsilyl (TBS) protected benzyl alcohols as reactive handles. Suzuki-Miyaura cross-coupling of **IV.4** and diboronate **IV.5** gave macrocycles **IV.6** and **IV.7** in a 28% combined yield. Global deprotection of both macrocycles followed by H<sub>2</sub>SnCl<sub>4</sub>-promoted reductive aromatization provided benzyl alcohol[8]CPP **IV.8** in 35% yield.<sup>26</sup> Deprotonation of the benzyl alcohols with sodium hydride and treatment with 1,3-propanesultone delivered disulfonated[8]CPP (**IV.1**) in 57% yield. The building block synthesis outlined here and the oligomeric nature of the nanohoop scaffold should provide access to various sizes of nanohoops, each with unique fluorescent profiles, excited state lifetimes, and Raman signatures due to the size-dependent nature of these properties.<sup>29, 38-42</sup> This structural control is a hallmark of the bottom-up organic synthesis of graphitic materials.





**Scheme 4.1.** The synthesis of disulfonate[8]CPP.

Characterization of the nano hoop with  $^1\text{H}$  and  $^{13}\text{C}\{^1\text{H}\}$  NMR spectroscopy revealed spectra consistent with the expected structure of **IV.1**. Importantly, the nano hoop is completely soluble in DMSO with photophysical properties that are comparable to the parent nano hoop [8]CPP (**Figure 4.2a**). Of note, the installation of two sulfonates was sufficient to render this nano hoop aqueous-soluble, a result which is consistent with our findings that these nonplanar structures are much more soluble than flat aromatics. Importantly, the photophysical properties of **IV.1** are retained in aqueous media (PBS buffer with 0.1% SDS). Similar to [8]CPP, the absorption maximum for **IV.1** is at 328 nm with a large molar extinction coefficient of  $5.8 \times 10^4 \text{ M}^{-1}\text{cm}^{-1}$ . Upon excitation, we observe a bright green fluorescence ( $\lambda_{\text{em}} = 510 \text{ nm}$ ) with a quantum yield of 0.17 and a large effective Stokes shift of over 180 nm. This is in stark contrast to common fluorophores such as fluorescein that has a Stokes shift of 41 nm.<sup>43</sup> The fluorescence emission is insensitive to acidic or basic environments (pH = 3-11), which is again in contrast to many common fluorophores (e.g., fluorescein, **Figure 4.2c**). Taken together, these findings illustrate that the desirable absorption and emission properties of the nano hoop are not perturbed when the nano hoop scaffold is manipulated to prepare aqueous-soluble versions that can be used for biological studies.

To probe the cytotoxicity of the nano hoop, we treated live HeLa cells with 5, 10, 25, 50, and 100  $\mu\text{M}$  solutions of **IV.1** for 2 h. We then monitored cell death using WST-8 formazan reduction (Experimental section, **Figure 4.7**).<sup>44</sup> Nano hoop **IV.1** showed no cytotoxicity at working concentrations of  $\leq 10 \mu\text{M}$ . Instead, cell death was only observed at concentrations of 25  $\mu\text{M}$  and above or with longer incubation times (Experimental section, **Figure 4.8**). We note that more extensive studies of nano hoop toxicology as a function of size, composition, and even encapsulated molecules are warranted in the future. Related studies for other graphitic nanomaterials are often plagued by the inherent heterogeneity of those materials, again highlighting the advantage of the bottom-up synthetic approach for the nano hoops.<sup>36</sup>

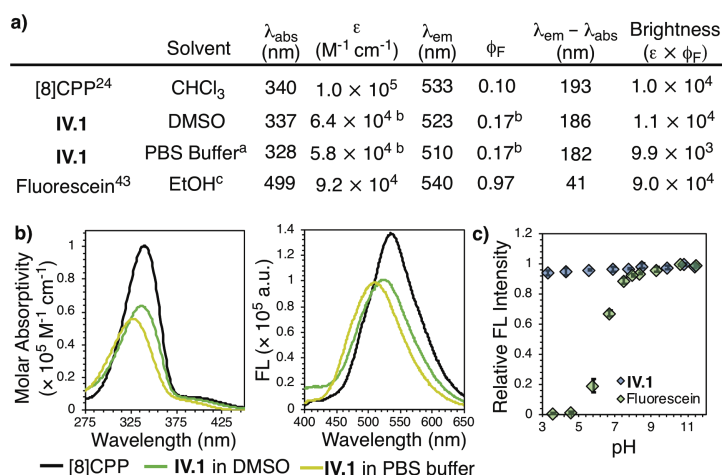


**Figure 4.2.** Characterization of disulfonate[8]CPP (**IV.1**). (a) Summary of nano hoop photophysical properties. (footnote a) Contains 0.1% SDS. (footnote b) Standard deviation is  $< 5\%$  of the measurement ( $n=3$ ). (footnote c) 0.01 M KOH in ethanol. (b)  $\lambda_{\text{ex}}$  and  $\lambda_{\text{em}}$  of 2  $\mu\text{M}$  solutions of [8]CPP (black), **IV.1** in DMSO (green), and **IV.1** in PBS buffer with 0.1% SDS (yellow). (c) pH vs fluorescence (FL) intensity of **IV.1** and fluorescein in a 1:1 MeOH:100 mM KCl, 100 mM KOH solution. Error bars represent standard deviation ( $n = 3$ ).

Next, using epifluorescence microscopy, we aimed to determine whether **IV.1** is cell permeable and whether the fluorescence of the nano hoop is sufficient to generate bright images in live cells. To test this, HeLa cells were treated with a 10  $\mu\text{M}$  solution of

**IV.1** in FBS free DMEM with 0.5% DMSO and the nuclear stain NucRed 647 for 1 h (**Figure 4.3**, E-H). Notably, after incubation and washing, bright green fluorescence from the nanohoop is clearly observed in the cells, which does not colocalize with the nuclear dye. Interestingly, the lack of localization of **IV.1** to specific cellular compartments is consistent with the previously reported localization of calixarenes in Chinese hamster ovary (CHO) cells.<sup>45</sup> Based on Pearson's correlation coefficients, we observe moderate colocalization to the cytosol (Celltracker Red CMTPX), and lower colocalization to the mitochondria (MitoTracker Red RM) and endoplasmic reticulum (ER-Tracker Red, Experimental section, **Figure 4.9** and **Table 4.2**).<sup>46</sup> In the absence of **IV.1** (**Figure 4.3**, A-D), no fluorescence was observed in the nanohoop channel confirming that the signal was not due to cellular autofluorescence. Additionally, no significant changes in cell morphology were observed through the differential interference contrast (DIC) channel after incubation with **IV.1**, confirming a low cytotoxicity of the nanohoop at this concentration.

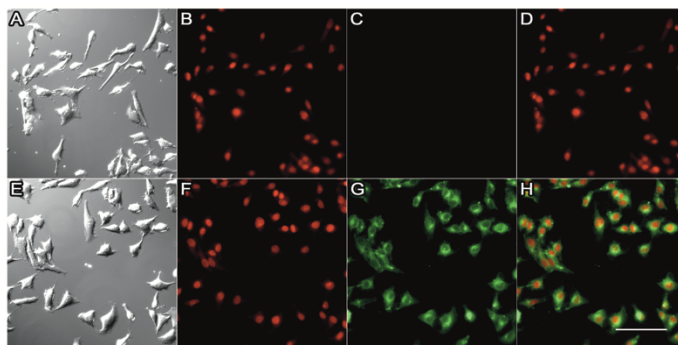


**Figure 4.3.** DIC and fluorescent images of live HeLa cells in the absence (A-D) or presence (E-H) of disulfonate[8]CPP (**IV.1**). (A,E) DIC; (B,F) NucRed live 647 imaged in CY5 channel; (C, G) **IV.1** imaged in DAPI-long-pass channel; and (D,H) merge of the CY5/DAPI-long-pass channel showing no significant colocalization. Scale bar = 100  $\mu\text{m}$ .

Encouraged by the robust imaging capabilities of **IV.1** in live cells we next sought to demonstrate the flexibility of this new fluorophore scaffold through the preparation of a “clickable” version of the nanohoop. We prepared azide[8]CPP **IV.9** using a scalable synthetic strategy similar to the methods described in **Scheme 4.1** (Experimental section).

In this case, we assumed the “clicked” moiety could provide the water solubility. To demonstrate the utility of azide **IV.9**, folate[8]CPP **IV.11** was synthesized using copper catalyzed azide-alkyne cycloaddition (**Figure 4.4a**). Folate receptors are known to be highly overexpressed on the surface of many cancer cells. Folic acid ( $K_D = 0.1$  nM) therefore can be an effective targeting group for imaging of cancer cells and even selective drug delivery.<sup>47, 48</sup>

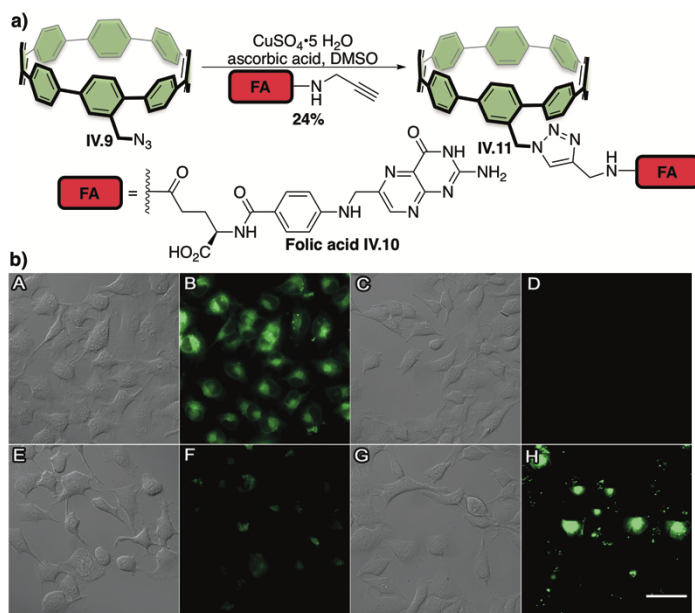


**Figure 4.4.** (a) Synthesis of folate-[8]CPP conjugate using copper catalyzed azide-alkyne click chemistry. (b) DIC and fluorescent images of live HeLa cells in the presence of **IV.11** (A, B, E, F) and absence of **IV.11** (C, D, G, H). As controls cells were treated with folic acid (E-F) and **IV.9** (G-H). (A, C, E, G) DIC channel; (B, D, F, H) DAPI-long-pass channel. Scale bar = 50  $\mu$ m.

HeLa cells were incubated with 10  $\mu$ M solution of **IV.11** in FBS free DMEM with 0.1% DMSO for 2 h (**Figure 4.4b**, A-B). The cells were then washed and incubated for 18 h with FBS free DMEM. After the second incubation period and washing, a bright fluorescent emission was observed from the nanohoop. In the absence of **IV.11**, no fluorescence is observed confirming that the signal was a result of the emission of **IV.11** and not cell autofluorescence (**Figure 4.4b**, C-D). To further support the role of folic acid

receptors on the cell uptake of **IV.11**, we preincubated cells with free folic acid for 30 min to saturate the folate receptors. Then we incubated the cells with a solution containing free folic acid and nanohoop **IV.11**. **Figure 4.4b**, E-F shows a marked decrease of cell fluorescence through the nanohoop channel consistent with the folic acid receptor mediated uptake of **IV.11**. Furthermore, when cells were treated with **IV.9** nonlocalized fluorescence was observed, which we attribute to aggregation of the azido nanohoop. These results demonstrate that azide[8]CPP **IV.9** can be functionalized with targeting groups and imaged in live cells.

### 4.3. Conclusion

These initial studies establish several important points regarding the nanohoop architecture, a growing class of conjugated molecules with radially oriented  $\pi$ -systems, as a new macrocyclic scaffold for fluorescent dye design. First, sulfonation is a viable strategy to render the nanohoops aqueous-soluble and retain their advantageous photophysical properties. Second, these aqueous-soluble nanohoops can penetrate live cells with minimal cytotoxicity and produce bright fluorescent images. Additionally, our solution measurements show that these materials are pH insensitive, an important consideration as we begin to develop the wide applicability of this unique molecular structure for intracellular probes where pH varies dramatically in each cellular compartment. Finally, we established that the nanohoop can be derivatized with targeting groups using “click“ chemistry and imaged in live cells. An exciting next step that we are currently pursuing is to establish nanohoops as multiplexed imaging tools utilizing the  $\lambda_{\text{abs}}$  shared by all nanohoops and their well resolved and size-dependent fluorescence, singlet lifetimes, and even Raman signatures. For example, based on modern imaging techniques and the synthetic methods available to prepare nanohoops, simultaneous imaging of 20 nanohoops in one experiment is feasible.<sup>19, 49</sup> As a more long-term prospect, we anticipate that the oligomeric nature and unique electron rich cavity of the nanohoop structure can be further engineered to allow for more complex function in biological settings. In conclusion, we have taken an important first step to demonstrate

nanohoops as an untapped class of fluorescent dyes that are viable for fluorescent probe development.

## 4.4. Experimental Sections

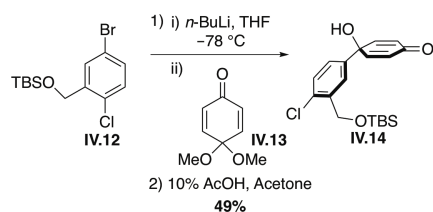
### 4.4.1. General Experimental Details

Moisture sensitive reactions were carried out under an inert atmosphere of nitrogen using standard Schlenk technique.  $^1\text{H}$  NMR spectra were recorded at 500 MHz Varian VNMR spectrometer or a Bruker Avance III-HD spectrometer or at 600 MHz on a Bruker Avance-III-HD NMR spectrometer.  $^{13}\text{C}$  NMR spectra were recorded at 125 MHz on a Varian VNMR Spectrometer or a Bruker Avance III-HD spectrometer or at 150 MHz on a Bruker Avance-III-HD NMR spectrometer. All  $^1\text{H}$  NMR spectra were taken in  $\text{CDCl}_3$  (referenced to TMS,  $\delta$  0.00 ppm), or  $\text{DMSO-d}_6$  (referenced to residual DMSO,  $\delta$  2.50 ppm). All  $^{13}\text{C}$  NMR spectra were taken in  $\text{CDCl}_3$  (referenced to chloroform,  $\delta$  77.16 ppm) or  $\text{DMSO-d}_6$  (referenced to DMSO,  $\delta$  39.52 ppm)

THF, DMF and Dioxane were dried by filtration through alumina according to the methods described by Grubbs.<sup>50</sup> Silica column chromatography was conducted with Zeochem Zeoprep 60 Eco 40-63  $\mu\text{m}$  silica gel. Automated flash chromatography was performed using a Biotage Isolera One. Thin Layer Chromatography (TLC) was performed using EMD Millipore Silica gel 60 F<sub>254</sub> plates for normal phase chromatography and EMD Millipore RP-18 modified silica gel 60 F<sub>254s</sub> plates for reverse phase chromatography. Developed plates were visualized using UV light at wavelengths of 254 and 265 nm. Preparatory silica gel chromatography was performed using 1000 micro Analtech silica gel GF thin layer chromatography plates. Reverse phase chromatography was conducted with Agela technologies bulk C<sub>18</sub> flash 50-60  $\mu\text{m}$  reverse phase silica gel. All glassware was oven or flame dried and cooled under an inert atmosphere of nitrogen unless otherwise noted. IR spectra were recorded on a Thermo Nicolet 6700 FT-IR. Masses were obtained by Dr. Haijun Yao at the University of Illinois Urbana-Champaign using a Waters Q-TOF Ultima ESI. Absorbance and fluorescence spectra were obtained using a Cary 100 spectrometer and a Horiba Jobin-Yvon FluoroMax-4 spectrometer respectively.

HeLa cells were purchased from ATCC and the CCK-8 cell viability kit was purchased from Doiundo Molecular Technologies Inc. Cell viability was measured using a Tecan Safire plate reader. Cell imaging experiments were performed on a Leica DMI8 fluorescence microscope equipped with an Andor Zyla 4.2+sCMOS detector. Compounds **IV.12**,<sup>51</sup> **IV.13**,<sup>52</sup> **IV.5**,<sup>26</sup> **IV.15**,<sup>53</sup> **IV.17**,<sup>26</sup> **IV.18**,<sup>54</sup> **IV.19**<sup>26</sup> and SPhos-Pd-G2<sup>55</sup> were prepared in accordance with previously reported procedures. For the synthesis of **IV.15** CHCl<sub>3</sub> was substituted for CCl<sub>4</sub> in the reported procedure. All spectra matched previously reported. All reagents were obtained commercially unless otherwise noted.

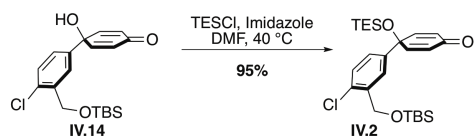
#### 4.4.2. Synthetic Details



4-bromo-1-chloro-2-[(*tert*-butyldimethylsilyl)oxymethyl]-benzene **IV.12** (10.0 g, 29.6 mmol, 1.30 equiv) was added to a flame dried flask and diluted with THF (99 mL). The solution was cooled to  $-78^{\circ}\text{C}$  for 30 min with stirring then *n*-BuLi (2.30 M in hexanes, 13.0 mL, 29.6 mmol, 1.30 equiv) was added to the mixture drop wise and the mixture was stirred at  $-78^{\circ}\text{C}$  for 30 min to give a light yellow solution. Quinone monoketal **IV.13** (3.20 mL, 22.8 mmol, 1.00 equiv) was added to the mixture dropwise to give a bronze colored solution and the mixture. After stirring at this temperature for 1 hour the reaction was quenched with denionized water (50 mL) and warmed to room temperature. The product was extracted with ethyl acetate (3 x 50 mL) and the combined organic layers were washed with deionized water (2 x 100 mL), brine (1 x 100 mL) then dried over sodium sulfate and concentrated to give a light brown oil.

A stir bar was added to the flask of crude product then the oil was diluted with acetone (100 mL). Under atmospheric conditions, a solution of 10% acetic acid in deionized water (100 mL) was added to the flask and the mixture was stirred for 2 hours. The reaction was quenched with a solution of saturated sodium bicarbonate (100 mL) and the

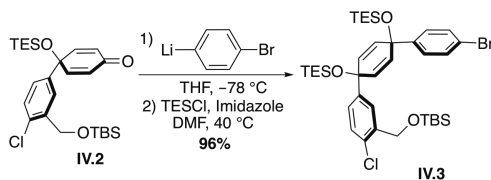
product was extracted with ethyl acetate (3 x 100 mL). The combined organic layers were washed with deionized water (2 x 100 mL), brine (1 x 100 mL) then dried over sodium sulfate and concentrated to give a bronze/red oil. Titration of the oil with hexanes gave the product as a powder after collection by vacuum filtration. The filtrate was concentrated and this process was repeated until no solid was precipitated upon titration of the resulting oil with hexanes to give the product **IV.14** as an ivory powder (5.25 g, 49%). mp 103-104 °C. <sup>1</sup>H NMR (600 MHz, CDCl<sub>3</sub>): δ 7.65 (d, *J* = 2.3 Hz, 1H), 7.39 (dd, *J* = 8.3, 2.3 Hz, 1H), 7.33 (d, *J* = 8.3 Hz, 1H), 6.86 (d, *J* = 10.1 Hz, 2H), 6.24 (d, *J* = 10.1 Hz, 2H), 4.76 (s, 2H), 2.35 (s, 1H), 0.94 (s, 9H), 0.10 (s, 6H); <sup>13</sup>C NMR (150 MHz, CDCl<sub>3</sub>): 185.36, 150.31, 139.73, 137.58, 131.50, 129.52, 127.29, 124.83, 124.61, 71.02, 62.21, 25.09, 18.45, -5.22; HRMS (TOF, ES+) (*m/z*): [M+Na]<sup>+</sup> calculated for C<sub>19</sub>H<sub>25</sub>ClO<sub>3</sub>SiNa, 387.1159; found: 387.1161. IR (neat): 3422.55, 3044.91, 2950.71, 2928.09, 2857.09, 1706.84, 1656.79, 1620.14, 1599.32, 1470.05, 1461.92, 1395.75, 1385.66, 1360.11, 1291.79, 1253.07, 1220.02, 1177.99, 1158.29, 1145.98, 1073.67, 1063.79, 1048.03, 997.91, 967.12, 933.97, 911.46, 874.25, 828.52, 772.59, 717.15, 704.40, 668.21, 628.20, 601.88, 585.71, 566.86 cm<sup>-1</sup>.



Chloroquinol **IV.14** (5.22 g, 14.3 mmol, 1.00 equiv) and imidazole (1.95 g, 28.6 mmol, 2.00 equiv) were added to a flame dried flask. The solids were dissolved in DMF (72 mL) and triethylsilylchloride (3.60 mL, 21.5 mmol, 1.5 equiv) was added dropwise to the mixture at room temperature. The reaction was heated to 40°C for 16 hours. The reaction was then cooled to room temperature and quenched with a saturated solution of sodium bicarbonate (50 mL). The product was extracted with ethyl acetate (3 x 100 mL) and the combined organic layers were washed with 5% LiCl in deionized water (4 x 50 mL), deionized water (1 x 50 mL), brine (1 x 50 mL) then dried over sodium sulfate and concentrated to give a brown oil. The product was purified via silica gel column chromatography (5-10% ethyl acetate/hexane) to give **IV.2** as a yellow oil (6.48 g, 95%). <sup>1</sup>H NMR (500 MHz, CDCl<sub>3</sub>): δ 7.65 (d, *J* = 2.1 Hz, 1H), 7.31 (dd, *J* = 8.33, 2.1 Hz, 1H),

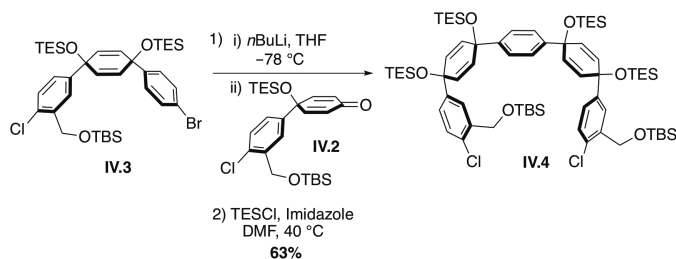


7.28 (d,  $J = 8.34$  Hz, 1H), 6.80 (d,  $J = 10.0$  Hz, 2H), 6.21 (d,  $J = 10.0$  Hz, 2H), 4.76 (a, 2H), 0.97 (t,  $J = 7.9$  Hz, 9H), 0.93 (s, 9H), 0.66 (q,  $J = 7.9$  Hz, 6H), 0.10 (s, 6H);  $^{13}\text{C}$  NMR (125 MHz,  $\text{CDCl}_3$ ):  $\delta$  185.75, 151.87, 139.40, 138.91, 131.00, 129.23, 126.80, 124.99, 124.58, 73.11, 62.31, 26.04, 18.49, 7.06, 6.36, -5.24; HRMS (TOF, ES+) ( $m/z$ ):  $[\text{M}+\text{Na}]^+$  calculated for  $\text{C}_{25}\text{H}_{39}\text{ClO}_3\text{Si}_2\text{Na}$ , 501.2024; found: 501.2028. IR (neat): 2954.09, 2876.38, 2856.77, 1672.52, 1630.53, 1603.95, 1470.87, 1405.93, 1386.72, 1252.39, 1215.18, 1167.69, 1145.84, 1099.76, 1058.64, 1039.63, 1003.85, 936.58, 890.07, 866.20, 835.69, 776.20, 744.39, 727.03, 727.06, 668.60, 613.16, 589.55, 550.91, 539.26, 528.01  $\text{cm}^{-1}$ .



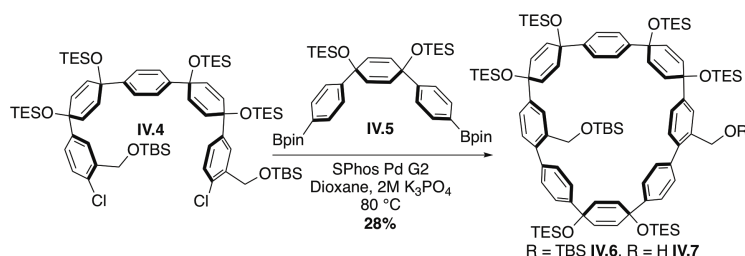
1,4-dibromobenzene (1.77 g, 7.51 mmol, 1.20 equiv) was dissolved in THF (25 mL) in a flame dried flask and cooled to  $-78^\circ\text{C}$  for 30 min. *n*-BuLi (2.30 M in hexane, 3.40 mL, 7.51 mmol, 1.20 equiv) was added drop wise to the cooled solution and stirred for another 20 min at that temperature to give a white precipitate. Chloro ketone **IV.2** (3.00 g, 6.26 mmol, 1 equiv) was diluted with THF (5 mL) and added to the cooled lithiate dropwise and the mixture was stirred for 1 hour at  $-78^\circ\text{C}$ . The reaction was quenched with the addition of deionized water (15 mL) at  $-78^\circ\text{C}$  then warmed to room temperature. The product was extracted with ethyl acetate (3 x 50 mL). The combined organic layers were washed with deionized water (2 x 100 mL), brine (1 x 100 mL) then dried over sodium sulfate and concentrated to give a brown oil. Imidazole (852 mg, 12.5 mmol, 2.00 equiv) was added to a flame dried flask and the crude brown oil was transferred to the flask with DMF (3 x 10 mL). Triethylsilylchloride (1.58 mL, 9.93 mmol, 1.50 equiv) was added to the mixture dropwise to the solution and the mixture was heated to  $40^\circ\text{C}$  for 16 hours. The reaction was then cooled to room temperature and quenched with a saturated solution of sodium bicarbonate (50 mL). The product was extracted with ethyl acetate (3 x 100 mL) and the combined organic layers were washed with 5% LiCl in deionized water (4 x 50 mL), deionized water (1 x 50 mL), brine (1 x 50 mL) then dried over

sodium sulfate and concentrated to give a brown oil. The product was purified via silica gel column chromatography (2% ethyl acetate/hexane) to give **IV.3** as a clear colorless oil (4.51 g, 96%). <sup>1</sup>H NMR (500 MHz, CDCl<sub>3</sub>): δ 7.64 (d, *J* = 2.2 Hz, 1H), 7.34 (d, *J* = 8.6 Hz, 2H), 7.19 (d, *J* = 8.3 Hz, 1H), 7.14 (d, *J* = 8.6 Hz, 2H), 7.07 (dd, *J* = 8.3, 2.2 Hz, 1H), 6.00 (d, *J* = 10.1 Hz, 2H), 5.91 (d, *J* = 10.1 Hz, 2H), 4.74 (s, 2H), 0.94 (t, *J* = 7.9 Hz, 9H), 0.91 (t, *J* = 7.9 Hz, 9H), 0.90 (s, 18H), 0.61 (q, *J* = 7.9 Hz, 6H), 0.57 (q, *J* = 7.9 Hz, 6H), 0.08 (s, 6H); <sup>13</sup>C NMR (125 MHz, CDCl<sub>3</sub>): 145.09, 144.76, 138.81, 131.63, 131.50, 131.33, 130.44, 128.64, 127.72, 125.56, 125.30, 121.31, 71.39, 71.22, 62.51, 26.04, 18.50, 7.19, 7.18, 6.56, -5.26. IR (neat): 2953.94, 2928.23, 2883.52, 2856.24, 1471.02, 1461.25, 1448.96, 1395.08, 1369.36, 1253.46, 1195.15, 1139.12, 1105.37, 1079.34, 1062.06, 1039.91, 1005.01, 938.44, 882.41, 833.34, 807.55, 775.85, 709.80, 668.29, 596.63, 569.09, 550.80, 530.65 cm<sup>-1</sup>.



Three ring bromo chloride **IV.3** (5.00 g, 6.67 mmol, 1.00 equiv) was dissolved in THF (22 mL) in a flame dried flask and cooled to  $-78^{\circ}\text{C}$  for 30 min. *n*-BuLi (2.30 M in hexane, 2.90 mL, 7.51 mmol, 1.00 equiv) was added drop wise to the cooled solution and stirred for another 20 min at that temperature to give a white precipitate. Chloro ketone **IV.2** (3.51 g, 7.33 mmol, 1.10 equiv) was diluted with THF (5 mL) and added to the cooled lithiate dropwise and the mixture was stirred for 1 hour at  $-78^{\circ}\text{C}$ . The reaction was quenched with the addition of deionized water (20 mL) at  $-78^{\circ}\text{C}$  then warmed to room temperature. The product was extracted with ethyl acetate (3 x 50 mL). The combined organic layers were washed with deionized water (2 x 100 mL), brine (1 x 100 mL) then dried over sodium sulfate and concentrated to give a brown oil. Imidazole (907 mg, 13.3 mmol, 2.00 equiv) was added to a flame dried flask and the crude brown oil was transferred to the flask with DMF (3 x 10 mL). Triethylsilylchloride (1.68 mL, 9.99 mmol, 1.50 equiv) was added to the mixture dropwise to the solution and the mixture was

heated to 40°C for 16 hours. The reaction was then cooled to room temperature and quenched with a saturated solution of sodium bicarbonate (50 mL). The product was extracted with ethyl acetate (3 x 100 mL) and the combined organic layers were washed with 5% LiCl in deionized water (4 x 50 mL), deionized water (1 x 50 mL), brine (1 x 50 mL) then dried over sodium sulfate and concentrated to give a brown oil. The product was precipitated from the crude oil by titration with ethanol to give **IV.4** as a pure white solid (5.34 g, 63%). mp 87-89 °C. <sup>1</sup>H NMR (600 MHz, CDCl<sub>3</sub>): δ 7.80 (d, *J* = 2.2 Hz, 2H), 7.18 (s, 4H), 7.09 (d, *J* = 8.3 Hz, 2H), 6.89 (dd, *J* = 8.3, 2.2 Hz, 2H), 5.95 (2, 8H), 4.76 (2, 4H), 0.93 (s, 18H), 0.91 (t, *J* = 7.9 Hz, 36H), 0.59 (q, *J* = 7.9 Hz, 12H), 0.58 (q, *J* = 7.9 Hz, 12H), 0.10 (s, 12H); <sup>13</sup>C NMR (150 MHz, CDCl<sub>3</sub>): 144.99, 144.93, 138.76, 131.86, 131.27, 130.29, 128.34, 125.72, 125.48, 125.44, 71.36, 71.27, 62.60, 26.11, 18.55, 7.20, 7.20, 6.58, 6.53, -5.20; HRMS (TOF, ES<sup>+</sup>) (*m/z*): [M+Na]<sup>+</sup> calculated for C<sub>68</sub>H<sub>112</sub>Cl<sub>2</sub>O<sub>6</sub>Si<sub>6</sub>Na, 1285.6349; found: 1285.6349. IR (neat): 2951.19, 2933.46, 2873.78, 1454.99, 1408.15, 1376.27, 1359.64, 1250.63, 1218.91, 1198.11, 1151.10, 1071.91, 1038.48, 999.19, 965.66, 928.69, 908.13, 885.02, 870.83, 835.28, 816.42, 776.64, 722.93, 707.97, 667.33, 644.15, 586.64, 565.03, 546.65, 540.80, 536.77, 531.92, 527.31 cm<sup>-1</sup>.

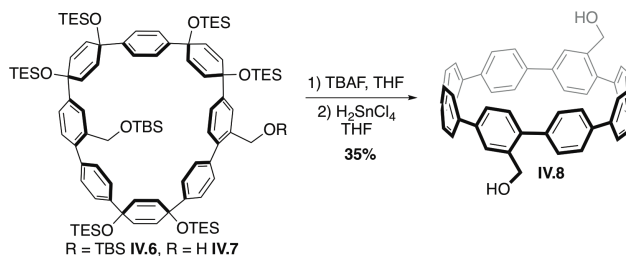


Five ring dichloride **IV.4** (1.50 g, 1.19 mmol, 1.00 equiv), previously reported three ring bisboronate **IV.5** (1.07 g, 1.44 mmol, 1.20 equiv) and SPhos-Pd-G2 catalyst (86.4 mg, 0.120 mmol, 0.100 equiv) were added to a flame dried flask. The flask was evacuated and backfilled with N<sub>2</sub> (5 x) then a septum put on the flask and the solids were purged with N<sub>2</sub> for 30 min. Dioxane (400 mL) and a solution of 2 M K<sub>3</sub>PO<sub>4</sub> in deionized water (40 mL) were sparged with nitrogen for 1 hour. The dioxane was added to the reaction flask via cannula and the solution was sparged for 2 hours while the 2 M K<sub>3</sub>PO<sub>4</sub> solution continued to sparge. The reaction flask was headed to 80°C for 30 min then the 2 M K<sub>3</sub>PO<sub>4</sub> solution was added. The reaction was stirred at this temperature for 16 hours then

cooled to room temperature. The mixture was filtered through celite rinsing with dichloromethane (3 x 75 mL) and the filtrate was concentrated to remove approximately 350 mL of dioxane. The product was extracted from this mixture with dichloromethane (3 x 100 mL) and the combined organic layers were washed with deionized water (2 x 100 mL), brine (1 x 100 mL) then dried over sodium sulfate and concentrated to give a black oily solid. The crude reaction was treated with silica gel column chromatography (0-15% ethyl acetate/hexane) to give impure **IV.6** and **IV.7** as clear oils. The products were purified by titration of the resulting oils with acetone to give **IV.6** and **IV.7** as white solids after collection with vacuum filtration. This process was repeated on the concentrated filtrates and fractions of mixed **IV.6** and **IV.7** were separated with silica gel column chromatography (0-15% ethyl acetate/hexane) to give **IV.6** (181 mg, 10%) and **IV.7** (314 mg, 18%) as white solids. **IV.6**: mp 215-216 °C. <sup>1</sup>H NMR (600 MHz, CDCl<sub>3</sub>): δ 7.86 (d, *J* = 1.8 Hz, 1H), 7.50 (d, *J* = 1.9 Hz, 1H), 7.48 (d, *J* = 8.5 Hz, 2H), 7.44 (d, *J* = 8.5 Hz, 2H), 7.41 (dd, *J* = 7.2, 1.9 Hz, H), 7.16 (d, *J* = 8.1 Hz, 2H), 7.13 (d, *J* = 8.1 Hz, 2H), 7.13 (d, *J* = 7.2 Hz, 1H), 7.12 (d, *J* = 8.4 Hz, 2H), 7.09 (d, *J* = 8.4 Hz, 2H), 7.05 (d, *J* = 8.0 Hz, 1H), 7.02 (dd, *J* = 8.0, 1.8 Hz, 1H), 6.17 (d, *J* = 10.3 Hz, 2H), 6.14 (d, *J* = 10.3 Hz, 2H), 6.04 (d, *J* = 10.1 Hz, 2H), 6.03 (d, *J* = 10.1 Hz, 2H), 5.96 (d, *J* = 10.1 Hz, 2H), 5.92 (d, *J* = 10.1 Hz, 2H), 4.57 (s, 2H), 4.55 (d, *J* = 5.0 Hz, 2H), 1.43 (t, *J* = 5.0 Hz, 1H), 1.00-0.95 (overlap, 36H), 0.93 (t, *J* = 7.9 Hz, 18H), 0.84 (s, 9H), 0.72-0.63 (overlap, 24H), 0.55 (q, *J* = 7.9 Hz, 12H), -0.05 (s, 6H); <sup>13</sup>C NMR (150 MHz, CDCl<sub>3</sub>): 146.03, 145.89, 145.85, 145.57, 143.63, 143.26, 139.71, 139.53, 139.29, 139.27, 138.28, 137.97, 132.41, 132.18, 132.03, 131.93, 131.36, 131.22, 129.94, 129.61, 128.80, 128.74, 126.46, 126.16, 126.07, 126.00, 125.98, 125.51, 124.66, 124.41, 72.49, 72.23, 71.35, 71.25, 70.91, 70.84, 63.45, 63.44, 26.07, 18.48, 7.29, 7.28, 7.21, 7.18, 6.65, 6.64, 6.62, 6.53, 6.52, -5.24; HRMS (TOF, ES+) (*m/z*): [M+Na]<sup>+</sup> calculated for C<sub>92</sub>H<sub>140</sub>O<sub>8</sub>Si<sub>7</sub>Na, 1591.8831; found: 1591.8867. IR (neat): 3533.67, 2952.07, 2874.99, 1589.20, 1485.35, 1470.21, 1412.17, 1245.71, 1190.90, 1099.95, 1078.85, 1004.50, 966.46, 878.16, 835.44, 774.58, 721.44, 668.29, 607.67, 525.03 cm<sup>-1</sup>.

**IV.7**: mp 131-134 °C. <sup>1</sup>H NMR (600 MHz, CDCl<sub>3</sub>): δ 7.54 (d, *J* = 1.4 Hz, 2H), 7.45 (s, 4H), 7.36 (dd, *J* = 7.9, 1.4 Hz, 2H), 7.17 (d, *J* = 7.9 Hz, 2H), 7.13 (d, *J* = 8.3 Hz, 4H), 7.10 (d, *J* = 8.3 Hz, 4H), 6.17 (s, 4H), 6.03 (d, *J* = 10.0 Hz, 4H), 5.95 (d, *J* = 10.0 Hz,

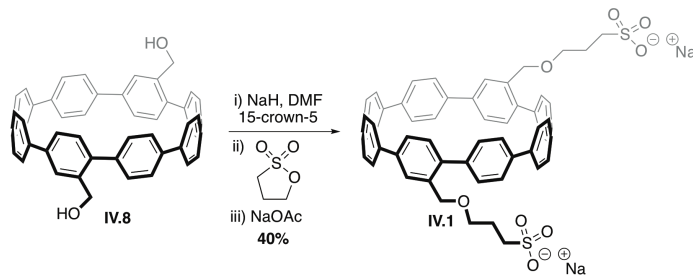
4H), 4.50 (d,  $J = 5.8$  Hz, 4H), 1.72 (d,  $J = 5.8$  Hz, 2H), 0.97 (t,  $J = 7.9$  Hz, 18H), 0.97 (t,  $J = 7.9$  Hz, 18H), 0.93 (t,  $J = 7.9$  Hz, 18H), 0.69-0.64 (overlap, 24H), 0.55 (q,  $J = 7.9$  Hz, 12H);  $^{13}\text{C}$  NMR (150 MHz,  $\text{CDCl}_3$ ):  $\delta$  145.95, 145.90, 143.59, 139.61, 139.33, 137.88, 132.40, 131.85, 131.39, 130.02, 128.74, 126.37, 125.96, 125.70, 124.95, 72.30, 71.20, 70.89, 63.25, 7.27, 7.27, 7.21, 6.64, 6.62, 6.53; HRMS (TOF, ES+) ( $m/z$ ):  $[\text{M}+\text{NH}_4]^+$  calculated for  $\text{C}_{86}\text{H}_{126}\text{O}_8\text{Si}_6\text{Na}$ , 1477.7966; found: 1477.7931. IR (neat): 3336.92, 2952.74, 2910.65, 2875.30, 1480.63, 1458.04, 1412.23, 1239.15, 1190.38, 1112.97, 1078.04, 1004.17, 964.87, 878.32, 859.10, 825.12, 793.42, 723.85, 668.13, 556.48, 536.69  $\text{cm}^{-1}$ .



Macrocycles **IV.6** and **IV.7** (**IV.6**: 181 mg, 0.115 mmol; **IV.7**: 314 mg, 0.215 mmol; combined as 1.00 equiv) were added to a flame dried flask and suspended in THF (3.30 mL) at room temperature. Tert-butyl ammonium fluoride (TBAF) (1.00 M in THF, 3.30 mL, 3.30 mmol, 10.0 equiv) was added to the suspension dropwise to give a yellow orange clear solution. The reaction was stirred for 2 hours then quenched with deionized water (10 mL) to give a colorless liquid. The mixture was concentrated to remove the THF and the resulting white solid was collect by vacuum filtration and rinsed with deionized water (50 mL) and dichloromethane (50 mL). The filtrate was discarded and the solid was dissolved in 1:1 acetone and deionized water then concentrated and dried thoroughly with high vacuum.

A 0.05 M solution of  $\text{H}_2\text{SnCl}_4$  was prepared by dissolving tin(II) dichloride dehydrate (1.13 g, 5.00 mmol, 1.00 equiv) in THF (100 mL) in a flame dried flask then adding HCl (12 M, 0.83 mL, 10 mmol) dropwise and stirring for 30 min. The free alcohol macrocycle obtained from the TBAF deprotection was suspended in THF (5 mL) in a flame dried flask and the  $\text{H}_2\text{SnCl}_4$  solution (0.05 M, 100 mL, 4.96 mmol, 15 equiv) was added via

cannula. The reaction immediately became clear and turned yellow then a precipitate formed after 30 min of reaction time. The mixture was stirred for 16 hours then the reaction was quenched with a solution of saturated sodium bicarbonate in deionized water (100 mL). The mixture was filtered through a pad of celite that was rinsed with deionized water (50 mL), acetone (50 mL) then dichloromethane (150mL). The dichloromethane layer was separated and the product was extracted from the aqueous layer with dichloromethane (2 x 100 mL). The combined organic layers were washed with deionized water (2 x 100 mL), brine (1 x 100 mL) dried over sodium sulfate and concentrated to give a yellow solid. The product was treated with silica gel column chromatography (0-5% methanol/dichloromethane) to give impure product as a yellow solid. The product was purified via preparatory silica gel thin layer chromatography eluting (10% methanol/dichloromethane) to give the desired product with minor impurities as a yellow solid. While the product was of sufficient purity to carry on, the remaining impurities were removed with silica gel column chromatography (0-5% methanol/dichloromethane) to give pristine **IV.8** as a yellow solid (71.8 mg, 35%). mp >250 °C decomp. <sup>1</sup>H NMR (600 MHz, CDCl<sub>3</sub>): δ 7.84 (d, *J* = 2.0 Hz, 2H), 7.52 (d, *J* = 8.6 Hz, 4H), 7.50 (s, 4H), 7.45 (s, 4H), 7.42 (d, *J* = 8.6 Hz, 4H), 7.40 (d, *J* = 8.5 Hz, 4H), 7.30 (d, *J* = 8.5 Hz, 4H), 7.00 (dd, *J* = 8.4, 2.0 Hz, 2H), 6.85 (d, *J* = 8.4 Hz, 2H), 5.04 (d, *J* = 4.5 Hz, 4H), 1.84 (t, *J* = 4.5 Hz, 2H); <sup>13</sup>C NMR (150 MHz, CDCl<sub>3</sub>): 139.03, 138.82, 138.81, 138.70, 138.53, 138.43, 137.98, 137.82, 137.54, 133.33, 129.86, 129.53, 128.14, 128.08, 127.86, 127.51, 127.41, 125.52, 63.67; HRMS (TOF, ES+) (*m/z*): [M+Na]<sup>+</sup> calculated for C<sub>50</sub>H<sub>36</sub>O<sub>2</sub>Na, 691.2631; found: 691.2634. IR (neat): 3391.76, 3021.32, 2919.87, 2849.76, 1668.20, 1586.23, 1558.53, 1481.25, 1386.63, 1261.31, 1182.68, 1000.17, 893.26, 841.29, 816.95, 731.30, 668.09, 648.4, 607.61, 550.82, 526.65 cm<sup>-1</sup>.

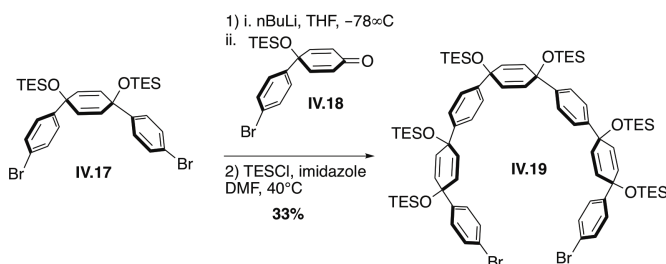


Nanohoop **IV.8** (20.1 mg, 0.0301 mmol, 1.00 equiv) was suspended in DMF (0.250 mL) at room temperature and the solution was briefly sonicated to promote dissolution of the nanohoop. Sodium hydride (5.9 mg, 0.148 mmol, 5.00 equiv) was added to the mixture as a solid and the suspension was stirred for 30 min after sonicating briefly. At this time, the reaction mixture had become a dark orange color and 15-crown-5 (24.4  $\mu$ L, 0.123 mmol, 4.00 equiv) was added to the flask and stirred for another 30 min. To the now brown suspension was added neat 1,3-propane sultone (42 mg, 0.344 mmol, 11.4 equiv) and the reaction was stirred for 16 hours. The reaction was quenched with the addition of deionized water (2.00 mL) and the mixture was stirred for 5 min. Sodium acetate (42.0 mg, 0.512 mmol, 17.0 equiv) was added to the light yellow solution and the mixture was stirred for 30 min. The crude reaction mixture was then concentrated, loaded on to reverse phase silica gel and purified with reverse phase silica gel chromatography (20-80% acetone/deionized water). Any recovered starting material or monosulfonated product was combined, resubjected to the same reaction conditions and purified as described. The disulfonated product was then rinsed with dichloromethane (4 x 5.00 mL) to give pure **IV.1** as an orange solid film (11.4 mg, 57%). A portion of monosulfonated product was also recovered as a yellow solid (8.1 mg, 35%). mp >220  $^{\circ}$ C decomp.  $^1$ H NMR (500 MHz,  $\text{CDCl}_3$ ):  $\delta$  7.82 (brs, 2H), 7.70 (d,  $J$  = 8.6 Hz, 4H), 7.67 (s, 4H), 7.68 (s, 4H), 7.57 (d,  $J$  = 8.3 Hz, 4H), 7.55 (d,  $J$  = 8.6 Hz, 4H), 7.37 (d,  $J$  = 8.7 Hz, 4H), 7.17 (d,  $J$  = 8.2 Hz, 2H), 6.93 (d,  $J$  = 8.2 Hz, 2H), 3.80 (s, 4H), 3.56 (t,  $J$  = 6.6 Hz, 4H), 3.56 (t,  $J$  = 6.6 Hz, 4H), 2.47 (t,  $J$  = 6.6 Hz, 4H), 1.86 (m, 4H);  $^{13}$ C NMR (125 MHz,  $\text{CDCl}_3$ ): 163.03, 138.39, 138.19, 137.46, 137.18, 137.15, 137.08, 136.51, 136.29, 135.63, 132.58, 129.19, 128.73, 127.61, 127.48, 127.37, 127.03, 126.21, 70.30, 69.41, 48.47, 25.77; HRMS (TOF, ES-) ( $m/z$ ):  $[M]^-$  calculated for  $\text{C}_{56}\text{H}_{47}\text{O}_8\text{S}_2$ , 911.2712; found: 911.2697. IR (neat): 3391.43, 3146.55, 3021.59, 2950.94, 2859.19, 1585.20, 1558.80, 1480.70,

1416.24, 1386.02, 1362.52, 1156.70, 1091.25, 1032.94, 1000.15, 890.28, 811.23, 726.96, 560.19, 554.04  $\text{cm}^{-1}$ .



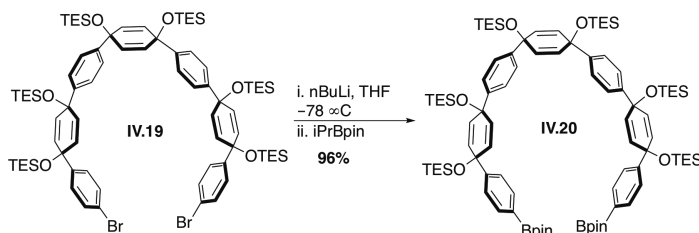
1,4-dibromo-2-(bromomethyl)-benzene **IV.15** (10.5 g, 32.3 mmol, 1.00 equiv) and sodium azide (3.15 g, 48.5 mmol, 1.50 equiv) were added to a flame dried flask then dissolved in dimethyl sulfoxide (430 mL). The mixture was stirred for 3 hours then the reaction was quenched with the addition of deionized water (250 mL). The product was extracted with dichloromethane (3 x 250 mL) and the combined organic layer wash washed with deionized water (4 x 250 mL), brine (1 x 250 mL) and dried over sodium sulfate then concentrated to give pure **IV.16** as a clear, colorless liquid (8.90 g, 95%).  $^1\text{H}$  NMR (500 MHz,  $\text{CDCl}_3$ ):  $\delta$  7.55 (s, 1H), 7.45 (d,  $J = 8.5$  Hz, 1H), 7.33 (d,  $J = 8.5$  Hz, 1H), 4.47 (s, 2H);  $^{13}\text{C}$  NMR (125 MHz,  $\text{CDCl}_3$ ): 137.26, 134.44, 132.84, 132.74, 122.12, 121.81, 54.24; HRMS (ASAP) ( $m/z$ ):  $[\text{M}]^+$  calculated for  $\text{C}_7\text{H}_5\text{Br}_2\text{N}_3$ , 288.8850; found: 288.8818. IR (neat): 3349.55, 3081.97, 2930.78, 2216.02, 2095.81, 1889.35, 1579.62, 1555.72, 1455.41, 1431.42, 1386.88, 1339.21, 1283.04, 1250.37, 1217.76, 1194.27, 1132.58, 1084.43, 1023.63, 946.40, 921.91, 874.16, 844.60, 808.34, 705.76, 685.26, 645.60, 583.54  $\text{cm}^{-1}$ .



Three ring dibromo **IV.17** (4.95 g, 7.60 mmol, 1.00 equiv) was dissolved in THF (38 mL) in a flame dried flask and cooled to  $-78^\circ\text{C}$  for 30 min then  $n\text{-BuLi}$  (2.20 M in hexane, 7.60 mL, 16.7 mmol, 2.2 equiv) was added to the reaction flask. Bromo ketone **IV.18** (6.34 g, 16.7 mmol, 2.20 equiv) in THF (56 mL) was immediately added to the cooled lithiate dropwise and the mixture was stirred for 1 hour at  $-78^\circ\text{C}$ . The reaction was quenched with the addition of deionized water (100 mL) at  $-78^\circ\text{C}$  then warmed to room

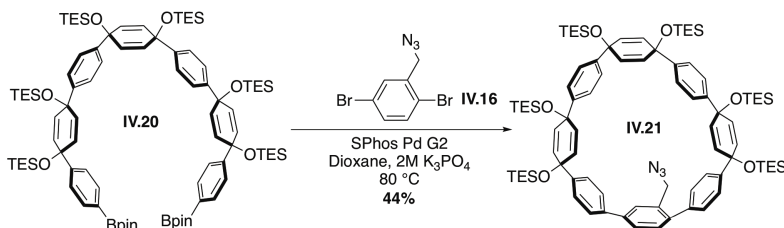


temperature. The product was extracted with ethyl acetate (2 x 100 mL). The combined organic layers were washed with deionized water (2 x 100 mL), brine (1 x 100 mL) then dried over sodium sulfate and concentrated to give a brown solid. This solid was suspended in hexanes and filtered to give a white powder. Imidazole (2.07 g, 30.4 mmol, 4.00 equiv) was added to a flame dried flask and the crude solid was added to the flask. The solids were dissolved in DMF (38 mL) and triethylsilylchloride (3.83 mL, 22.8 mmol, 3.00 equiv) was added to the mixture dropwise to the solution and the mixture was heated to 40°C for 16 hours. The reaction was then cooled to room temperature and quenched with a saturated solution of sodium bicarbonate (20 mL). The product was extracted with ethyl acetate (2 x 75 mL) and the combined organic layers were washed with 5% LiCl in deionized water (4 x 50 mL), deionized water (1 x 50 mL), brine (1 x 50 mL) then dried over sodium sulfate and concentrated to give a maroon oil. The product was purified via silica gel column chromatography (20-30% dichloromethane/hexane) to give **IV.19** as a clear, colorless, sticky oil (3.68 g, 33%). Characterization of this compound is consistent with previously reports.<sup>26</sup>



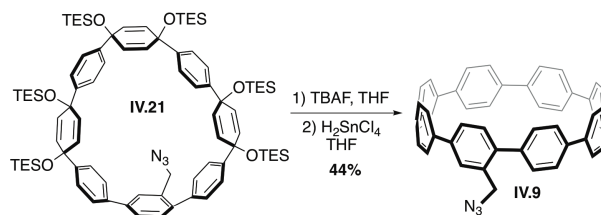
Seven ring dibromide **IV.19** (3.68 g, 2.48 mmol, 1.00 equiv) was dissolved in THF (12 mL) in a flame dried flask and cooled to -78°C for 30 min. *n*-BuLi (2.20 M in hexane, 2.49 mL, 5.47 mmol, 2.20 equiv) was added drop wise to the cooled. 2-Isopropoxy-4,4,5,5-tetramethyl-1,3,2-dioxaborolane (2.04 mL, 10.0 mmol, 4.03 equiv) was then immediately added to the cooled lithiate dropwise and the mixture was stirred for 1 hour at -78°C. The reaction was quenched with the addition of deionized water (20 mL) at -78°C then warmed to room temperature. The product was extracted with ethyl acetate (2 x 50 mL) and the combined organic layers were washed with deionized water (2 x 25 mL), brine (1 x 25 mL) then dried over sodium sulfate and concentrated to give **IV.20** as a white foamy solid (3.94 g, 96%). mp: 82-85 °C. <sup>1</sup>H NMR (500 MHz, CDCl<sub>3</sub>): δ 7.68 (d,

$J = 7.5$  Hz, 4H), 7.31 (d,  $J = 7.5$  Hz, 4H), 7.21 (overlap, 8H), 5.97 (d,  $J = 9.6$  Hz, 4H), 5.96 (s, 4H), 5.92 (d,  $J = 9.6$  Hz, 4H), 1.32 (s, 24H). 0.94-0.91 (overlap, 36H), 0.88 (t,  $J = 7.9$  Hz, 18H), 0.62-0.58 (overlap, 24H), 0.55 (q,  $J = 7.9$  Hz, 12H);  $^{13}\text{C}$  NMR (125 MHz,  $\text{CDCl}_3$ ): 149.31, 145.14, 144.96, 134.79, 131.71, 131.56, 131.38, 125.82, 125.79, 125.28, 83.82, 71.76, 71.50, 71.36, 25.01, 7.21, 7.19, 7.16, 6.62, 6.59.; HRMS (ASAP) ( $m/z$ ):  $[\text{M}]^+$  calculated for  $\text{C}_{90}\text{H}_{142}\text{B}_2\text{O}_{10}\text{Si}_6$ , 1572.9405; found: 1572.9364. IR (neat): 3032.71, 2952.95, 2910.00, 2874.71, 1608.85, 1499.88, 1457.91, 1398.38, 1359.09, 1318.74, 1272.06, 1237.84, 1189.66, 1144.53, 1115.90, 1067.97, 1003.77, 958.13, 879.53, 859.40, 825.62, 720.67, 674.36, 657.32  $\text{cm}^{-1}$ .



SPhos-Pd-G2 catalyst (41.0 mg, 0.0565 mmol, 0.100 equiv) was added to a flame dried flask. The flask was evacuated and backfilled with  $\text{N}_2$  (5 x) then a septum was put on the flask and the solid was purged with  $\text{N}_2$  for 30 min. During the  $\text{N}_2$  purge seven ring bisboronate **IV.20** (847 mg, 0.565 mmol, 1.00 equiv) was added to a separate flame dried flask, dissolved in dioxane (10 mL) and sparged for 30 min. At the same time dibromide **IV.16** (197 mg, 0.678 mmol, 1.20 equiv) was added to another flame dried flask, dissolved in dioxane (10 mL) and sparged for 30 min. The solutions of **IV.20** and **IV.16** cannulated into the flask containing SPhos-Pd-G2, rinsing each flask with dioxane (1 x 5 mL). Dioxane (158 mL) was also added to the flask and the solution was sparged with  $\text{N}_2$  while sonicating the flask for 50 min. Meanwhile, a solution of 2 M  $\text{K}_3\text{PO}_4$  in deionized water was sparged with nitrogen for 1 hour. The reaction flask was headed to  $80^\circ\text{C}$  for 30 min then the 2 M  $\text{K}_3\text{PO}_4$  solution (18.8 mL) was added. The reaction was stirred at this temperature for 16 hours then cooled to room temperature. The mixture was concentrated to remove the dioxane and the resulting solution was filtered through celite rinsing with dichloromethane (3 x 50 mL). The resulting organic layer was separated and the product was extracted further form the aqueous layer with dichloromethane (3 x 75 mL). The combined organic layers were washed with deionized water (2 x 100 mL), brine (1 x 100

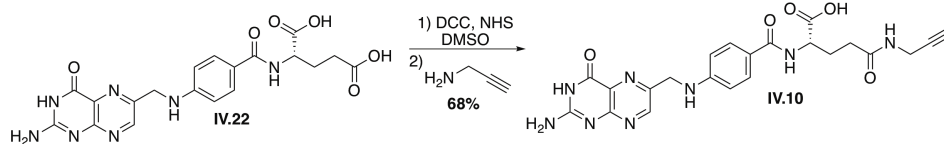
mL) then dried over sodium sulfate and concentrated to give a brown solid. The crude reaction was purified with silica gel column chromatography (20-50% dichloromethane/hexane) to give the desired product as a mostly pure white solid. This solid was suspended in acetone and filtered to give pure **IV.21** as white solid (363 mg, 44%). mp 153-155 °C. <sup>1</sup>H NMR (500 MHz, CDCl<sub>3</sub>): δ 7.63 (s, 1H), 7.44 (d, *J* = 8.1 Hz, 1H), 7.40 (d, *J* = 7.8 Hz, 2H), 7.34 (d, *J* = 7.8 Hz, 2H), 7.25-7.22 (overlap, 8H), 7.10 (d, *J* = 8.5 Hz, 2H), 7.08 (d, *J* = 8.1 Hz, 1H), 7.04 (d, *J* = 8.5 Hz, 2H), 6.14 (d, *J* = 10.2 Hz, 2H), 6.11 (d, *J* = 10.2 Hz, 2H), 6.06 (d, *J* = 10.1 Hz, 2H), 6.03 (d, *J* = 10.3 Hz, 2H), 6.00 (d, *J* = 10.3 Hz, 2H), 5.93 (d, *J* = 10.1 Hz, 2H), 4.43 (t, 2H), 1.01 (t, *J* = 7.8 Hz, 9H), 0.98 (t, *J* = 7.8 Hz, 9H), 0.93 (t, *J* = 7.8 Hz, 9H), 0.90-0.85 (overlap, 27H), 0.93 (q, *J* = 7.8 Hz, 6H), 0.93 (q, *J* = 7.8 Hz, 6H), 0.93 (q, *J* = 7.8 Hz, 6H), 0.93 (q, *J* = 7.8 Hz, 6H), 0.51-0.44 (overlap, 12H); <sup>13</sup>C NMR (125 MHz, CDCl<sub>3</sub>): 146.54, 146.18, 144.65, 144.63, 144.55, 144.53, 140.85, 140.46, 139.71, 139.13, 133.97, 132.79, 132.44, 132.27, 131.88, 131.71, 131.34, 129.07, 128.41, 127.81, 127.48, 126.53, 126.18, 125.99, 125.91, 125.85, 125.81, 72.24, 71.68, 71.62, 71.46, 69.58, 69.48, 52.95, 7.32, 7.29, 7.24, 7.21, 7.19, 7.15, 6.77, 6.75, 6.65, 6.63, 6.61, 6.60; HRMS (ASAP) (*m/z*): [M]<sup>+</sup> calculated for C<sub>85</sub>H<sub>123</sub>N<sub>3</sub>O<sub>6</sub>Si<sub>6</sub>, 1449.8027; found: 1449.8158. IR (neat): 3033.73, 2951.82, 2909.02, 2873.90, 2097.09, 1490.69, 1481.27, 1457.48, 1403.30, 1342.72, 1237.52, 1188.11, 1113.49, 1059.66, 1003.84, 960.19, 940.27, 909.87, 973.68, 857.40, 829.40, 817.66, 557.06 cm<sup>-1</sup>.



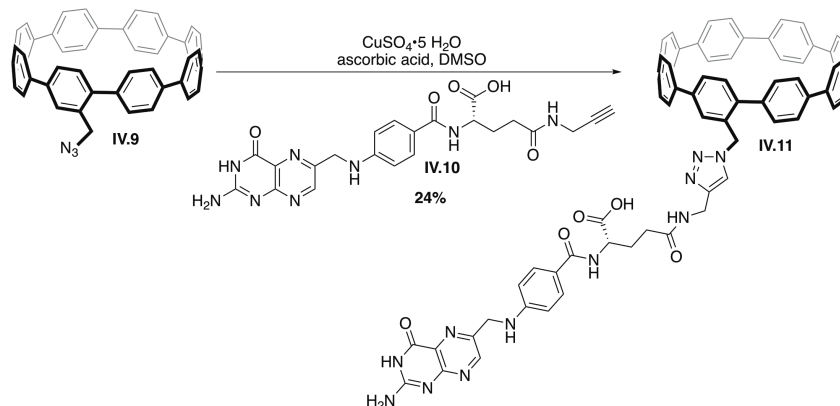
Macrocycle **IV.21** (350 mg, 0.241 mmol, 1.00 equiv) were added to a flame dried flask and suspended in THF (2.4 mL) at room temperature. Tert-butyl ammonium fluoride (TBAF) (1.00 M in THF, 1.60 mL, 1.60 mmol, 6.50 equiv) was added to the suspension dropwise to give a yellow orange clear solution. The reaction was stirred for 2 hours at which time a white precipitate was formed. The reaction was then quenched with deionized water (10 mL) and concentrated to remove the THF. The resulting white solid

was collected by vacuum filtration and rinsed with deionized water (25 mL) and dichloromethane (25 mL) to give a crude white solid that was carried on to the aromatization.

A 0.05 M solution of  $\text{H}_2\text{SnCl}_4$  was prepared by dissolving tin(II) dichloride dehydrate (545 mg, 2.41 mmol) in THF (50 mL) in a flame dried flask then adding HCl (12 M, 0.371 mL, 4.83 mmol) dropwise and stirring for 30 min. The  $\text{H}_2\text{SnCl}_4$  solution (0.05 M, 34 mL, 1.69 mmol, 7 equiv) was added to the crude free alcohol macrocycle solid (0.2414 mmol, 1.00 equiv) in a flame dried flask. The reaction immediately became clear and turned yellow. The mixture was stirred for 3 hours then the reaction was quenched with a solution of saturated sodium bicarbonate in deionized water (50 mL). The mixture was filtered through a pad of celite that was rinsed with deionized water (10 mL) and dichloromethane (150 mL). The dichloromethane layer was separated and the product was extracted from the aqueous layer with dichloromethane (2 x 100 mL). The combined organic layers were washed with deionized water (2 x 100 mL), brine (1 x 100 mL) dried over sodium sulfate and concentrated to give a yellow solid. The product was dry loaded onto celite and purified with silica gel column chromatography (25-28% dichloromethane/hexanes) to give the product **IV.9** as a pristine yellow solid. (78.5 mg, 49%). mp >230 °C decomp.  $^1\text{H}$  NMR (500 MHz,  $\text{CDCl}_3$ ):  $\delta$  7.73 (s, 1H), 7.55 (d,  $J$  = 8.6 Hz, 2H), 7.53 (d,  $J$  = 8.5 Hz, 4H), 7.52-7.46 (overlap, 14H), 7.43 (d,  $J$  = 8.5 Hz, 4H), 7.39 (d,  $J$  = 8.4 Hz, 2H), 7.27 (d,  $J$  = 8.2 Hz, 2H), 7.03 (d,  $J$  = 8.4 Hz, 1H), 6.86 (d,  $J$  = 8.4 Hz, 1H), 4.71 (s, 2H);  $^{13}\text{C}$  NMR (125 MHz,  $\text{CDCl}_3$ ): 139.48, 139.40, 138.99, 138.44, 138.42, 138.07, 138.00, 137.97, 137.95, 137.95, 137.92, 137.87, 137.87, 137.60, 137.45, 133.84, 132.31, 130.72, 129.63, 128.26, 128.03, 127.69, 127.66, 127.64, 127.55, 127.50, 127.49, 127.47, 126.12, 53.13; HRMS (ASAP) ( $m/z$ ):  $[\text{M}]^+$  calculated for  $\text{C}_{50}\text{H}_{36}\text{O}_2\text{Na}$ , 663.2674; found: 663.2640. IR (neat): 3017.59, 2920.89, 2092.86, 1585.15, 1481.11, 1386.17, 1336.02, 1263.71, 1179.60, 1112.10, 998.76, 938.76, 850.28, 807.17, 724.55  $\text{cm}^{-1}$ .



This procedure was adapted from a previously reported procedure.<sup>56</sup> Folic acid **IV.22** (1.00 g, 2.23 mmol, 1.00 equiv) was suspended in DMSO (45 mL) in a flame dried flask and dissolved with light heating in a water bath at 50°C for 30 min. N-Hydroxysuccinimide (287 mg, 2.49 mmol, 1.1 equiv) and N,N'-Dicyclohexylcarbodiimide (514 mg, 2.49 mmol, 1.1 equiv) were added to the flask and the reaction was stirred at room temperature for 18 hours at which time a white precipitate was observed. The resulting precipitate was collected via gravity filtration and the filtrate reaction mixture was added to a flame dried flask. Then triethylamine (0.38 mL, 2.72 mmol, 1.2 equiv) and propargyl amine (0.17 mL, 2.72 mmol, 1.2 equiv) were added to the reaction flask and stirred for another 18 hours. The reaction was quenched with the addition of a solution of 20% acetone in ether (100 mL) and the resulting solid was collected via centrifugation, rinsed with acetone (50 mL) then collected again via centrifugation. This solid was dissolve in water (50 mL) with heating at 50°C with sonication for 30 min. Then the red solution was acidified with 12M HCl and the resulting filtrate was collected via vacuum filtration and then rinsed with MeCN (3 x 20 mL) and ether (2 x 20 mL). The resulting orange solid gave **IV.10** as the major product contaminated with **IV.22** and the  $\alpha$ -substituted folate isomer (1.08 g, 68%). The product mixture is consistent with previous reports with **IV.10** as the major product.<sup>48</sup>



This procedure was adapted from a previously reported procedure.<sup>48</sup> Folate **IV.10** as a mixture from the previous reaction (17.0 mg, 0.0362 mmol, 1.60 equiv), azide[8]CPP **IV.9** (15.0 mg, 0.0226 mmol, 1.00 equiv), sodium ascorbate (8 mg, 0.0452 mmol, 2.00 equiv) and  $\text{CuSO}_4 \cdot 5\text{H}_2\text{O}$  (1.1 mg, 0.00450 mmol, 0.2 equiv) were added to a flame dried microwave vial and suspended DMSO (1.0 mL). The reaction mixture was stirred in the microwave for 1 hour at 70°C then the resulting brown reaction mixture was quenched with acetone (10 mL). This solution was stirred in an ice bath for 30 min then the resulting solid was collected via centrifugation, rinsed with dichloromethane (2 x 10 mL) acetonitrile (2 x 10 mL) collecting each time with centrifugation. The solid was suspended in water with aid of sonication for 30 min then acidified with 12M HCl. The resulting solid was collected via vacuum filtration and rinsed with deionized water (2 x 5 mL), MeCN (2 x 5 mL) and diethyl ether (2 x 5 mL). This solid was dissolved in 0.1 M NaOH in methanol and filtered over cotton to remove any undissolved solids and the filtrate was acidified with 12 M HCl to give a yellow precipitate. The solid was collected via vacuum filtration to give **IV.11** as a yellow solid contaminated with the  $\alpha$ -substituted folate isomer (4.5 mg, 24%). mp >250 °C decomp. <sup>1</sup>H NMR (600 MHz, DMSO):  $\delta$  8.64 (s, 1H), 8.34 (overlap, 1H), 8.18 (d, 8.0 Hz, 1H), 7.97 (s) 7.93 (s) (1H), 7.72-7.68 (overlap, 9H), 7.65-7.62 (overlap, 13H), 7.60 (d,  $J$  = 8.2 Hz, 2H), 7.56 (d,  $J$  = 8.3 Hz, 2H), 7.49 (d,  $J$  = 8.2 Hz, 2H), 7.39 (d,  $J$  = 7.3 Hz, 2H), 7.14 (d,  $J$  = 8.4 Hz, 1H), 6.93 (overlap, 1H), 6.89 (m, 1H), 6.63 (overlap, 2H), 5.95 (s) 5.94 (s) (2H), 4.48 (s, 2H), 4.32-4.22 (overlap, 3H), 2.27-2.18 (overlap, 2H) 2.07(m) 1.98 (m) (1 H), 1.89 (m, 1H); <sup>13</sup>C NMR (150 MHz, DMSO): 174.10, 173.83, 171.86, 171.50, 166.36, 160.84, 156.61, 153.72, 150.77, 148.71, 148.47, 145.30, 138.13, 138.07, 137.62, 137.08, 136.76, 136.59, 136.56, 136.25,

136.13, 133.54, 132.83, 132.78, 129.64, 129.47, 129.00, 127.95, 127.80, 127.52, 127.19, 127.18, 127.14, 127.04, 123.10, 111.17, 51.13, 45.91, 40.43, 34.25, 31.80, 31.53, 30.57; HRMS (ASAP) ( $m/z$ ):  $[M]^+$  calculated for  $C_{71}H_{55}N_{11}O_5$ , 691.2631; found: 691.2634. IR (neat): 3628.17, 3325.00, 3066.00, 3023.12, 2941.83, 2859.01, 1696.98, 1639.38, 1693.53, 1524.02, 1500.93, 1481.87, 1381.47, 1331.61, 1251.83, 1183.37, 1112.36, 1052.02, 999.56, 956.17, 884.17, 816.42, 766.34, 725.77  $cm^{-1}$ .

#### 4.4.3. Cell Culture, Cytotoxicity, and Confocal Microscope Details

HeLa cells were cultured in high glucose Dulbecco's modified Eagle's medium (DMEM) supplemented with 10% fetal bovine serum (FBS) and 1% penicillin/streptomycin at 37 °C under 5% CO<sub>2</sub> atmosphere. For disulfonate[8]CPP **IV.1** studies, confluent HeLa cells were incubated in FBS-free DMEM containing 1 (0.5 – 10  $\mu$ M) with 0.5% DMSO for up to 24 hours in a 96-well plate (10<sup>4</sup> cells/well). For the surfactant studies (section 4.4.4.), surfactant solubilized [8] or [12]CPP, confluent cells were incubated in FBS-free DMEM with the nano hoop in 1 or 5 wt% Pluronic F108 for 2 hours in a 96-well plate (10<sup>4</sup> cells/well). For cytotoxicity studies control groups were treated with FBS-free DMEM with 0.5% DMSO for **IV.1** or 0.1 wt% Pluronic F108 for surfactant studies. After treatment with vehicle, 100  $\mu$ L of FBS-free DMEM containing 10% CCK-8 solution was added to each well and the cells were incubated for 2 hours more at 37 °C. The absorbance at 450 nm was measured with a microplate reader and the cell viability was calculated and normalized to the control group.

For live cell imaging HeLa cells were plated in poly-D-lysine coated plates (MatTek) containing 2 mL of DMEM and incubated at 37 °C under 5% CO<sub>2</sub> atmosphere for 24 hours. The confluent cells were washed with PBS buffer then co-incubated with **IV.1** (10  $\mu$ M), or surfactant solubilized [8] or [12]CPP, and NucRed dye (2 drops) in FBS-free DMEM for 1 hour. After removing extracellular vehicle by washing with PBS, cells were bathed in 2 mL of PBS while cell imaging was performed on the cells using a Lecia DMI8 fluorescent microscope equipped with a Excelitas X-Cite 110LED light source. All cubes for imaging were purchased from Chroma.

**Table 4.1.** Details for the cubes used in the experiments outlined in this document and in the manuscript.

Cube	Excitation filter	Excitation range (nm)	Emission filter	Emission range (nm)	Band-stop filter
DAPI/FluoroGold Longpass	AT350/50x	300-398	ET425lp	422-600	T400lp
49006-ET-Cy5	ET620/60x	585-654	ET700/75m	659-745	T660lpxr

For colocalization experiments the cell culture procedures described above were followed to give confluent cells on poly-D-lysine coated plates (MatTek). The DMEM medium was removed and the cells were washed with PBS buffer then incubated with 500 nM of CellTracker Red CMTPX, ER-Tracker Red and MitoTracker Red RM in FBS-free DMEM for 30 minutes then washed with PBS buffer. The cells were then incubated with a 1  $\mu$ M solution of **IV.1** in FBS-free DMEM for 1 hour then washed with PBS buffer, then bathed in 2 mL of PBS for cell imaging.

For the FA[8]CPP **IV.11** experiments the cell culture procedures described above were followed to give confluent cells on poly-D-lysine coated plates (MatTek). The DMEM medium was removed and the cells were washed with PBS buffer. The cells were then incubated with **IV.11** (10  $\mu$ M) or **IV.9** (10  $\mu$ M) for 2 hours in FBS-free DMEM. For the free folic acid experiments, the cells were incubated with folic acid (5 mM) for 30 minutes before incubation with **IV.11**. The cells were then washed with PBS buffer and incubated in FBS-free DMEM for 18 hours. For imaging the cells were washed with PBS buffer then bathed in 2 mL of PBS.

#### 4.4.4. Nano hoop Surfactant Images

[8]CPP (5.6 mg, 0.0092 mmol) or [12]CPP (5.8 mg, 0.0064 mmol) were dissolved in 5 mL of 5 wt% Pluronic F108 in fetal bovine serum (FBS) free Dulbecco's Modified



Eagle's Medium (DMEM) by stirring the solutions at high speed for 21 hours. Undissolved nano hoop was separated from the solution by centrifugation of the resulting suspension for 1 hour at 4300 rpm at 25 °C. The supernant was removed, analyzed with UV-Vis spectroscopy and kept as the nano hoop stock solution. Cells were incubated with the [8] or [12]CPP solutions as described in the cell culture and cytotoxicity procedures section of this supporting information with solutions (1 or 5 wt% Pluronic F108 in DMEM) composed of 100%, 50% or 25% of the nano hoop stock solution. Cytotoxicity was measured using the CCK8 cell assay and the nano hoop was visualized in HeLa cells with confocal microscopy.

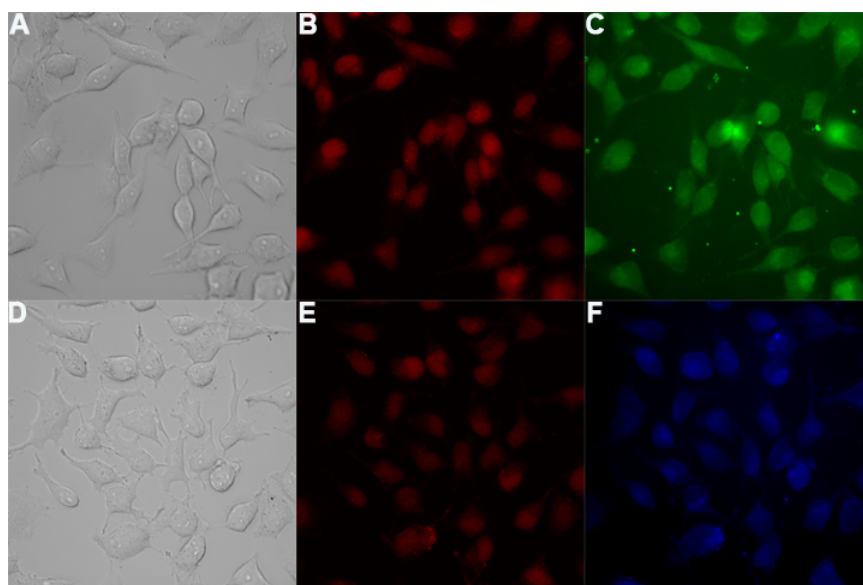


**Figure 4.5.** Fluorescent images of [8]CPP and [12]CPP in live cells. HeLa cells were incubated with nuclear stain NucRed® live 647 (A-F) in the presence of a [8]CPP in a 5 wt% solution of pluronic F108 (A-C) or in the presence of a [12]CPP in a 5 wt% solution of pluronic F108 (D-F) for 1 hour and washed before imaging. The channels shown are the differential interference contrast (A and D), CY5 (colored red, B and E), DAPI-LP (colored green, C) and DAPI (colored blue, F). Channels C and F were treated with 3x3 binning and 3s exposure times to visualize the fluorescent emission.

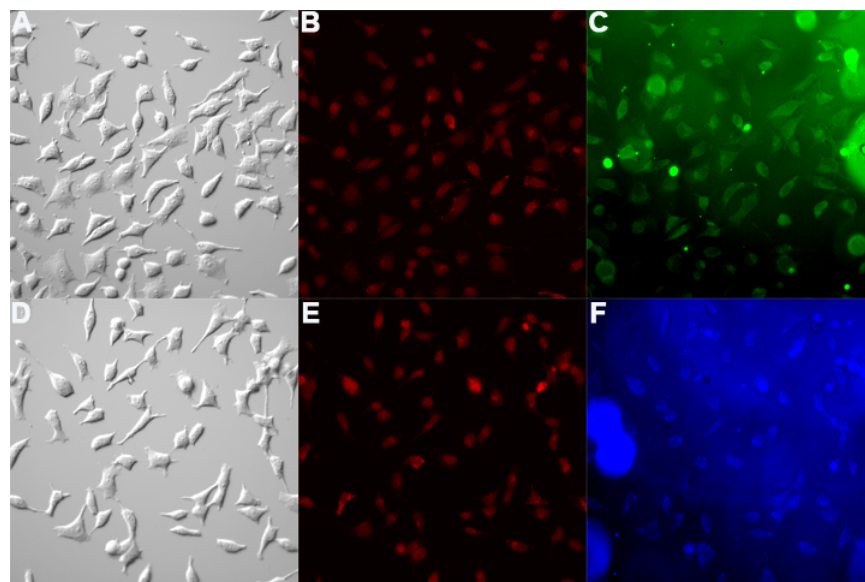


**Figure 4.6.** Fluorescent images of [8]CPP and [12]CPP in live cells. HeLa cells were incubated with nuclear stain NucRed® live 647 (A-F) in the presence of a [8]CPP in a 5 wt% solution of pluronic F108 and cetrimonium bromide (CTBA) (A-C) or in the presence of a [12]CPP in a 5 wt% solution of pluronic F108 and CTAB (D-F) for 1 hour and washed before imaging. The channels shown are the differential interference contrast (A and D), CY5 (colored red, B and E), DAPI-LP (colored green to represent the emission of [8]CPP, C) and DAPI (colored blue to represent the emission of [12]CPP, F). Channels C and F were treated with 3x3 binning to visualize the fluorescent emission. Large aggregated structures are clearly visible in the nanohoop channels (C and F).

#### 4.4.5. Nanohoop Cytotoxicity

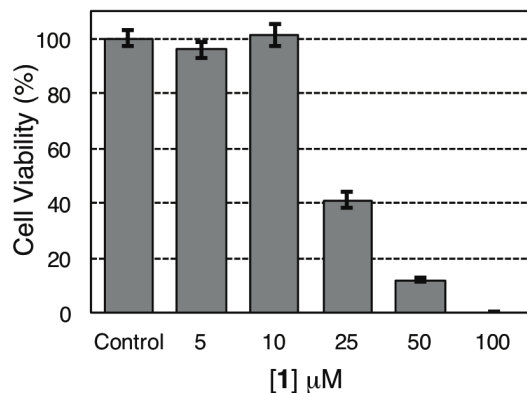


**Figure 4.7.** Cell viability of disulfonate[8]CPP **IV.1** in HeLa cells. The results are expressed as the mean with error bars representing the standard error in measurement (n=6).

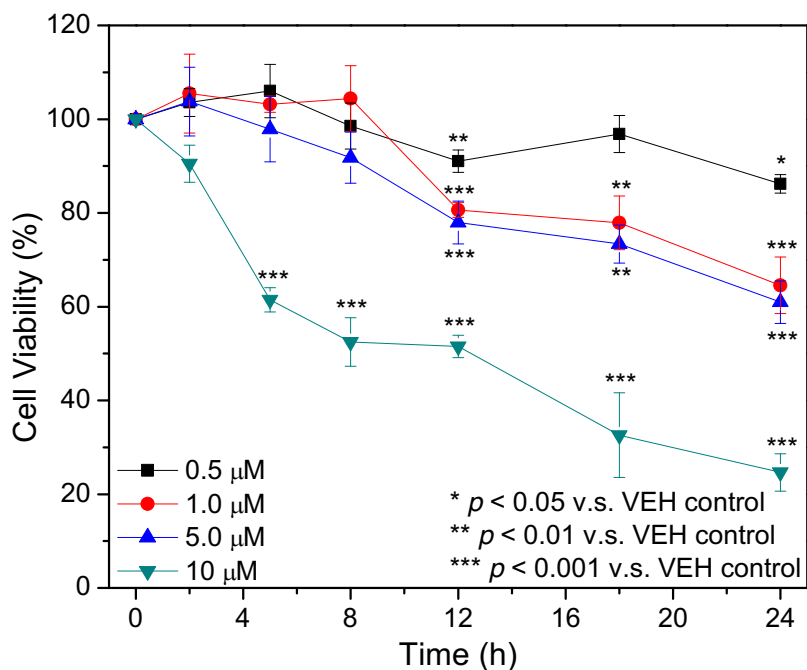


**Figure 4.8.** Long-term cell viability of disulfonate[8]CPP **IV.1** in HeLa cells. The results are expressed as the mean with error bars representing the standard error in measurement (n=6).

#### 4.4.6. Colocalization Experiments

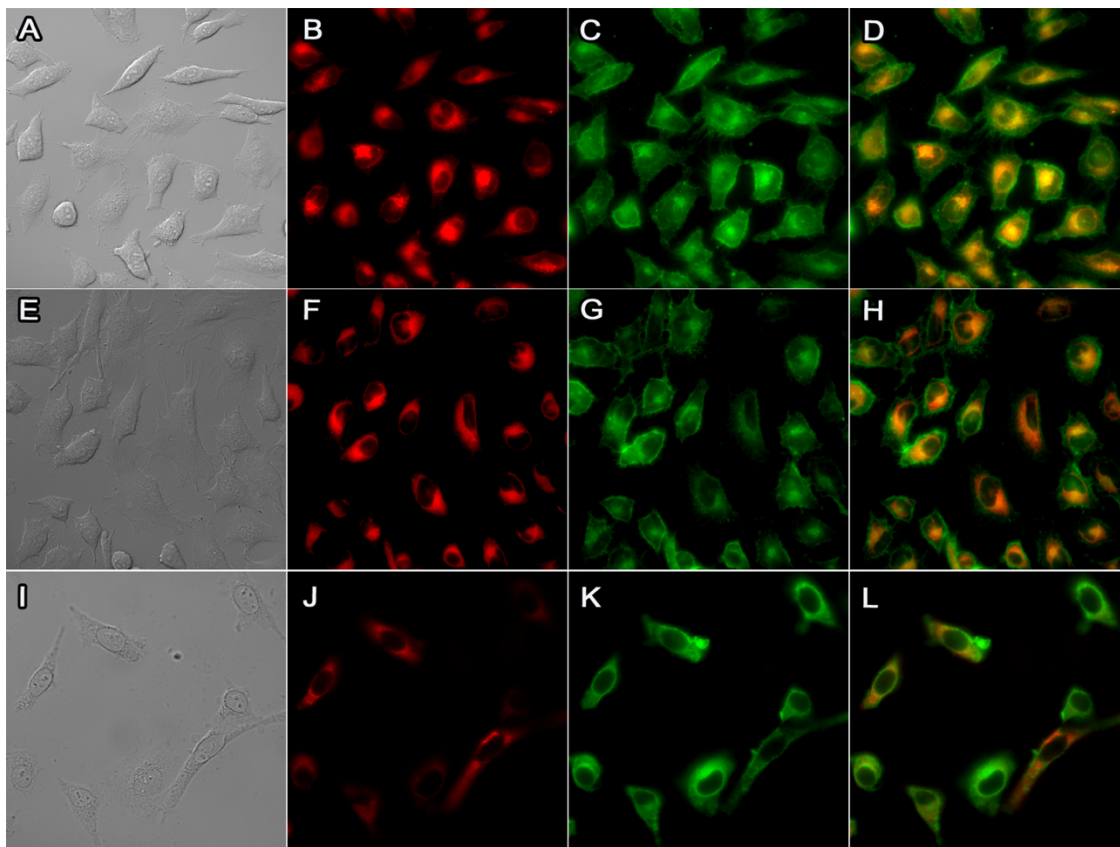


**Figure 4.9.** DIC and fluorescent images of live HeLa cells for colocalization experiments of disulfonate[8]CPP **IV.1** with CellTracker Red CMTX (A-D), ER-Tracker Red (E-H) and MitoTracker Red RM (I-L). DIC (A, E, I); CY5 (B, F, J); DAPI-long-pass (C, G, K); CY5 and DAPI-long-pass overlay (C, H, L).

**Table 4.2.** Pearson's colocalization coefficients for the images shown in **Figure 4.8** and **Figure 4.3**.

Localization Dye	Organelle	Pearson's coefficient
CellTracker Red CMTPX	--	0.78
ER-Tracker Red	Endoplasmic reticulum	0.63
Mito Tracker Red RM	Mitochondria	0.38
NucRed® 647	Nucleus	0.33

#### 4.4.7. Methods of Optical Characterization

The quantum yield of disulfonate[8]CPP **IV.1** (DMSO and PBS Buffer with 0.1% SDS) and **IV.9** (DCM) was determined as described by Jobin Yvon Horiba<sup>58</sup> using anthracene (ethanol) and quinine sulfate (0.1M H<sub>2</sub>SO<sub>4</sub>) as standards while exciting at 330nm for **IV.1** and 335 for **IV.9**. The fluorescence of **IV.1** and **IV.9** were integrated from 420-650 nm while anthracene was integrated from 360-480 nm and quinine sulfate was integrated from 400-600 nm.

For pH studies, 10  $\mu$ M solutions of either disulfonate[8]CPP **IV.1** or fluorescein in 1:1 MeOH:100 mM KCl, 100 mM KOH were prepared from 20mM DMSO stock solutions. The pH of three samples of either **IV.1** or fluorescein were measured using a SevenMulti Mettler Toledo pH probe and adjusted to the same value using 1 M - 100 mM solutions of HCl or KOH. The absorbance and fluorescence of each sample was measured and plotted as an average against the measured pH value of the sample from pH 12 - 3.

For photobleaching studies solutions of disulfonate[8]CPP **IV.1** (0.12  $\mu$ M) and fluorescein (0.12  $\mu$ M) were prepared in PBS buffer with 0.1% SDS and PBS buffer solutions respectively that had been sparged with O<sub>2</sub> for 1 hour. The fluorescence emission was measured every 10 minutes while the sample was under constant irradiation for 6 hours.

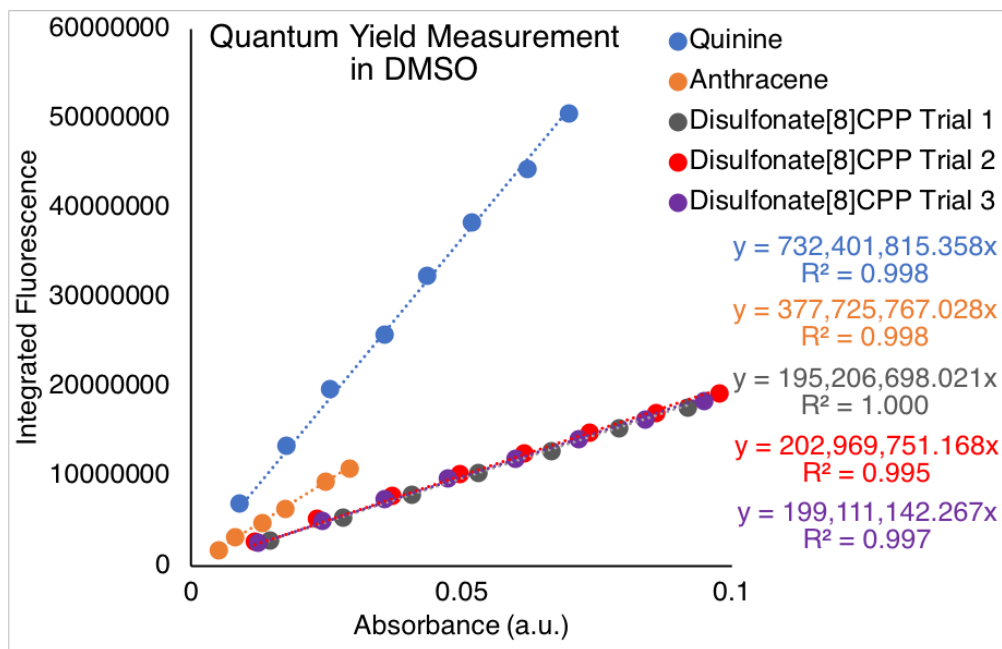


Figure 4.10. Quantum yield measurement of IV.1 in DMSO.

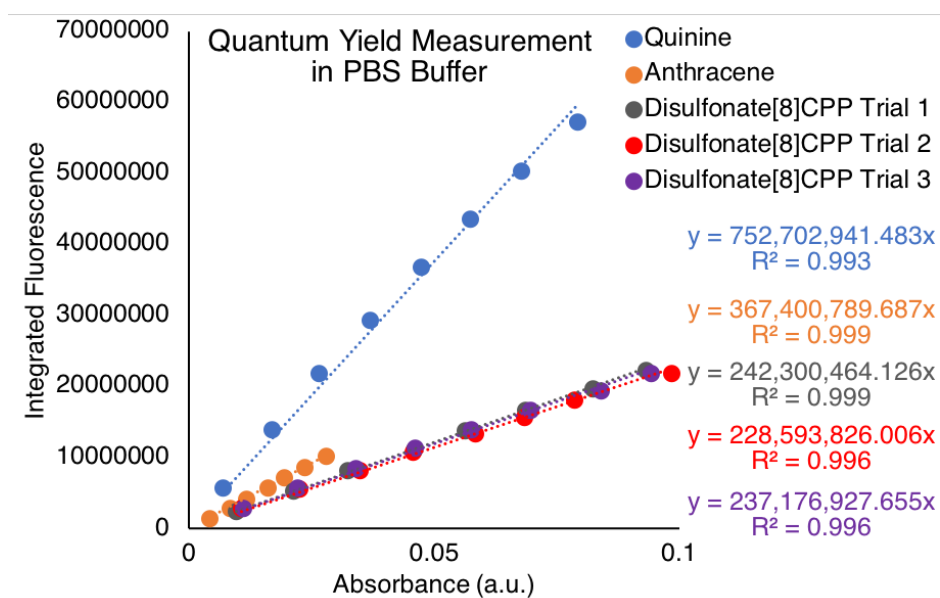
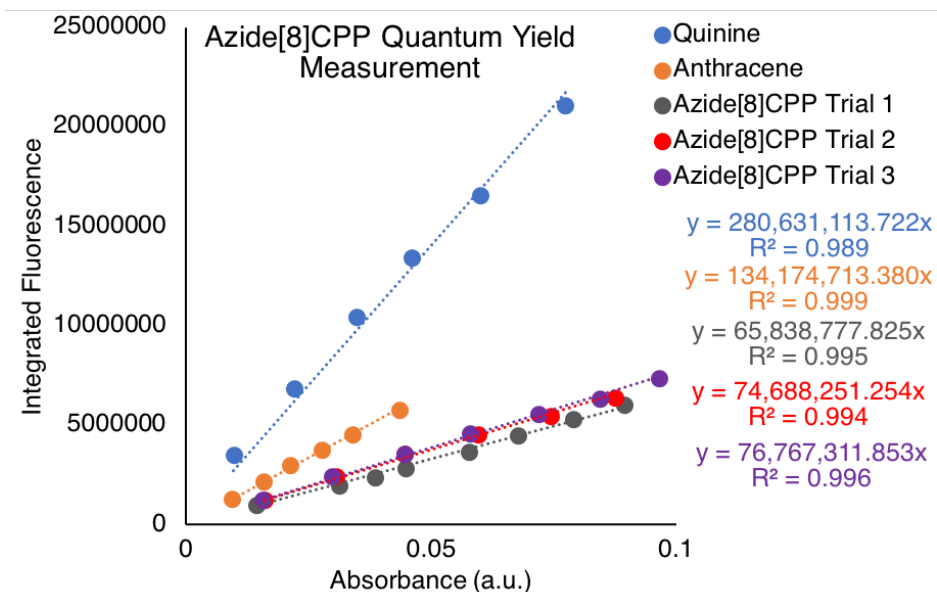
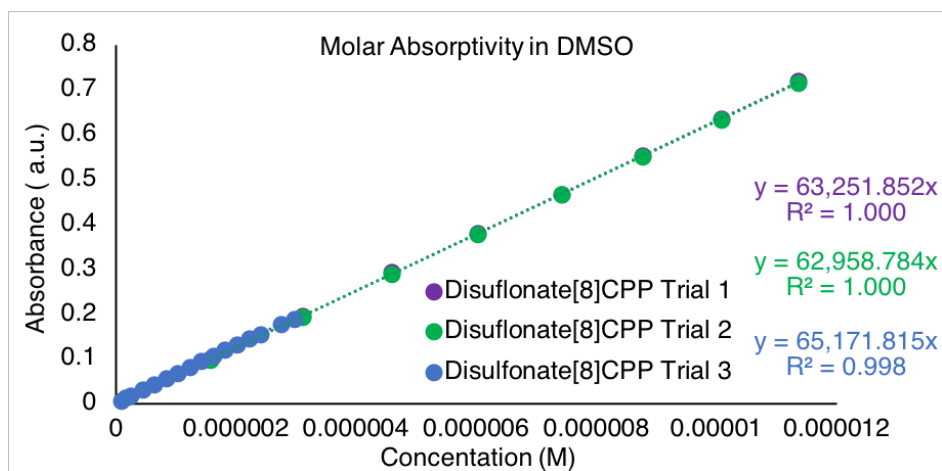


Figure 4.11. Quantum yield measurement of IV.1 in PBS Buffer with 0.1% SDS.



**Figure 4.12.** Quantum yield measurement of **IV.9** in dichloromethane.



**Figure 4.13.** Molar absorptivity measurement of **IV.1** in DMSO.

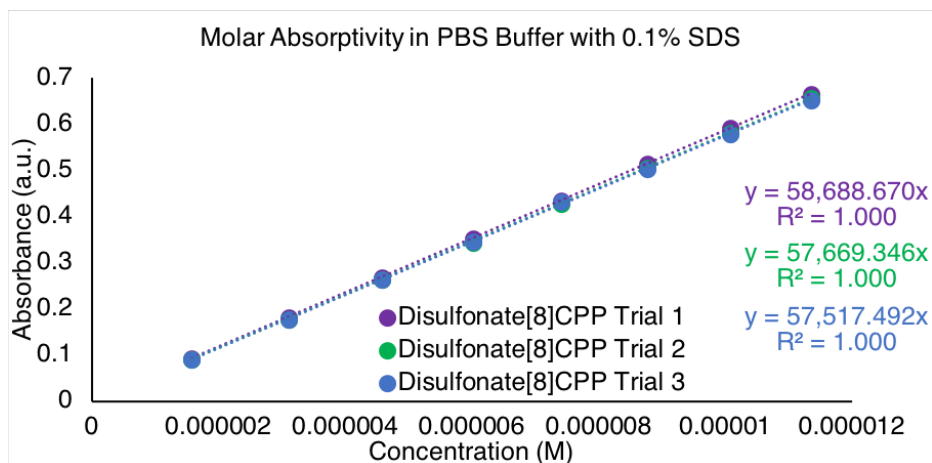


Figure 4.14. Molar absorptivity measurement of IV.1 in PBS Buffer with 0.1% SDS.

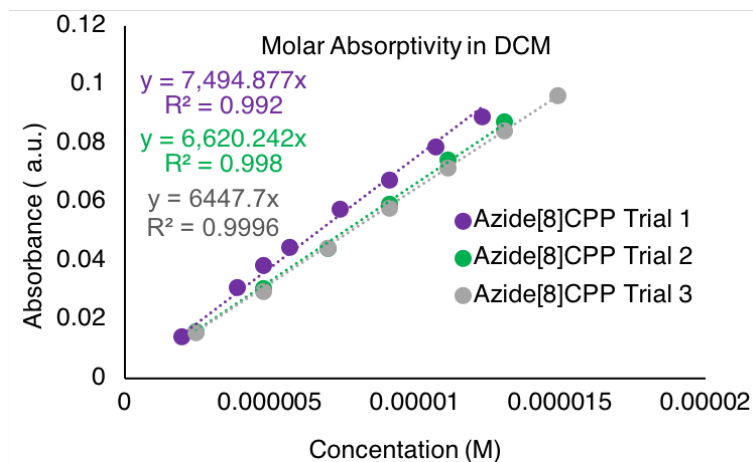
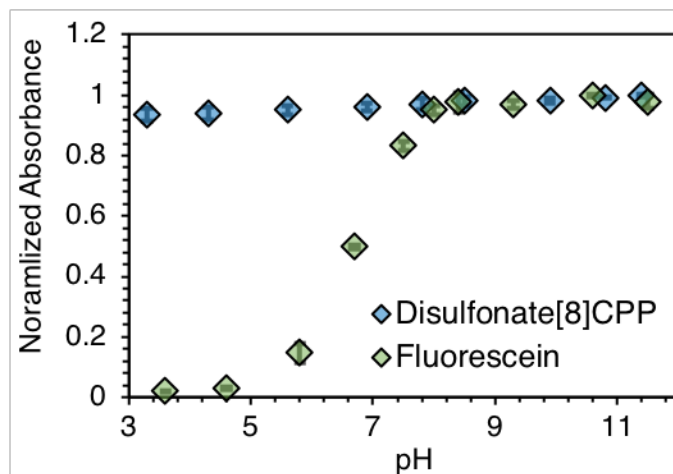


Figure 4.15. Molar absorptivity measurement of IV.9 in dichloromethane.



**Table 4.3.** Summary of the optical properties of disulfonate[8]CPP **IV.1** and azide[8]CPP **IV.9** using the data presented in this section (n=3).

Compound	Measurement	Solvent	Average	Standard Deviation
<b>IV.1</b>	$\phi$	DMSO	0.174	0.003
<b>IV.1</b>	$\phi$	PBS Buffer	0.168	0.005
<b>IV.9</b>	$\phi$	DCM	0.16	0.01
<b>IV.1</b>	$\epsilon$	DMSO	$6.4 \times 10^4$	$0.1 \times 10^4$
<b>IV.1</b>	$\epsilon$	PBS Buffer	$5.80 \times 10^4$	$0.06 \times 10^4$
<b>IV.9</b>	$\epsilon$	DCM	$6.8 \times 10^3$	$0.6 \times 10^3$



**Figure 4.16.** The absorbance of **IV.1** at 330 nm remains constant as pH changes while the absorbance of fluorescein at 494 nm is pH dependent. Error bars represent standard deviation (n=3).

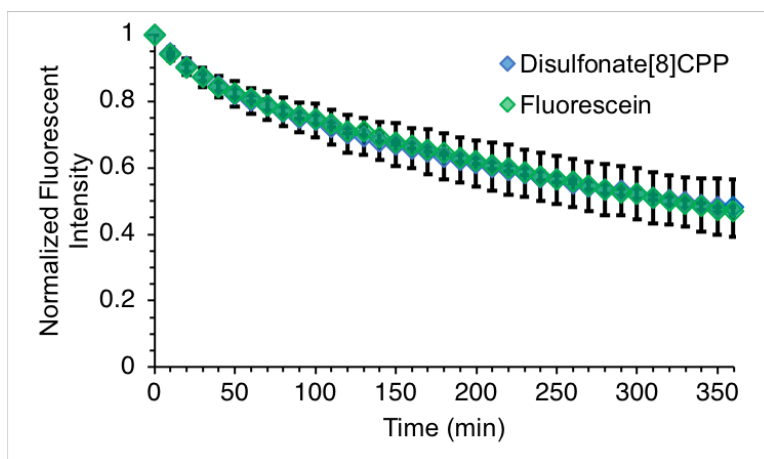


**Figure 4.17.** Photobleaching of nano hoop **IV.1** and fluorescein under constant irradiation over time in a cuvette. The nano hoop was excited at 328 nm and the emission was monitored at 510 nm while fluorescein was excited 494 nm and the emission was monitored 512 nm.

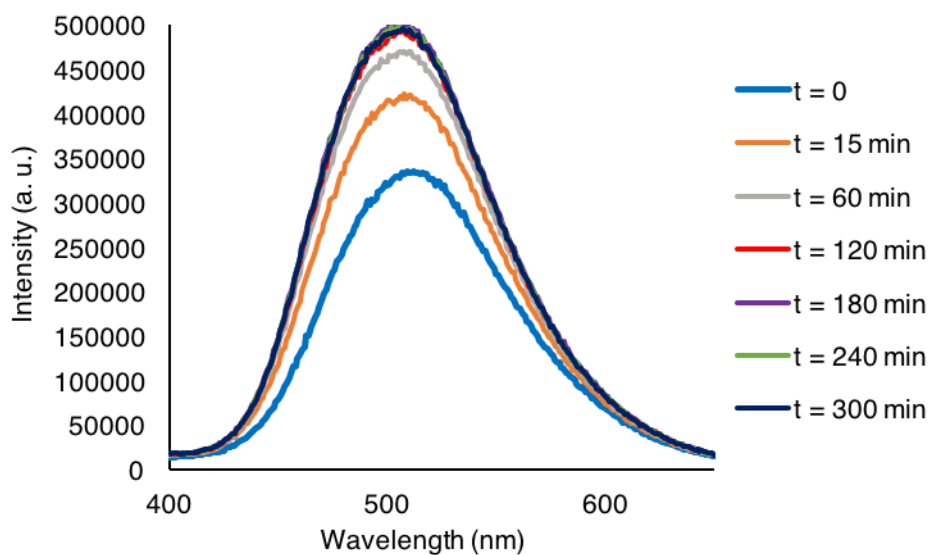


**Figure 4.18.** The fluorescence of **IV.1** (excitation at 330 nm) in PBS buffer solution with 10% fetal bovine serum (FBS). The initial increase in fluorescence is likely due to increased solubility of **IV.1** in the 10% FBS solution.

#### 4.4.8. Optical Characterization and Cytotoxicity Studies for Surfactant Solubilized Nano hoops

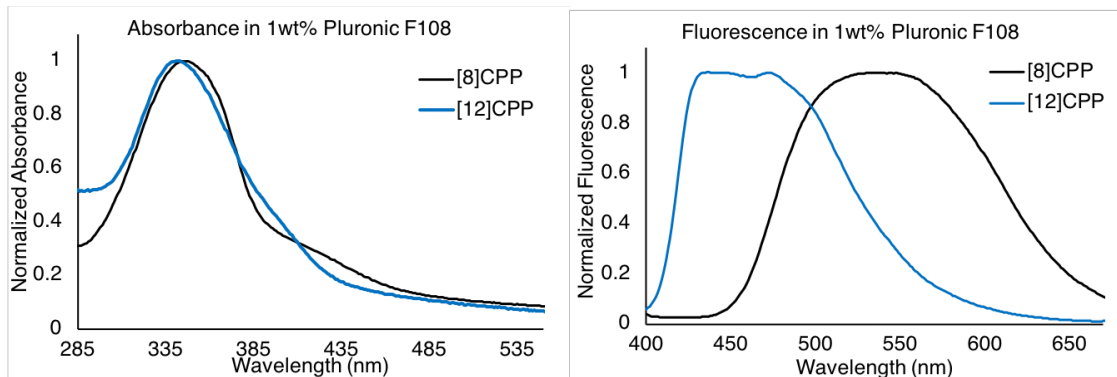


**Figure 4.19 (left) and Figure 4.20 (right).** Absorption and emission spectra of [8] and [12]CPP stock solutions (nanohoop in deionized water with 1wt% pluronic F108). Absorption and emission normalized by scaling the maxima to 1.

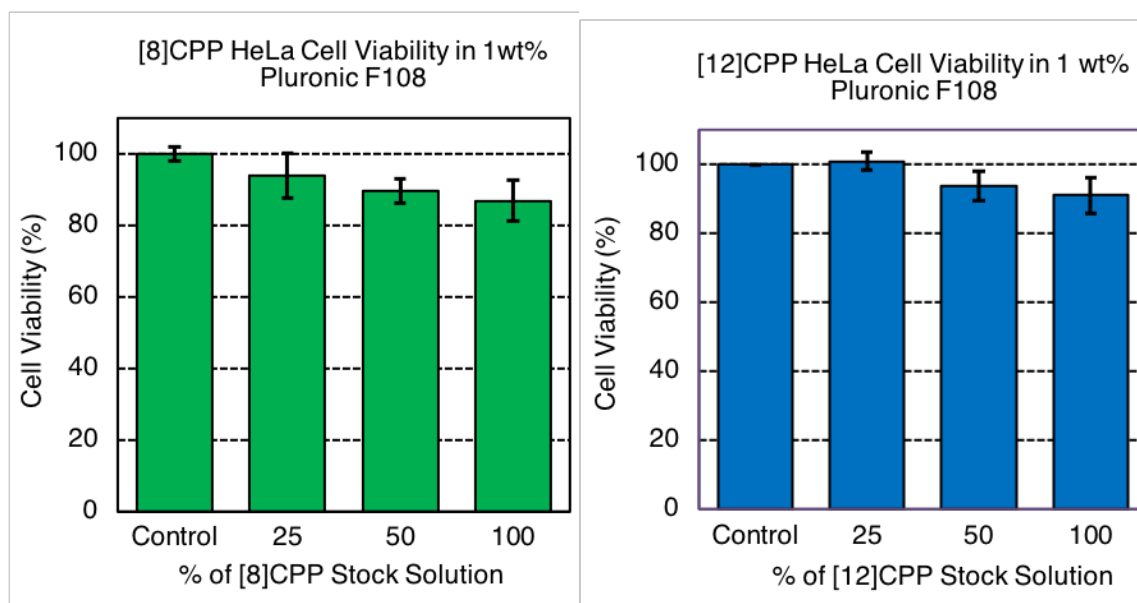


**Figure 4.21 (left) and Figure 4.22 (right).** Cell viability of [8] and [12]CPP in HeLa cells with 1 wt% pluronic F108. Error bars show standard error in measurement (n=6).

#### **4.5. Bridge to Chapter V**

In this chapter the first example of nanohoops as a new class of biocompatible fluorophores is described. We found that the unique optical properties of this scaffold are retained when aqueous solubilizing functional groups are appended to the backbone, presenting this cyclic architecture as new chemical space for fluorescent probe design. In the next chapter the development of a synthetic strategy to prepare nanohoops containing the linear acene pentacene is described. The effect that the macrocyclic backbone has on the properties of traditional linear organic materials is examined to present nanohoop incorporation as a design strategy for the synthesis of novel organic materials.

## CHAPTER V

### THE SYNTHESIS OF A PENTACENE INCORPORATED NANOHOOP

This chapter includes unpublished co-authored material. Experimental work was performed by either myself or Cyrus Waters under my direction. This chapter was written by myself with editorial assistance from Professor Ramesh Jasti.

The development of synthetic strategies that modify the electronics of organic compounds such as pentacene have unveiled important structural-property relationships that dictate the performance of these materials in a variety of applications. Macrocyclic formation has recently emerged as a strategy to alter the properties of organic materials resulting novel compounds with device properties that outperform their linear counterparts. The unique structural effects afforded by the cyclic, conjugated structure of cycloparaphenylenes present this class of molecules as a promising scaffold for the design of new types of organic materials with altered electronic structures. In this study we investigate the effects that the nanohoop architecture has on the properties of pentacene, a well-characterized linear organic semiconductor. We describe a novel synthetic strategy to build curvature into this planar acene and enabled the incorporation of pentacene into advanced intermediates towards the synthesis of pentacene[10]CPP. Our initial studies demonstrate that the nanohoop structure alters the electronic state of pentacene making isolation of the target molecule challenging. We hypothesize that the instability of this product is a result of structural deformation that enhances the diradical character of pentacene and propose experiments to probe this behavior in the future.

#### **5.1. Introduction**

Organic semiconducting molecules are promising materials in molecular electronics because they are light-weight, flexible and their structures are easily tuned with chemical modification.<sup>1-5</sup> In particular, pentacene has demonstrated remarkable properties as a component of organic light emitting diodes (OLEDs), organic field effect

transistors (OFETs) and photovoltaic devices (**Figure 5.1**).<sup>6-10</sup> This broad applicability arises in part from the development of synthetic strategies to incorporate functional groups that tune the electronic and structural properties of pentacene.<sup>11-16</sup> For example, the singlet fission (SF) capabilities of this molecule are dramatically impacted by functional groups that change the electronic delocalization and conjugation of the scaffold.<sup>17-20</sup> Functionalization of pentacene with bulky solubilizing groups such as triisopropylsilylethynyl (TIPS) promotes 2D  $\pi$ -stacking in the solid state to give derivatives with improved performance as components of OFETs.<sup>12</sup> Therefore, the design of unique pentacene derivatives with altered electronic and structural properties can provide access to novel types of organic nanomaterials for molecular electronics.

Conjugated macrocycles such as [n]cycloparaphenylenes, also known as nanohoops, have presented themselves as new types of organic materials with altered electronic and solid state properties (**Figure 5.1**).<sup>21-24</sup> In these molecules subtle structural effects, that are a result of their macrocyclic architecture, result in a bent, radially oriented  $\pi$ -system with small dihedral angles that increase conjugation and electronic delocalization around the hoop.<sup>22, 25</sup> This results in tunable, size-dependent electronic properties where the HOMO $\rightarrow$ LUMO gap of the nanohoop decreases as the diameter of the hoop decreases in stark contrast to many linear conjugated systems.<sup>22, 26</sup> Additionally, the electron rich pore of the nanohoop afforded by the bent  $\pi$ -system provides a hydrophobic cavity for the formation of host-guest complexes with complementary guests.<sup>27-29</sup> These unique properties are maintained in derivatives of nanohoops where the benzene rings are substituted with heteroarenes presenting nanohoop formation as a design strategy to tune the electronic properties of organic molecules.<sup>30-38</sup>

Recently, the Nuckolls lab has demonstrated that the performance of linear, conjugated donor-acceptor systems can be improved in molecular electronics by bending these systems into conjugated macrocycles.<sup>39-41</sup> Motivated by these results, the tunable structure of pentacene and unique properties afforded by the nanohoop structure we sought to prepare pentacene[10]CPP (**V.1**) and study the impact that the nanohoop architecture has on the electronic properties of pentacene (**Figure 5.1**). Herein, we describe our progress towards the synthesis of **V.1** and provide insight on the reactivity of this molecule. Our novel synthetic strategy takes advantage of the reactivity of pentacene

and  $^1\text{O}_2$  to prepare curved advanced intermediates with the *cis*-stereochemistry required for nano hoop synthesis.<sup>15</sup> This study provides a general synthetic strategy for the preparation curved, advanced intermediates towards acene containing macrocycles with altered electronic structures as novel organic nanomaterials.

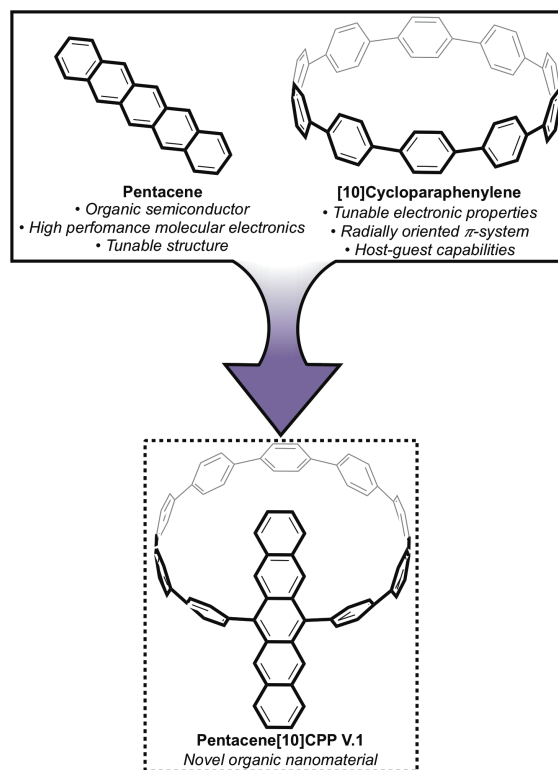


**Figure 5.1.** Pentacene and [10]cycloparaphenylene combine to create novel organic nanomaterial **V.1**.

## 5.2. Results

The main synthetic challenge towards the preparation of cycloparaphenylenes and their derivatives stems from the large amount of strain associated with bending linear oligophenylenes into cyclic structures. Strategies to overcome this strain utilize “corner units” that provided curvature to linear precursors and favor macrocycle formation.<sup>30,42</sup> In particular, our lab has pioneered the use of cyclohexadienes with *cis*-stereochemistry as corner units that are reduced in the final step of the synthetic sequence to give the fully aromatized nano hoop.<sup>23, 24, 43</sup> To adapt this synthetic approach for the preparation of **V.1**

we first aimed to prepare an advanced intermediate with *cis*-stereochemistry about the 6 and 13 positions of pentacene. Our synthesis began with the monolithiation of 1,4-dibromobenzene and subsequent addition of two equivalents this nucleophile into 6,13-pentacenequinone **V.2** (**Figure 5.2**). In our hands, this addition only gave dibromide **V.3** as the *trans*-isomer in 57% yield. Following a previously reported procedure, **V.3** was aromatized with  $\text{H}_2\text{SnCl}_4$  then stirred as dilute solution under an  $\text{O}_2$  atmosphere in the presence of sunlight to give endoperoxide **V.4** in 61% yield over two steps.<sup>44</sup> The preparation of **V.4** was key towards the synthesis of **V.1** as it positions the oxygens on the same face of the molecule, providing the desired *cis*-stereochemistry at the 6 and 13 positions of pentacene. Reduction of the endoperoxide by heating **V.4** with Pd/C and aqueous base gave dibromide **V.5** as the *cis*-isomer in 66% yield. Interestingly, when **V.4** was treated with more harsh reducing conditions, by stirring with Pd/C under  $\text{H}_2$  atmosphere, fully reduced product was observed.<sup>45</sup> Suzuki-Miyaura cross-coupling of **V.5** and dibromide **V.6** gave macrocycle **V.7** in 34% yield (**Figure 5.2**). The  $^1\text{H}$  NMR spectrum **V.7** shows broad peaks in the cyclohexadiene region that resolve upon cooling, demonstrating the sterically congested nature of this intermediate (**Figure 5.4**). Treatment of **V.7** with tetrabutylammonium fluoride delivered deprotected macrocycle **V.8** in 79% yield.

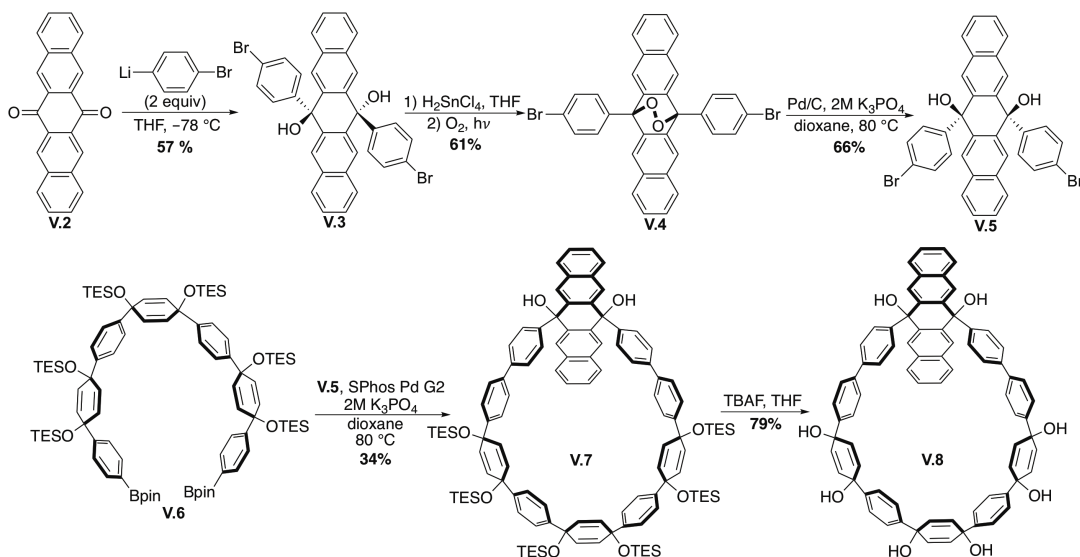


**Figure 5.2.** Synthesis of pentacene containing macrocycles utilizing endoperoxide formation to access *cis*-stereochemistry.



With the advanced macrocyclic intermediate in hand, we began our studies on the reduction of **V.8** to yield the final compound **V.1**. When **V.8** was treated with standard  $\text{H}_2\text{SnCl}_4$  aromatization conditions, the reaction solution immediately became a dark purple color consistent with the formation of the reduced pentacene backbone (**Figure 5.3**).<sup>46</sup> This color persisted for the entire reaction and was maintained during the work-up. However, purification via crystallization or column chromatography resulted in the color fading to give a yellow tinted solution. The  $^1\text{H}$  NMR spectrum of the crude reaction showed one major product with peaks consistent with nanohoop formation. Purification of this mixture with column chromatography and analysis of the major product by  $^1\text{H}$  NMR and  $^{13}\text{C}$  NMR revealed the identity the product as diol **V.9**. Despite being the major product of this reaction by  $^1\text{H}$  NMR, **V.9** was isolated in only 22% yield.

Although the purple color observed during the  $\text{H}_2\text{SnCl}_4$  mediated reaction sequence suggest that **V.1** was formed, we hypothesized that **V.9** might be a result of incomplete aromatization during our initial attempt. Resubjecting **V.9** to  $\text{H}_2\text{SnCl}_4$  aromatization conditions again resulted in the formation of a purple colored reaction solution that faded upon purification to yield **V.9** as recovered starting material (**Figure 5.3**). Treatment of **V.9** with harsh reducing conditions, utilizing sodium hypophosphite and refluxing acetic acid, resulted in the isolation of a green powder identified as over reduced product **V.10** on small scale.<sup>15</sup> Surprisingly, oxidation of **V.10** with 2,3-dihydro-5,6-dicyano-1,4-benzoquinone (DDQ) gave **V.9** as identified by the crude reaction mixture.<sup>35</sup>

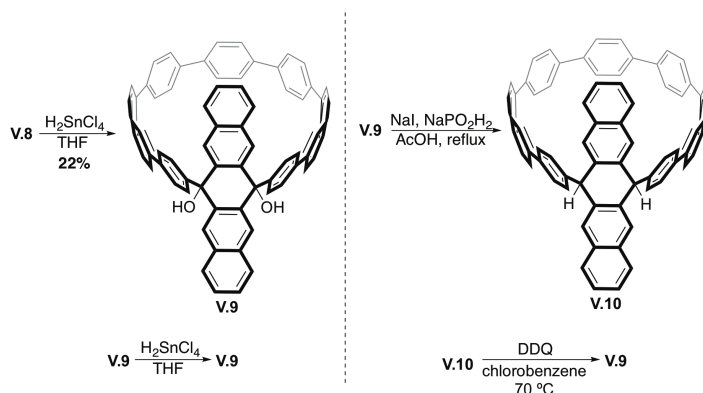


**Figure 5.3.** Reduction and oxidation attempts to prepare target compound **V.1**.

### 5.3. Discussion

Taken together our results thus far suggest that the pentacene backbone of the desired product **V.1** is extremely reactive, complicating its isolation. The purple color observed when **V.8** or **V.9** are subjected to the  $\text{H}_2\text{SnCl}_4$  mediated reaction conditions suggests that the pentacene portion of the molecule is fully aromatized. Analysis of the crude reaction mixture with UV-vis spectrometry shows peaks in the acene fingerprint region at 519 nm, 560 nm and 604 nm that overlay identically with the spectrum of 6,13-diphenylpentacene. Additionally, when the progress of the reaction is monitored with UV-vis these peaks appear almost immediately after  $\text{H}_2\text{SnCl}_4$  is introduced to the solution, further supporting the formation of **V.1**. These results led us to hypothesize that once **V.1** is formed, this nanohoop reacts readily  $^1\text{O}_2$  in a formal [4+2] cycloaddition reaction to give a highly strained endoperoxide intermediate. This intermediate could then be easily reduced to give **V.9** under the  $\text{H}_2\text{SnCl}_4$  or DDQ promoted aromatization conditions.

However, the formation of **V.10** from **V.9** (via **V.1**) with sodium hypophosphite mediated reduction suggests that the mechanism of decomposition for **V.1** may be more complex than the cycloaddition reaction initially proposed. In addition, attempts to isolate other cycloaddition products by quenching aromatization reactions with dienes, such as maleic anhydride, resulted in irreproducible and complex reaction mixtures with no identifiable cycloaddition products. Alternatively, the decomposition of **V.1** may involve the formation of a diradical intermediate as a result of electronic and structural deformation of the pentacene portion of the nanohoop backbone.<sup>47, 48</sup> Although pentacene is traditionally a closed shell (CS) singlet without diradical character, theoretical studies ((U)B3LYP/6-31G(d,p)) suggest that structural deformations can cause a decrease in the HOMO→LUMO gap, and ultimately decrease the singlet→triplet gap, resulting in an increase in diradical character of pentacene. In this study, the authors found that when the HOMO→LUMO gap is less than 2.2 eV, pentacene begins to exhibit this behavior.<sup>49</sup> Computations ((R)B3LYP/6-31G(d,p)) show, that both the HOMO and the LUMO of **V.1** are localized on the pentacene portion of this nanohoop (**Figure 5.6**). The structural

effects from the nanohoop architecture of **V.1** cause a decrease in the HOMO→LUMO gap to a value of 1.95 eV. An increase in diradical character could also explain the lack of other products peak besides **V.9** in the <sup>1</sup>H NMR spectrum since diradicals that populate low lying triplet states and become <sup>1</sup>H NMR inactive.<sup>50, 51</sup> Investigations are currently underway to characterize this diradical intermediate experimentally with VT-NMR and <sup>2</sup>D-NMR and theoretically.

## 5.4. Conclusion and Future Work

The nanohoop architecture provides a unique opportunity to tune the electronic structure of organic semiconducting materials. We have designed a synthetic strategy that takes advantage of the reactivity of acenes towards <sup>1</sup>O<sub>2</sub> to prepare corner units with the *cis*-stereochemistry required for nanohoop synthesis. Our methodology provided access to advanced intermediate towards the synthesis of pentacene[10]CPP **V.1**. The highly reactive nature of **V.1** complicated the isolation and characterization of this product. Initial studies suggest that the decomposition of **V.1** is due to the induction of diradical character at the pentacene portion of the nanohoop backbone. Studies are currently underway to fully characterize this reactive intermediate and demonstrate the electronic effect that the nanohoop architecture has on incorporated acenes.

## 5.5. Experimental Sections

### 5.5.1. General Experimental Details

Moisture sensitive reactions were carried out under an inert atmosphere of nitrogen using standard Schlenk technique. <sup>1</sup>H NMR spectra were recorded at 400 MHz, 500 MHz, or 600 MHz on a (400 MHz or 500 MHz) Varian VNMR spectrometer or at 600 MHz or 500 MHz on a Bruker Avance-III-HD NMR spectrometer. <sup>13</sup>C NMR spectra were recorded at 100 MHz or 125 MHz on a Varian VNMR Spectrometer or at 150 MHz or 125 MHz on a Bruker Avance-III-HD NMR spectrometer. All <sup>1</sup>H NMR spectra were taken in CDCl<sub>3</sub> (referenced to TMS, δ 0.00 ppm) or DMSO-d<sub>6</sub> (referenced to residual

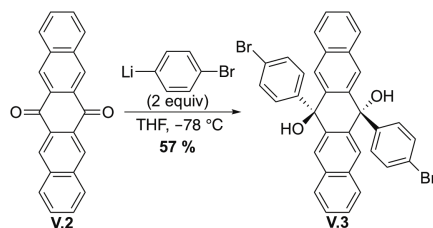
DMSO  $\delta$  2.50 ppm). All  $^{13}\text{C}$  NMR spectra were taken in  $\text{CDCl}_3$  (referenced to chloroform,  $\delta$  77.16 ppm) or  $\text{DMSO-d}_6$  (referenced to DMSO,  $\delta$  39.51 ppm).

THF, dichloromethane, and DMF were dried by filtration through alumina according to the methods described by Grubbs.<sup>52</sup> Column chromatography was conducted with Zeochem Zeoprep 60 Eco 40-63  $\mu\text{m}$  silica gel unless otherwise noted. Alumina column chromatography was performed with Sorbent Technologies 50-200  $\mu\text{m}$  basic activity I-II alumina. Thin Layer Chromatography (TLC) was performed using Sorbent Technologies Silica Gel XHT TLC plates. Developed plates were visualized using UV light at wavelengths of 254 and 265 nm. Recycling gel permeation chromatography (GPC) was performed using a Japan Analytical Industry LC-9101 preparative HPLC with JAIGEL-1H/JAIGEL-2H columns in series using  $\text{CHCl}_3$ . All glassware was oven or flame dried and cooled under an inert atmosphere of nitrogen unless otherwise noted.

Compound **V.6** was prepared in accordance with previously reported procedures and all spectra matched previously reported.<sup>53</sup> All reagents were obtained commercially unless otherwise noted.

All calculations were carried out with Gaussian 09 package at B3LYP/6-3(dp) level of theory.<sup>54</sup> Geometries were optimized in the gas phase. The fully optimized structures were confirmed to be true minima by vibrational analysis. Structures were minimized with no symmetry restrictions.

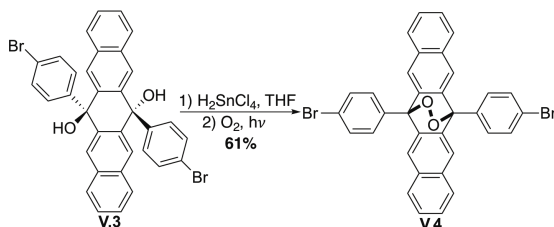
### 5.5.2. Synthetic Details



1,4-dibromobenzene (5.05 g, 21.4 mmol, 2.20 equiv) was dissolved in THF (214 mL) and cooled to  $-78\text{ }^\circ\text{C}$  for 30 min. To this solution, was added *n*-BuLi (1.90 M in hexanes, 11.8 mL, 22.4 mmol, 2.30 equiv). This reaction mixture was stirred for 30 min at  $-78\text{ }^\circ\text{C}$  for 30 min to give a white precipitate. In a separate flask 6,13-Pentacenequinone **V.2** (3.00 g, 9.73 mmol, 1.00 equiv) was dissolved in THF (97.0 mL)

to give a dark orange solution. The lithiated bromobenzene reaction solution was cannulated dropwise into the solution of **V.2** to give a cloudy dark orange reaction mixture and the reaction was stirred for 90 min. The reaction was quenched with deionized water (150 mL) and warmed to room temperature. The product was extracted with ethyl acetate (5 x 100 mL) and the combined organic layers were washed with brine (1 x 150 mL), deionized water (2 x 150 mL) then brine (1 x 150 mL) and dried over sodium sulfate and concentrated to give a dark orange oil. This oil was suspended in chloroform and crystallized in the freezer overnight. The resulting solid was collected by vacuum filtration to give the trans-isomer **V.3** as a yellow solid (3.43 g, 57%).

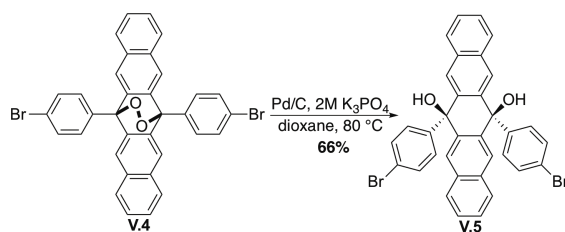
$^1\text{H}$  NMR (600 MHz,  $\text{CDCl}_3$ ):  $\delta$  8.33 (s, 4H), 7.90 (dd,  $J = 6.2, 3.3$  Hz, 4H), 7.57 (dd,  $J = 6.2, 3.3$  Hz, 4H), 6.65 (d,  $J = 8.7$  Hz, 4H), 6.54 (d,  $J = 8.7$  Hz, 4H), 2.14 (s, 2H);  $^{13}\text{C}$  NMR (150 MHz,  $\text{CDCl}_3$ ):  $\delta$  140.74, 139.00, 133.47, 132.83, 129.35, 128.32, 127.56, 126.88, 125.20, 76.07.



Tin (II) chloride dihydrate (12.3 g, 54.3 mmol, 10 equiv) was dissolved in HCl (12.1 M, 44 mL, 532 mmole, 98.0 equiv) and stirred for 10 min to give a colorless solution. In a separate flask pentacene dibromide **V.3** (3.38 g, 5.43 mmol, 1.00 equiv) was dissolved in THF (108 mL) to give a light yellow solution. The tin solution was cannulated into the solution of **V.3** dropwise and stirred for 15 min to give a dark purple solution. The reaction was quenched with deionized water (130 mL) and the resulting dark purple precipitate was collected with vacuum filtration. This solid was suspended in chloroform (1,360 mL) and sparged with oxygen for 4 hours. The reaction mixture was then stirred for 48 hours in direct sunlight to give a light yellow solution that was concentrated to give a purple sticky solid. This mixture was dissolved in dichloromethane (100 mL) and filtered through a pad of celite rinsing with dichloromethane (600 mL). The resulting filtrate was concentrated to give the crude product as a orange solid that was suspended in hexanes and collected via vacuum filtration to give pure **V.4** as a light

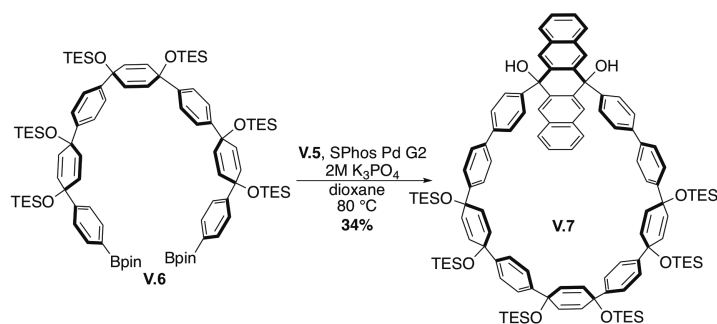
yellow solid. The filtrate was concentrated to give a dark orange oil and remaining product was purified from this mixture with column chromatography (40-100% dichloromethane/hexanes) to give endoperoxide **V.4** as a light yellow solid (2.07 g total, 61%).

$^1\text{H}$  NMR (600 MHz,  $\text{CDCl}_3$ ):  $\delta$  7.88 (d,  $J = 8.4$  Hz, 2H), 7.73 (d,  $J = 8.4$  Hz, 2H), 7.71 (dd,  $J = 6.3, 3.2$  Hz, 4H), 7.59 (s, 4H), 7.45 (dd,  $J = 6.3, 3.2$  Hz, 4H);  $^{13}\text{C}$  NMR (150 MHz,  $\text{CDCl}_3$ ):  $\delta$  136.42, 132.59, 132.18, 131.90, 129.55, 128.38, 127.14, 123.11, 122.92, 83.91.



Endoperoxide **V.4** (2.08 g, 3.36 mmol, 1.00 equiv) and palladium on carbon (10 wt %, 208 mg) were added to a round bottom flask, evacuated and backfilled with  $\text{N}_2$ . The reaction flask was capped and then purged with  $\text{N}_2$  for 30 min then dissolved in dioxane (120 mL). A solution of  $\text{K}_3\text{PO}_4$  in deionized water (2 M, 12 mL) was added to the reaction flask and reaction mixture was heated to 80 °C for 18 hours. The reaction was cooled to room temperature and quenched with deionized water (20 mL) and carefully filtered over celite rinsing with ethyl acetate (100 mL) and deionize water (100 mL). The product was extracted further with ethyl acetate (6 x 50 mL) and the combined organic layers were washed with deionized water (2 x 100 mL) and brine (1 x 100 mL), dried over sodium sulfate and concentrated to give an orange solid. The product was purified with column chromatography (0-100% dichloromethane/hexanes) to give the desired product as the cis-isomer **V.5** as a light yellow solid (1.37 g, 66%).

$^1\text{H}$  NMR (600 MHz,  $\text{CDCl}_3$ ):  $\delta$  8.39 (s, 4H), 7.95 (dd,  $J = 6.2, 3.3$  Hz, 4H), 7.58 (dd,  $J = 6.2, 3.3$  Hz, 4H), 6.89 (d,  $J = 8.7$  Hz, 4H), 6.57 (d,  $J = 8.7$  Hz, 4H), 3.04 (s, 2H);  $^{13}\text{C}$  NMR (150 MHz,  $\text{CDCl}_3$ ):  $\delta$  141.43, 139.06, 132.89, 130.67, 129.73, 128.30, 126.96, 125.30, 121.88, 76.26.



SPhos-Pd-G2 catalyst (35.0 mg, 0.050 mmol, 0.0500 equiv) and pentacene dibromide **V.5** (615 mg, 0.989 mmol, 1.00 equiv) were added to a flame dried flask. The flask was evacuated and backfilled with N<sub>2</sub> (5 x) then a septum was put on the flask and the solid was purged with N<sub>2</sub> for 30 min. During the N<sub>2</sub> purge previously reported seven ring bisboronate **V.6** (1.53 g, 0.989 mmol, 1.00 equiv) was added to a separate flame dried flask, dissolved in dioxane (100 mL) and sparged for 1 hour. Dioxane (50 mL) was added to the flask with SPhos-Pd-G2 and **V.5** and the solution of **V.6** was cannulated into this flask. The resulting solution was sparged with N<sub>2</sub> while sonicating the flask for 1 hour, then sparged with stirring for 1 hour. Meanwhile, a solution of 2 M K<sub>3</sub>PO<sub>4</sub> in deionized water was sparged with nitrogen for 1 hour. The reaction flask was heated to 80 °C for 30 min then the 2 M K<sub>3</sub>PO<sub>4</sub> solution (33 mL) was added. The reaction was stirred at this temperature for 16 hours then cooled to room temperature to give a clear brown solution. The mixture was concentrated to remove the dioxane and the resulting solution was filtered through celite rinsing with ethyl acetate (3 x 50 mL). The resulting organic layer was separated and the product was extracted further from the aqueous layer with ethyl acetate (3 x 100 mL). The combined organic layers were washed with deionized water (2 x 100 mL), brine (1 x 100 mL) then dried over sodium sulfate and concentrated to give a brown solid. The crude reaction was purified with silica gel column chromatography (15-100% ethyl acetate/hexane) to give the desired product **V.7** as a light orange solid (599 mg, 34%).

<sup>1</sup>H NMR (600 MHz, CDCl<sub>3</sub>): δ 8.65 (s, 4H), 8.03 (dd, *J* = 6.0, 3.5 Hz, 4H), 7.58 (dd, *J* = 6.0, 3.5 Hz, 4H), 7.13 (d, *J* = 8.4 Hz, 4H), 7.07 (d, *J* = 8.7 Hz, 4H), 7.04 (d, *J* = 8.7 Hz, 4H), 7.00 (d, *J* = 8.4 Hz, 4H), 6.93 (d, *J* = 8.6 Hz, 4H), 6.86 (d, *J* = 8.6 Hz, 4H), 6.04-5.97 (overlap, 8H), 5.85-5.79 (overlap, 4H), 2.92 (s, 2H), 0.92 (t, *J* = 8.0 Hz, 18H), 0.90 (t, *J* = 7.8 Hz, 18H), 0.87 (t, *J* = 7.8 Hz, 18H), 0.62 (q, *J* = 7.8 Hz, 12H), 0.56 (q, *J* = 8.0 Hz, 12H), 0.50 (q, *J* = 7.8 Hz, 12H).

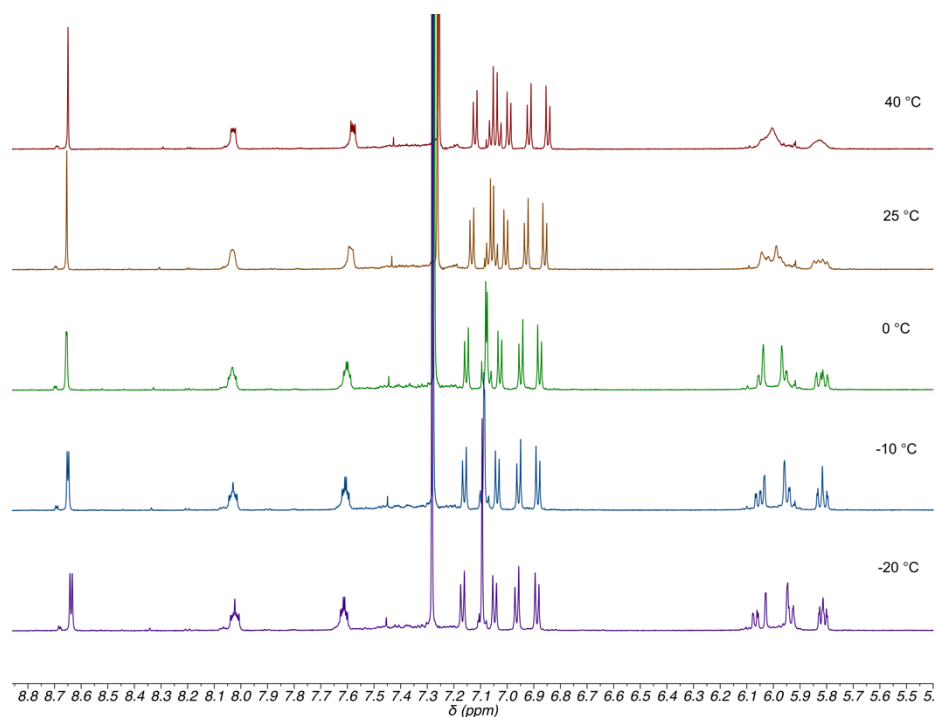
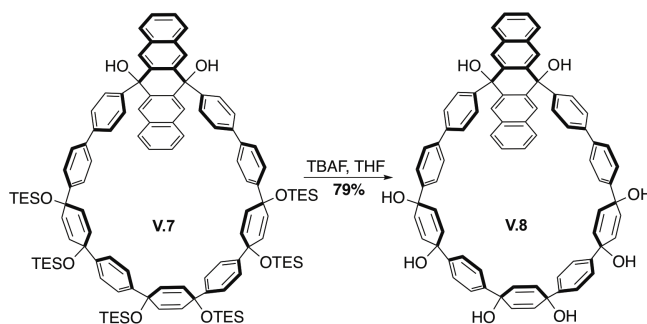


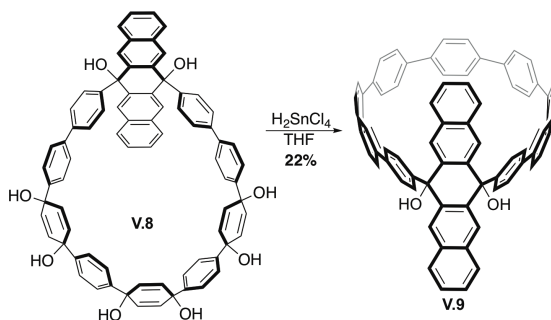
**Figure 5.4.** VT- $^1\text{H}$  NMR of macrocycle **V.7**.



Macrocycle **V.7** (599 mg, 0.341 mmol, 1.00 equiv) was added to a flame dried flask and suspended in THF (7.0 mL) at room temperature. Tert-butyl ammonium fluoride (TBAF) (1.00 M in THF, 2.73 mL, 2.73 mmol, 8.00 equiv) was added to the suspension dropwise to give a clear brown colored solution. The reaction was stirred for 3 hours at which time a white precipitate was formed. The reaction was then quenched with deionized water (20 mL) and concentrated to remove the THF. The resulting yellow solid was suspended in dichloromethane with sonication and collect by vacuum filtration. The resulting solid was rinsed with deionized water (25 mL) and dichloromethane (25 mL) to give **V.8** as a pure white solid (294 mg, 79%).



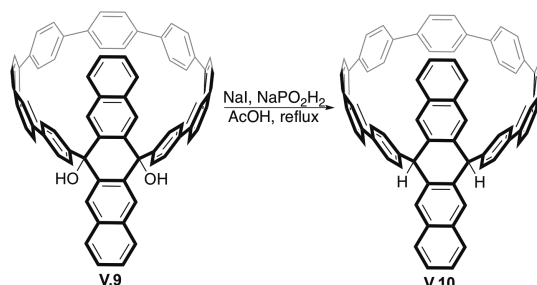
$^1\text{H}$  NMR (600 MHz,  $\text{DMSO-d}_6$ ):  $\delta$  8.62 (s, 4H), 8.10 (dd,  $J = 6.3, 3.3$  Hz, 4H), 7.59 (dd,  $J = 6.3, 3.3$  Hz, 4H), 7.21 (d,  $J = 8.6$  Hz, 4H), 7.17 (d,  $J = 8.6$  Hz, 4H), 7.15 (d,  $J = 8.5$  Hz, 4H), 7.11 (d,  $J = 8.5$  Hz, 4H), 6.99 (d,  $J = 8.3$  Hz, 4H), 6.74 (d,  $J = 8.3$  Hz, 4H), 5.96 (s, 4H), 5.82 (d,  $J = 10.0$  Hz, 4H), 5.82 (d,  $J = 10.0$  Hz, 4H);  $^{13}\text{C}$  NMR (150 MHz,  $\text{DMSO-d}_6$ ):  $\delta$  146.18, 145.07, 144.78, 144.19, 140.15, 138.16, 137.64, 132.17, 131.83, 131.08, 131.03, 128.01, 127.89, 126.10, 125.67, 125.48, 125.21, 125.15, 125.05, 124.98, 74.41, 68.43, 67.98, 67.70, 57.48.



A 0.05 M solution of  $\text{H}_2\text{SnCl}_4$  was prepared by dissolving tin(II) dichloride dihydrate (360 mg, 1.60 mmol) in THF (20 mL) in a flame dried flask then adding HCl (12 M, 0.160 mL, 1.94 mmol) dropwise and stirring for 30 min. In a separate flask macrocycle **V.8** (230 mg, 0.185 mmol, 1.00 equiv) was suspended in THF (18.5 mL). The  $\text{H}_2\text{SnCl}_4$  solution (0.05 M, 18.5 mL, 0.925 mmol, 5.00 equiv) was added the flask with macrocycle **V.8**. The reaction immediately became dark purple color and this color persists overnight while the reaction is stirred for 3 hours. The reaction was quenched with a solution of saturated sodium bicarbonate in deionized water (20 mL) and the product was extracted with dichloromethane (3 x 20 mL). The combined organic layers were washed with deionized water (3 x 20 mL) and brine (1 x 20 mL) then dried over sodium sulfate and concentrated to give the crude product as a dark purple solid. The product was purified with column chromatography over basic alumina (0-20% methanol/dichloromethane) to give **V.9** as the isolated product (42.0 mg, 22%). The purple and blue colors of the reaction mixture remain on the baseline of the column.

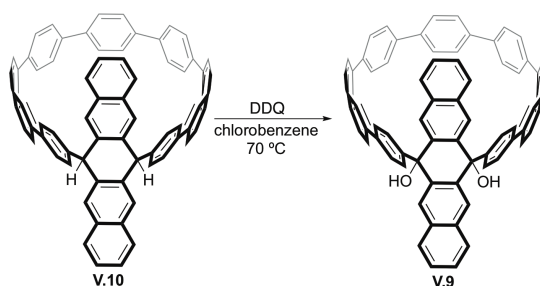
$^1\text{H}$  NMR (600 MHz,  $\text{DMSO-d}_6$ ):  $\delta$  8.55 (s, 4H), 7.96 (dd,  $J = 6.3, 3.3$  Hz, 4H), 7.09 (d,  $J = 8.7$  Hz, 2H), 7.59 (s, 4H), 7.57-7.63 (overlap, 12H), 7.48 (d,  $J = 8.8$  Hz, 4H), 7.45 (d,  $J = 8.8$  Hz, 4H), 7.43 (d,  $J = 8.4$  Hz, 4H), 7.37 (d,  $J = 8.4$  Hz, 4H), 7.34 (d,

$J = 8.6$  Hz, 4H), 7.25 (d,  $J = 8.6$  Hz, 4H);  $^{13}\text{C}$  NMR (150 MHz, DMSO- $d_6$ ):  $\delta$  171.21, 146.73, 139.61, 139.43, 139.28, 138.64, 138.49, 138.18, 137.58, 137.52, 133.16, 128.06, 127.74, 127.69, 127.55, 127.48, 127.26, 127.23, 127.14, 127.12, 126.58, 126.55, 74.71.



Macrocycle **V.9** (10.0 mg, 0.0100 mmol, 1.00 equiv), sodium iodide (11.0 mg, 0.0700 mmol, 7.00 equiv) and sodium hypophosphite monohydrate (12.0 mg, 0.110 mmol, 11.0 equiv) added to a flame dried flask and suspended in glacial acetic acid (1.00 mL). The mixture was heated to reflux for 90 min then cooled to room temperature and quenched with the addition of deionized water (5.00 mL) and the resulting precipitate was collected via vacuum filtration washing with deionized water (2 x 10 mL) and methanol (2 x 10 mL) to give a green tinted solid as reduced macrocycle **V.10** as a crude reaction mixture.

$^1\text{H}$  NMR (500 MHz, DMSO- $d_6$ ):  $\delta$  8.06 (s, 4H), 7.09 (dd,  $J = 6.2, 3.3$  Hz, 4H), 7.57 (s, 4H), 7.53 (s, 8H), 7.46 (d,  $J = 9.0$  Hz, 4H), 7.46 (dd,  $J = 6.2, 3.3$  Hz, 4H), 7.43 (d,  $J = 9.0$  Hz, 4H), 7.41 (d,  $J = 8.7$  Hz, 4H), 7.36 (d,  $J = 8.7$  Hz, 4H), 7.24 (d,  $J = 8.5$  Hz, 4H), 7.20 (d,  $J = 8.5$  Hz, 4H), 5.97 (s, 2H);  $^{13}\text{C}$  NMR (125 MHz, DMSO- $d_6$ ):  $\delta$  145.21, 139.71, 139.29, 138.87, 138.73, 138.68, 138.31, 137.74, 137.67, 136.50, 132.73, 129.16, 128.70, 127.88, 127.83, 127.62, 127.60, 127.59, 127.39, 127.36, 127.28, 127.02, 125.99.



The crude reaction mixture from the sodium hypophosphate reduction was added to a flame dried flask with 2,3-dichloro-5,6-dicyano-1,4-benzoquinone (12.0 mg, 0.0500 mmol, 5.00 equiv) and suspended in chlorobenzene (4.00 mL) to give a cloudy orange solution. The reaction was heated to 70 °C for 90 min then cooled to room temperature and quenched with the addition of deionized water (10 ml). The product was extracted with dichloromethane (3 x 10 mL) and the combined organic layers were washed with deionized water (4 x 10 mL) and brine (1 x 10 mL) then dried over sodium sulfate and concentrated to give a black oil as macrocycle **V.9**. Characterization is consistent with the spectra reported in this experimental section.

### 5.5.3. Computational Coordinates of Minimized Geometries and HOMO, LUMO Levels

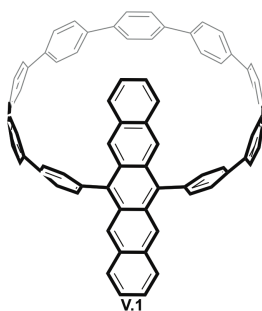


**Figure 5.5.** Structure of macrocycle **V.1** represented with the computational coordinates listed below.

C	6.17407	0.82705	-4.99219
C	5.96125	0.32097	-3.66751
C	5.87749	-1.11079	-3.47496
C	5.99135	-1.96298	-4.62335

C	6.18536	-1.43842	-5.87007
C	6.28103	-0.02213	-6.05735
C	5.8137	1.15226	-2.56405
C	5.63593	0.65625	-1.25145
C	5.63452	-0.79118	-1.04359
C	5.70293	-1.61632	-2.19123
C	5.38114	1.54463	-0.17022
C	5.52945	1.05126	1.1554
C	5.63709	-0.39185	1.3653
C	5.48398	-1.2965	0.27803
C	5.49822	1.87982	2.30213
C	5.67134	1.38913	3.59176
C	5.86028	-0.03208	3.78945
C	5.8129	-0.87239	2.68378
C	5.68217	2.24695	4.74155
C	5.87642	1.73834	5.99482
C	6.07591	0.33367	6.18767
C	6.06958	-0.52064	5.12125
C	4.66598	2.82465	-0.45662
C	4.85779	-2.62712	0.54098
C	3.48422	2.69374	-1.21468
C	2.58068	3.73411	-1.34024
C	2.79555	4.97244	-0.70875
C	4.01708	5.14651	-0.03819
C	4.93875	4.09922	0.07391
C	5.22871	-3.87187	-0.00154
C	4.37204	-4.97679	0.05935
C	3.12209	-4.89328	0.69364
C	2.81551	-3.68919	1.35265
C	3.65309	-2.59034	1.27346
C	1.63892	5.90355	-0.65754

C	2.01629	-5.87772	0.56365
C	0.774	6.01925	-1.75982
C	-0.52802	6.47825	-1.60611
C	-1.02515	6.85	-0.34338
C	-0.09534	6.93056	0.70975
C	1.20864	6.46261	0.55787
C	1.13116	-6.102	1.63247
C	-0.14722	-6.60169	1.41269
C	-0.59662	-6.89967	0.11342
C	0.35982	-6.87259	-0.9178
C	1.64069	-6.3699	-0.69805
C	-2.49379	6.84302	-0.11554
C	-2.05737	-6.91779	-0.15732
C	-3.4258	7.09188	-1.1411
C	-4.73915	6.63869	-1.04824
C	-5.18367	5.92149	0.0779
C	-4.30619	5.84791	1.17392
C	-2.99415	6.29538	1.07896
C	-2.53587	-6.22204	-1.28116
C	-3.8605	-5.81546	-1.36825
C	-4.78164	-6.08816	-0.34078
C	-4.34493	-6.94271	0.69001
C	-3.01406	-7.34353	0.78268
C	-6.36751	5.02494	0.05177
C	-7.05252	4.64407	1.22067
C	-7.8259	3.48779	1.25641
C	-7.95072	2.66008	0.1249
C	-7.42678	3.14758	-1.08487
C	-6.65302	4.30282	-1.12036
C	-8.33141	1.22835	0.22707
C	-6.02274	-5.27588	-0.25112

C	-7.88953	0.49539	1.34204
C	-7.8341	-0.89167	1.31816
C	-8.22561	-1.62353	0.18226
C	-8.83222	-0.89712	-0.86065
C	-8.8787	0.49497	-0.84167
C	-6.5374	-4.89872	1.00322
C	-7.39341	-3.81138	1.1383
C	-7.75644	-3.02493	0.02924
C	-7.4015	-3.52344	-1.23802
C	-6.56897	-4.62866	-1.37501
H	6.24322	1.90279	-5.13065
H	5.92389	-3.03814	-4.47905
H	6.2714	-2.09476	-6.73107
H	6.43851	0.37212	-7.05693
H	5.85228	2.22704	-2.70866
H	5.64084	-2.68991	-2.07516
H	5.3567	2.94547	2.17997
H	5.93154	-1.94082	2.83224
H	5.53567	3.31363	4.59303
H	5.88354	2.39885	6.8569
H	6.23154	-0.04778	7.1925
H	6.21783	-1.58778	5.26407
H	3.23954	1.72991	-1.64635
H	1.64339	3.55591	-1.85667
H	4.24868	6.10593	0.41659
H	5.87448	4.27867	0.59424
H	6.18909	-3.98106	-0.49554
H	4.67522	-5.90835	-0.41098
H	1.85553	-3.58355	1.84717
H	3.33417	-1.65414	1.71725
H	1.09767	5.65907	-2.73188

H	-1.2016	6.43251	-2.45582
H	-0.41722	7.28155	1.68584
H	1.86322	6.42638	1.4242
H	1.41501	-5.79233	2.6341
H	-0.8457	-6.64225	2.24277
H	0.07243	-7.16256	-1.92437
H	2.31505	-6.24789	-1.54104
H	-3.10457	7.59142	-2.05056
H	-5.41181	6.79198	-1.88746
H	-4.60968	5.3091	2.06582
H	-2.31485	6.08892	1.89953
H	-1.83444	-5.87454	-2.03255
H	-4.14486	-5.16297	-2.1864
H	-5.04031	-7.25253	1.46458
H	-2.70317	-7.94979	1.62899
H	-6.92705	5.22538	2.12972
H	-8.28915	3.1897	2.19262
H	-7.50865	2.54433	-1.98371
H	-6.15216	4.56817	-2.04613
H	-7.45926	1.02001	2.18903
H	-7.35882	-1.40138	2.14906
H	-9.22542	-1.42218	-1.72623
H	-9.30018	1.02119	-1.69362
H	-6.18141	-5.39224	1.90194
H	-7.71326	-3.52141	2.1343
H	-7.68992	-2.97837	-2.13114
H	-6.27194	-4.93614	-2.37286

**Table 5.1.** HOMO and LUMO levels of **V.1** from its minimized structure (in hartrees and eV).

Compound	HOMO level	LUMO level
<b>V.1</b>	Hartrees: -0.16373	Hartrees: -0.09216
	eV: 4.46	eV: 2.51

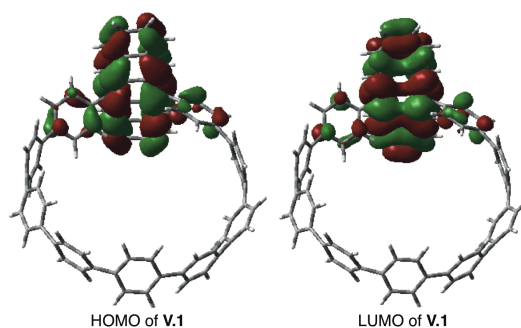


**Figure 5.6.** HOMO and LUMO surfaces of **V.1**.

#### CONCLUDING REMARKS

In summary, the studies highlighted in this dissertation provide synthetic approaches to access selectively functionalized version of nanohoops. The methodology was utilized to prepare nanohoops that are soluble in aqueous media and enabled the first study of these compounds as a novel class of biocompatible fluorophores. This seminal study has launched numerous investigations into the unique properties of the nanohoop scaffold that can be harnessed for biological imaging. Additionally, the synthetic approach developed in our lab was leveraged to prepared a pentacene incorporated nanohoop with modulated properties. These findings are the first steps towards the development of novel types of carbon nanomaterials based on the nanohoop scaffold.



## REFERENCES CITED

### Chapter I.

1. Mallinson, J.; Collins, I. Macrocycles in new drug discovery. *Future Med. Chem.* **2012**, *4*, 1409-1438.
2. Yudin, A. K. Macrocycles: Lessons from the distant past, recent developments, and future directions. *Chem. Sci.* **2015**, *6*, 30-49.
3. Bogdan, A. R.; Jerome, S. V.; Houk, K. N.; James, K. Strained cyclophane macrocycles: Impact of progressive ring size reduction on synthesis and structure. *J. Am. Chem. Soc.* **2012**, *134*, 2127-2138.
4. Allen, S. E.; Dokholyani, N. V.; Bowers, A. A. Dynamic docking of conformationally constrained macrocycles: Methods and applications. *ACS Chem. Biol.* **2016**, *11*, 10-24.
5. Over, B.; Matsson, P.; Tyrchan, C.; Artursson, P.; Doak, B. C.; Foley, M. A.; Hilgendorf, C.; Johnston, S. E.; Lee, M. D.; Lewis, R. J.; McCarren, P.; Muncipinto, G.; Norinder, U.; Perry, M. W. D.; Duvall, J. R.; Kihlberg, J. Structural and conformational determinants of macrocycle cell permeability. *Nat. Chem. Biol.* **2016**, *12*, 1065-1074.
6. Gulder, T.; Baran, P. S. Strained cyclophane natural products: Macrocyclization at its limits. *Nat. Prod. Rep.* **2012**, *29*, 899-934.
7. Tao, Z. F.; Wang, L.; Stewart, K. D.; Chen, Z. H.; Gu, W.; Bui, M. H.; Merta, P.; Zhang, H. Y.; Kovar, P.; Johnson, E.; Park, C.; Judge, R.; Rosenberg, S.; Sowin, T.; Lin, N. H. Structure-based design, synthesis, and biological evaluation of potent and selective macrocyclic checkpoint kinase 1 inhibitors. *J. Med. Chem.* **2007**, *50*, 1514-1527.
8. Cogdell, R. J.; Gall, A.; Kohler, J. The architecture and function of the light-harvesting apparatus of purple bacteria: From single molecules to in vivo membranes. *Q. Rev. Biophys.* **2006**, *39*, 227-324.
9. De Vico, L.; Anda, A.; Osipov, V. A.; Madsen, A. O.; Hansen, T. Macrocyclic ring deformation as the secondary design principle for light-harvesting complexes. *Proc. Natl. Acad. Sci. U. S. A.* **2018**. Accepted.
10. Iyoda, M.; Yamakawa, J.; Rahman, M. J. Conjugated macrocycles: Concepts and applications. *Angew. Chem., Int. Ed.* **2011**, *50*, 10522-10553.
11. Iyoda, M.; Shimizu, H. Multifunctional pi-expanded oligothiophene macrocycles. *Chem. Soc. Rev.* **2015**, *44*, 6411-6424.

12. Darzi, E. R.; Jasti, R. The dynamic, size-dependent properties of [5]-[12]cycloparaphenylenes. *Chem. Soc. Rev.* **2015**, *44*, 6401-6410.
13. Spitler, E. L.; Johnson, C. A.; Haley, M. M. Renaissance of annulene chemistry. *Chem. Rev.* **2006**, *106*, 5344-5386.
14. Golder, M. R.; Jasti, R. Syntheses of the smallest carbon nanohoops and the emergence of unique physical phenomena. *Acc. Chem. Res.* **2015**, *48*, 557-566.
15. Segawa, Y.; Yagi, A.; Matsui, K.; Itami, K. Design and synthesis of carbon nanotube segments. *Angew. Chem., Int. Ed.* **2016**, *55*, 5136-5158.
16. Kromer, J.; Rios-Carreras, I.; Fuhrmann, G.; Musch, C.; Wunderlin, M.; Debaerdemaeker, T.; Mena-Osteritz, E.; Bauerle, P. Synthesis of the first fully alpha-conjugated macrocyclic oligothiophenes: Cyclo[n]thiophenes with tunable cavities in the nanometer regime. *Angew. Chem., Int. Ed.* **2000**, *39*, 3481-3486.
17. Fuhrmann, G.; Debaerdemaeker, T.; Bauerle, P. C-C bond formation through oxidatively induced elimination of platinum complexes - A novel approach towards conjugated macrocycles. *Chem. Commun.* **2003**, 948-949.
18. Zhang, F.; Gotz, G.; Winkler, H. D. F.; Schalley, C. A.; Bauerle, P. Giant cyclo[n]thiophenes with extended pi conjugation. *Angew. Chem., Int. Ed.* **2009**, *48*, 6632-6635.
19. Ball, M.; Fowler, B.; Li, P. P.; Joyce, L. A.; Li, F.; Liu, T. F.; Paley, D.; Zhong, Y.; Li, H. X.; Xiao, S. X.; Ng, F.; Steigerwald, M. L.; Nuckolls, C. Chiral conjugated corrals. *J. Am. Chem. Soc.* **2015**, *137*, 9982-9987.
20. Yamago, S.; Watanabe, Y.; Iwamoto, T. Synthesis of [8]cycloparaphenylene from a square-shaped tetranuclear platinum complex. *Angew. Chem., Int. Ed.* **2010**, *49*, 757-759.
21. Hoffmann, M.; Wilson, C. J.; Odell, B.; Anderson, H. L. Template-directed synthesis of a pi-conjugated porphyrin nanoring. *Angew. Chem., Int. Ed.* **2007**, *46*, 3122-3125.
22. Bols, P. S.; Anderson, H. L. Shadow mask templates for site-selective metal exchange in magnesium porphyrin nanorings. *Angew. Chem., Int. Ed.* **2018**, *57*, 7874-7877.
23. Hoffmann, M.; Karnbratt, J.; Chang, M. H.; Herz, L. M.; Albinsson, B.; Anderson, H. L. Enhanced pi conjugation around a porphyrin[6] nanoring. *Angew. Chem., Int. Ed.* **2008**, *47*, 4993-4996.

24. O'Sullivan, M. C.; Sprafke, J. K.; Kondratuk, D. V.; Rinfray, C.; Claridge, T. D. W.; Saywell, A.; Blunt, M. O.; O'Shea, J. N.; Beton, P. H.; Malfois, M.; Anderson, H. L. Vernier templating and synthesis of a 12-porphyrin nano-ring. *Nature* **2011**, *469*, 72-75.
25. Kondratuk, D. V.; Perdigao, L. M. A.; Sullivan, M. C. O.; Svatek, S.; Smith, G.; Shea, J. N. O.; Beton, P. H.; Anderson, H. L. Two vernier-templated routes to a 24-porphyrin nanoring. *Angew. Chem., Int. Ed.* **2012**, *51*, 6696-6699.
26. Rickhaus, M.; Jentzsch, A. V.; Tejerina, L.; Griibner, I.; Jirasek, M.; Claridge, T. D. W.; Anderson, H. L. Single-acetylene linked porphyrin nanorings. *J. Am. Chem. Soc.* **2017**, *139*, 16502-16505.
27. Jasti, R.; Bhattacharjee, J.; Neaton, J. B.; Bertozzi, C. R. Synthesis, characterization, and theory of [9]-, [12]-, and [18]cycloparaphenylene: Carbon nanohoop structures. *J. Am. Chem. Soc.* **2008**, *130*, 17646-17647.
28. Sisto, T. J.; Golder, M. R.; Hirst, E. S.; Jasti, R., Selective synthesis of strained [7]cycloparaphenylene: An orange-emitting fluorophore. *J. Am. Chem. Soc.* **2011**, *133* (40), 15800-15802.
29. Xia, J. L.; Bacon, J. W.; Jasti, R., Gram-scale synthesis and crystal structures of [8]- and [10]CPP, and the solid-state structure of C-60@[10]CPP. *Chem. Sci.* **2012**, *3* (10), 3018-3021.
30. Darzi, E. R.; Sisto, T. J.; Jasti, R., Selective Syntheses of [7]-[12]cycloparaphenylenes using orthogonal suzuki-miyaura cross-coupling reactions. *J. Org. Chem.* **2012**, *77*, 6624-6628.
31. Kayahara, E.; Patel, V. K.; Xia, J. L.; Jasti, R.; Yamago, S., Selective and gram-scale synthesis of [6]cycloparaphenylene. *Synlett* **2015**, *26*, 1615-1619.
32. Sisto, T. J.; Jasti, R., Overcoming molecular strain: Synthesis of [7]cycloparaphenylene. *Synlett* **2012**, *4*, 483-489.
33. Evans, P. J.; Darzi, E. R.; Jasti, R., Efficient room-temperature synthesis of a highly strained carbon nanohoop fragment of buckminsterfullerene. *Nat. Chem.* **2014**, *6*, 404-408.
34. Takaba, H.; Omachi, H.; Yamamoto, Y.; Bouffard, J.; Itami, K. Selective synthesis of [12]cycloparaphenylene. *Angew. Chem., Int. Ed.* **2009**, *48*, 6112-6116.
35. Tour, J. M. Molecular electronics. Synthesis and testing of components. *Acc. Chem. Res.* **2000**, *33*, 791-804.

36. Delbosco, N.; De Winter, J.; Moins, S.; Persoons, A.; Dubois, P.; Coulembier, O. Macrocyclic P3HT obtained by intramolecular McMurry coupling of linear bis-aldehyde polymer: A direct comparison with linear homologue. *Macromolecules* **2017**, *50*, 1939-1949.
37. Bhaskar, A.; Ramakrishna, G.; Hagedorn, K.; Varnavski, O.; Mena-Osteritz, E.; Bauerle, P.; Goodson, T. Enhancement of two-photon absorption cross-section in macrocyclic thiophenes with cavities in the nanometer regime. *J. Phys. Chem. B* **2007**, *111*, 946-954.
38. Zhang, F.; Gotz, G.; Mena-Osteritz, E.; Weil, M.; Sarkar, B.; Kaim, W.; Bauerle, P. Molecular and electronic structure of cyclo[10]thiophene in various oxidation states: Polaron pair vs. bipolaron. *Chem. Sci.* **2011**, *2*, 781-784.
39. Ito, H.; Mitamura, Y.; Segawa, Y.; Itami, K. Thiophene-based, radial pi-conjugation: Synthesis, structure, and photophysical properties of cyclo-1,4-phenylene-2',5'-thienylenes. *Angew. Chem., Int. Ed.* **2015**, *54*, 159-163.
40. Shimizu, H.; Gonzalez, J. D. C.; Hasegawa, M.; Nishinaga, T.; Haque, T.; Takase, M.; Otani, H.; Rabe, J. P.; Iyoda, M. Synthesis, structures, and photophysical properties of pi-expanded oligothiophene 8-mers and their saturn-like C-60 complexes. *J. Am. Chem. Soc.* **2015**, *137*, 3877-3885.
41. Zhang, S. Q.; Liu, Z. Y.; Fu, W. F.; Liu, F.; Wang, C. M.; Sheng, C. Q.; Wang, Y. F.; Deng, K.; Zeng, Q. D.; Shu, L. J.; Wan, J. H.; Chen, H. Z.; Russell, T. P. Donor-acceptor conjugated macrocycles: Synthesis and host-guest coassembly with fullerene toward photovoltaic application. *ACS Nano* **2017**, *11*, 11701-11713.
42. Leriche, P.; Frere, P.; Cravino, A.; Aleveque, O.; Roncali, J. Molecular engineering of the internal charge transfer in thiophene-triphenylamine hybrid pi-conjugated systems. *J. Org. Chem.* **2007**, *72*, 8332-8336.
43. Liu, C. Y.; Yang, G. C.; Si, Y. L.; Liu, Y. J.; Pan, X. M. Understanding photophysical properties of chiral conjugated corrals for organic photovoltaics. *J. Mater. Chem. C* **2017**, *5*, 3495-3503.
44. Ball, M.; Zhong, Y.; Fowler, B.; Zhang, B. Y.; Li, P. P.; Etkin, G.; Paley, D. W.; Decatur, J.; Dalsania, A. K.; Li, H. X.; Xiao, S. X.; Ng, F.; Steigerwald, M. L.; Nuckolls, C. Macrocyclization in the design of organic n-type electronic materials. *J. Am. Chem. Soc.* **2016**, *138*, 12861-12867.
45. Zhang, B. Y.; Trinh, M. T.; Fowler, B.; Ball, M.; Xu, Q. Z.; Ng, F.; Steigerwald, M. L.; Zhu, X. Y.; Nuckolls, C.; Zhong, Y. Rigid, Conjugated macrocycles for high performance organic photodetectors. *J. Am. Chem. Soc.* **2016**, *138*, 16426-16431.

46. Ball, M. L.; Zhang, B. Y.; Xu, Q. Z.; Paley, D. W.; Ritter, V. C.; Ng, F.; Steigerwald, M. L.; Nuckolls, C. Influence of molecular conformation on electron transport in giant, conjugated macrocycles. *J. Am. Chem. Soc.* **2018**, *140*, 10135-10139.
47. Zhang, B. Y.; Sanchez, R. H.; Zhong, Y.; Ball, M.; Terban, M. W.; Paley, D.; Billinge, S. J. L.; Ng, F.; Steigerwald, M. L.; Nuckolls, C. Hollow organic capsules assemble into cellular semiconductors. *Nat. Commun.* **2018**, *9*, 1957-1963.
48. Bakulin, A. A.; Rao, A.; Pavelyev, V. G.; van Loosdrecht, P. H. M.; Pshenichnikov, M. S.; Niedzialek, D.; Cornil, J.; Beljonne, D.; Friend, R. H. The role of driving energy and delocalized states for charge separation in organic semiconductors. *Science* **2012**, *335*, 1340-1344.
49. Yong, C. K.; Parkinson, P.; Kondratuk, D. V.; Chen, W. H.; Stannard, A.; Summerfield, A.; Sprafke, J. K.; O'Sullivan, M. C.; Beton, P. H.; Anderson, H. L.; Herz, L. M. Ultrafast delocalization of excitation in synthetic light-harvesting nanorings. *Chem. Sci.* **2015**, *6*, 181-189.
50. Sprafke, J. K.; Kondratuk, D. V.; Wykes, M.; Thompson, A. L.; Hoffmann, M.; Drevinskas, R.; Chen, W. H.; Yong, C. K.; Karnbratt, J.; Bullock, J. E.; Malfois, M.; Wasielewski, M. R.; Albinsson, B.; Herz, L. M.; Zigmantas, D.; Beljonne, D.; Anderson, H. L. Belt-shaped pi-systems: Relating geometry to electronic structure in a six-porphyrin nanoring. *J. Am. Chem. Soc.* **2011**, *133*, 17262-17273.
51. Rousseaux, S. A. L.; Gong, J. Q.; Haver, R.; Odell, B.; Claridge, T. D. W.; Herz, L. M.; Anderson, H. L. Self-assembly of russian doll concentric porphyrin nanorings. *J. Am. Chem. Soc.* **2015**, *137*, 12713-12718.
52. Jiang, H. W.; Tanaka, T.; Mori, H.; Park, K. H.; Kim, D.; Osuka, A. Cyclic 2,12-porphyrinylene nanorings as a porphyrin analogue of cycloparaphenylenes. *J. Am. Chem. Soc.* **2015**, *137*, 2219-2222.
53. Kang, H. S.; Sisto, T. J.; Peurifoy, S.; Arias, D. H.; Zhang, B. Y.; Nuckolls, C.; Blackburn, J. L. Long-lived charge separation at heterojunctions between semiconducting single-walled carbon nanotubes and perylene diimide electron acceptors. *J. Phys. Chem. C* **2018**, *122*, 14150-14161.
54. Hong, G. S.; Diao, S. O.; Antaris, A. L.; Dai, H. J. Carbon nanomaterials for biological imaging and nanomedicinal therapy. *Chem. Rev.* **2015**, *115*, 10816-10906.
55. Li, P. H.; Sisto, T. J.; Darzi, E. R.; Jasti, R. The effects of cyclic conjugation and bending on the optoelectronic properties of paraphenylenes. *Org. Lett.* **2014**, *16*, 182-185.
56. Iwamoto, T.; Watanabe, Y.; Sakamoto, Y.; Suzuki, T.; Yamago, S. Selective and random syntheses of [n]cycloparaphenylenes (n=8-13) and size dependence of their electronic properties. *J. Am. Chem. Soc.* **2011**, *133*, 8354-8361.

57. Adamska, L.; Nayyar, I.; Chen, H.; Swan, A. K.; Oldani, N.; Fernandez-Alberti, S.; Golder, M. R.; Jasti, R.; Doorn, S. K.; Tretiak, S. Self-trapping of excitons, violation of condon approximation, and efficient fluorescence in conjugated cycloparaphenylenes. *Nano Lett.* **2014**, *14*, 6539-6546.
58. Kayahara, E.; Sun, L. S.; Onishi, H.; Suzuki, K.; Fukushima, T.; Sawada, A.; Kaji, H.; Yamago, S. Gram-scale syntheses and conductivities of [10]cycloparaphenylene and its tetraalkoxy derivatives. *J. Am. Chem. Soc.* **2017**, *139*, 18480-18483.
59. Darzi, E. R.; Hirst, E. S.; Weber, C. D.; Zakharov, L. N.; Lonergan, M. C.; Jasti, R. Synthesis, properties, and design principles of donor-acceptor nano hoops. *ACS Cent. Sci.* **2015**, *1*, 335-342.
60. Van Raden, J. M.; Darzi, E. R.; Zakharov, L. N.; Jasti, R. Synthesis and characterization of a highly strained donor-acceptor nano hoop. *Org. Biomol. Chem.* **2016**, *14*, 5721-5727.
61. Kuwabara, T.; Orii, J.; Segawa, Y.; Itami, K. Curved oligophenylenes as donors in shape-persistent donor-acceptor macrocycles with solvatochromic properties. *Angew. Chem., Int. Ed.* **2015**, *54*, 9646-9649.

## Chapter II.

1. Nguyen, S. T.; Johnson, L. K.; Grubbs, R. H.; Ziller, J. W. Ring-opening metathesis polymerization (ROMP) of norbornene by a group-viii carbene complex in protic media. *J. Am. Chem. Soc.* **1992**, *114*, 3974-3975.
2. Bielawski, C. W.; Grubbs, R. H. Living ring-opening metathesis polymerization. *Prog. Polym. Sci.* **2007**, *32*, 1-29.
3. Schrock, R. R. Living ring-opening metathesis polymerization catalyzed by well-characterized transition-metal alkylidene complexes. *Acc. Chem. Res.* **1990**, *23*, 158-165.
4. Schrock, R. R.; Hoveyda, A. H. Molybdenum and tungsten imido alkylidene complexes as efficient olefin-metathesis catalysts. *Angew. Chem., Int. Ed.* **2003**, *42*, 4592-4633.
5. Gulder, T.; Baran, P. S. Strained cyclophane natural products: Macrocyclization at its limits. *Nat. Prod. Rep.* **2012**, *29*, 899-934.
6. Villar, E. A.; Beglov, D.; Chennamadhavuni, S.; Porco, J. A.; Kozakov, D.; Vajda, S.; Whitty, A. How proteins bind macrocycles. *Nat. Chem. Biol.* **2014**, *10*, 723-731.

7. Xia, J. L.; Bacon, J. W.; Jasti, R. Gram-scale synthesis and crystal structures of [8]- and [10]CPP, and the solid-state structure of C-60@[10]CPP. *Chem. Sci.* **2012**, *3*, 3018-3021.
8. Iwamoto, T.; Watanabe, Y.; Takaya, H.; Haino, T.; Yasuda, N.; Yamago, S. Size- and orientation-selective encapsulation of C-70 by cycloparaphenylenes. *Chem. Eur. J.* **2013**, *19*, 14061-14068.
9. Iwamoto, T.; Watanabe, Y.; Sadahiro, T.; Haino, T.; Yamago, S. Size-selective encapsulation of C-60 by [10]cycloparaphenylene: Formation of the shortest fullerene-peapod. *Angew. Chem., Int. Ed.* **2011**, *50*, 8342-8344.
10. Iwamoto, T.; Slanina, Z.; Mizorogi, N.; Guo, J. D.; Akasaka, T.; Nagase, S.; Takaya, H.; Yasuda, N.; Kato, T.; Yamago, S. Partial charge transfer in the shortest possible metallofullerene peapod, La@C<sub>82</sub> subset of [11]cycloparaphenylene. *Chem. Eur. J.* **2014**, *20*, 14403-14409.
11. Matsuno, T.; Sato, S.; Iizuka, R.; Isobe, H. Molecular recognition in curved pi-systems: Effects of pi-lengthening of tubular molecules on thermodynamics and structures. *Chem. Sci.* **2015**, *6*, 909-916.
12. Sato, S.; Yamasaki, T.; Isobe, H. Solid-state structures of peapod bearings composed of finite single-wall carbon nanotube and fullerene molecules. *Proc. Natl. Acad. Sci. U. S. A.* **2014**, *111*, 8374-8379.
13. Isobe, H.; Hitosugi, S.; Yamasaki, T.; Iizuka, R. Molecular bearings of finite carbon nanotubes and fullerenes in ensemble rolling motion. *Chem. Sci.* **2013**, *4*, 1293-1297.
14. Hitosugi, S.; Iizuka, R.; Yamasaki, T.; Zhang, R.; Murata, Y.; Isobe, H. Assessment of fullerene derivatives as rolling journals in a finite carbon nanotube Bearing. *Org. Lett.* **2013**, *15*, 3199-3201.
15. Burns, N. Z.; Krylova, I. N.; Hannoush, R. N.; Baran, P. S. Scalable total synthesis and biological evaluation of haouamine A and its atropisomer. *J. Am. Chem. Soc.* **2009**, *131*, 9172-9173.
16. Baran, P. S.; Burns, N. Z. Total synthesis of (+/-)-haouamine A. *J. Am. Chem. Soc.* **2006**, *128*, 3908-3909.
17. Lloyd-Williams, P.; Giralt, E. Atropisomerism, biphenyls and the Suzuki coupling: Peptide antibiotics. *Chem. Soc. Rev.* **2001**, *30*, 145-157.

18. Evans, D. A.; Wood, M. R.; Trotter, B. W.; Richardson, T. I.; Barrow, J. C.; Katz, J. L. Total syntheses of vancomycin and eremomycin aglycons. *Angew. Chem., Int. Ed.* **1998**, *37*, 2700-2704.
19. Nicolaou, K. C.; Li, H.; Boddy, C. N. C.; Ramanjulu, J. M.; Yue, T. Y.; Natarajan, S.; Chu, X. J.; Brase, S.; Rubsam, F. Total synthesis of vancomycin - Part 1: Design and development of methodology. *Chem. Eur. J.* **1999**, *5*, 2584-2601.
20. Boger, D. L.; Miyazaki, S.; Kim, S. H.; Wu, J. H.; Castle, S. L.; Loiseleur, O.; Jin, Q. Total synthesis of the vancomycin aglycon. *J. Am. Chem. Soc.* **1999**, *121*, 10004-10011.
21. Cram, D. J.; Cram, J. M. Cyclophane chemistry - Bent and battered benzene rings. *Acc. Chem. Res.* **1971**, *4*, 204-213.
22. Evans, P. J.; Darzi, E. R.; Jasti, R. Efficient room-temperature synthesis of a highly strained carbon nanohoop fragment of buckminsterfullerene. *Nat. Chem.* **2014**, *6*, 404-408.
23. Dhital, R. N.; Sakurai, H. Oxidative coupling of organoboron compounds. *Asian J. Org. Chem.* **2014**, *3*, 668-684.
24. Iafe, R. G.; Kuo, J. L.; Hochstatter, D. G.; Saga, T.; Turner, J. W.; Merlic, C. A. Increasing the efficiency of the transannular diels-alder strategy via palladium(II)-catalyzed macrocyclizations. *Org. Lett.* **2013**, *15*, 582-585.
25. Iafe, R. G.; Chan, D. G.; Kuo, J. L.; Boon, B. A.; Faizi, D. J.; Saga, T.; Turner, J. W.; Merlic, C. A. Cyclization strategies to polyenes using Pd(II)-catalyzed couplings of pinacol vinylboronates. *Org. Lett.* **2012**, *14*, 4282-4285.
26. Darzi, E. R.; White, B. M.; Loventhal, L. K.; Zakharov, L. N.; Jasti, R. An operationally simple and mild oxidative homocoupling of aryl boronic esters to access conformationally constrained macrocycles. *J. Am. Chem. Soc.* **2017**, *139*, 3106-3114.
27. Nagumo, S.; Ishizawa, S.; Nagai, M.; Inoue, T. Studies on the constituents of Aceraceae plants .13. Diarylheptanoids and other phenolics from *Acer nikoense*. *Chem. Pharm. Bull.* **1996**, *44*, 1086-1089.
28. Sung, S. H.; Lee, M. Anti-adipogenic activity of a new cyclic diarylheptanoid isolated from *Alnus japonica* on 3T3-L1 cells via modulation of PPAR gamma, C/EBP alpha and SREBP1c signaling. *Bioorg. Med. Chem. Lett.* **2015**, *25*, 4648-4651.
29. Ogura, T.; Usuki, T. Total synthesis of acerogenins E, G and K, and centrololol. *Tetrahedron* **2013**, *69*, 2807-2815.



30. Smyth, J. E.; Butler, N. M.; Keller, P. A. A twist of nature - the significance of atropisomers in biological systems. *Nat. Prod. Rep.* **2015**, *32*, 1562-1583.
31. Pattawong, O.; Salih, M. Q.; Rosson, N. T.; Beaudry, C. M.; Cheong, P. H. Y. The nature of persistent conformational chirality, racemization mechanisms, and predictions in diarylether heptanoid cyclophane natural products. *Org. Biomol. Chem.* **2014**, *12*, 3303-3309.
32. Slocum, D. W.; Reinscheld, T. K.; White, C. B.; Timmons, M. D.; Shelton, P. A.; Slocum, M. G.; Sandlin, R. D.; Holland, E. G.; Kusmic, D.; Jennings, J. A.; Tekin, K. C.; Nguyen, Q.; Bush, S. J.; Keller, J. M.; Whitley, P. E. ortho-Lithiations reassessed: The advantages of deficiency catalysis in hydrocarbon media. *Organometallics* **2013**, *32*, 1674-1686.
33. Diorazio, L. J.; Widdowson, D. A.; Clough, J. M. Regiospecific synthesis of 2-fluoro-3-O-methylestrone using cesium fluorosulfate. *J. Chem. Soc. Perk. Trans. 1* **1992**, 421-425.
34. Semmelhack, M. F.; Chlenov, A. (Arene)Cr(CO)<sub>3</sub> complexes: Arene lithiation/reaction with electrophiles. *Top. Organomet. Chem.* **2004**, *7*, 21-42.
35. Ricci, P.; Kramer, K.; Larrosa, I. Tuning reactivity and site selectivity of simple arenes in C-H activation: ortho-Arylation of anisoles via arene-metal pi-complexation. *J. Am. Chem. Soc.* **2014**, *136*, 18082-18086.
36. Pangborn, A. B.; Giardello, M. A.; Grubbs, R. H.; Rosen, R. K.; Timmers, F. J. Safe and convenient procedure for solvent purification. *Organometallics* **1996**, *15*, 1518-1520.
37. Sheldrick, G. M.; Bruker AXS: Madison, WI, **1998**.
38. Sheldrick, G. M. A short history of SHELX. *Acta Crystallogr A* **2008**, *64*, 112-122.
39. Frisch, M. J.; Trucks, G. W.; Schlegel, H. B.; Scuseria, G. E.; Robb, M. A.; Cheeseman, J. R.; Scalmani, G.; Barone, V.; Mennucci, B.; Petersson, G. A.; Nakatsuji, H.; Caricato, M.; Li, X.; Hratchian, H. P.; Izmaylov, A. F.; Bloino, J.; Zheng, G.; Sonnenberg, J. L.; Hada, M.; Ehara, M.; Toyota, K.; Fukuda, R.; Hasegawa, J.; Ishida, M.; Nakajima, T.; Honda, Y.; Kitao, O.; Nakai, H.; Vreven, T.; Montgomery, J. A.; Peralta, J. E.; Ogliaro, F.; Bearpark, M.; Heyd, J. J.; Brothers, E.; Kudin, K. N.; Staroverov, V. N.; Kobayashi, R.; Normand, J.; Raghavachari, K.; Rendell, A.; Burant, J. C.; Iyengar, S. S.; Tomasi, J.; Cossi, M.; Rega, N.; Millam, J. M.; Klene, M.; Knox, J. E.; Cross, J. B.; Bakken, V.; Adamo, C.; Jaramillo, J.; Gomperts, R.; Stratmann, R. E.; Yazyev, O.; Austin, A. J.; Cammi, R.; Pomelli, C.; Ochterski, J. W.; Martin, R. L.; Morokuma, K.; Zakrzewski, V. G.; Voth, G. A.; Salvador, P.; Dannenberg, J. J.; Dapprich, S.; Daniels, A. D.; Farkas, Foresman, J. B.; Ortiz, J. V.; Cioslowski, J.; Fox, D. J. Wallingford CT, **2009**.

### Chapter III.

1. Iijima, S. Helical microtubules of graphitic carbon. *Nature* **1991**, *354*, 56-58.
2. Yu, M. F.; Lourie, O.; Dyer, M. J.; Moloni, K.; Kelly, T. F.; Ruoff, R. S. Strength and breaking mechanism of multiwalled carbon nanotubes under tensile load. *Science* **2000**, *287*, 637-640.
3. Tang, Z. K.; Zhang, L. Y.; Wang, N.; Zhang, X. X.; Wen, G. H.; Li, G. D.; Wang, J. N.; Chan, C. T.; Sheng, P. Superconductivity in 4 angstrom single-walled carbon nanotubes. *Science* **2001**, *292*, 2462-2465.
4. Joselevich, E. Electronic structure and chemical reactivity of carbon nanotubes: A chemist's view. *ChemPhysChem* **2004**, *5*, 619-624.
5. Misewich, J. A.; Martel, R.; Avouris, P.; Tsang, J. C.; Heinze, S.; Tersoff, J. Electrically induced optical emission from a carbon nanotube FET. *Science* **2003**, *300*, 783-786.
6. Sgobba, V.; Guldi, D. M. Carbon nanotubes-electronic/electrochemical properties and application for nanoelectronics and photonics. *Chem. Soc. Rev.* **2009**, *38*, 165-184.
7. Segawa, Y.; Ito, H.; Itami, K. Structurally uniform and atomically precise carbon nanostructures. *Nat. Rev. Mater.* **2016**, *1*, 15002.
8. Saito, N.; Haniu, H.; Usui, Y.; Aoki, K.; Hara, K.; Takanashi, S.; Shimizu, M.; Narita, N.; Okamoto, M.; Kobayashi, S.; Nomura, H.; Kato, H.; Nishimura, N.; Taruta, S.; Endo, M. Safe clinical use of carbon nanotubes as innovative biomaterials. *Chem. Rev.* **2014**, *114*, 6040-6079.
9. Hong, G. S.; Diao, S. O.; Antaris, A. L.; Dai, H. J. Carbon nanomaterials for biological imaging and nanomedicinal therapy. *Chem. Rev.* **2015**, *115*, 10816-10906.
10. Bachilo, S. M.; Balzano, L.; Herrera, J. E.; Pompeo, F.; Resasco, D. E.; Weisman, R. B. Narrow (n,m)-distribution of single-walled carbon nanotubes grown using a solid supported catalyst. *J. Am. Chem. Soc.* **2003**, *125*, 11186-11187.
11. Chiang, W. H.; Sankaran, R. M. Linking catalyst composition to chirality distributions of as-grown single-walled carbon nanotubes by tuning Ni<sub>x</sub>Fe<sub>1-x</sub> nanoparticles. *Nat. Mater.* **2009**, *8*, 882-886.
12. Tu, X. M.; Manohar, S.; Jagota, A.; Zheng, M. DNA sequence motifs for structure-specific recognition and separation of carbon nanotubes. *Nature* **2009**, *460*, 250-253.

13. Jasti, R.; Bertozzi, C. R. Progress and challenges for the bottom-up synthesis of carbon nanotubes with discrete chirality. *Chem. Phys. Lett.* **2010**, *494*, 1-7.
14. Tian, X.; Jasti, R., Cycloparaphenylenes: The shortest segment of armchair carbon nanotubes. In *Fragments of fullerene and carbon nanotubes: Designed synthesis, unusual reactions, and coordination chemistry*, Petrukhina, M. A.; Scott, L. T., Eds. John Wiley & Sons, Inc.: Hoboken, N. J., **2012**, 291.
15. Jasti, R.; Bhattacharjee, J.; Neaton, J. B.; Bertozzi, C. R. Synthesis, characterization, and theory of [9]-, [12]-, and [18]cycloparaphenylene: Carbon nanohoop structures. *J. Am. Chem. Soc.* **2008**, *130*, 17646-17647.
16. Yu, X. C.; Zhang, J.; Choi, W.; Choi, J. Y.; Kim, J. M.; Gan, L. B.; Liu, Z. F. Cap formation engineering: From opened C<sub>60</sub> to single-walled carbon nanotubes. *Nano Lett.* **2010**, *10*, 3343-3349.
17. Liu, B. L.; Liu, J.; Li, H. B.; Bhola, R.; Jackson, E. A.; Scott, L. T.; Page, A.; Irle, S.; Morokuma, K.; Zhou, C. W. Nearly exclusive growth of small diameter semiconducting single-wall carbon nanotubes from organic chemistry synthetic end-cap molecules. *Nano Lett.* **2015**, *15*, 586-595.
18. Omachi, H.; Nakayama, T.; Takahashi, E.; Segawa, Y.; Itami, K. Initiation of carbon nanotube growth by well-defined carbon nanorings. *Nat. Chem.* **2013**, *5*, 572-576.
19. Sanchez-Valencia, J. R.; Dienel, T.; Groning, O.; Shorubalko, I.; Mueller, A.; Jansen, M.; Amsharov, K.; Ruffieux, P.; Fasel, R. Controlled synthesis of single-chirality carbon nanotubes. *Nature* **2014**, *512*, 61-64.
20. Golder, M. R.; Colwell, C. E.; Wong, B. M.; Zakharov, L. N.; Zhen, J. X.; Jasti, R. Iterative reductive aromatization/ring-closing metathesis strategy toward the synthesis of strained aromatic belts. *J. Am. Chem. Soc.* **2016**, *138*, 6577-6582.
21. Povie, G.; Segawa, Y.; Nishihara, T.; Miyauchi, Y.; Itami, K. Synthesis of a carbon nanobelt. *Science* **2017**, *356*, 172-175.
22. Hirst, E. S.; Jasti, R. Bending benzene: Syntheses of [n]cycloparaphenylenes. *J. Org. Chem.* **2012**, *77*, 10473-10478.
23. Darzi, E. R.; Sisto, T. J.; Jasti, R. Selective syntheses of [7]-[12]cycloparaphenylenes using orthogonal Suzuki-Miyaura cross-coupling reactions. *J. Org. Chem.* **2012**, *77*, 6624-6628.
24. Xia, J. L.; Bacon, J. W.; Jasti, R. Gram-scale synthesis and crystal structures of [8]- and [10]CPP, and the solid-state structure of C<sub>60</sub>@[10]CPP. *Chem. Sci.* **2012**, *3*, 3018-3021.

25. Takaba, H.; Omachi, H.; Yamamoto, Y.; Bouffard, J.; Itami, K. Selective synthesis of [12]cycloparaphenylene. *Angew. Chem., Int. Ed.* **2009**, *48*, 6112-6116.
26. Sisto, T. J.; Golder, M. R.; Hirst, E. S.; Jasti, R. Selective synthesis of strained [7]cycloparaphenylene: An orange-emitting fluorophore. *J. Am. Chem. Soc.* **2011**, *133*, 15800-15802.
27. Xia, J. L.; Jasti, R. Synthesis, characterization, and crystal structure of [6]cycloparaphenylene. *Angew. Chem., Int. Ed.* **2012**, *51*, 2474-2476.
28. Segawa, Y.; Senel, P.; Matsuura, S.; Omachi, H.; Itami, K. [9]Cycloparaphenylene: Nickel-mediated synthesis and crystal Structure. *Chem. Lett.* **2011**, *40*, 423-425.
29. Segawa, Y.; Miyamoto, S.; Omachi, H.; Matsuura, S.; Senel, P.; Sasamori, T.; Tokitoh, N.; Itami, K. Concise synthesis and crystal structure of [12]cycloparaphenylene. *Angew. Chem., Int. Ed.* **2011**, *50*, 3244-3248.
30. Iwamoto, T.; Watanabe, Y.; Sakamoto, Y.; Suzuki, T.; Yamago, S. Selective and random syntheses of [n]cycloparaphenylenes (n=8-13) and size dependence of their electronic properties. *J. Am. Chem. Soc.* **2011**, *133*, 8354-8361.
31. Evans, P. J.; Darzi, E. R.; Jasti, R. Efficient room-temperature synthesis of a highly strained carbon nanohoop fragment of buckminsterfullerene. *Nat. Chem.* **2014**, *6*, 404-408.
32. Kayahara, E.; Patel, V. K.; Yamago, S. Synthesis and characterization of [5]cycloparaphenylene. *J. Am. Chem. Soc.* **2014**, *136*, 2284-2287.
33. Omachi, H.; Matsuura, S.; Segawa, Y.; Itami, K. A modular and size-selective synthesis of [n]cycloparaphenylenes: A step toward the selective synthesis of [n, n] single-walled carbon nanotubes. *Angew. Chem., Int. Ed.* **2010**, *49*, 10202-10205.
34. Kayahara, E.; Patel, V. K.; Xia, J. L.; Jasti, R.; Yamago, S. Selective and gram-scale synthesis of [6]cycloparaphenylene. *Synlett* **2015**, *26*, 1615-1619.
35. Patel, V. K.; Kayahara, E.; Yamago, S. Practical synthesis of [n]cycloparaphenylenes (n=5, 7-12) by H<sub>2</sub>SnCl<sub>4</sub>-mediated aromatization of 1,4-dihydroxycyclo-2,5-diene precursors. *Chem. Eur. J.* **2015**, *21*, 5742-5749.
36. Segawa, Y.; Yagi, A.; Matsui, K.; Itami, K. Design and synthesis of carbon nanotube segments. *Angew. Chem., Int. Ed.* **2016**, *55*, 5136-5158.
37. Golder, M. R.; Jasti, R. Syntheses of the smallest carbon nanohoops and the emergence of unique physical phenomena. *Acc. Chem. Res.* **2015**, *48*, 557-566.

38. Darzi, E. R.; Jasti, R. The dynamic, size-dependent properties of [5]-[12]cycloparaphenylenes. *Chem. Soc. Rev.* **2015**, *44*, 6401-6410.
39. Iwamoto, T.; Watanabe, Y.; Sakamoto, Y.; Suzuki, T.; Yamago, S. Selective and random syntheses of [n]cycloparaphenylenes (n=8-13) and size dependence of their electronic properties. *J. Am. Chem. Soc.* **2011**, *133*, 8354-8361.
40. Iwamoto, T.; Watanabe, Y.; Sadahiro, T.; Haino, T.; Yamago, S. Size-selective encapsulation of C<sub>60</sub> by [10]cycloparaphenylene: Formation of the shortest fullerene-peapod. *Angew. Chem., Int. Ed.* **2011**, *50*, 8342-8344.
41. Hashimoto, S.; Kayahara, E.; Mizuhata, Y.; Tokitoh, N.; Takeuchi, K.; Ozawa, F.; Yamago, S. Synthesis and physical properties of polyfluorinated cycloparaphenylenes. *Org. Lett.* **2018**, *20*, 5973-5976.
42. Leonhardt, E.; Van Raden, J. M.; Miller, D.; Zakharov, L. N.; Aleman, B.; Jasti, R. A bottom-up approach to solution-processed, atomically precise graphitic cylinders on surfaces. *ChemRxiv.* **2018**.
43. Kayahara, E.; Sun, L.; Onishi, H.; Suzuki, K.; Fukushima, T.; Sawada, A.; Kaji, H.; Yamago, S. Gram-scale synthesis and conductivities of [10]cycloparaphenylene and its tetraalkoxy derivatives. *J. Am. Chem. Soc.* **2018**, *139*, 18480-18483.
44. Darzi, E. R.; Hirst, E. S.; Weber, C. D.; Zakharov, L. N.; Lonergan, M. C.; Jasti, R. Synthesis, properties, and design principles of donor-acceptor nano hoops. *ACS Cent. Sci.* **2015**, *1*, 335-342.
45. Van Raden, J. M.; Darzi, E. R.; Zakharov, L. N.; Jasti, R. Synthesis and characterization of a highly strained donor-acceptor nano hoop. *Org. Biomol. Chem.* **2016**, *14*, 5721-5727.
46. Della Sala, P.; Talotta, C.; Caruso, T.; De Rosa, M.; Soriente, A.; Neri, P.; Gaeta, C. Tuning cycloparaphenylene host properties by chemical modification. *J. Org. Chem.* **2017**, *82*, 9885-9889.
47. Tran-Van, A. F.; Wegner, H. A. Nano-rings with a handle - Synthesis of substituted cycloparaphenylenes. *Beilstein J. Nanotechnol.* **2014**, *5*, 1320-1333.
48. Li, S. J.; Huang, C. F.; Thakellapalli, H.; Farajidizaji, B.; Popp, B. V.; Petersen, J. L.; Wang, K. K. Syntheses and structures of functionalized [9]cycloparaphenylenes as carbon nano hoops bearing carbomethoxy and N-phenylphthalimido groups. *Org. Lett.* **2016**, *18*, 2268-2271.
49. Kayahara, E.; Qu, R.; Yamago, S. Bromination of cycloparaphenylenes: Strain-induced site-selective bis-addition and its application for late-stage functionalization. *Angew. Chem., Int. Ed.* **2017**, *56*, 10428-10432.

50. Li, P. H.; Sisto, T. J.; Darzi, E. R.; Jasti, R. The effects of cyclic conjugation and bending on the optoelectronic properties of paraphenylenes. *Org. Lett.* **2014**, *16*, 182-185.
51. Darzi, E. R.; White, B. M.; Loventhal, L. K.; Zakharov, L. N.; Jasti, R. An operationally simple and mild oxidative homocoupling of aryl boronic esters to access conformationally constrained macrocycles. *J. Am. Chem. Soc.* **2017**, *139*, 3106-3114.
52. Sisto, T. J.; Zakharov, L. N.; White, B. M.; Jasti, R. Towards pi-extended cycloparaphenylenes as seeds for CNT growth: Investigating strain relieving ring-openings and rearrangements. *Chem. Sci.* **2016**, *7*, 3681-3688.
53. Jackson, E. P.; Sisto, T. J.; Darzi, E. R.; Jasti, R. Probing Diels-Alder reactivity on a model CNT sidewall. *Tetrahedron* **2016**, *72*, 3754-3758.
54. Jung, M. E.; Hatfield, G. L. Preparation of bromides from alcohols via treatment with trimethylsilyl bromide. *Tetrahedron Lett.* **1978**, 4483-4486.
55. Pangborn, A. B.; Giardello, M. A.; Grubbs, R. H.; Rosen, R. K.; Timmers, F. J. Safe and convenient procedure for solvent purification. *Organometallics* **1996**, *15*, 1518-1520.

#### Chapter IV.

1. Garland, M.; Yim, J. J.; Bogoy, M. A bright future for precision medicine: advances in fluorescent chemical probe design and their clinical application. *Cell Chem. Biol.* **2016**, *23*, 122-136.
2. Lavis, L. D.; Raines, R. T. Bright ideas for chemical biology. *ACS Chem. Biol.* **2008**, *3*, 142-155.
3. Liu, Z.; Lavis, L. D.; Betzig, E. Imaging live-cell dynamics and structure at the single-molecule level. *Mol. Cell* **2015**, *58*, 644-659.
4. Jones, K. A.; Porterfield, W. B.; Rathbun, C. M.; McCutcheon, D. C.; Paley, M. A.; Prescher, J. A. Orthogonal luciferase-luciferin pairs for bioluminescence imaging. *J. Am. Chem. Soc.* **2017**, *139*, 2351-2358.
5. Michie, M. S.; Gotz, R.; Franke, C.; Bowler, M.; Kumari, N.; Magidson, V.; Levitus, M.; Loncarek, J.; Sauer, M.; Schnermann, M. J. Cyanine Conformational restraint in the far-red range. *J. Am. Chem. Soc.* **2017**, *139*, 12406-12409.

6. Chattopadhyay, P. K.; Gaylord, B.; Palmer, A.; Jiang, N.; Raven, M. A.; Lewis, G.; Reuter, M. A.; Rahman, A. K. M. N. U.; Price, D. A.; Betts, M. R.; Roederer, M. Brilliant violet fluorophores: A new class of ultrabright fluorescent compounds for immunofluorescence experiments. *Cytometry, Part A* **2012**, *81a*, 456-466.
7. Lavis, L. D. Chemistry is dead. Long live chemistry! *Biochemistry* **2017**, *56*, 5165-5170.
8. Xue, L.; Karpenko, I. A.; Hiblot, J.; Johnsson, K. Imaging and manipulating proteins in live cells through covalent labeling. *Nat. Chem. Biol.* **2015**, *11*, 917-923.
9. Rodriguez, E. A.; Campbell, R. E.; Lin, J. Y.; Lin, M. Z.; Miyawaki, A.; Palmer, A. E.; Shu, X. K.; Zhang, J.; Tsien, R. Y. The growing and glowing toolbox of fluorescent and photoactive proteins. *Trends Biochem. Sci.* **2017**, *42*, 111-129.
10. Kairdolf, B. A.; Qian, X. M.; Nie, S. M. Bioconjugated nanoparticles for biosensing, in vivo imaging, and medical diagnostics. *Anal. Chem.* **2017**, *89*, 1015-1031.
11. Butkevich, A. N.; Lukinavicius, G.; D'Este, E.; Hell, S. W. Cell-permeant large Stokes shift dyes for transfection-free multicolor nanoscopy. *J. Am. Chem. Soc.* **2017**, *139*, 12378-12381.
12. Lee, H. L. D.; Lord, S. J.; Iwanaga, S.; Zhan, K.; Xie, H. X.; Williams, J. C.; Wang, H.; Bowman, G. R.; Goley, E. D.; Shapiro, L.; Twieg, R. J.; Rao, J. H.; Moerner, W. E. Superresolution Imaging of targeted proteins in fixed and living cells using photoactivatable organic fluorophores. *J. Am. Chem. Soc.* **2010**, *132*, 15099-15101.
13. Banala, S.; Maurel, D.; Manley, S.; Johnsson, K. A caged, localizable rhodamine derivative for superresolution microscopy. *ACS Chem. Biol.* **2012**, *7*, 289-293.
14. Chozinski, T. J.; Gagnon, L. A.; Vaughan, J. C. Twinkle, twinkle little star: Photoswitchable fluorophores for super-resolution imaging. *FEBS Lett.* **2014**, *588*, 3603-3612.
15. Lavis, L. D.; Raines, R. T. Bright building blocks for chemical biology. *ACS Chem. Biol.* **2014**, *9*, 855-866.
16. Grimm, J. B.; English, B. P.; Chen, J. J.; Slaughter, J. P.; Zhang, Z. J.; Revyakin, A.; Patel, R.; Macklin, J. J.; Normanno, D.; Singer, R. H.; Lionnet, T.; Lavis, L. D. A general method to improve fluorophores for live-cell and single-molecule microscopy. *Nat. Methods* **2015**, *12*, 244-250.
17. Grimm, J. B.; Muthusamy, A. K.; Liang, Y.; Brown, T. A.; Lemon, W. C.; Patel, R.; Lu, R.; Macklin, J. J.; Keller, P. J.; Ji, N.; Lavis, L. D. A general method to fine-tune fluorophores for live-cell and in vivo imaging. *Nat. Methods* **2017**, *14*, 987-994.

18. Qu, J. Q.; Kohl, C.; Pottel, M.; Mullen, K. Ionic perylenetetracarboxydiimides: Highly fluorescent and water-soluble dyes for biolabeling. *Angew. Chem., Int. Ed.* **2004**, *43*, 1528-1531.
19. Hu, F. H.; Zeng, C.; Long, R.; Miao, Y. P.; Wei, L.; Xu, Q. Z.; Min, W. Supermultiplexed optical imaging and barcoding with engineered polyynes. *Nat. Methods* **2018**, *15*, 194-200.
20. Lin, H. A.; Sato, Y.; Segawa, Y.; Nishihara, T.; Sugimoto, N.; Scott, L. T.; Higashiyama, T.; Itami, K. A water-soluble warped nanographene: synthesis and applications for photoinduced cell death. *Angew. Chem., Int. Ed.* **2018**, *57*, 2874-2878.
21. Wan, H.; Yue, J. Y.; Zhu, S. J.; Uno, T.; Zhang, X. D.; Yang, Q. L.; Yu, K.; Hong, G. S.; Wang, J. Y.; Li, L. L.; Ma, Z. R.; Gao, H. P.; Zhong, Y. T.; Su, J.; Antaris, A. L.; Xia, Y.; Luo, J.; Liang, Y. Y.; Dai, H. J. A bright organic NIR-II nanofluorophore for three-dimensional imaging into biological tissues. *Nat. Commun.* **2018**, *9*, 1171.
22. Golder, M. R.; Jasti, R. Syntheses of the smallest carbon nanohoops and the emergence of unique physical phenomena. *Acc. Chem. Res.* **2015**, *48*, 557-566.
23. Jasti, R.; Bhattacharjee, J.; Neaton, J. B.; Bertozzi, C. R. Synthesis, characterization, and theory of [9]-, [12]-, and [18]cycloparaphenylene: carbon nanohoop structures. *J. Am. Chem. Soc.* **2008**, *130*, 17646-17647.
24. Scott, L. T. Conjugated belts and nanorings with radially oriented p orbitals. *Angew. Chem., Int. Ed.* **2003**, *42*, 4133-4135.
25. Darzi, E. R.; Sisto, T. J.; Jasti, R. Selective syntheses of [7]-[12]cycloparaphenylenes using orthogonal Suzuki-Miyaura cross-coupling reactions. *J. Org. Chem.* **2012**, *77*, 6624-6628.
26. Patel, V. K.; Kayahara, E.; Yamago, S. Practical synthesis of [n]cycloparaphenylenes (n=5, 7-12) by H<sub>2</sub>SnCl<sub>4</sub>-mediated aromatization of 1,4-dihydroxycyclo-2,5-diene precursors. *Chem. Eur. J.* **2015**, *21*, 5742-5749.
27. Segawa, Y.; Yagi, A.; Matsui, K.; Itami, K. Design and synthesis of carbon nanotube segments. *Angew. Chem., Int. Ed.* **2016**, *55*, 5136-5158.
28. Pena-Alvarez, M.; Qiu, L. L.; Taravillo, M.; Baonza, V. G.; Delgado, M. C. R.; Yamago, S.; Jasti, R.; Navarrete, J. T. L.; Casado, J.; Kertesz, M. From linear to cyclic oligoparaphenylenes: electronic and molecular changes traced in the vibrational Raman spectra and reformulation of the bond length alternation pattern. *Phys. Chem. Chem. Phys.* **2016**, *18*, 11683-11692.
29. Darzi, E. R.; Jasti, R. The dynamic, size-dependent properties of [5]-[12]cycloparaphenylenes. *Chem. Soc. Rev.* **2015**, *44*, 6401-6410.



30. Adamska, L.; Nayyar, I.; Chen, H.; Swan, A. K.; Oldani, N.; Fernandez-Alberti, S.; Golder, M. R.; Jasti, R.; Doorn, S. K.; Tretiak, S. "Self-trapping of excitons, violation of Condon approximation and efficient fluorescence in conjugated cycloparaphenylenes." *Nano Lett.* **2014**, *14*, 6539-6546.
31. Iwamoto, T.; Watanabe, Y.; Sakamoto, Y.; Suzuki, T.; Yamago, S. Selective and random syntheses of [n]cycloparaphenylenes (n=8-13) and size dependence of their electronic properties. *J. Am. Chem. Soc.* **2011**, *133*, 8354-8361.
32. Darzi, E. R.; Hirst, E. S.; Weber, C. D.; Zakharov, L. N.; Lonergan, M. C.; Jasti, R. Synthesis, properties, and design principles of donor-acceptor nanohoops. *ACS Cent. Sci.* **2015**, *1*, 335-342.
33. Kuwabara, T.; Orii, J.; Segawa, Y.; Itami, K. Curved oligophenylenes as donors in shape-persistent donor-acceptor macrocycles with solvatofluorochromic properties. *Angew. Chem., Int. Ed.* **2015**, *54*, 9646-9649.
34. Van Raden, J. M.; Darzi, E. R.; Zakharov, L. N.; Jasti, R. Synthesis and characterization of a highly strained donor-acceptor nanohoop. *Org. Biomol. Chem.* **2016**, *14*, 5721-5727.
35. Sisto, T. J.; Zakharov, L. N.; White, B. M.; Jasti, R. Towards pi-extended cycloparaphenylenes as seeds for CNT growth: investigating strain relieving ring-openings and rearrangements. *Chem. Sci.* **2016**, *7*, 3681-3688.
36. Hong, G. S.; Diao, S. O.; Antaris, A. L.; Dai, H. J. Carbon nanomaterials for biological imaging and nanomedicinal therapy. *Chem. Rev.* **2015**, *115*, 10816-10906.
37. Cherukuri, P.; Gannon, C. J.; Leeuw, T. K.; Schmidt, H. K.; Smalley, R. E.; Curley, S. A.; Weisman, R. B. Mammalian pharmacokinetics of carbon nanotubes using intrinsic near-infrared fluorescence. *Proc. Natl. Acad. Sci. U. S. A.* **2006**, *103*, 18882-18886.
38. Segawa, Y.; Fukazawa, A.; Matsuura, S.; Omachi, H.; Yamaguchi, S.; Irlle, S.; Itami, K. Combined experimental and theoretical studies on the photophysical properties of cycloparaphenylenes. *Org. Biomol. Chem.* **2012**, *10*, 5979-5984.
39. Hines, D. A.; Darzi, E. R.; Jasti, R.; Kamat, P. V. Carbon nanohoops: excited singlet and triplet behavior of [9]- and [12]-cycloparaphenylene. *J. Phys. Chem. A* **2014**, *118*, 1595-1600.
40. Chen, H.; Golder, M. R.; Wang, F.; Jasti, R.; Swan, A. K. Raman spectroscopy of carbon nanohoops. *Carbon* **2014**, *67*, 203-213.

41. Pena-Alvarez, M.; Burrezo, P. M.; Kertesz, M.; Iwamoto, T.; Yamago, S.; Xia, J. L.; Jasti, R.; Navarrete, J. T. L.; Taravillo, M.; Baonza, V. G.; Casado, J. Properties of sizeable [n]cycloparaphenylenes as molecular models of single-wall carbon nanotubes elucidated by raman spectroscopy: structural and electron-transfer responses under mechanical stress. *Angew. Chem., Int. Ed.* **2014**, *53*, 7033-7037.
42. Yamago, S.; Watanabe, Y.; Iwamoto, T. Synthesis of [8]cycloparaphenylene from a square-shaped tetranuclear platinum complex. *Angew. Chem., Int. Ed.* **2010**, *49*, 757-759.
43. Seybold, P. G.; Gouterman, M.; Callis, J. Calorimetric, photometric and lifetime determinations of fluorescence yields of fluorescein dyes. *Photochem. Photobiol.* **1969**, *9*, 229-242.
44. Dojindo Molecular Technologies, Inc. Cell Counting Kit-8: Technical Manual. [https://www.dojindo.com/TechnicalManual/Manual\\_CK04.pdf](https://www.dojindo.com/TechnicalManual/Manual_CK04.pdf). (accessed Aug 19, 2018).
45. Lalor, R.; Baillie-Johnson, H.; Redshaw, C.; Matthews, S. E.; Mueller, A. Cellular uptake of a fluorescent calix[4]arene derivative. *J. Am. Chem. Soc.* **2008**, *130*, 2892-2893.
46. Dunn, K. W.; Kamocka, M. M.; McDonald, J. H. A practical guide to evaluating colocalization in biological microscopy. *Am. J. Physiol. Cell Physiol.* **2011**, *300*, C723-C742.
47. Consoli, G. M. L.; Granata, G.; Fragassi, G.; Grossi, M.; Sallese, M.; Geraci, C. Design and synthesis of a multivalent fluorescent folate—calix[4]arene conjugate: cancer cell penetration and intracellular localization. *Org. Biomol. Chem.* **2015**, *13*, 3298-3307.
48. Consoli, G. M. L.; Granata, G.; Geraci, C. Design, synthesis, and drug solubilising properties of the first folate—calixarene conjugate. *Org. Biomol. Chem.* **2011**, *9*, 6491-6495.
49. Huang, T.; Phelps, C.; Wang, J.; Lin, L. J.; Bittel, A.; Scott, Z.; Jacques, S.; Gibbs, S. L.; Gray, J. W.; Nan, X. L. Simultaneous multicolor single-molecule tracking with single-laser excitation via spectral imaging. *Biophys. J.* **2018**, *114*, 301-310.
50. Pangborn, A. B.; Giardello, M. A.; Grubbs, R. H.; Rosen, R. K.; Timmers, F. J. Safe and convenient procedure for solvent purification. *Organometallics* **1996**, *15*, 1518-1520.
51. Golder, M. R.; Colwell, C. E.; Wong, B. M.; Zakharov, L. N.; Zhen, J. X.; Jasti, R. Iterative reductive aromatization/ring-closing metathesis strategy towards the synthesis of strained aromatic belts. *J. Am. Chem. Soc.* **2016**, *138*, 6577-6582.

52. Li, P. H.; Sisto, T. J.; Darzi, E. R.; Jasti, R. The effects of cyclic conjugation and bending on the optoelectronic properties of oligophenylenes. *Org. Lett.* **2014**, *16*, 182-185.
53. David, S.; Lonergan, M. C. Varying anionic functional group density in sulfonate-functionalized polyfluorenes by a one-phase suzuki polycondensation. *Macromolecules* **2013**, *46*, 4361-4369.
54. Jackson, E. P.; Sisto, T. J.; Darzi, E. D.; Jasti, R. Probing Diels-Alder Reactivity on a Model CNT Sidewall. *Tetrahedron*. **2016**, *72*, 3754-3758.
55. Brodnik, H.; Pozgan, F.; Stefane, B. Synthesis of 8-heteroaryl nitroxoline analogues via one-pot sequential Pd-catalyzed coupling reactions. *Org. Biomol. Chem.* **2016**, *14*, 1969-1981.
56. Trindade, A. F.; Frade, R. F.; Maçôas, E. M. S.; Graça, C.; Rodrigues, C. A. B.; Martinho, J. M. G.; Afonso, C. A. M. "Click and go": simple and fast folic acid conjugation. *Org. Biomol. Chem.* **2014**, *12*, 3181-3190.
58. Jobin Yvon Horiba. "A Guide to Recording Fluorescence Quantum Yields." <http://www.horiba.com/fileadmin/uploads/Scientific/Documents/Fluorescence/quantumyieldstrad.pdf> (accessed Aug 19, 2018).

## Chapter V.

1. Facchetti, A. Organic semiconductors: Made to order. *Nat. Mater.* **2013**, *12*, 598-600.
2. Nelson, J. Organic semiconductors: A map to find winners. *Nat. Mater.* **2017**, *16*, 969-970.
3. Henson, Z. B.; Mullen, K.; Bazan, G. C. Design strategies for organic semiconductors beyond the molecular formula. *Nat. Chem.* **2012**, *4*, 699-704.
4. Li, M. M.; An, C. B.; Pisula, W.; Mullen, K. Cyclopentadithiophene-benzothiadiazole donor-acceptor polymers as prototypical semiconductors for high-performance field-effect transistors. *Acc. Chem. Res.* **2018**, *51*, 1196-1205.
5. Ying, L.; Huang, F.; Bazan, G. C. Regioregular narrow-bandgap-conjugated polymers for plastic electronics. *Nat. Commun.* **2017**, *8*, 14047.
6. Lee, W. H.; Park, J.; Sim, S. H.; Lim, S.; Kim, K. S.; Hong, B. H.; Cho, K. Surface-directed molecular assembly of pentacene on monolayer graphene for high-performance organic transistors. *J. Am. Chem. Soc.* **2011**, *133*, 4447-4454.

7. Park, S. K.; Jackson, T. N.; Anthony, J. E.; Mourey, D. A. High mobility solution processed 6,13-bis(triisopropyl-silylethynyl) pentacene organic thin film transistors. *Appl. Phys. Lett.* **2007**, *91*, 063514.
8. Dorel, R.; Echavarren, A. M. Strategies for the synthesis of higher acenes. *Eur. J. Org. Chem.* **2017**, 14-24.
9. Anthony, J. E. The larger acenes: Versatile organic semiconductors. *Angew. Chem., Int. Ed.* **2008**, *47*, 452-483.
10. Cui, X.; Xiao, C.; Winands, T.; Koch, T.; Li, Y.; Zhang, L.; Doltsinis, N. L.; Wang, Z. Hexacenediimides. *J. Am. Chem. Soc.* **2018**, *140*, 12175-12180.
11. Anthony, J. E.; Gierschner, J.; Landis, C. A.; Parkin, S. R.; Sherman, J. B.; Bakus, R. C. A new functionalization strategy for pentacene. *Chem. Commun.* **2007**, 4746-4748.
12. Anthony, J. E.; Brooks, J. S.; Eaton, D. L.; Parkin, S. R. Functionalized pentacene: Improved electronic properties from control of solid-state order. *J. Am. Chem. Soc.* **2001**, *123*, 9482-9483.
13. Bheemireddy, S. R.; Ubaldo, P. C.; Rose, P. W.; Finke, A. D.; Zhuang, J. P.; Wang, L. C.; Plunkett, K. N. Stabilizing pentacene by cyclopentannulation. *Angew. Chem., Int. Ed.* **2015**, *54*, 15762-15766.
14. Dai, G. L.; Chang, J. J.; Luo, J.; Dong, S. Q.; Aratani, N.; Zheng, B.; Huang, K. W.; Yamada, H.; Chi, C. Y. Z-Shaped Pentaleno-acene dimers with high stability and small band gap. *Angew. Chem., Int. Ed.* **2016**, *55*, 2693-2696.
15. Kaur, I.; Jia, W. L.; Kopreski, R. P.; Selvarasah, S.; Dokmeci, M. R.; Pramanik, C.; McGruer, N. E.; Miller, G. P. Substituent effects in pentacenes: Gaining control over HOMO-LUMO gaps and photooxidative resistances. *J. Am. Chem. Soc.* **2008**, *130*, 16274-16286.
16. Griffith, O. L.; Anthony, J. E.; Jones, A. G.; Shu, Y.; Lichtenberger, D. L. Substituent effects on the electronic characteristics of pentacene derivatives for organic electronic devices: Dioxolane-substituted pentacene derivatives with triisopropylsilylethynyl functional groups. *J. Am. Chem. Soc.* **2012**, *134*, 14185-14194.
17. Sanders, S. N.; Kumarasamy, E.; Pun, A. B.; Trinh, M. T.; Choi, B.; Xia, J. L.; Taffet, E. J.; Low, J. Z.; Miller, J. R.; Roy, X.; Zhu, X. Y.; Steigerwald, M. L.; Sfeir, M. Y.; Campos, L. M. Quantitative intramolecular singlet fission in bipentacenes. *J. Am. Chem. Soc.* **2015**, *137*, 8965-8972.

18. Kumarasamy, E.; Sanders, S. N.; Tayebjee, M. J. Y.; Asadpoordarvish, A.; Hele, T. J. H.; Fuemmeler, E. G.; Pun, A. B.; Yablon, L. M.; Low, J. Z.; Paley, D. W.; Dean, J. C.; Choi, B.; Scholes, G. D.; Steigerwald, M. L.; Ananth, N.; McCamey, D. R.; Sfeir, M. Y.; Campos, L. M. Tuning singlet fission in pi-bridge-pi chromophores. *J. Am. Chem. Soc.* **2017**, *139*, 12488-12494.
19. Liu, H. Y.; Wang, R.; Shen, L.; Xu, Y. Q.; Xiao, M.; Zhang, C. F.; Li, X. Y. A covalently linked tetracene trimer: Synthesis and singlet exciton fission property. *Org. Lett.* **2017**, *19*, 580-583.
20. Fuemmeler, E. G.; Sanders, S. N.; Pun, A. B.; Kumarasamy, E.; Zeng, T.; Miyata, K.; Steigerwald, M. L.; Zhu, X. Y.; Sfeir, M. Y.; Campos, L. M.; Ananth, N. A direct mechanism of ultrafast intramolecular singlet fission in pentacene dimers. *ACS Cent. Sci.* **2016**, *2*, 316-324.
21. Iyoda, M.; Yamakawa, J.; Rahman, M. J. Conjugated macrocycles: concepts and applications. *Angew. Chem., Int. Ed.* **2011**, *50*, 10522-10553.
22. Darzi, E. R.; Jasti, R. The dynamic, size-dependent properties of [5]-[12]cycloparaphenylenes. *Chem. Soc. Rev.* **2015**, *44*, 6401-6410.
23. Golder, M. R.; Jasti, R. Syntheses of the smallest carbon nano hoops and the emergence of unique physical phenomena. *Acc. Chem. Res.* **2015**, *48*, 557-566.
24. Segawa, Y.; Yagi, A.; Matsui, K.; Itami, K. Design and synthesis of carbon nanotube segments. *Angew. Chem., Int. Ed.* **2016**, *55*, 5136-5158.
25. Segawa, Y.; Fukazawa, A.; Matsuura, S.; Omachi, H.; Yamaguchi, S.; Irle, S.; Itami, K. Combined experimental and theoretical studies on the photophysical properties of cycloparaphenylenes. *Org. Biomol. Chem.* **2012**, *10*, 5979-5984.
26. Iwamoto, T.; Watanabe, Y.; Sakamoto, Y.; Suzuki, T.; Yamago, S. Selective and random syntheses of [n]cycloparaphenylenes (n=8-13) and size dependence of their electronic properties. *J. Am. Chem. Soc.* **2011**, *133*, 8354-8361.
27. Iwamoto, T.; Watanabe, Y.; Sadahiro, T.; Haino, T.; Yamago, S. Size-selective encapsulation of C-60 by [10]cycloparaphenylene: Formation of the shortest fullerene-peapod. *Angew. Chem., Int. Ed.* **2011**, *50*, 8342-8344.
28. Xia, J. L.; Bacon, J. W.; Jasti, R. Gram-scale synthesis and crystal structures of [8]- and [10]CPP, and the solid-state structure of C-60@[10]CPP. *Chem. Sci.* **2012**, *3*, 3018-3021.
29. Della Sala, P.; Talotta, C.; Caruso, T.; De Rosa, M.; Soriente, A.; Neri, P.; Gaeta, C. Tuning cycloparaphenylene host properties by chemical modification. *J. Org. Chem.* **2017**, *82*, 9885-9889.

30. Tran-Van, A. F.; Wegner, H. A. Nano-rings with a handle - Synthesis of substituted cycloparaphenylenes. *Beilstein J. Nanotechnol.* **2014**, *5*, 1320-1333.
31. Darzi, E. R.; Hirst, E. S.; Weber, C. D.; Zakharov, L. N.; Lonergan, M. C.; Jasti, R. Synthesis, properties, and design principles of donor-acceptor nano hoops. *ACS Cent. Sci.* **2015**, *1*, 335-342.
32. Van Raden, J. M.; Darzi, E. R.; Zakharov, L. N.; Jasti, R. Synthesis and characterization of a highly strained donor-acceptor nano hoop. *Org. Biomol. Chem.* **2016**, *14*, 5721-5727.
33. Kuwabara, T.; Orii, J.; Segawa, Y.; Itami, K. Curved oligophenylenes as donors in shape-persistent donor-acceptor macrocycles with solvatochromic properties. *Angew. Chem., Int. Ed.* **2015**, *54*, 9646-9649.
34. Della Sala, P.; Capobianco, A.; Caruso, T.; Talotta, C.; De Rosa, M.; Neri, P.; Peluso, A.; Gaeta, C. An anthracene-incorporated [8]cycloparaphenylene derivative as an emitter in photon upconversion. *J. Org. Chem.* **2018**, *83*, 220-227.
35. Li, S. J.; Huang, C. F.; Thakellapalli, H.; Farajidizaji, B.; Popp, B. V.; Petersen, J. L.; Wang, K. K. Syntheses and structures of functionalized [9]cycloparaphenylenes as carbon nano hoops bearing carbomethoxy and N-phenylphthalimido groups. *Org. Lett.* **2016**, *18*, 2268-2271.
36. Kayahara, E.; Sun, L.; Onishi, H.; Suzuki, K.; Fukushima, T.; Sawada, A.; Kaji, H.; Yamago, S. Gram-scale synthesis and conductivities of [10]cycloparaphenylene and its tetraalkoxy derivatives. *J. Am. Chem. Soc.* **2018**, *139*, 18480-18483.
37. Liu, Y. Y.; Lin, J. Y.; Bo, Y. F.; Xie, L. H.; Yi, M. D.; Zhang, X. W.; Zhang, H. M.; Loh, T. P.; Huang, W. Synthesis and crystal structure of highly strained [4]cyclofluorene: Green-emitting fluorophore. *Org. Lett.* **2016**, *18*, 172-175.
38. Hashimoto, S.; Kayahara, E.; Mizuhata, Y.; Tokitoh, N.; Takeuchi, K.; Ozawa, F.; Yamago, S. Synthesis and physical properties of polyfluorinated cycloparaphenylenes. *Org. Lett.* **2018**, *20*, 5973-5976.
39. Ball, M.; Zhong, Y.; Fowler, B.; Zhang, B. Y.; Li, P. P.; Etkin, G.; Paley, D. W.; Decatur, J.; Dalsania, A. K.; Li, H. X.; Xiao, S. X.; Ng, F.; Steigerwald, M. L.; Nuckolls, C. Macrocyclization in the design of organic n-type electronic materials. *J. Am. Chem. Soc.* **2016**, *138*, 12861-12867.
40. Zhang, B. Y.; Trinh, M. T.; Fowler, B.; Ball, M.; Xu, Q. Z.; Ng, F.; Steigerwald, M. L.; Zhu, X. Y.; Nuckolls, C.; Zhong, Y. Rigid, Conjugated macrocycles for high performance organic photodetectors. *J. Am. Chem. Soc.* **2016**, *138*, 16426-16431.

41. Ball, M. L.; Zhang, B. Y.; Xu, Q. Z.; Paley, D. W.; Ritter, V. C.; Ng, F.; Steigerwald, M. L.; Nuckolls, C. Influence of molecular conformation on electron transport in giant, conjugated macrocycles. *J. Am. Chem. Soc.* **2018**, *140*, 10135-10139.
42. Sun, Z.; Miyamoto, N.; Sato, S.; Tokuyama, H.; Isobe, H. An obtuse-angled corner unit for fluctuating carbon nano hoops. *Chem. Asian J.* **2017**, *12*, 271-275.
43. Jasti, R.; Bhattacharjee, J.; Neaton, J. B.; Bertozzi, C. R. Synthesis, characterization, and theory of [9]-, [12]-, and [18]cycloparaphenylene: Carbon nano hoop structures. *J. Am. Chem. Soc.* **2008**, *130*, 17646-17647.
44. Miao, Q.; Chi, X. L.; Xiao, S. X.; Zeis, R.; Lefenfeld, M.; Siegrist, T.; Steigerwald, M. L.; Nuckolls, C. Organization of acenes with a cruciform assembly motif. *J. Am. Chem. Soc.* **2006**, *128*, 1340-1345.
45. Sparfel, D.; Gobert, F.; Rigaudy, J. Thermal transformations of meso-acenic photooxides. VI pentacenic photooxides. *Tetrahedron* **1980**, *36*, 2225-2235.
46. Patel, V. K.; Kayahara, E.; Yamago, S. Practical synthesis of [n]cycloparaphenylenes (n=5, 7-12) by H<sub>2</sub>SnCl<sub>4</sub>-mediated aromatization of 1,4-dihydroxycyclo-2,5-diene precursors. *Chem. Eur. J.* **2015**, *21*, 5742-5749.
47. Ueda, A.; Nishida, S.; Fukui, K.; Ise, T.; Shiomi, D.; Sato, K.; Takui, T.; Nakasuji, K.; Morita, Y. Three-dimensional intramolecular exchange interaction in a curved and nonalternant pi-conjugated system: Corannulene with two phenoxyl radicals. *Angew. Chem., Int. Ed.* **2010**, *49*, 1678-1682.
48. Wang, Q.; Hu, P.; Tanaka, T.; Gopalakrishna, T. Y.; Heng, T. S.; Phan, H.; Zeng, W. D.; Ding, J.; Osuka, A.; Chi, C. Y.; Siegel, J.; Wu, J. S. Curved -conjugated corannulene dimer diradicaloids. *Chem. Sci.* **2018**, *9*, 5100-5105.
49. Yang, H. F.; Chen, M. Z.; Song, X. Y.; Bu, Y. X. Structural fluctuation governed dynamic diradical character in pentacene. *Phys. Chem. Chem. Phys.* **2015**, *17*, 13904-13914.
50. Dressler, J. J.; Teraoka, M.; Espejo, G. L.; Kishi, R.; Takamuku, S.; Gomes-Garcis, C. J.; Zakharov, L. N.; Nakano, M.; Casado, J.; Haley, M. M. Thiophene and its sulfur inhibit indenoindenodibenzothiophene diradicals from low-energy lying thermal triplets. *Nat. Chem.* **2018**, Article ASAP.
51. Rudebusch, G. E.; Zafra, J. L.; Jorner, K.; Fukuda, K.; Marshall, J. L.; Arrechea-Marcos, I.; Espejo, G. L.; Ortiz, R. P.; Gomez-Garcia, C. J.; Zakharov, L. N.; Nakano, M.; Ottosson, H.; Casado, J.; Haley, M. M. Diindeno-fusion of an anthracene as a design strategy for stable organic biradicals. *Nat. Chem.* **2016**, *8*, 753-759.

52. Pangborn, A. B.; Giardello, M. A.; Grubbs, R. H.; Rosen, R. K.; Timmers, F. J. Safe and convenient procedure for solvent purification. *Organometallics* **1996**, *15*, 1518-1520.
53. White, B. M.; Zhao, Y.; Kawashima, T. E.; Branchaud, B. P.; Pluth, M. D.; Jasti, R. Expanding the chemical space of biocompatible fluorophores: Nanohoops in cells. *ACS Cent. Sci.* **2018**, *4*, 1173-1178.
54. Frisch, M. J.; Trucks, G. W.; Schlegel, H. B.; Scuseria, G. E.; Robb, M. A.; Cheeseman, J. R.; Scalmani, G.; Barone, V.; Mennucci, B.; Petersson, G. A.; Nakatsuji, H.; Caricato, M.; Li, X.; Hratchian, H. P.; Izmaylov, A. F.; Bloino, J.; Zheng, G.; Sonnenberg, J. L.; Hada, M.; Ehara, M.; Toyota, K.; Fukuda, R.; Hasegawa, J.; Ishida, M.; Nakajima, T.; Honda, Y.; Kitao, O.; Nakai, H.; Vreven, T.; Montgomery, J. A.; Peralta, J. E.; Ogliaro, F.; Bearpark, M.; Heyd, J. J.; Brothers, E.; Kudin, K. N.; Staroverov, V. N.; Kobayashi, R.; Normand, J.; Raghavachari, K.; Rendell, A.; Burant, J. C.; Iyengar, S. S.; Tomasi, J.; Cossi, M.; Rega, N.; Millam, J. M.; Klene, M.; Knox, J. E.; Cross, J. B.; Bakken, V.; Adamo, C.; Jaramillo, J.; Gomperts, R.; Stratmann, R. E.; Yazyev, O.; Austin, A. J.; Cammi, R.; Pomelli, C.; Ochterski, J. W.; Martin, R. L.; Morokuma, K.; Zakrzewski, V. G.; Voth, G. A.; Salvador, P.; Dannenberg, J. J.; Dapprich, S.; Daniels, A. D.; Farkas; Foresman, J. B.; Ortiz, J. V.; Cioslowski, J.; Fox, D. J. Wallingford CT, **2009**.